EPFL

Thèse n° 9487

Dispatch-aware Optimal Planning of Active Distribution Networks including Energy Storage Systems

Présentée le 13 février 2023

Faculté des sciences et techniques de l'ingénieur
Laboratoire des systèmes électriques distribués
Programme doctoral en génie électrique

pour l'obtention du grade de Docteur ès Sciences

par

Ji Hyun YI

Acceptée sur proposition du jury

Prof. A. Skrivervik Favre, présidente du jury
Prof. M. Paolone, Dr S.-R. Cherkaoui, directeurs de thèse
Prof. V. Miranda, rapporteur
Prof. F. Pilo, rapporteur
Prof. J.-Y. Le Boudec, rapporteur

École polytechnique fédérale de Lausanne

2023

To my family

Acknowledgements

This work has been possible, thanks to the help and support of many kind people. I would like to thank each and everyone who have contributed to completion of my thesis.

Firstly, I would like to express my deepest gratitude to my supervisor, Prof. Mario Paolone for providing me the opportunity to purse my Ph.D. thesis under his supervision. I am incredibly appreciative of his thorough and unwavering supervision during the past four years of my doctoral studies. Under his guidance, I have continually developed as a researcher, and grown both in personal and professional way . I'm also grateful to Dr. Rachid Cherkaoui, my thesis co-director, for his unwavering support during my doctoral studies. Aside from his invaluable technical inputs, he has been a constant source of energy and warmth during my PhD.

Then, I want to express my deepest gratitude to my collaborators at ABB and Hitachi Energy Research for funding this dissertation. In particular, I would like to thank Dr. Katarina Knezovic and Dr. Dmitry Shchetinin for their resourceful and friendly collaboration.

Then, I wish to express my thanks to Sophie and Eulalia for handling administrative and non-technical matters.

I would like to thanks to my friends and colleagues. In particular to my office-mate Simone for having a good company. I want to thank Yihui, Vladimir, Johanna, Alex, Francesco, Sherif, Willem, Georgios, and others for making the lab life memorable. A special thank you to Rahul for being at my side always. Thanks to your constant encouragement and support, I have come this far.

I would like to thank all my friends in Lausanne, with whom I have shared incredible moments. In particular, many thanks go to my dearest flatmates, Ohyeon, Sohyeong, Yeonju, and Sim. They have become my family in Switzerland.

Last but not least, my heartfelt and eternal gratitude to my devoted parents for their devotion, many years of support, unending love, and immeasurable patience and compassion. I would like to convey my deepest gratitude to my sister Jieun. This dissertation is dedicated to them.

Lausanne, 24 October 2022 Ji Hyun Yi

Abstract

Distributed generation (DG) units are progressively installed into the power distribution network and may actively controlled to achieve specific operational objectives paving the way to realise the concept of the so-called active distribution network (ADN). Nonetheless, the penetration of renewable energy resources (RER) is prominently rising among DG units within ADNs leading to significant volatility in the power-flows and difficulty in achieving network controllability. As a result, several operational issues arise for both distribution and transmission networks. The stochasticity and variability of RERs may cause technical issues regarding system operating condition of ADNs such as degradation of power supply in terms of reliability and voltage quality, line congestion, etc. Simultaneously, the reserve requirements at the transmission level, to manage the power imbalance caused by highly stochastic prosumption at the distribution level, are increasing significantly. This brings the interest in attenuating such power imbalances at the distribution network level by delegating the financial responsibility from transmission system operators (TSOs) to distribution system operators (DSOs). With this change in the regulatory environment, the DSOs' operational objectives may include achieving the local dispatchability of the ADN. *Dispatchability* identifies the capability of a resource, or a network, to control the realized active power flow through the resource, or the network, to follow a pre-defined power schedule with high fidelity. A promising solution is to integrate energy storage systems (ESSs) within the ADN for compensating the dispatch error, thereby enhancing the ADN's dispatchability. In this context, the thesis develops a planning framework for ADNs to achieve their dispatchability by means of ESS allocation while ensuring a reliable and secure operation of ADNs. Then, the framework is extended to include grid reinforcements and ESSs planning. Finally, the thesis also develops a distribution network expansion planning (DNEP) strategy to consider hosting newly integrated stochastic generation resources and customers.

The first part of the thesis develops the framework for the optimal sizing and siting ESSs to achieve ADNs dispatchability. The planning strategy is developed by embedding operational constraints of the grid by means of both linearized and exact optimal power flow models. In this regard, the proposed formulation relies on the so-called Augmented Relaxed Optimal Power Flow (AR-OPF) method: it expresses a convex full AC optimal power flow, which is proven to provide a global optimal and exact solution in the case of radial power grids. The AR-OPF is appropriately modified to be coupled with the proposed dispatching control resulting in a two-level optimization problem. In the first block, the optimal level of dispatchability

and the ESS allocation is determined based on the trade-off between the imbalance penalty cost and the ESS investment cost. The following block determines the site and size of the ESS assets by evaluating the system states over operating scenarios representing seasonal variability and prediction uncertainty. To solve such a large-scale planning problem, the Benders decomposition technique is utilized to break down the planning problem into investment and parallel operation problems, each representing the daily operation of a typical day type.

The second part of the thesis tackles how the optimal investment in existing lines has to be integrated to develop a joint planning problem considering ESSs and line reinforcement to achieve the optimal dispatch level while ensuring sufficient hosting capacity for increasing stochastic renewable generation. The line reinforcement investment is suitably modeled along with corresponding adjustments on the network admittance matrix and the grid constraints to be incorporated in the modified AR-OPF model. Finally, the above methods are extended to formulate a distribution network expansion planning (DNEP) strategy that considers hosting newly integrated stochastic generation resources and customers. The investment in new lines is suitably modeled and embedded into the AR-OPF model-based operation. This is achieved by converting the model to account for the change of network topology and adjacency matrix associated with assets investment. The large computational burden of the DNEP problem is mitigated by employing a specific sequential algorithm that consists of two sub-stages: the first sub-stage sequentially integrates new nodes while determining lines for reinforcement and nodes for ESS allocation, while the second sub-stage determines the capacity of lines and ESSs. The performance of the proposed methodology is verified through simulations on various sizes of distribution networks by showing that it can determine the optimal level of dispatchability while securing the required hosting capacity of the ADN under increasing stochastic prosumption.

Keywords: Active distribution networks, Benders decomposition, distribution network, expansion planning, energy storage systems, grid reinforcement, line reinforcement, optimal power flow, dispatchability, stochastic optimization.

Résumé

Les unités de production distribuée (DG) sont progressivement installées dans les réseaux de distribution d'électricité et sont activement contrôlées pour atteindre des objectifs opérationnels spécifiques, ouvrant la voie à la réalisation de réseaux de distribution actifs (ADN). Néanmoins, la pénétration des ressources énergétiques renouvelables (RER) est en forte augmentation parmi les unités DG au sein des ADN, ce qui entraîne une volatilité importante des flux d'énergie et par conséquent une difficulté à assurer la contrôlabilité du réseau. En conséquence, plusieurs problèmes opérationnels se posent à la fois au sein du réseau de distribution et du réseau de transmission. La stochasticité et la variabilité des RER peuvent entraîner des problèmes techniques concernant l'état de fonctionnement des ADN, tels que la dégradation de l'alimentation électrique en termes de fiabilité et de qualité de la tension, la congestion des lignes, etc. Simultanément, les exigences de réserve au niveau du transport, pour gérer le déséquilibre de puissance causé par la nature stochastique de la production/-demande au niveau de la distribution, augmentent de manière significative. Cela présente l'intérêt d'atténuer ces déséquilibres de puissance au niveau du réseau de distribution en déléguant la responsabilité financière des gestionnaires de réseau de transport (TSO) aux gestionnaires de réseau de distribution (DSO). Avec cette évolution de la réglementation, l'objectif opérationnel intéressant les DSO pourraient inclure la réalisation de la dispatchabilité de l'ADN. La dispatchabilité identifie la capacité d'une ressource, ou d'un réseau, à contrôler le flux de puissance active réalisé à travers la ressource, ou le réseau, pour suivre un profil de puissance prédéfini de manière aussi précise que possible. Une solution prometteuse consiste à intégrer et à utiliser les ESS au sein de l'ADN pour compenser la distribution des erreurs, améliorant ainsi la dispatchabilité de l'ADN. Dans ce contexte, cette thèse développe un outil de planification permettant aux ADN d'atteindre leur dispatchabilité moyennant l'installation d'ESS, tout en assurant simultanément un fonctionnement fiable et sécurisé des ADN. Deuxièmement, le cadre est étendu pour inclure des renforcements du réseau en même temps que la planification des ESS. Enfin, la thèse développe également une stratégie de planification de l'expansion du réseau de distribution (DNEP) pour envisager l'intégration de nouvelles ressources de production stochastiques et de nouveaux clients.

La première partie de la thèse développe un schéma de dimensionnement et d'implantation optimal des ESS pour la dispatchabilité des ADN. La stratégie de planification est développée en intégrant les contraintes opérationnelles du réseau par un modèle exact de

calcul de flux de puissance optimal. À cet égard, la formulation proposée s'appuie sur la méthode dite Augmented Relaxed Optimal Power Flow (AR-OPF) : elle formule un modèle de flux de puissance optimal convexe en régime alternatif, dont il a été prouvé qu'il fournit une solution globale optimale et exacte dans le cas de réseaux électriques radiaux. L'AR-OPF est modifié de manière appropriée pour être couplé avec le contrôle de dispatchabilité proposé résultant en un problème d'optimisation à deux niveaux. Dans le premier bloc, le niveau optimal de dispatchabilité et l'allocation ESS sont déterminés sur la base du compromis entre le coût de pénalité de déséquilibre et le coût d'investissement ESS. Le bloc suivant détermine le site et la taille des actifs d'ESS en fonction de l'évaluation des conditions du système à partir de scénarios d'exploitation représentant la variabilité saisonnière et l'incertitude des prévisions. Pour résoudre un tel problème de planification à grande échelle, la technique de décomposition de Benders est utilisée pour décomposer le problème de planification en problèmes d'investissement et en problèmes d'exploitation en parallèle, chacun de ces derniers représentant le fonctionnement quotidien d'une journée typique.

La deuxième partie de la thèse considère l'investissement dans les lignes existantes qui est intégré pour développer un problème de planification conjointe prenant en compte les ESS et le renforcement des lignes pour atteindre le niveau de dispatchabilité optimal tout en assurant une capacité d'accueil suffisante pour augmenter la production renouvelable stochastique. L'investissement du renforcement de la ligne est modélisé de manière appropriée avec les ajustements correspondants dans la matrice d'admittance du réseau et dans les contraintes de réseau à incorporer dans le modèle AR-OPF modifié.

Enfin, la thèse propose que les méthodes ci-dessus soient étendues pour formuler une stratégie de planification de l'expansion du réseau de distribution (DNEP) qui considère l'installation de nouvelles ressources de production stochastiques et l'intégration de nouveaux clients. L'investissement de nouvelles lignes est modélisé de manière appropriée et intégré dans le problème d'exploitation basé sur le modèle AR-OPF. Ceci est réalisé en convertissant le modèle pour tenir compte du changement de la topologie du réseau et de la matrice d'adjacence associée aux investiments. La charge de calcul du problème DNEP est atténuée en utilisant un algorithme séquentiel spécifique qui se compose de deux sous-étapes : la première sous-étape intègre séquentiellement de nouveaux nœuds tout en déterminant les lignes pour le renforcement et les nœuds pour l'allocation des ESS, tandis que la deuxième sous-étape détermine la capacité des lignes et des ESS. La performance de la méthodologie proposée est vérifiée à travers des simulations sur différentes tailles de réseaux de distribution en montrant qu'elle peut déterminer le niveau optimal de dispatchabilité tout en sécurisant la capacité d'hébergement requise de l'ADN sous une probabilité stochastique croissante de la production/demande.

Mots-clés : Réseaux de distribution actifs, décomposition de Benders, planification de l'expansion du réseau de distribution, systèmes de stockage d'énergie, renforcement du réseau, renforcement de la ligne, flux de puissance optimal, planification de la dispatchabilité, optimisation stochastique

Contents

Acknowledgements **i**

Abstract **iii**

List of figures **xi**

List of tables **xiii**

1 Introduction **1**
1.1 Motivation of the Thesis . . . 3
1.2 Objectives and Contributions of the Thesis . . . 4
1.3 Thesis Outline . . . 6

2 Optimal Planning of Energy Storage Systems accounting for Active Distribution Networks' Dispatchability **9**
2.1 Highlights . . . 9
2.2 Organization of the Chapter . . . 9
2.3 State-of-the-art of ADN Operation Considering Prosumption Uncertainty . . . 10
2.4 State-of-the-art of ESS Planning . . . 12
2.5 Problem Statement and Contributions . . . 14
2.6 Achieving the ADN's Dispatchability . . . 14
2.6.1 Definition of ADN's Dispatchability . . . 14
2.6.2 Embedding the ESS's Offset Profile within the Dispatch Plan . . . 16
2.7 Integration of ADN's Dispatchability into the Power Flow Model . . . 17
2.7.1 Formulation of PWL-OPF Model . . . 17
2.8 System Description . . . 20
2.9 Problem Formulation . . . 21
2.9.1 Operation-aware ADNs' planning problem . . . 21
2.9.2 ADNs' planning algorithm using Benders decomposition . . . 24
2.10 Simulations . . . 27
2.10.1 Simulation Configuration . . . 27
2.10.2 Simulation Result . . . 28

2.10.3 Approximation Accuracy of PWL-OPF model with Different Discretization Steps . . . 30
2.10.4 Discussion on the Integration of the Offset Profile . . . 32
2.11 Conclusion . . . 33

3 Optimal Planning of Energy Storage Systems based on Exact Convexified OPF Model 35
3.1 Highlights . . . 35
3.2 Organization of the Chapter . . . 35
3.3 State-of-the-art of the OPF Model Embedded in Planning Strategies . . . 36
3.4 Problem Statement and Contributions . . . 38
3.5 Augmented Relaxed Optimal Power Flow . . . 38
3.5.1 Discussion on the Exactness and the Applicability of the Model for Various Operational Objectives . . . 40
3.6 Problem Formulation . . . 41
3.6.1 Key Differences with the Planning Approach in Ch. 2 . . . 42
3.6.2 1st Block Problem . . . 44
3.6.3 2nd Block Problem . . . 46
3.7 Simulations . . . 49
3.7.1 Simulation Configuration . . . 49
3.7.2 Planning with 1 Day under Hourly Dispatch . . . 50
3.7.3 Planning with Full Scenarios with 30 min Dispatch Intervals . . . 51
3.7.4 Sensitivity Analysis Regarding the Initial ESS SoE . . . 53
3.7.5 Numerical Comparison with Operation Model Using PWL-OPF, R-OPF, and AR-OPF Model . . . 54
3.7.6 Comparison with Planning Approach Using AR-OPF and R-OPF Model . . . 55
3.8 Conclusion . . . 56

4 Optimal Co-planning of ESS Allocation and Line Reinforcement Considering the ADN's Dispatchability 57
4.1 Highlights . . . 57
4.2 Organization of the Chapter . . . 57
4.3 State-of-the-art of Co-optimization of Line Reinforcement and ESS Allocation . . . 58
4.4 Problem Statement and Contributions . . . 59
4.5 System Description . . . 60
4.6 Problem Formulation . . . 61
4.6.1 1st Block Problem . . . 61
4.6.2 2nd Block Problem . . . 62
4.7 Simulations . . . 72
4.7.1 Simulation Configuration . . . 72
4.7.2 Effect of Co-optimized Planning : Comparison between the Case with ESSs only, and the Case with both ESSs and Line Reinforcement . . . 73
4.7.3 Planning Results with Different Levels of PV Capacities . . . 75

4.7.4 Numerical Assessment on the Effect of Separation of Siting and Sizing Problems . . . 78
4.7.5 Scalability Analysis Regarding the Network Size . . . 79
4.8 Conclusion . . . 81

5 Expansion Planning of Active Distribution Networks Achieving their Dispatchability 83
5.1 Highlight . . . 83
5.2 Organization of the Chapter . . . 83
5.3 State-of-the-art of ADN Expansion Planning . . . 84
5.4 Problem Statement and Contributions . . . 86
5.5 System Description . . . 87
5.6 Problem Formulation . . . 89
5.7 Sequential Approach . . . 90
5.7.1 1st Block Problem . . . 90
5.7.2 2nd Block Problem . . . 91
5.8 Simultaneous Approach . . . 98
5.8.1 Master Problem . . . 101
5.8.2 Subproblem . . . 101
5.8.3 Selection of the Best Network Topology . . . 105
5.9 Comparison between the Sequential and the Simultaneous Approach . . . 106
5.9.1 Simulation Configuration . . . 107
5.9.2 Planning Results Comparison between the Sequential and the Simultaneous Approach . . . 107
5.10 Performance Validation of the Expansion Planning Tool with the Sequential Approach . . . 109
5.10.1 The simulation Configuration . . . 109
5.10.2 Distribution Network Expansion Assessment on a Real Swiss Power Distribution Network . . . 111
5.10.3 Scalability Analysis Regarding Varying Investment Candidates . . . 115
5.10.4 Scalability Analysis Regarding Varying System Size . . . 115
5.10.5 Statistical Analysis on Varying Number of Operating Scenarios . . . 116
5.11 Conclusion . . . 117

6 Conclusion 119

A Appendix 123
A.1 Scenario Generation . . . 123
A.1.1 Defining the Operating Scenario set: Discussion on the Decision on the Minimum Number of Scenarios to Represent the Uncertainty . . . 124
A.2 Benders Decomposition . . . 127
A.2.1 Master problem . . . 127
A.2.2 Sub-problems . . . 127

Bibliography **139**

Curriculum Vitae **141**

List of Figures

2.1 The piecewise linear approximation of a quadratic function. 18
2.2 Classic two-port Π model of a transmission line adopted for the formulation of the OPF relaxed constraints. Adapted from [1]. 19
2.3 The full algorithm of the proposed planning strategy. 25
2.4 Considered real 55 node distribution network. 28
2.5 Prosumption prediction, dispatch plan and active power through the GCP in each scenario (sc): (a) Case 0 (No ESS), (b) Case 1 (With ESS integrated with offset profile), (c) Case 2 (With ESS and without offset profile). 31
2.6 Normalized error in longitudinal current (%) with respect to PWL-OPF models with different discretization step numbers. 32

3.1 Full algorithm of the proposed method. 43
3.2 The full algorithm: (a) Ch. 2, (b) this chapter. 44
3.3 Considered real 55 bus distribution network. 50
3.4 Prosumption prediction, dispatch plan and active power through GCP in each scenario (not labeled for the sake of readability): (a) Day 1(No ESS), (b) Day 1(With ESS (Imbalance price : \$897/MWh)). 53
3.5 Error in longitudinal current (A). 55

4.1 Solution algorithm overview of the proposed method. 62
4.2 Detailed structure of the 2nd block problem. 63
4.3 The resistance model of lossy ESS adopted from [2]. 69
4.4 Fitting of line parameters as function of ampacity. Line data adapted from MV cable and overhead line manufactures. 73
4.5 ADN topology used for the joint ESS allocation and line reinforcement. 75
4.6 (a) Energy reservoir (kWh), (b) Power rating (kVA). 76
4.7 Dispatch result of Day 1: (a) Aggregated prosumption scenarios and prosumption prediction, (b) Power flow through GCP of scenarios, prosumption prediction and dispatch plan (Imbalance price : \$897/MWh). 77
4.8 (a) Topology with ESS allocation and line reinforcement, (b) ESS allocation (2nd block problem), (c) Line reinforcement (2nd block problem). 78
4.9 Obtained optimal cost value of (a) First block problem, (b) Second block problem. 79

4.10 Convergence of Benders decompostion: (a) Approach 1, (b) siting sub-stage (Approach 2), (c) sizing sub-stage (Approach 2). 80
4.11 (a) Average computation time per Benders iteration (BI) for distribution networks with different sizes, (b) Total computation time for distribution networks with different sizes. 82

5.1 Full algorithm of the proposed method. 91
5.2 Full structure of the 2nd block problem. 92
5.3 Flow chart of the simultaneous approach. 100
5.4 Network topology with: (a) candidate nodes for ESS allocation and new nodes, (b) with line candidates, (c) with ESSs, new lines and line reinforcement. 112
5.5 Example of dispatch result for Day-type 4, year 10: (a) aggregated prosumption scenarios and prosumption prediction, (b) power flow through GCP of scenarios, prosumption prediction and dispatch plan (DP). 113
5.6 The 1st block cost result. 113
5.7 Computation time with different number of candidates. 115
5.8 (a) CDF of initial scenario set and reduced scenario sets with different number of reduced scenarios regarding the value of a single random variable (PV irradiation value at timestep 75, day-type 1, and year 1), (b) Boxplot of objective values of planning problem with different number of prosumption scenarios. 118

A.1 (a) CDF of initial scenario set and reduced scenario sets with different number of reduced scenarios, (b) Average of normalized distance between initial and reduced scenario sets with different number of reduced scenarios 126

List of Tables

2.1 ESS main parameters and candidate nodes for simulation 28
2.2 ESS allocation results of PWL-OPF based ESS planning strategies with offset profile (Case 1) and without (Case 2). 29
2.3 Cost and Operational advantage comparison of PWL-OPF based ESS planning strategies with offset profile (Case 1) and without (Case 2). 30
2.4 Comparison on accuracy of longitudinal current calculation with respect to PWL-OPF models with different discretization step numbers. 32

3.1 Imbalance prices for ESS allocation. 50
3.2 ESS allocation result for Case 1 (original ampacity) and Case 2 (reduced ampacity). 51
3.3 Comparison between the result of 1st block and 2nd block for Case 1 (original ampacity) and Case 2 (reduced ampacity). 51
3.4 ESS allocation results with different imbalance prices. 52
3.5 Planning cost and Operational benefits with differnt imbalance prices. 52
3.6 ESS allocation result with different initial SoE levels. 53
3.7 Cost and Operational benefits with different initial SoE levels. 54
3.8 Comparison on accuracy of longitudinal current calculation with respect to different OPF models. 55
3.9 ESS allocation result using AR-OPF and R-OPF model. 56
3.10 Cost and Operational benefits using AR-OPF and R-OPF models. 56
3.11 Error in longitudinal line current (A) of AR-OPF and R-OPF models. 56

4.1 Parameters related to line reinforcement. 72
4.2 The investment solutions of Strategy 1 and 2 in the case of 500 % PV capacity. . 74
4.3 The planning cost of Strategy 1 and 2 in the case of 500 % PV capacity. 75
4.4 The planning results comparison (Approach 1 vs. Approach 2). 80
4.5 Total computation times and number of Benders iteration for distribution networks with different sizes. 81

5.1 Investment solutions with the sequential approach and the simultaneous approaches (AR-OPF and R-OPF) 108
5.2 Objective values and the computation times with the sequential approach and the simultaneous approaches (AR-OPF and R-OPF models). 108

5.3 Investment solutions with sequential approach and simultaneous approaches (10 new nodes). 109
5.4 Objective values and the computation times with sequential approach and simultaneous approaches (10 new nodes). 110
5.5 Parameters related to line investment. 110
5.6 Investment result 111
5.7 Planning cost and Operational benefits. 113
5.8 Computation time (sec) for the expansion planning with the sequential approach. 114
5.9 Computation time (hours) with various number of candidates (28-node system). 115
5.10 Computation time (sec) of the 2nd block with respect to system size. 116
5.11 Post analysis with respect to different number of scenarios (tested on 13-node system, 4 day-types, 24 timesteps, 2 ESS node candidates, 1 new line candidate). 117

Nomenclature

Abbreviation

ADN	Active Distribution Network
AR-OPF	Augement Releaxed Optimal Power Flow
CDF	Cumulative Distribution Function
DER	Distributed Energy Resources
DG	Distributed Generation
DNEP	Distribution Network Expansion Planning
DSO	Distribution System Operator
ESS	Energy Storage System
GCP	Grid Connection Point
LDER	Leftover Dispatch Error Rate
MAR-OPF	Modified Augement Releaxed Optimal Power Flow
MILP	Mixed Integer Linear Programming
MISOCP	Mixed Integer Second Order Cone Programming
MP	Master Problem
MV	Medium Voltage
OPF	Optimal Power Flow
PSO	Particle Swarm Optimization
PV	Photovoltaic
PWL	Piecewise Linearization
PWL-OPF	Piecewise Linearization Optimal Power Flow
R-OPF	Relaxed Optimal Power Flow
RER	Renewable Energy Resources
SOCP	Second Order Cone Programming
SP	Subproblem
TSO	Transmission System Operator

Notation

$(.)^*$	Optimal value of $(.)$
$\mathscr{R}(.)$	Real part of $(.)$
j	Imaginary unit
$up(.)$	Node connected upstream to node $(.)$

Chapter 2

Sets and Indices

$l, up(l) \in \mathscr{L}$	Index and set of nodes
$t \in \mathscr{T}$	Index and set of time steps
$\phi \in \Phi_{dy}$	Index and set of scenarios for day d and year y
$d \in \mathscr{D}$	Index and set of day-types
$y \in \mathscr{Y}$	Index and set of years
$\beta \in \mathscr{B}$	Index and set of benders iterations
$v \in \mathscr{U}$	Index and set of discretization steps for piecewise linearization

Variables

$U \in \{0,1\}$	Installation status of the ESS
C	Energy reservoir of the ESS
R	Power rating of the ESS
$\tilde{p}$	Prosumption prediction (Average of the active prosumption over all scenarios)
Δp	Deviation of prosumption scenario from the prosumption prediction ($\tilde{p}$)
$\tilde{f}$	Average of squared longitudinal line current over all scenarios
Δf	Deviation of squared longitudinal line current from $\tilde{f}$
DP	Dispatch plan at the GCP
F^E	Offset profile for the ESS
ω	Compensated amount of prosumption deviation by the ESSs
ϵ	Uncovered dispatch error
f	Squared longitudinal line current
v	Squared nodal voltage magnitude
$s=p+jq$	Nodal prosumption
$S^t=P^t+jQ^t$	Complex power flow to a line from its upstream node
$S^b=P^b+jQ^b$	Complex power flow from a line to its downstream node
$s^E=p^E+jq^E$	Complex power flow of ESS
I^b	Squared line current magnitude at a line's downstream node
I^t	Squared line current magnitude at a line's upstream node
E^E	State-of-energy of ESS
Δ_v^y	vth discretization steps used for piecewise linearzing y^2
IC_E	ESS investment cost
TC	Total planning cost
OC	Operation cost
MC	Master problem cost
SC	Subproblem cost
UB	Upper-bound of total planning cost
LB	Lower-bound of total planning cost
α	Proxy subproblem costs

$\Gamma^{(\beta)}$	Benders cut accumulated at βth Benders iteration
μ/ϑ	Dual values linked to constraints in subproblem fixing the value of ESS power rating/energy reservoir replicate variable to the power rating/energy reservoir solution of previous master problem

Parameters

Υ	Number of discretization steps in the piecewise linear approximation function
θ_v^y	Slope of the v-th slope in the discretization of y
$\bar{y}$	Maximum value of y
T	Time horizon of the daily OPF problem
Δt	Time duration of dispatch interval
$\lambda_{\phi d}$	Probability of scenario ϕ on day d
N_{dy}	Number of days in day-type d in year y
Y	ESS planning horizon
r_{dis}	Discount rate
$\mathbf{H}$	Adjacency matrix
b	Half of the total line shunt susceptance
$z = r + jx$	Total longitudinal line impedance
I^{max}	Upper limit on the line current
P^{max}, Q^{max}	Maximum value of active and reacitve line power flows
v^{max}/v^{min}	Upper-bounds/lower-bounds of the squared nodal voltage magnitude
ic_E^f, ic_E^e, ic_E^p	Investment cost parameter for ESS installation, energy reservoir, power rating
C^{max}/C^{min}	Maximum/minimum ESS energy reservoir
R^{max}/R^{min}	Maximum/minimum possible ESS power rating capacity
CR^{max}	Maximum power ramping rate of ESS
$\boldsymbol{\alpha}, \boldsymbol{\beta}, \boldsymbol{\kappa}$	Vectors defining the slope and the intercepts, respectively, of the set of lines which approximate the power capability curve of ESS
SoE_{ini}	Initial level of ESS state-of-energy level
SoE^{min}/SoE^{max}	Minimum/maximum allowed state-of-energy level
Δ_{ini}^{fin}	Maximum difference between the final and initial state-of-energy level with respect to the ESS energy reservoir capacity
N_c	Allowed number of cycles per day chosen as a function of the targeted ESS lifetime
w_l, w_f, w_e	Weight coefficients for the grid losses, offset profile, and dispatch error
$\underline{\alpha}$	Lower-bound of proxy subproblem cost

Functions

$f(y, \bar{y}, \Upsilon)$	Piecewise linearization function of y^2 for PWL-OPF model

Chapter 3

Sets and Indices

$l, up(l) \in \mathscr{L}$	Index and set of nodes
$t \in \mathscr{T}$	Index and set of time steps
$\phi \in \Phi_{dy}$	Index and set of scenarios for day d and year y
$d \in \mathscr{D}$	Index and set of day-types
$y \in \mathscr{Y}$	Index and set of years
$\beta \in \mathscr{B}$	Index and set of benders iterations
$m \in \mathscr{M}$	Index and set of solving iteration number of subproblem of 2nd block problem

Variables

$\tilde{p}$	Prosumption prediction (Average of the active prosumption over all scenarios)
Δp	Deviation of prosumption scenario from the prosumption prediction ($\tilde{p}$)
$\tilde{f}$	Average of squared longitudinal line current over all scenarios
Δf	Deviation of squared longitudinal line current from $\tilde{f}$
DP	Dispatch plan at the GCP
ϵ	Uncovered dispatch error
θ	Leftover dispatch error rate of prosumption scenario
f	Squared longitudinal line current
$\bar{f}$	Auxiliary upper-bound variable of square of longitudinal current
v	Squared nodal voltage magnitude
$\bar{v}$	Auxiliary upper-bound variable of square of nodal voltage magnitude
$s=p+jq$	Nodal prosumption
$S^t=P^t+jQ^t$	Complex power flow to a line from its upstream node
$S^b=P^b+jQ^b$	Complex power flow from a line to its downstream node
$\bar{S}^t = \bar{P}^t+j\bar{Q}^t$	Upper-bound variable for complex power flow to a line from its upstream node
$\hat{S}^t = \hat{P}^t+j\hat{Q}^t$	Lower-bound variable for complex power flow to a line from its upstream node
$\bar{S}^b = \bar{P}^b+jQ^b$	Upper-bound variable for complex power flow from a line to its downstream node
$\hat{S}^b = \hat{P}^b+j\hat{Q}^b$	Lower-bound variable for complex power flow from a line to its downstream node
$s^E=p^E+jq^E$	Complex power flow of ESS
$s'=p'+jq'$	Complex nodal prosumption excluding the unserved load
I^b	Squared line current magnitude at a line's downstream node
I^t	Squared line current magnitude at a line's upstream node

E^E	State-of-energy of ESS
up^+/up^-	Positive/negative unserved active prosumption
uq^+/uq^-	Positive/negative unserved reactive prosumption
γ	Slack variable for the realized losses deviation
ζ	Slack variable for the additional realization of losses deviation
C	ESS energy reservoir
R	ESS power rating
μ/ϑ	Dual values linked to constraints in subproblem fixing the value of ESS power rating/energy reservoir replicate variable to the power rating/energy reservoir solution of previous master problem
$\Gamma^{(\beta)}$	Benders cut accumulated at βth Benders iteration
MC	Master problem cost
SC	Subproblem cost
IC^E	ESS investment cost
UB	Upper-bound of total planning cost
LB	Lower-bound of total planning cost

Parameters

$\lambda_{\phi d}$	Probability of scenario ϕ on day d
N_{dy}	Number of days in day-type d in year y
Y	ESS planning horizon
r_{dis}	Discount rate
$\mathbf{H}$	Adjacency matrix
b	Half of the total line shunt susceptance
$z = r + jx$	Total longitudinal line impedance
I^{max}	Upper limit on the line current
P^{max}, Q^{max}	Maximum value of active and reacitve line power flows
v^{max}/v^{min}	Upper bounds/Lower bounds of the squared nodal voltage magnitude
w_d	Weight coefficients for the dispatch error
w, w_u	Weight coefficients for the grid losses and unserved energy

Chapter 4

Sets and Indices

$l, up(l) \in \mathscr{L}$	Index and set of nodes
$\mathscr{L}^E$	Set of virtual buses connected to the real ESS candidate buses and set of virtual lines connected upstream to the virtual buses
$t \in \mathscr{T}$	Index and set of time steps
$\phi \in \Phi_{dy}$	Index and set of scenarios for day d and year y
$d \in \mathscr{D}$	Index and set of day-types
$y \in \mathscr{Y}$	Index and set of years
$m \in \mathscr{M}_1/\mathscr{M}_2$	Index and set of solving iteration number of the siting/sizing stage sub-problem of 2nd block problem
$\beta \in \mathscr{B}_1/\mathscr{B}_2$	Index and set of Benders iteration number of the siting/sizing stage of 2nd block problem
$v \in \mathscr{U}$	Index and set of discretization steps for piecewise linearization

Variables

U	Installation status of the ESS
C	Energy reservoir of the ESS
R	Power rating of the ESS
X	Reinforcement investment status of existing line
A	Updated ampacity of line
ΔA	Change in ampacity of line
IC	Total investment cost
IC	Investment cost of line reinforcement
IC_b	Investment cost associated with binary investment decisions
IC_c	Investment cost associated with continuous investment decisions
MC^1/MC^2	Master problem cost of siting/sizing of 2nd block problem
SC^1/SC^2	Subproblem cost of siting/sizing of 2nd block problem
UB_1/UB_2	Upper-bound of planning cost of siting/sizing stage
LB_1/LB_2	Lower-bound of total planning cost of siting/sizing stage
$\alpha^{1st}/\alpha^{2nd}$	Proxy subproblem costs of siting/sizing stage problem
τ	Dual values linked to constraints in subproblem fixing the value of ESS location status replicate variable to the ESS location solution of previous master problem
χ	Dual values linked to constraints in subproblem fixing the value of line investment status replicate variable to the line investment solution of previous master problem
$\Gamma 1/\Gamma 2$	Benders cut for siting/sizing sub-stage of 2nd block problem
$\tilde{p}$	Prosumption prediction (Average of the active prosumption over all scenarios)

Δp	Deviation of prosumption scenario from the prosumption prediction ($\tilde{p}$)
$\tilde{f}$	Average of squared longitudinal line current over all scenarios
Δf	Deviation of squared longitudinal line current from $\tilde{f}$
ϵ	Uncovered dispatch error
θ	Leftover dispatch error rate of prosumption scenario
f	Squared longitudinal line current
$\bar{f}$	Auxiliary upper-bound variable of square of longitudinal current
v	Squared nodal voltage magnitude
$\bar{v}$	Auxiliary upper-bound variable of square of nodal voltage magnitude
$s=p+jq$	Nodal prosumption
$S^t=P^t+jQ^t$	Complex power flow to a line from its upstream node
$S^b=P^b+jQ^b$	Complex power flow from a line to its downstream node
$\bar{S}^t=\bar{P}^t+j\bar{Q}^t$	Upper-bound variable for complex power flow to a line from its upstream node
$\hat{S}^t=\hat{P}^t+j\hat{Q}^t$	Lower-bound variable for complex power flow to a line from its upstream node
$\bar{S}^b=\bar{P}^b+jQ^b$	Upper-bound variable for complex power flow from a line to its downstream node
$\hat{S}^b=\hat{P}^b+j\hat{Q}^b$	Lower-bound variable for complex power flow from a line to its downstream node
$s^E=p^E+jq^E$	Complex power flow of ESS
$s'=p'+jq'$	Complex nodal prosumption excluding the unserved load
I^b	Squared line current magnitude at a line's downstream node
I^t	Squared line current magnitude at a line's upstream node
E^E	State-of-energy of ESS
up^+/up^-	Positive/negative unserved active prosumption
uq^+/uq^-	Positive/negative unserved reactive prosumption
γ	Slack variable for the realized losses deviation
ζ	Slack variable for the additional realization of losses deviation
μ/ϑ	Dual values linked to constraints in subproblem fixing the value of ESS power rating/energy reservoir replicate variable to the power rating/energy reservoir solution of previous master problem
ι	Dual values linked to constraints in subproblem fixing the value of line ampacity replicate variable to the line ampacity solution of previous master problem

Parameters

ic_E^f, ic_E^e, ic_E^p	Investment cost parameter for ESS installation, energy reservoir, power rating
ic^r	Fixed cost parameter for line reinforcement of line
C^{max}/C^{min}	Maximum/minimum ESS energy reservoir
R^{max}/R^{min}	Maximum/minimum possible ESS power rating capacity
CR^{max}	Maximum power ramping rate of ESS
A^{max}/A^{min}	Maximum/minimum possible ampacity of line conductor
ΔA^{max}	Maximum possible change in ampacity of line conductor
$\delta_2, \delta_1, \delta_0$	Coefficient for quadratic, linear, constant term of line conductor cost function with respect to line ampacity, respectively
ρ	Line length
$\underline{\alpha}^{1st}/\underline{\alpha}^{2nd}$	Lower-bound of proxy subproblem cost in siting/sizing stage
$\lambda_{\phi d}$	Probability of scenario ϕ on day d
N_{dy}	Number of days in day-type d in year y
Y	ESS planning horizon
r_{dis}	Discount rate
$\mathbf{H}$	Adjacency matrix
b	Half of the total line shunt susceptance
$z = r + jx$	Total longitudinal line impedance
I^{max}	Upper limit on the line current
v^{max}	Upper-bound of the squared nodal voltage magnitude
w_l, w_u	Weight coefficients for the grid losses and unserved energy, respectively
a_v, b_v	Slope and y-intersept of piecewise linearized functions of squared line ampacity
Υ	Number of discretization steps for PWL of squared line ampacity

Functions

$L(A^2)$	Piecewise linearization of squared line ampacity

Chapter 5

Sets and Indices

$i \in \mathcal{N}$	Index and set of nodes in the (expanded) grid
$n' \in \mathcal{N}'$	Index and set of new nodes to be added to the grid
$k \in \mathcal{K}(n')$	Index and set of candidate lines for connecting new node n'
$l \in \mathcal{L}$	Index and set of line and the node indices connected downstream
$j \in \mathcal{J}$	Index and set of lines within the union set of existing lines and candidate lines
$D \in \mathcal{D}^*$	Index and set of unique solutions of new lines determined for different day-types
$\mathcal{L}^E$	Set of virtual buses connected to the real ESS candidate buses and set of virtual lines connected upstream to the virtual buses
$t \in \mathcal{T}$	Index and set of time steps
$\phi \in \Phi_{dy}$	Index and set of scenarios for day d and year y
$d \in \mathcal{D}$	Index and set of day-types
$y \in \mathcal{Y}$	Index and set of years
$m \in \mathcal{M}_1/\mathcal{M}_2$	Index and set of solving iteration number of the siting/sizing stage sub-problem of 2nd block problem
$\beta \in \mathcal{B}_1/\mathcal{B}_2$	Index and set of Benders iteration number of the siting/sizing stage of 2nd block problem
$v \in \mathcal{U}$	Index and set of discretization steps for piecewise linearization

Variables

U	Installation status of the ESS
C	Energy reservoir of the ESS
R	Power rating of the ESS
X	Reinforcement investment status of existing line
X'	Installation investment status of new line candidate
A	Updated ampacity of existing line
A'	Ampacity of new line
ΔA	Change in ampacity of line
IC	Total investment cost
IC_E	ESS investment cost
Π	Investment status of existing lines and the candidate routes represented by binary variables
Ψ	Connection status of existing lines and the candidate routes
A''	Line ampacities of existing lines and the cadidate routes
θ	Leftover dispatch error rate of prosumption scenario
f	Squared longitudinal line current
$\bar{f}$	Auxiliary upper-bound variable of square of longitudinal current

v	Squared nodal voltage magnitude
$\bar{v}$	Auxiliary upper-bound variable of square of nodal voltage magnitude
$s=p+jq$	Nodal prosumption
$S^t=P^t+jQ^t$	Complex power flow to a line from its upstream node
$S^b=P^b+jQ^b$	Complex power flow from a line to its downstream node
$\bar{S}^t=\bar{P}^t+j\bar{Q}^t$	Upper-bound variable for complex power flow to a line from its upstream node
$\hat{S}^t=\hat{P}^t+j\hat{Q}^t$	Lower-bound variable for complex power flow to a line from its upstream node
$\bar{S}^b=\bar{P}^b+jQ^b$	Upper-bound variable for complex power flow from a line to its downstream node
$\hat{S}^b=\hat{P}^b+j\hat{Q}^b$	Lower-bound variable for complex power flow from a line to its downstream node
$s^E=p^E+jq^E$	Complex power flow of ESS
$s'=p'+jq'$	Complex nodal prosumption excluding the unserved load
I^b	Squared line current magnitude at a line's downstream node
I^t	Squared line current magnitude at a line's upstream node
up^+/up^-	Positive/negative unserved active prosumption
uq^+/uq^-	Positive/negative unserved reactive prosumption
ζ	Slack variable for the additional realization of losses deviation
MC^1/MC^2	Master problem cost of siting/sizing of 2nd block problem
SC^1/SC^2	Subproblem cost of siting/sizing of 2nd block problem
UB_1/UB_2	Upper-bound of planning cost of siting/sizing stage
LB_1/LB_2	Lower-bound of total planning cost of siting/sizing stage
$\alpha^{1st}/\alpha^{2nd}$	Proxy subproblem costs of siting/sizing stage problem
$\Gamma 1/\Gamma 2$	Benders cut for siting/sizing sub-stage of 2nd block problem
τ	Dual values linked to constraints in subproblem fixing the value of ESS location status replicate variable to the ESS location solution of previous master problem
χ	Dual values linked to constraints in subproblem fixing the value of line investment status replicate variable to the line investment solution of previous master problem
TP	Total planning cost with the network topology
$\bar{vv}, vv$	Auxiliary variables representing nodal voltage linked to the new line candidates
SC^{MISOCP}	MISOCP subproblem cost of 2nd block problem
μ/ϑ	Dual values linked to constraints in subproblem fixing the value of ESS power rating/energy reservoir replicate variable to the power rating/energy reservoir solution of previous master problem
ι	Dual values linked to constraints in subproblem fixing the value of line ampacity replicate variable to the line ampacity solution of previous master problem

Parameters

L	Number of (connected) lines in the (expanded) grid
N'	Number of new nodes
N	Number of nodes in the (expanded) grid
K	Number of line candidates for connecting the new node
ic_E^f, ic_E^e, ic_E^p	Investment cost parameter for ESS installation, energy reservoir, power rating
ic^r	Fixed cost parameter for line reinforcement of line
ic^c	Fixed cost parameter for new line candidate
$\delta_2, \delta_1, \delta_0$	Coefficient for quadratic, linear, constant term of line conductor cost function with respect to line ampacity, respectively
ρ	Line length
M	Big number used for the big-M method
$\mathbf{H}$	Adjacency matrix
b	Half of the total line shunt susceptance
$z = r + jx$	Total longitudinal line impedance
I^{max}	Upper limit on the line current
v^{max}	Upper-bound of the squared nodal voltage magnitude
$\underline{\alpha}^{1st}/\underline{\alpha}^{2nd}$	Lower-bound of proxy subproblem cost in siting/sizing stage
A^{max}/A^{min}	Maximum/minimum possible ampacity of line conductor
ΔA^{max}	Maximum possible change in ampacity of line conductor
$\lambda_{\phi d}$	Probability of scenario ϕ on day d
N_{dy}	Number of days in day-type d in year y
Y	ESS planning horizon
r_{dis}	Discount rate
w_l, w_u	Weight coefficients for the grid losses and unserved energy, respectively
C^{max}/C^{min}	Maximum/minimum ESS energy reservoir
R^{max}/R^{min}	Maximum/minimum possible ESS power rating capacity
CR^{max}	Maximum power ramping rate of ESS
a_v, b_v	Slope and y-intersept of piecewise linearized functions of squared line ampacity
Υ	Number of discretization steps for PWL of squared line ampacity

Functions

$L(A^2)$	Piecewise linearization of squared line ampacity

1 Introduction

In the last two decades, the penetration of distributed generation (DG) units has largely increased in distribution networks. Among DG units, the share of distributed renewable energy resources (RER) is notably rising, and this trend will only accelerate due to the global decarbonization objectives for the electricity production. However, the inherent stochastic nature of RERs poses operational issues for the power distribution and transmission networks. On the one hand, it increases power imbalances at the transmission level. On the other hand, it is causing grid constraint violations (such as nodal voltage violations and lines/transformer congestions) at the distribution level. Therefore, achieving the direct controllability of networks is essential for distribution system operators (DSOs) to incorporate RERs [3] seamlessly. This fact is aided by developments in energy technologies such as energy storage systems (ESSs) and information and communication technologies (ICTs), bringing to reality the possibility of efficient control and coordination of heterogeneous energy resources [4]. The mentioned technical advancement increases the potential of distribution networks transitioning from passive to active distribution networks (ADNs) [5].

In this context, it is worth recalling that ADNs are defined as *"distribution networks that have systems in place to control a combination of distributed energy resources (DERs) (*i.e.*, DG, controllable loads or ESSs.)"* [6]. The changes in distribution networks is tightly coupled within the evolving role of DSOs. The advent of various DERs requires DSOs to be provided with more network observability and controllability, causing them to adopt the concept of ADNs. DSOs should be capable of actively managing power flows of ADNs by exploiting DERs and/or a flexible network topology. This enables DSOs to gain more system flexibility, not only for managing the ADN in a safe and reliable manner, but also to provide other ancillary services to transmission networks, such as balancing, frequency control, voltage support, etc [7]. In this respect, the active management of network and DERs strengthen the coupling of operation and planning of the systems. For instance, DERs dramatically alter the net-load prediction as well as the peak load profiles, which is an essential factor driving network reinforcement. In this context, the suitability of current distribution network planning procedures for ADNs should be assessed in view of such developments.

Traditional planning schemes used deterministic approaches mainly based on worst-case

scenarios of power system operation such as: peak load profiles, worst-case voltage drops, and contingency-based security constraints [6, 8]. These approaches when applied to distribution networks planning to accommodate a large number of RERs, result in large sub-optimal costs. In this regard, traditional planning approaches are an impediment to increase the DERs penetration, which calls for a radical transition in distribution networks planning strategies.

The required key changes for developing a modern planning strategy in distribution networks are linked with the followings: data modeling; network operation assessment; planning options; and planning objectives [9]. In contrast to the traditional planning strategy, time-series models of load profiles and generations should be considered for better analysis of temporal interactions between DERs and resulting system operating condition. Moreover, the operating condition of the ADN should be assessed probabilistically to properly take into account the various uncertainties associated to DERs. The active operation of DSOs starts from allocating controllable infrastructures within the network, preferably embedding the control schemes to maximize the usage of existing and newly allocated assets for operational purposes. Therefore, the modern planning methodology should provide both network and non-network solutions (ex., allocation of DERs) as planning choices, while taking into account DSOs' various operational objectives that the candidate solutions can distinctively support. In this way, the DSO can identify the optimal decision between the traditional infrastructure investment versus other technologies.

The aforementioned requirements for the modern ADN planning raised the interest of researchers and power industry, prompting the development of several planning models and approaches to address the features discussed above and to tackle resulting complexities of ADN planning decision-making processes.

Numerous studies suggest ADN planning strategies to incorporate active management schemes that can tackle the technical challenges introduced by various DERs integration such as degraded voltage quality, and binding hosting capacity [10, 11]. Furthermore, economic risks associated with DERs, such as financial penalties associated with significant imbalances, load-shedding or generation curtailment, can be avoided and even converted into economic gains with the right use of active management schemes [12, 13]. The corresponding active management approaches include network reconfiguration [14], dispatch of DERs such as DGs, ESSs, demand response (DR) [15]. Especially, the optimal allocation of DGs has become an essential candidate for ADN planning solutions thanks to their benefits such as satisfying the peak load [16], network reinforcement deferral [17], reduction of grid losses [18] and ensuring the system reliability [19]. Another notable finding in recent studies is that the optimal ESS allocation is widely integrated in the ADN planning strategies, in order to benefit from ESSs' versatile services, such as peak load shaving [20], voltage control [21], improvement of power quality [22] and reliability [20], deferral of network reinforcement via management of line congestion [23]. It is noteworthy that a variety of operational purposes were modeled in the planning framework to mitigate the aforementioned technological challenges, such that the ADN planning strategies were formulated as multi-objective optimization problems [12, 14, 20].

The optimal utilization of the allocated active components through active management schemes, certainly affect the ADN planning. By acknowledging such coupling between the operation and planning, many of above-mentioned studies developed simultaneous optimization schemes integrating both planning and operation [10, 11, 13, 14, 20–22], in order to evaluate the operational benefits of active management schemes and ultimately their impact on planning solutions. In this regard, the operation models were incorporated into the planning problems, constructing *operation-aware planning strategies*.

Finally, the ADN operation can be largely affected by the high uncertainty levels from a variety of sources, such as loads demand, RERs, and power market. Not only the uncertainty from each source may cause economical and technical issues to DSOs, but also the uncertainties can collectively exacerbate their influence to the system operation.

In this regard, some studies considered the uncertainties by formulating robust optimization planning frameworks for risk aversion [24]. To avoid unnecessary over-investment, others developed stochastic optimization planning strategies [10, 11, 14] to obtain cost-effective investment solutions considering accepted risk of network constraint violation in extreme cases. In many studies, the stochastic planning problem was discretely approximated by representing the distribution of the prosumption with a set of scenarios to improve computational efficiency [11, 14].

1.1 Motivation of the Thesis

It is becoming more crucial for transmission system operators (TSOs) and DSOs to have a right strategy to tackle issues originated from the continuous displacement of conventional centralized power plants towards DGs mainly composed by RERs. The stochasticity of RERs may causes risks in ADNs operating conditions such as power supply degradation in terms of voltage quality, grid reliability, etc. At transmission level, the security of the power system has been traditionally sustained by central procurement of regulating power from fast generating units. However, the growing uncertainty associated to power generation of stochastic resources calls for higher expenses for the procurement of conventional reserve. Meanwhile, as investments in traditional large power plants decline, so does the provision of ancillary services from bulk power plants. Such system inflexibility increases the risk of frequent extreme price occurrences in power markets [25] and overall rise in system operation costs to manage system imbalances. It is needless to mention that the system uncertainty increased by RERs integration will exacerbate such operational risks. Furthermore, the increased stress placed on the power system would necessitate huge expenditures in grid strengthening to preserve the reliability and quality of electricity supply.

In order to prevent the above-mentioned imminent challenges, procurement of flexibility within the grid is being identified as a promising resolution for the aforementioned issues. *Flexibility* can be defined as *"the ability of the system components to adjust their operating point, in timely and harmonized manner, to accommodate expected, as well as unexpected, changes in system operating conditions"* [26].

In this respect, the recent literature has advocated the provision of flexibility from ADNs through actively managing DERs and enhancing the controllability of ADNs, not only for the sake of ensuring the reliable ADNs operation, but also for providing the flexibility to the upper-grid [27]. In particular, there has been growing interest in using ESSs in ADNs to compensate for the uncertainty of non-dispatchable local resources (e.g., [28, 29]), hence attaining the dispatchability of ADNs. The term *dispatchability* refers to a controllability of a resource such that the resource's realized active power output adheres to a pre-defined set-point with high accuracy. By analogy, the *dispatchability of an ADN* signifies the capability of the ADN active power flow through the grid connecting point (GCP) with the transmission network to strictly follow a day-ahead power schedule [30]. Efforts have been made to achieve *dispatchability* of the ADNs in view of the inherent advantages such as reduction of the bulk system reserve provision [31] and mitigation of the imbalance penalty charges imposed on DSOs [30, 32].

This thesis focuses on the optimal planning for ADNs with a particular reference to the provision of the local flexibility via ESS allocation that can enhance the reliability of the distribution network operation and achieve ADN's dispatchability in presence of uncertainty of renewable generation. [1] Moreover, grid reinforcement and expansion planning schemes are jointly developed along with the ESS allocation to appropriately and effectively account for the full interaction between the flexible resources and the network operation condition. The ultimate goal of the thesis is to provide a powerful planning tool to DSOs to determine the optimal strategies to enhance the operation of ADN infrastructures.

1.2 Objectives and Contributions of the Thesis

This thesis aims to address the challenges regarding the planning of ADNs with particular reference to their dispatchability supported by ESSs. In this context, an operation-aware ESS allocation strategy employing both exact and approximated optimal power flow (OPF) models is proposed to achieve an optimal level of dispatchability in ADNs. Then, the co-optimized planning of the ESS allocation and the line reinforcement is developed to ensure adequate renewable energy hosting capacity. Finally, a distribution network expansion planning (DNEP) strategy is proposed to integrate new customers into the system while achieving a sufficient level of dispatchability. In the following section, the main contributions of the thesis are elaborated based on the issues detailed in the Introduction.

Optimal Planning of ESSs in ADNs to Achieve ADNs Dispatchability

Introduction of ADNs dispatchability by means of OPF models

The thesis first introduces the concept of ADN's dispatchability by using the OPF model. A piece-wise linear approximation is applied to the OPF model to convexify the full AC-OPF problem while taking into account the nodal voltage and line ampacity constraints. Moreover, the ESSs control strategy is embedded in the OPF model to maximize the exploitation of these assets.

[1] Note that in this thesis we consider the prosumption uncertainty as the only source of system uncertainties. However, there can be other sources of uncertainty, for instance, uncertainty in imbalance price. Consideration of the market uncertainty can be explored in future works.

Development of a stochastic optimization model for ESS planning considering achieving dispatchability of ADN

A scenario-based stochastic two-stage optimization problem is developed for the optimal siting and sizing of ESSs in ADNs to achieve their dispatchability while considering the uncertainty and seasonal variability of prosumption. The Benders decomposition technique is utilized to derive a computationally-tractable formulation of a scenario-based operation-aware planning problem.

Optimal Planning of Energy Storage Systems based on an Exact Convexified OPF model

An operation-driven planning strategy of ESS is proposed to achieve the dispatchability of the ADN based on the non-approximated, convexified AC-OPF model or the Augmented Relaxed Optimal Power Flow (AR-OPF) model. Achieving the ADN disatchability requires a substantial and non-trivial modification of the AR-OPF model, resulting in the so-called modified AR-OPF (MAR-OPF) model and the development of a solution approach to reach the exactness of the OPF model. In this regard, we formulated the planning problem in two blocks by modifying the objective term, constraints, and variables related to the dispatch error. Meanwhile, we apply the Benders decomposition to handle the multi-layered decisions with numerous scenarios.

Optimal Co-planning of ESS and Line Reinforcement considering the ADN's Dispatchability

Inclusion of line reinforcement into the planning problem

A joint planning problem considering ESS allocation and line reinforcement is proposed to achieve ADNs dispatchability while ensuring sufficient hosting capacity for increasing stochastic prosumption. The line reinforcement investment is suitably modeled along with corresponding adjustments to the network admittance matrix and the grid constraints in order to be incorporated into the MAR-OPF model.

Decomposition of planning problem to facilitate the convergence to the optimal solution

The inclusion of numerous binary variables associated with line reinforcement investment necessitates the reformulation of the planning problem for the sake of improving the solution efficiency. The planning framework resulting from the proposed reformulation determines the siting and sizing of the investment assets sequentially, thereby accelerating the convergence of the Benders decomposition algorithm.

Expansion Planning of Active Distribution Networks Achieving their Dispatchability

Introduction of network expansion to the planning problem

The DNEP strategy is proposed to ensure sufficient hosting capacity and achieve ADNs dispatchability when integrating new stochastic RERs and demand. The new line investment is suitably modeled and introduced to planning options. The ESSs and lines investment decisions are optimized based on the accurate evaluation of the ADN operation via the MAR-

OPF model. The MAR-OPF model is appropriately converted by employing the Big-M method to consider the change of network topology and adjacency matrix associated with assets investment.

Development of solution approaches to tackle the computational complexity of the distribution network expansion planning problem

The computational burden of the DNEP problem is mitigated by employing two approaches: the sequential approach and the simultaneous approach. Both algorithms consist of siting and sizing sub-stages. In the sequential approach, the siting sub-stage sequentially integrates new nodes while determining lines for reinforcement and nodes for the ESS allocation, and the sizing sub-stage determines the capacity of lines and ESSs. On the other hand, in the simultaneous approach, the siting sub-stage's problem structure is transformed to simultaneously determine all of the new lines' installation.

1.3 Thesis Outline

The structure of the rest of the thesis dissertation is as follows.

Chater 2 begins with introducing the concept of ADNs' dispatchability. Then it presents a procedure for the optimal siting and sizing of ESSs in ADNs hosting a large amount of stochastic RERs. The optimization objective is to minimize the ADN's day-ahead computed dispatch error. The allocation of ESSs is determined while taking advantages from their operational features regarding the ADN's dispatchability. The proposed ESSs planning is defined by formulating, and solving, a scenario-based non-linear non-convex OPF. The OPF problem is converted to a piecewise linearized OPF (PWL-OPF). The ESSs control strategy is embedded to fully exploit the energy capacity of the ESSs. It is integrated within the PWL-OPF to achieve the ADN's dispatchability regarding all operating scenarios. The Benders decomposition technique is employed to tackle the computational complexity of the proposed planning problem. The problem is decomposed into two sub-ones: a master problem where the allocation of the ESSs is decided, and several subproblems where the dispatchability of ADN with the support of the allocated ESS is evaluated through the scenario-based OPF. The performance of the planning tool and the benefit of ESS control strategy are shown by numerical simulations conducted on a real ADN.

Chapter 3 presents a different method for the optimal siting and sizing of ESSs in ADNs to achieve their dispatchability. Compared to Ch. 2, the peculiarity of the method proposed in this chapter is that the proposed formulation relies on the AR-OPF model: it expresses a convex full AC-OPF, which is proven to provide a global optimal and exact solution in the case of radial power grids. The AR-OPF is coupled with the proposed ADN dispatching resulting in a two-level optimization problem. In the first block, the site and size of the ESSs are decided along with the level of dispatchability that the ADN can achieve. Then, in the second block, the adequacy of the ESS allocations and the feasibility of the grid operating points are verified over operating scenarios using the Benders decomposition technique.

Consequently, the optimal size and site of the ESSs are adjusted. To validate the proposed method, simulations are conducted on a real ADN hosting a large amount of Photovoltaic (PV) generation. Comparative analyses on the solution accuracy with planning tools employing other OPF models are also discussed.

Chapter 4 presents a method for the co-optimization of ESS allocation and line reinforcement in ADNs. The ADN operational objective is the same as the one adopted in Ch. 2 and Ch. 3. The proposed formulation relies on a modified formulation of the AR-OPF model where the changes of line characteristic are modeled and embedded into the AR-OPF model according to the line reinforcement investment decisions. To tackle the complexity and computational burden of the proposed planning problem, the Benders decomposition algorithm is used and, in order to enhance the convergence speed of the numerical solution of the proposed problem, the Benders decomposition has been suitably modified to determine the assets' site and size sequentially. To assess the performance of the proposed method, the planning simulations exercises are conducted with respect to varying PV capacity to assess the effectiveness of the co-optimization planning method.

Chapter 5 presents a combined framework for DNEP and ESS allocation in ADNs hosting large amount of PV generations and loads. The proposed DNEP ensures the reliable operation of the targeted ADN with the objective of achieving its dispatchability while minimizing grid losses by determining both the optimal grid expansion to connect new nodes and the reinforcement of existing lines. The DNEP problem's complexity is handled by employing two solution approaches: a sequential algorithm where new nodes are added sequentially following the priorities determined by the user while another approach optimizes simultaneously the investment of new lines. In both approaches, the siting and sizing problems associated with the ESSs and lines investment are solved separately to enhance the convergence speed of the Benders decomposition. Simulations are conducted to compare the two approaches in terms of solution optimality and computational efficiency.

Chapter 6 reviews the primary contributions of this research and looks ahead to potential future works.

2 Optimal Planning of Energy Storage Systems accounting for Active Distribution Networks' Dispatchability

2.1 Highlights

In this chapter, we first introduce the concept of ADNs' dispatchability. Then, we present an optimal procedure for the siting and sizing ESSs within ADNs hosting a large amount of stochastic distributed and uncontrollable RERs. The optimization objective is to minimize the ADN's day-ahead computed dispatch error. The allocation of ESSs is determined while taking advantage of their operational features regarding the ADN's dispatchability. The proposed ESSs planning is defined by formulating and solving a scenario-based non-linear, non-convex OPF. The OPF problem is converted to a PWL-OPF model. The ESS control strategy is employed to maximize their energy capacity exploitation and integrated within the PWL-OPF model to achieve the ADN's dispatchability regarding all operating scenarios. The Benders decomposition technique is employed to tackle the computational complexity of the proposed planning problem. The problem is decomposed into two sub-ones: a master problem where the allocation of the ESSs is decided, and subproblems where the dispatchability of the ADN via the control of the allocated ESSs is evaluated through a scenario-based OPF. To validate the proposed method, extensive simulations are conducted on a real Swiss network embedding significant PV generation.

This chapter presents the work published in:

Yi, Ji Hyun, Rachid Cherkaoui, and Mario Paolone. "Dispatch-aware planning of energy storage systems in active distribution network." ***Electric Power Systems Research*** **190 (2021): 106644**

2.2 Organization of the Chapter

The first part of the chapter is devoted to the background associated with the research motivation, followed by the literature review about the dispatchability of ADNs and the ESS allocation. The second part includes a description of the core elements of the planning methodology. Then, the concept of achieving ADN's dispatchability by embedding a suitable control of ESSs is introduced, along with the detailed formulation of the PWL-OPF model. The third part elaborates on the structure of the ESS allocation problem and how the large-

scale planning problem is decomposed by employing the Benders decomposition technique. The mathematical formulation of the decomposed problems is given. Finally, the proposed methodology is applied on a real Swiss distribution system.

2.3 State-of-the-art of ADN Operation Considering Prosumption Uncertainty

Power balancing is becoming an increasingly challenging task due to the growing volatility of electricity generation in power systems introduced by the high penetration of non-dispatchable and stochastic DERs. More specifically, in the distribution network, the *prosumption*[2] forecast uncertainties are originated not only from the load consumption but also from the distributed RERs, causing a significant amount of power deviations from the scheduled power exchange with the upper network. In this way, at the transmission level, the spinning reserve requirement is growing to tackle not only the peak demand but also the unpredictable system imbalances stemming from the stochastic prosumption. The significant cost increase of reserves is expected to mitigate the system imbalance through market balancing mechanisms.

The central management of system imbalance may exhibit limitations, and several studies have called for the necessity of modifying electricity market frameworks to encourage appropriate cooperation between TSOs and DSOs to handle the system imbalance [33]. Furthermore, in [34], a reformation of the market operating rules is suggested to correctly allocate the balancing responsibility to the local DSOs based on the cost-causality principle. The new cost allocation scheme would highly incentivise DSOs to manage the prosumption uncertainty locally. In [31], it is studied how the so-called *dispatched by-design distribution networks* significantly reduce the reserve requirement for the bulk power system, producing the least total costs for operating the bulk power system.

In this context, there has been increasing interest in using ESSs as a flexible resource to compensate for system imbalances [35], [36]. The European Network of Transmission System Operators for Electricity published a draft grid code addressing the possibility of ESSs becoming balancing serving providers [37]. However, European Union's regulatory directive is currently prohibiting DSOs' ownership of ESSs used for balancing and congestion management purposes to prevent distortion of a competitive market for ESSs [38]. Yet, in [39], the Authors pointed out the necessity and possibility of modifying the regulatory framework regarding the ownership of ESSs to promote their further exploitation for balancing, congestion management, and other ancillary services.

For this reason, despite the lack of an already established market and regulatory framework, we assume that: 1) a market environment with a modified regulatory framework allows DSOs to invest in ESSs and to control them for balancing service but not for energy arbitrage; 2) the DSO is the financial representative for the imbalance caused within its ADN, which is penalized as an imbalance cost paid to the TSO. With the above assumptions, DSOs have enough

[2] Prosumption is defined as the load consumption minus the locally generated power.

motivation to integrate the ESSs to compensate for the dispatch error, thereby enhancing the *dispatchability* of their ADNs and mitigating the aforementioned financial risk. The *dispatchability* identifies the capability of a resource, or an ADN, to control the realized active power output of the resources, or active power flow at the GCP of the ADN, to follow a pre-defined power schedule with high fidelity.

There have already been studies addressing the optimal control strategies of ESSs to improve the dispatchability of stochastic resources [28, 32, 40, 41]. Furthermore, efforts have been made to achieve *dispatchability of ADNs* in view of the inherent advantages such as reduction of the bulk system reserve provision [31] and mitigation of the imbalance penalty charges imposed on DSOs [30, 32, 42]. Based on the probabilistic forecast of the prosumption and forecast errors, the Authors of [32] compute an optimal dispatch schedule by minimizing the power exchange through the GCP while limiting the occurrences of dispatch error during the whole operation horizon. Meanwhile, a robust optimization approach with an emphasis on a control strategy for ESSs is proposed to achieve the dispatchability of a distribution feeder in [30]. In a day-ahead operation, the power schedule is computed following the prediction point of prosumption. An ESS is controlled such that the active power flow through the ADN GCP tracks the power schedule with minor deviations. The possible realization of prediction error is modeled based on the historical load consumption and RERs production data. The dispatching problem is formulated as a robust optimization problem such that the worst case of the prediction error is compensated by maximizing the exploitation of given ESSs located at the GCP. The Author proposed to embed the so-called *offset profile* which aims to restore an adequate ESS state-of-energy (SoE) so that, during operation, enough up/down flexibility is available to compensate for the mismatch between prosumption prediction and realization.

However, the algorithm proposed in [30, 32] did not consider the network model and associated operational constraints, which may lead to physically inapplicable solutions during the real operation. The operational constraints were addressed to compute an optimal dispatch plan in [43]. The studies mentioned above clearly state that the feasibility of the formulated problems regarding the imbalance constraint heavily depends on the ESSs' power and energy capacities. Inevitably, such a study on the control strategy of ESSs raises another crucial research question regarding how ESSs' sites and sizes should be determined to achieve ADN's dispatchability. In this respect, the optimal allocation of ESSs to achieve ADN's dispatchability becomes the research question to be tackled in this chapter.

A robust optimization-based planning framework may ensure perfect dispatchability (*i.e.*, the dispatch plan is followed perfectly for all prosumption scenarios); however it often leads to an over-investment decision. Alternatively, the prosumption uncertainty can be considered by formulating a stochastic optimization problem for the dispatching problem. Compared to the robust optimization approach, the stochastic optimization problem can avoid over-investment because it aims to achieve the economically optimal investment solution with larger risk. To reduce the computational burden, the stochastic optimization problem can be discretely approximated by expressing the distribution of prosumption with a set of scenarios. In this regard, the dispatching problem is modeled as a scenario-based stochastic optimization

problem. The ADN's dispatchability is evaluated based on a set of operating scenarios, which represent the prediction uncertainty.

2.4 State-of-the-art of ESS Planning

ESSs are widely acknowledged as beneficial and commercially exploitable due to their multiple uses within various levels of a power system. To observe the value of ESSs more distinctively, it is better to group the literature concerning the purpose of using ESSs within the power system and the perspective of whom that ESS is exploited for.

Operational objective: the TSO perspective

Efforts have been made to procure system flexibility at the transmission level by installing grid-scale ESSs within the transmission network [44, 45]. The Author of [44] suggests that co-optimizing ESS investments, along with transmission and generation investments, can be cost-effective in coping with uncertainties and variabilities associated with large RERs portfolios. The Author of [45] proposes a joint expansion planning of transmission and ESSs for a large-scale wind farm integrated power system to maintain adequate system reliability. The flexible resources also can be procured in an aggregated manner as proposed in [46]. The Author proposed a method to aggregate the resources within distribution systems to procure the frequency control reserve. In [31], the Authors evaluated the economic advantages of achieving dispatchability of a distribution network via exploiting ESSs to reduce the bulk power system reserve.

Operational objective: the DSO perspective

Numerous papers have tackled the topic of optimal siting and sizing ESSs in ADN with various objectives. For the technical aspects, [14, 47, 48] focused on the advantage of ESSs for minimizing network losses, while [14, 49, 50] considered the distribution network's voltage control problem. Providing services to mitigate line congestions [14], and improving the quality of power supply [47, 51] were also regarded as operational objectives in the ESS allocation. A substantial amount of literature addressed the economic benefit of ESS for DSOs, such as minimizing operation cost [52], maximizing the DSOs' profit by providing ancillary services [53] to the transmission network, or mitigating the risk in energy markets via load shifting and power arbitrage [54]. In [55], the Authors presented a control-aware optimal placement and sizing of ESSs by embedding receding horizon control strategies within a linearized OPF model. The operational objective of the problem was to maximize PV utilization. There are also extensive works on sizing ESSs with special attention on forecast uncertainties of stochastic resources [56, 57]. Meanwhile, relatively few studies were dedicated to ESSs planning for achieving the dispatchability of ADNs.

There have been studies in the probabilistic estimation of the required ESSs capacity to compensate for the renewable generation uncertainty to a pre-defined extent from the prosumer's side [58, 59]. The Authors of [60] and [61] proposed an algorithm to size a wind farm ESS to achieve its dispatchability. In [60], the ESS dispatch strategy is coupled with assessing its capacity and expected lifetime based on the confidence level of the power output

w.r.t the pre-defined schedule. In [61], specific ESS control algorithms are proposed along with a linear regression forecasting algorithm to compensate energy imbalance between the real power output and the pre-defined schedule of stochastic DERs. Furthermore, the impact of the balance service on the ESS's life is assessed.

To ensure the economic optimality of decision-making, it is worth evaluating the optimal allocation of ESSs in the of DSOs' economic profit by considering the trade-off between its investment cost and the expected advantages while respecting the technical requirements for the preferred operational condition of the ADN. In this regard, ESS planning methodologies proposed in [54, 62–64] are developed by formulating and solving OPF model-based planning problems. These studies addressed the financial risk of DSOs in the energy market regarding the imbalance caused within their ADNs. The work in [54] proposed a method for the optimal allocation of ESSs through a cost-benefit analysis while integrating a control strategy of ESSs to compensate for the gap between the actual prosumption and the purchased energy from a forward market, mitigating the DSO's risk in the real-time energy market. In [62], by using the same market framework as in [54], the Authors proposed a scenario-based ESSs planning strategy and the optimal operation of DSOs considering the optimal bidding strategy in the day-ahead market and the optimal real-time operation of ESSs to minimize the imbalance cost regarding operating scenarios representing prediction uncertainties. In [63], a similar objective was considered in the ESSs planning problem modeled as a scenario-based stochastic optimization problem while considering controllable DG units and ESSs. In [64], the ESSs capacity is determined for multiple agents, such as DSOs, wind farms, PV stations, and ADNs demand aggregators. The approach is based on the game theory to reduce each agent's transaction cost risk due to the resources' forecast errors. However, only three scenarios (high, middle, and low levels of prosumption) were considered to model the forecast errors.

In several studies mentioned above, decomposition techniques are used to tackle the computational complexity of large-scale multi-layered planning problems, and the Benders decomposition is widely used. For instance, in [65], the stochastic planning problem is decomposed into two stages using the Benders decomposition methods [54, 62]. In the master problem, the decision variables are determined based on the system operation evaluation assessed through solving suitably defined subproblems.

The performance and reliability of the planning tools for ADNs can be guaranteed only when the operational conditions of the system are accurately modeled through a proper power flow model. The insight is underpinned by observing from the studies mentioned above that they tackled the problem of the ESSs sizing and placement while considering the ESSs operation's characteristics and the system's subsequent operational conditions. In short, the quality of the operation solution relies on the accuracy of the network operation model and the prosumption stochastic model. Indeed, considering prosumption uncertainty renders the planning exercise a stochastic optimization problem, which is further discretely approximated as a scenario-based stochastic optimization problem to improve computational efficiency. Moreover, the advantages of using scenarios are related to considering generic parametric and non-parametric distributions of prosumptions forecasts.

Analyzing the stochasticity of consumption and local generation and the generation of operating scenarios is out of the scope of this thesis. Therefore, the operating scenarios are assumed to be given by the modeler. Yet, the relevant scenario generation method utilized in this work is included in the appendix (see Sec. A.1) for readers' interest.

2.5 Problem Statement and Contributions

We model and solve the ESS allocation problem while considering the dispatchability of ADNs. The control strategy of ESSs assets is embedded into the ADN operation problem formulated based on the piecewise linearized OPF (PWL-OPF) model (described later in Sec. 2.7.1). The resulting planning problem is a large-scale two-stage scenario-based stochastic optimization problem, which is computationally burdensome. Therefore, the planning problem is decomposed into a master and parallel subproblems by employing the Benders decomposition [66], Contributions of the chapter are two, as described below.

1. The optimal allocation of ESSs is determined based on a piecewise linear approximation of the full AC-OPF to achieve the dispatchability of an ADN hosting high-capacity stochastic renewable generation.

2. The control-aware approach embeds the maximum exploitation of ESSs capacity and is integrated into the ESSs planning problem.

2.6 Achieving the ADN's Dispatchability

2.6.1 Definition of ADN's Dispatchability

The dispatching problem is modeled as a scenario-based stochastic problem. Therefore, the ADN's dispatchability is evaluated based on a set of operating scenarios representing the prediction uncertainty.

The uncertainty in prosumption in each day-type is represented by operating scenarios indexed with $\phi \in \Phi$ with probability λ_ϕ for each scenario. The dispatch interval is identified by the index $t \in \{1,...,T\} = \mathcal{T}$, where T corresponds to the scheduling horizon of the daily operation. Time indices are separated by a constant timestep Δt. Each node of the ADN has a non-dispatchable aggregated prosumption ($s_{l\phi t}$) defined for each scenario and time interval. The aggregated ADN active powers through the GCP (supposed to be the first node of the ADN topology) to an upper layer network in all scenarios ($P_{1\phi t}, \forall \phi \in \Phi$) are expected to follow a day-ahead determined daily dispatch plan for each time interval (DP_t), which is derived with the support of a forecasting tool. Note that in this dispatching problem, we compute a dispatch plan only for the active power. The gap between the dispatch plan and the realized active power flow at GCP is defined as *dispatch error*. Then, ESSs allocated within the network are dispatched for each scenario and time interval according to active power ($p^E_{l\phi t}$) and reactive power ($q^E_{l\phi t}$). The dispatched active power compensates for the gap between active power through the GCP and the dispatch plan, which results from the deviation of realized total prosumption from the total prosumption prediction. Consequently, the observed dispatch error at GCP can be minimized and the ESS capacity determines the

capability of compensating for the dispatch error, defined as *dispatchability of the ADN*.

The active and reactive prosumption scenarios for each day-type are generated, assuming that the prosumption profile follows a normal distribution[3]. Therefore, the mean of the prosumption over the scenarios is equal to the given prosumption prediction. The expected line losses resulting from operating the ADN with the given prosumption prediction are calculated by averaging the line losses over the scenarios [30]. $p_{l\phi t}$ is aggregated active prosumption at bus l, scenario ϕ, time t, and $f_{l\phi t}$ is square of longitudinal current magnitude causing losses in line l, scenario ϕ, and time t. r_l is the total longitudinal resistance of line l. $\tilde{p}_{lt}$ and $\tilde{f}_{lt}$ are average of the active prosumption and squared longitudinal line current causing losses over all scenarios at bus l, time t, respectively. $\Delta p_{l\phi t}$ and $\Delta f_{l\phi t}$ are deviation of prosumption and squared longitudinal line current causing losses for scenario ϕ and time t from $\tilde{p}_{lt}$ and $\tilde{f}_{lt}$, respectively. (2.1a) and (2.1b) express the prosumption at bus l and the line losses of line l by these variables. In (2.1c), a dispatch plan DP_t follows the predicted point of the total prosumption considering the predicted grid losses.

$$p_{l\phi t} = \tilde{p}_{ltdy} - \Delta p_{l\phi t}, \qquad \forall l \in \mathscr{L}, \forall \phi \in \Phi, \forall t \in \mathscr{T}, \tag{2.1a}$$

$$r_l f_{l\phi t} = r_l \tilde{f}_{lt} - r_l \Delta f_{l\phi t}, \qquad \forall l \in \mathscr{L}, \forall \phi \in \Phi, \forall t \in \mathscr{T}, \tag{2.1b}$$

$$DP_t = \sum_{l \in \mathscr{L}} (\tilde{p}_{lt} + r_l \tilde{f}_{lt}), \qquad \forall t \in \mathscr{T}. \tag{2.1c}$$

$P^t_{1\phi t}$ represents the active power through the GCP for each scenario and time interval. In other words, it is the aggregate of all prosumption, including the total grid losses in the ADN. In this context, the *dispatch error* with no dispatchable resources in ADN is formally defined as the total dispatch error of prosumption plus the losses over the lines as indicated in the left-hand side of (2.2). As in the right-hand side of (2.2), the active powers of the ESS can be controlled to compensate for the GCP power flow deviation. The compensated amount of deviation is indicated by $\omega_{l\phi t}$. $\epsilon_{l\phi t}$ represents the residual deviation that cannot be covered at bus l, scenario ϕ, and time t. To quantify the covered (or not covered) error by the ESSs, we express that the sum of the two parts, shown in the right-hand side of (2.2), is equal to the dispatch error in case of no dispatchable resources. On the other hand, the dispatch error at the GCP is expressed as (2.3).

$$\sum_{l \in \mathscr{L}} (\Delta p_{l\phi t} + r_l \Delta f_{l\phi t}) = \sum_{l \in \mathscr{L}} (\epsilon_{l\phi t} + \omega_{l\phi t}), \qquad \forall \phi \in \Phi, \forall t \in \mathscr{T}, \tag{2.2}$$

$$DP_t - P^t_{1\phi t} = \sum_{l \in \mathscr{L}} \epsilon_{l\phi t}, \qquad \forall \phi \in \Phi, \forall t \in \mathscr{T}. \tag{2.3}$$

[3] Since the proposed method relies on a scenario-based approach, the modeler can use generic parametric and non-parametric distributions to model the prosumptions. Modeling the prosumption uncertainty can affect the fidelity of the optimal solution regarding the allocation of ESS and the dispatchabiliy level of an ADN. However, as modeling of prosumption stochasticity is not the scope of this paper, the prosumption scenarios are generated simply assuming that the prosumption follows a normal distribution, while the temporal correlation is neglected. Nevertheless, when a modeler is equipped with a robust scenario generator which models accurately the distribution of the consumption load and generation and their temporal correlations, the proposed approach can guarantee the reliable performance.

Finally, the objective is to minimize the active power deviation at the GCP from the daily dispatch plan for all scenarios during the operation horizon and it is expressed mathematically as follows.

$$\min_{p^E} \sum_{t\in\mathscr{T}} \sum_{\phi\in\Phi} \lambda_\phi \left| \sum_{l\in\mathscr{L}} \epsilon_{l\phi t} \right| \tag{2.4}$$

2.6.2 Embedding the ESS's Offset Profile within the Dispatch Plan

The daily dispatch plan can include the ESSs control strategy, so-called *offset profile*, to maximize the exploitation of the ESSs capacity for covering the uncertainty of the prosumption [30]. The objective of the offset profile is to restore an adequate ESSs SoE so that enough flexibility is available within ESSs to compensate for upcoming errors between the predicted and the realized prosumption during operation. For example, assume that the current SoE of a generic ESS is near its limit, and high uncertainty (*i.e.*, the realized prosumption deviates from the forecasted prosumption with large magnitude) is expected in upcoming time intervals. Then, the offset profile assigned to each allocated ESS can bias the dispatch plan to charge/discharge the ESS so that the SoE level is adjusted to a value capable of compensating for the upcoming realizations of prosumption forecast errors. In practice, it gives the ESS a high capability of compensating for the uncertainty projected up to the end of the dispatch horizon.

Eq. (2.5) indicates that the offset profile F^E_{lt} is assigned to the ESS allocated at node l. The ESS active power dispatch at node l is determined for every time interval t with the offset profile and the power compensating for the dispatch error, as shown in (2.6).

$$|F^E_{lt}| \le R_l, \qquad \forall l \in \mathscr{L}, \forall t \in \mathscr{T}, \tag{2.5}$$

$$p^E_{l\phi t} = F^E_{lt} + \omega_{l\phi t}, \qquad \forall l \in \mathscr{L}, \forall \phi \in \Phi, \forall t \in \mathscr{T}. \tag{2.6}$$

Each offset profile assigned to an ESS is added to the dispatch plan. In this way, the energy required to restore the appropriate SoE can be embedded in the dispatch plan. The dispatch plan for an ADN is finally expressed as (2.7) by using (2.1a) and (2.1b), along with the offset profiles.

$$DP_t = \sum_{l\in\mathscr{L}} F^E_{lt} + \sum_{l\in\mathscr{L}} (\tilde{p}_{lt} + r_l \tilde{f}_{lt}), \qquad \forall t \in \mathscr{T}. \tag{2.7}$$

In summary, the equations for modeling the ESS's role of compensating for the dispatch error and the ESS's control strategy for maximizing its capability correspond to (2.1a), (2.1b), (2.2), (2.3), (2.5)-(2.7). For the sake of simplicity, they are collectively defined as $\Xi(v) \ge 0$, where $v = \{p_E, \epsilon, \omega, F^E\}$. Note that the variables indicated without subscript are defined for $\forall l \in \mathscr{L}, \forall \phi \in \Phi, \forall t \in \mathscr{T}$.

2.7 Integration of ADN's Dispatchability into the Power Flow Model

In this section, the definition of the ADN's dispatchability is integrated within the OPF model to apply the concept of dispatchability on a real distribution network, achieving *dispatched-by-design* ADN. Moreover, we embed the ESS's operational strategy to optimally utilize their energy capacities to cope with uncertainty in the power flow through the ADN.

In this chapter, we account for the ADN's operational constraints via a linearized model[4], referred to as the PWL-OPF model. It relies on linear approximation of the non-linear power flow equations for its convexification. Thanks to this linearization, the planning problem is more tractable although at the expense of the exactness of the formulation (*i.e.*, the optimal solution of the approximated model may not be equivalent to the optimal solution of the original OPF problem). It is widely used in tackling various research interests in power systems thanks to its flexibility of implementation [67–69]. Likewise, the PWL-OPF model is used in this chapter because embedding the ESS control strategy requires the optimization problem to have more flexibility concerning the objective function. Moreover, it is noteworthy that the approximation accuracy of the model can be adjusted by changing the proper number of discretizations. It can achieve the optimal solution with reasonable quality and minor approximation errors from the original OPF solution. Unlike the existing work relying on the PWL-OPF method, we consider the shunt element of the lines, which can significantly impact the line's current flows, especially in networks with long underground coaxial cables.

2.7.1 Formulation of PWL-OPF Model

Piecewise linearization function

The piecewise linearization function $f(y, \bar{y}, \Upsilon)$, which approximates y^2, illustrated in Fig. 2.1. Note that $\bar{y}$ is equivalent to the maximum possible value of y. Υ indicates the number of discretization steps in the piecewise linearization function. The function approximates a quadratic function of y as shown in (2.8a).

$$y^2 \approx f(y, \bar{y}, \Upsilon) = \sum_{\upsilon=1}^{\Upsilon} \theta_\upsilon^y \Delta_\upsilon^y, \tag{2.8a}$$

$$y = y^+ - y^-, \quad y^+, y^- \in \mathbb{R}^+, \tag{2.8b}$$

$$y^+ + y^- = \sum_{\upsilon=1}^{\Upsilon} \Delta_\upsilon^y, \tag{2.8c}$$

$$0 \le \Delta_\upsilon^y \le \bar{y}/\Upsilon, \qquad \forall \upsilon \in \mathscr{U}, \tag{2.8d}$$

$$\theta_\upsilon^y = (2\upsilon - 1)\,\bar{y}/\Upsilon, \qquad \forall \upsilon \in \mathscr{U}. \tag{2.8e}$$

(2.8b) says that y is expressed by subtracting two non-negative variables y^+ and y^-, which represent the positive and the negative values of y, respectively. In this way, the absolute

[4] A better OPF model will be employed in the next Chapter. Here, we use a linear OPF model for the sake of simplicity of problem formulation.

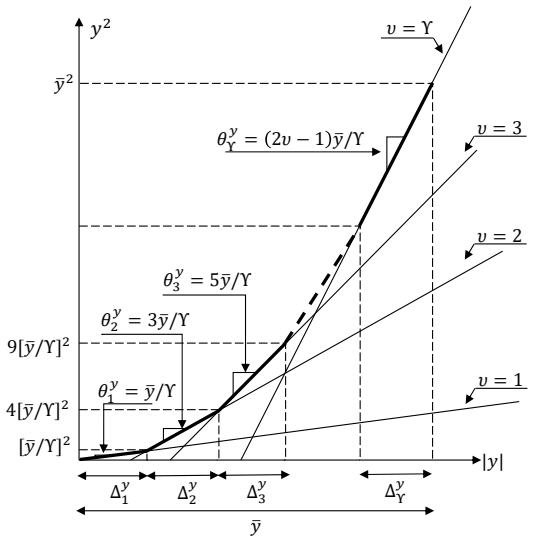

Figure 2.1: The piecewise linear approximation of a quadratic function.

value of y can be expressed by the two variables as shown in the left-hand side of (2.8c).[5] An auxiliary variable $\Delta^y_\upsilon, \forall \upsilon \in \mathscr{U}$ ($|\mathscr{U}| = \Upsilon$), is introduced to determine the step size for the piecewise linearization of the absolute value of y. Each step size is optimally decided within the range specified in (2.8d), which is governed by the number of discretized segments Υ and $\bar{y}$. For each discretization step, θ^y_υ, the slope of the curve at each break-point, is estimated by (2.8e). Then the slope is assigned to construct the set of line segments, which all together approximate the value of y (see (2.8a)). Note that the PWL approximation is by nature relaxing the quadratic constraint, and therefore it requires including active/reactive power, or grid losses related objective terms in the objective function to tighten the relaxation. The set of equations (2.8a)-(2.8e) can be notated as:

$$P(\varrho^y) \geq 0, \text{where } \varrho^y = \{\Delta^y, y^+, y^-\} \tag{2.9}$$

. Note that Δ^y implies $\Delta^y_\upsilon, \forall \upsilon \in \mathscr{U}$. The readers can refer to [67] for more details.

The application of PWL function to the OPF model

The OPF formulation for a radial power network is derived by applying the Kirchhoff's law to Fig. 2.2, which depicts the line model for a radial power network. The power flow equations are given in (2.10a)-(2.10e). $\mathbf{H}$ is the adjacency matrix of the network, where $\mathbf{H}_{k,l}$ is defined for $k, l \in \mathscr{L}$ and $\mathbf{H}_{k,l} = 1$ if $k = up(l)$ or 0 if not. (2.10a), (2.10b) indicates the power balance equations at the upstream of line l, and at the downstream of line l, respectively. (2.10c) represents the nodal voltage equation, where $\Re(.)$ represents the real part of a complex number. (2.10e) defines the squared value of the longitudinal current of line l. The network security constraints regarding nodal voltages and the line ampacity defined at the upstream

[5] The substitution of y with the two non-negative variables implies a relaxation of the absolute value of y. Therefore, the minimization of y should be included either implicitly or explicitly in the objective function.

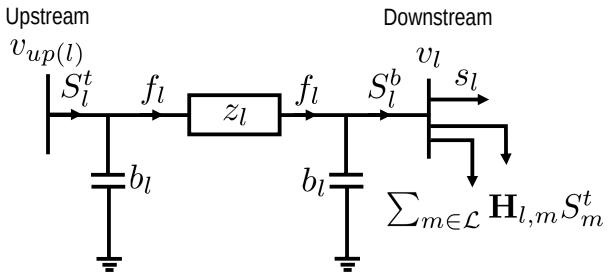

Figure 2.2: Classic two-port Π model of a transmission line adopted for the formulation of the OPF relaxed constraints. Adapted from [1].

and downstream nodes of line l are expressed with (2.10d) and (2.10f), (2.10g) respectively.

$$S_l^t = s_l + \sum_{m\in\mathscr{L}} \mathbf{H}_{l,m} S_l^t + z_l f_l - (v_{up(l)} + v_l) b_l, \qquad \forall l \in \mathscr{L}, \tag{2.10a}$$

$$S_l^b = s_l + \sum_{m\in\mathscr{L}} \mathbf{H}_{l,m} S_l^t, \qquad \forall l \in \mathscr{L}, \tag{2.10b}$$

$$v_l = v_{up(l)} - 2\Re\left(z_l^* \left(S_l^t + j v_{up(l)} b_l\right)\right) + |z_l|^2 f_l, \qquad \forall l \in \mathscr{L}, \tag{2.10c}$$

$$v^{min} \le v_l \le v^{max}, \qquad \forall l \in \mathscr{L}, \tag{2.10d}$$

$$f_l = \frac{|P_l^t|^2 + |Q_l^t + v_{up(l)} b_l|^2}{v_{up(l)}} = \frac{|P_l^b|^2 + |Q_l^b - v_l b_l|^2}{v_l}, \qquad \forall l \in \mathscr{L}, \tag{2.10e}$$

$$\frac{|P_l^t|^2 + |Q_l^t|^2}{v_{up(l)}} \le (I_l^{max})^2, \qquad \forall l \in \mathscr{L}, \tag{2.10f}$$

$$\frac{|P_l^b|^2 + |Q_l^b|^2}{v_l} \le (I_l^{max})^2, \qquad \forall l \in \mathscr{L}. \tag{2.10g}$$

Eqs. (2.10e)-(2.10g) contain quadratic and fraction terms that make these constraints non-convex. Therefore, we apply the previously introduced piecewise linearization to the non-linear terms. The first step is to simplify the fraction term by replacing the denominator variables associated with the nodal voltage magnitudes in (2.10e)-(2.10g) with the voltage lower bound (v^{min}). This results in a conservative constraints of the line current and the current causing the grid losses. By taking the second part of (2.10e), the equation is simplified to (2.11a). (2.10f) and (2.10g) are replaced with (2.11b) and (2.11c).

$$v^{min} f_l = |P_l^t|^2 + |Q_l^b - v_l b_l|^2, \qquad \forall l \in \mathscr{L}, \tag{2.11a}$$

$$|P_l^t|^2 + |Q_l^t|^2 \le v^{min} I_l^{max}, \qquad \forall l \in \mathscr{L}, \tag{2.11b}$$

$$|P_l^b|^2 + |Q_l^b|^2 \le v^{min} I_l^{max}, \qquad \forall l \in \mathscr{L}. \tag{2.11c}$$

Then, we linearize (2.11a)-(2.11c) by applying the PWL function on the quadratic terms: $|P_l^t|^2$, $|P_l^b|^2$, $|Q_l^t|^2$, $|Q_l^b|^2$, and $|Q_l^b - v_l b_l|^2$, each formulated by the equations below.

$$|P_l^t|^2 \approx f(P_l^t, P_l^{max}, \Upsilon), \qquad \forall l \in \mathscr{L}, \tag{2.12a}$$
$$|Q_l^t|^2 \approx f(Q_l^t, Q_l^{max}, \Upsilon), \qquad \forall l \in \mathscr{L}, \tag{2.12b}$$
$$|P_l^b|^2 \approx f(P_l^b, P_l^{max}, \Upsilon), \qquad \forall l \in \mathscr{L}, \tag{2.12c}$$
$$|Q_l^b|^2 \approx f(Q_l^b, Q_l^{max}, \Upsilon), \qquad \forall l \in \mathscr{L}, \tag{2.12d}$$
$$|Q_l^t - v_l b_l|^2 \approx f(Q_l^b - v_l b_l, Q_l^{max}, \Upsilon), \qquad \forall l \in \mathscr{L}. \tag{2.12e}$$

where P_l^{max} and Q_l^{max} are chosen as the maximum active and reactive power flows over all scenarios and timesteps for each line, which are obtained by running a preliminary load flow with the selected stochastic prosumption scenarios. It should be noted that the set of variables and equations shown in (2.9) should be defined for $P_l^t, P_l^b, Q_l^t, Q_l^b$, and $Q_l^b - v_l b_l$, respectively. The set of equations are not indicated here to avoid repetition. Instead, they are noted as:

$$\left\{ P(\varrho^{P_l^t}), P(\varrho^{P_l^b}), P(\varrho^{Q_l^t}), P(\varrho^{Q_l^b}), P(\varrho^{Q_l^b - v_l b_l}) \right\} \geq 0, \qquad \forall l \in \mathscr{L}. \tag{2.13}$$

By using the piecewise linearization function, all the quadratic terms indicated in the OPF formulation can be replaced. Therefore, (2.11a) can be replaced with (2.14a), and (2.11b), (2.11c) with (2.14b) and (2.14c), respectively.

$$v^{min} f_l = f(P_l^t, P_l^{max}, \Upsilon) + f(Q_l^b - v_l b_l, Q_l^{max}, \Upsilon), \qquad \forall l \in \mathscr{L}, \tag{2.14a}$$
$$f(P_l^t, P_l^{max}, \Upsilon) + f(Q_l^t, Q_l^{max}, \Upsilon) \leq v^{min} I_l^{max}, \qquad \forall l \in \mathscr{L}, \tag{2.14b}$$
$$f(P_l^b, P_l^{max}, \Upsilon) + f(Q_l^b, Q_l^{max}, \Upsilon) \leq v^{min} I_l^{max}, \qquad \forall l \in \mathscr{L}. \tag{2.14c}$$

For the sake of readability, (2.10a)-(2.10d),(2.13),(2.14) are grouped and represented by $\Theta_{PWL}(\varphi) \geq 0$, where $\varphi = \{S^t, v, f, s, \varrho^{P^t}, \varrho^{P^b}, \varrho^{Q^t}, \varrho^{Q^b}, \varrho^{Q^b - vb}\}$, is the set of variables. The notation without subscript corresponds to the vector of variable for all nodes/lines. The PWL problem is defined as (2.15a), where $C(r_l f_l)$ is a cost function associated with the grid losses.

$$\min_{\varphi} \sum_{\forall l \in \mathscr{L}} C(r_l f_l) \tag{2.15a}$$
$$\text{subject to: } \Theta_{PWL}(\varphi) \geq 0. \tag{2.15b}$$

2.8 System Description

The studied network is a radial distribution network and is considered to be balanced without any coupling between the phases. The objective of the problem is to determine the optimal sizes and sites of ESSs so that the power flow through the ADN GCP follows a daily dispatch plan with minimal deviation. As previously mentioned, by embedding the offset

profile within the dispatch plan, we can maximize the exploitation of the installed ESSs to cope with the uncertainty caused by the stochastic nature of the resources.

The optimal allocation of ESSs is determined based on the operation of the ADN over the planning horizon Y, while the prosumption profiles are expected to grow each year at the constant rate r_i. Each year is indexed with $y \in \{1, ..., Y\} = \mathscr{Y}$. We classify days into day-types indexed with $d \in \mathscr{D}$. To represent the seasonal variability of prosumption, the set of operating scenarios representing prediction uncertainty is defined differently for all day-types and years (*i.e.*, the operation scenario set Φ_{dy} is defined $\forall d \in \mathscr{D}$ and $\forall y \in \mathscr{Y}$). The uncertainty in prosumption in each day-type and year is represented by operating scenarios indexed with $\phi \in \Phi_{dy}$ with probability λ_ϕ for each scenario.

To evaluate the ADN operation for each day-type, the dispatching problem is solved such that the ADN's dispatchability described in Sec. 2.6.1 is achieved. During the operation of day-type d and year y, the aggregated ADN active powers through the GCP to an upper layer network in all scenarios ($P_{1\phi t}$, $\forall \phi \in \Phi_{dy}$) are expected to follow a daily dispatch plan for each time interval (DP_{tdy}). To achieve it for all day-types and years, an ESS is allocated at l (*i.e.*, $U_l = 1$, where $U_l \in \{0, 1\}$), with the energy reservoir of C_l, and the power rating of R_l. The ESS's active power ($p^E_{l\phi t}$) and reactive power ($q^E_{l\phi t}$) are controlled for each scenario and time interval so that they compensate for the difference between the active power flow of each operating scenario at GCP and the dispatch plan. As a result, the observed dispatch error at GCP can be reduced.

In summary, the defined ESS allocation problem to achieve dispatchability is formulated as a two-stage stochastic MILP model. The first stage has the binary decision variables on the location of the ESSs (U_l) and the continuous decision variables on the capacity of the ESS energy reservoirs (C_l) and their power rating (R_l). The second stage deals with daily dispatch problems, determining the decision variables given by the ESSs' active and reactive powers for all operating scenarios.

2.9 Problem Formulation

2.9.1 Operation-aware ADNs' planning problem

The operation-aware planning problem is formulated as two-stage stochastic MILP problem as explained in Sec. 2.8. In this section, the problem is mathematically formulated taking into account the cost objectives, ESS investment and network operation model considering the ESS exploitation for achieving dispatchability.

Modeling of ESSs investment

The ESS investment is modeled through (2.16a)-(2.16c). In reality, available power ratings and energy capacities are often restrained as in (2.16a) and (2.16b) due to various physical constraints involving, for instance, manufacture or geographical factors. CR^{max} is the maximum value for the rate at which ESS is charged/discharged relatively to its maximum energy capacity. The power rating and energy reservoir is determined considering this relationship as

in (2.16c). The ESS investment cost consists of fixed installation costs, power rating costs, and energy reservoir costs as shown in (2.16)[6].

$$R^{min}U_l \le R_l \le R^{max}U_l, \qquad \forall l \in \mathscr{L}, \tag{2.16a}$$
$$C^{min}U_l \le C_l \le C^{max}U_l, \qquad \forall l \in \mathscr{L}, \tag{2.16b}$$
$$R_l \le \frac{C_l}{CR^{max}}, \qquad \forall l \in \mathscr{L}, \tag{2.16c}$$
$$IC_E = \sum_{l \in \mathscr{L}} (ic_E^f U_l + ic_E^p R_l + ic_E^e C_l), \qquad \forall l \in \mathscr{L}. \tag{2.16d}$$

Modeling of ESSs operation

The operational characteristics of an ideal ESS located at node l are represented as (2.17b)-(2.17g). To consider the ESS for the daily operation of ADN, the model of the ESS operation should be included in the set of power flow equations defined for all scenarios and time intervals within the daily dispatch horizon. Note that all the operation variables indicated in (2.17b)-(2.17g) are defined for $\forall t \in \mathscr{T}$. Eq. (2.17a) refers to the circular curve of ESS active and reactive power capability defined by the power rating of the ESS converter. It is approximated by a set of linear constraints inscribed within the original curve as in (2.17b). $\boldsymbol{\alpha}_l$, $\boldsymbol{\beta}_l$ and $\boldsymbol{\kappa}_l$ are vectors defining the slope and the intercepts of the set of linear constraints which approximate the power capability curve of the ESS located at node l. Eq. (2.17c) expresses the ESS' SoE with charge/discharge power for each time interval. Eq. (2.17d) indicates SoE limits on during the day. As in (2.17e), the initial SoE is set to be equal to SoE^{ini} and the final SoE is set to be within $\pm\Delta_{ini}^{fin} * 100\%$ of the initial SoE as in (2.17f). Moreover, we account for the aging of the ESS caused by its operation by (2.17g). This constraint keeps the ESS energy exchange within a threshold, which minimizes the ESS aging during its daily operation [70]. ω is a positive parameter that depends on $p_{l\phi t}^E$, and we chose the maximum value stated in [70] ($\omega = 1$). N_c is the allowed number of cycles per day chosen as a function of the targeted ESS lifetime [70].

$$(p_{lt}^E)^2 + (q_{lt}^E)^2 \le R_l^2, \qquad \forall t \in \mathscr{T}, \tag{2.17a}$$
$$\boldsymbol{\alpha}_l p_{lt}^E + \boldsymbol{\beta}_l q_{lt}^E \le \boldsymbol{\kappa}_l R_l, \qquad \forall t \in \mathscr{T}, \tag{2.17b}$$
$$E_{l(t+1)}^E = E_{lt}^E + \Delta t p_{lt}^E, \qquad \forall t \in \mathscr{T}, \tag{2.17c}$$
$$SoE^{min}C_l \le E_{lt}^E \le SoE^{max}C_l, \qquad \forall t \in \mathscr{T}, \tag{2.17d}$$
$$E_{l(1)}^E = SoE^{ini} * C_l, \qquad \forall t \in \mathscr{T}, \tag{2.17e}$$
$$E_{l(1)}^E - \Delta_{ini}^{fin}C_l \le E_{l(T+1)}^E \le E_{l(1)}^E + \Delta_{ini}^{fin}C_l, \qquad \forall t \in \mathscr{T}, \tag{2.17f}$$
$$\frac{\Delta t}{2 * 1h}\left|\omega p_{lt}^E\right| \le N_c C_l, \qquad \forall t \in \mathscr{T}. \tag{2.17g}$$

The equations linked to the ideal ESS operation are grouped and defined as $\Lambda(\pi_l) \ge 0$,

[6] In this thesis, the three mentioned types of costs are considered for ESS investment. However, there are other accessory costs required for ESS investment, such as costs for power electronics. These accessory costs can be included in future works.

where $\pi_l = \{p_l^E, q_l^E, E_l^E\}$. The power balance equations through lines should be converted to include ESS power injections at their receiving ends as shown in (2.18a), (2.18b).

$$S_l^t = s_l + s_l^E + \sum_{m \in \mathscr{L}} \mathbf{H}_{l,m} S_l^t + z_l f_l - (v_{up(l)} + v_l) b_l, \qquad \forall l \in \mathscr{L}, \tag{2.18a}$$

$$S_l^b = s_l + s_l^E + \sum_{m \in \mathscr{L}} \mathbf{H}_{l,m} S_l^t, \qquad \forall l \in \mathscr{L}. \tag{2.18b}$$

Henceforth, (2.10a), (2.10b) from $\Theta_{PWL}(\varphi) \geq 0$ are replaced by (2.18a), (2.18b), converting the collective notation of PWL-OPF model including ESSs as $\Theta_{PWL}^E(\varphi_{\phi t}^E) \geq 0, \forall \phi \in \Phi_{dy}, \forall t \in \mathscr{T}$, while $\varphi^E = \{S^t, v, f, s, s^E, \varrho^{P^t}, \varrho^{P^b}, \varrho^{Q^t}, \varrho^{Q^b}, \varrho^{Q^b - vb}\}$.

Mathematical formulation of ADNs' planning problem

The total planning cost (TC) is the sum of ESS investment cost and the total operation cost during the planning horizon, and it is mathematically formulated as below, where OC_{dy} represents the operation cost for day d, and year y. w_f, w_e and w_l are the weight coefficients for the offset profile, the dispatch error, and the grid losses, respectively. When ESS assets with a specific capacity of energy reservoir and power rating are invested (by paying for the ESS investment cost), the operation condition of an ADN is evaluated in terms of the operation cost associated with total dispatch error and grid losses during the operation horizon. The operation condition should be checked for prosumption scenarios of different days and years spanning the planning horizon to evaluate accurately the operational benefit of ESSs' investment. The objective function of dispatch operation for day-type d and year y is given in (2.19b). The objective of the subproblem is to minimize the uncovered dispatch error, the absolute value of the offset profile, and the grid losses, with the set of optimization variables defined by (2.19g). Note that, instead of taking into account the operation of all days within the planning horizon, only a number of representative day-types are chosen for the evaluation of ADN's operation. The operation cost of each day-type is multiplied by the number of days classified to that day-type. Discount rate r_{dis} is considered to calculate the annual operation cost of each operation year. The optimization variables of the problem consists of two-stage decision variables. The first stage decision variabels include binary variables associated with ESS installation, ESS energy reservoir, and power rating variables as shown in (2.20e). The second stage variables include operation associated variables such as power flow, current, voltage, and ESS power as given in (2.19g).

$$\min_{\Omega_1, \Omega_2} : TC = IC_E + \sum_y \sum_d \frac{N_{dy}}{(1+r_{dis})^y} OC_{dy} \tag{2.19a}$$

$$where\ OC_{dy} = \sum_{t \in \mathscr{T}} (w_f \sum_{l \in \mathscr{L}} |F_{lt}^E| + \sum_{\phi \in \Phi_{dy}} \lambda_\phi (w_e | \sum_{l \in \mathscr{L}} \epsilon_{l\phi t}| + w_l \sum_{l \in \mathscr{L}} r_l f_{l\phi t}))$$

$$\forall d \in \mathscr{D}, \forall y \in \mathscr{Y}$$

subject to:

$$(2.16), \tag{2.19b}$$

$$\Theta^{E}_{PWL}(\varphi^{E}_{\phi t}) \geq 0, \qquad \forall \phi \in \Phi_{dy}, \forall t \in \mathscr{T}, \forall d \in \mathscr{D}, \forall y \in \mathscr{Y}, \tag{2.19c}$$

$$\Xi(v_{dy}) \geq 0, \qquad \forall d \in \mathscr{D}, \forall y \in \mathscr{Y}, \tag{2.19d}$$

$$\Lambda(\pi_{l\phi}) \geq 0, \qquad \forall l \in \mathscr{L}, \forall \phi \in \Phi_{dy}, \forall d \in \mathscr{D}, \forall y \in \mathscr{Y}, \tag{2.19e}$$

$$\Omega_1 = \{U, C, R\}, \tag{2.19f}$$

$$\Omega_2 = \{\varphi^{E}_{\phi t}, v, \pi_{l\phi}\}, \qquad \forall l \in \mathscr{L}, \forall t \in \mathscr{T}, \forall \phi \in \Phi_{dy}, \forall d \in \mathscr{D}, \forall y \in \mathscr{Y}. \tag{2.19g}$$

The constraints for the planning problem consists of two parts. First set of constraints is associated with ESS investment (see (2.16)). The other part is related to the ADN's operation, which includes power flow equations and security constraints (see (2.19c)) along with the set of equations related to the dispatch scheme (see (2.19d)) described in Sec. 2.6.1. To achieve the ADN's dispatchability, the invested ESSs are controlled, with their operation characteristics governed by (2.19e).

2.9.2 ADNs' planning algorithm using Benders decomposition

The formulated planning problem is a large scale two-stage stochastic MILP problem. The computational burden for solving the planning problem increases significantly with the number of years, day-types, and scenarios. To tackle the complexity of the problem, the Benders decomposition technique is employed to decompose it into smaller problems following the structure of the two-stage optimization problem shown in Fig. 2.3. The master problem stands for the first stage problem and determines the sites and sizes of the ESSs. Each subproblem stands for the second stage problem and represents the daily operation for different day types where the fitness of the determined allocations is evaluated with respect to the grid losses and the dispatch error. After solving the master problem, the values of the investment decision variables are fixed temporarily in the following subproblems, such that the given planning problem is reduced to an operational problem parameterized by the value of the investment decision variables vector. Then, the optimal value of this vector is updated by a cutting-plane approach, or Bender's cuts, constructed by objective values obtained from subproblems and dual values associated with the investment constraints fixing the investment variables' values to the master problem's solutions. The theory related to the Benders decomposition technique is recalled in Sec. A.2.

The whole structure of the planning algorithm is illustrated in Fig. 2.3. The Benders decomposition starts with the evaluation of the operational condition of the ADN in a default configuration (when there is no ESS). The evaluation is fed back into the master problem in the form of Benders cuts, which are built with subproblem objective values and the dual values associated with the ESSs power rating and energy reservoir capacities. The master problem updates the optimal ESS allocation in view of improvement on the operational condition, while the lower bound (LB) of the total planning cost is obtained by determining the investment

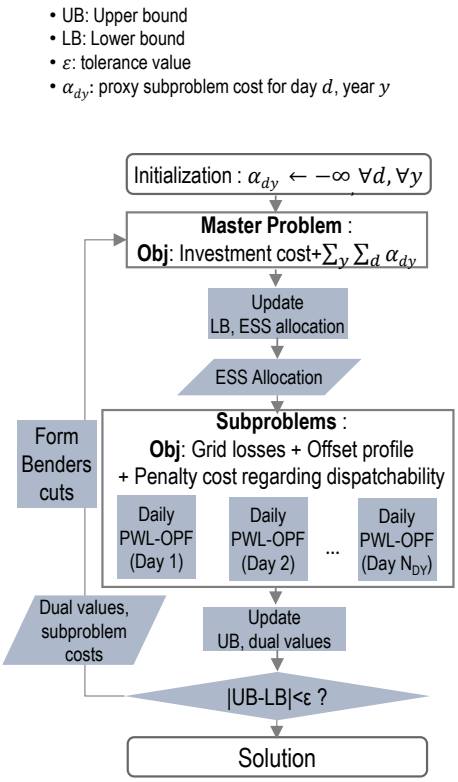

Figure 2.3: The full algorithm of the proposed planning strategy.

cost and estimating the expected subproblem costs by accumulated Benders cuts. In the following subproblems, the benefits of updated ESS allocation solutions are evaluated, and the upper bound (UB) of the total planning cost is obtained by adding the investment cost from the previous master problem to the calculated subproblem costs. The decomposition procedure goes through a number of iterations between solving the master problem and several subproblems until the gap between LB and the UB reduces to below the pre-defined tolerance value (ε), reaching a convergence.

Master Problem - Investment Stage

In the master problem, the optimal siting and sizing of the ESSs is determined considering the investment cost and the proxy subproblem costs. The formulation of the master problem is given in (2.20a), minimizing the total planning cost computed by adding the investment cost with the sum of lower approximations for the subproblem costs with respect to the determined ESS allocation. The optimization variables of the problem are given in (2.20e) and the constraints are given as (2.20b)-(2.20d).

$$\min_{\Omega_1} : MC = IC_E + \sum_{y \in \mathscr{Y}} \sum_{d \in \mathscr{D}} \alpha_{dy} \tag{2.20a}$$

Subject to:

$$(2.16a) - (2.16c), \tag{2.20b}$$

$$\alpha_{dy} \geq \underline{\alpha}, \qquad \forall d \in \mathscr{D}, \forall y \in \mathscr{Y}, \tag{2.20c}$$

$$\alpha_{dy} \geq \Gamma_{dy}^{(\beta)}, \qquad \forall d \in \mathscr{D}, \forall y \in \mathscr{Y}, \forall \beta \in \mathscr{B}, \tag{2.20d}$$

$$\Omega_1 = \{U_l, C_l, R_l, \alpha_{dy}\}, \qquad \forall d \in \mathscr{D}, \forall y \in \mathscr{Y}. \tag{2.20e}$$

The constraints related to the ESS allocation are given by (2.16a)-(2.16c). In the initial stage of the Benders decomposition, the approximated cost of the subproblem associated with day d and year y (α_{dy}), is assigned with the pre-defined lower bound for the subproblem cost $\underline{\alpha}$. As the decomposition algorithm progresses, it improves the approximation by the set of Benders cuts ($\Gamma_{dy}^{(\beta)}, \forall d \in \mathscr{D}, \forall y \in \mathscr{Y}, \forall \beta \in \mathscr{B}$), which are added to the master problem for all the Benders iteration ($\forall \beta \in \mathscr{B}$) as shown in (2.20d) (see (2.24)).

$$LB = \sum_{l \in \mathscr{L}} (ic_E^f U_l^{(\beta)*} + ic_E^p R_l^{(\beta)*} + ic_E^e C_l^{(\beta)*}) + \sum_{y \in \mathscr{Y}} \sum_{d \in \mathscr{D}} \alpha_{dy}^* \tag{2.21}$$

After solving the master problem, the lower bound for the total planning cost (LB) is updated with the optimal objective value as shown in (2.21) ((β)* indicates that it is the identified optimal solution at βth Benders iteration).

Subproblem - Operation Stage

In the subproblem associated with day d and year y, a daily PWL-OPF model evaluates the operational benefits of ESSs with respect to the dispatchability and losses minimization under the compliance with the grid constraints. The dispatch plan embedding the offset profile is computed to follow the prosumption scenarios. Meanwhile, the dispatchability with respect to the dispatch plan is evaluated in terms of uncovered dispatch error while maximizing the exploitation of the determined ESS for compensation of the dispatch error. The subproblem corresponding to the dispatch operation for day-type d and year y is given in (2.22). As indicated in (2.22a), the objective of the subproblem is to minimize the uncovered dispatch error, the absolute value of the offset profile, and the grid losses, with the set of optimization variables defined by (2.22g). The constraints include power flow equations and security constraints (see (2.22b)) along with the set of equations associated with the dispatch (see (2.22c)) described in Sec. 2.6.1. Moreover, (2.22d) represents the constraints determining the operation characteristics of an ideal ESSs. The constraints (2.22e) and (2.22f) modelling the ESSs' power ratings and energy reservoirs are fixed to the optimal solution given by the master problem.

$$\min_{\Omega_2} : SC_{dy} = N_{dy} \sum_{t \in \mathscr{T}} (w_f \sum_{l \in \mathscr{L}} |F_{lt}^E| + \sum_{\phi \in \Phi_d} \lambda_\phi (w_e | \sum_{l \in \mathscr{L}} \epsilon_{l\phi t}| + w_l \sum_{l \in \mathscr{L}} r_l f_{l\phi t})) \tag{2.22a}$$

Subject to:

$$\Theta^{E}_{PWL}(\varphi^{E}_{\phi t}) \geq 0, \qquad \forall \phi \in \Phi_{dy}, \forall\, t \in \mathscr{T}, \tag{2.22b}$$

$$\Xi(\nu_{dy}) \geq 0, \tag{2.22c}$$

$$\Lambda(\pi_{l\phi}) \geq 0, \qquad \forall\, l \in \mathscr{L}, \forall \phi \in \Phi_{dy}, \tag{2.22d}$$

$$R_l = R_l^{(\beta)*} : \mu_{ldy}, \qquad \forall\, l \in \mathscr{L}, \tag{2.22e}$$

$$C_l = C_l^{(\beta)*} : \vartheta_{ldy}, \qquad \forall\, l \in \mathscr{L}, \tag{2.22f}$$

$$\Omega_2 = \{\varphi^{E}_{\phi t}, \nu, \pi_{\phi}\}, \qquad \forall\, l \in \mathscr{L}, \forall\, t \in \mathscr{T}, \forall \phi \in \Phi_{dy}. \tag{2.22g}$$

where w_f, w_e and w_l are the weight coefficients for the offset profile, the dispatch error, and the grid losses, respectively. μ_{ldy} and ϑ_{ldy} are the dual variables associated with constraints fixing the value ESS power rating and energy reservoir to the optimal solution of the master problem. The upper bound of the total planning cost UB is calculated by adding the optimal investment cost obtained from the master problem and the sum of parallel subproblem costs over all day-types and years as shown in (2.23).

$$UB = \sum_{l \in \mathscr{L}} (ic^{f}_{E} U_l^{(\beta)*} + ic^{p}_{E} R_l^{(\beta)*} + ic^{e}_{E} C_l^{(\beta)*}) + \sum_{y \in \mathscr{Y}} \sum_{d \in \mathscr{D}} SC^{*}_{dy}. \tag{2.23}$$

Values of the dual variables linked to the subproblem for day-type d and year y obtained at βth iteration are provided as inputs to the master problem in the next iteration to form the Benders cuts as shown in (2.24)).

$$\Gamma^{(\beta)}_{dy} = \big[SC^{*}_{dy} - \sum_{l \in \mathscr{L}} (\mu_{ldy}(R_l - R_l^{(\beta)*}) - \vartheta_{ldy}(C_l - C_l^{(\beta)*}))\big]. \tag{2.24}$$

2.10 Simulations

2.10.1 Simulation Configuration

In this section, the proposed method is tested with respect to an existing Swiss distribution network hosting a large capacity of renewable generation (see Fig. 2.4). The network's base voltage is 21kV, and the base 3 phase power is 6MVA. The total capacity of the PV generation is 2.7MWp, whereas the total capacity of hydropower generation is 805kVA. The power generation from PV panels is uncontrollable and inherently stochastic. By contrast, we assume that the hydropower generation can be dispatched and thus the generation uncertainty is negligible.[7] The planning horizon is set to 10 years. The annual growth rate of load consumption is considered as 3%. The discount rate r_{dis} is set to 7%. The load consumption is considered to be constant. All the parameters related to the investment of ESSs are listed in Table 2.1. The candidate nodes for ESSs installation are set according to the indications of the operator of this network. The stochastic nature of load consumption and PV injections is considered

[7] However, in reality, weather, and in particular precipitation and runoff, is of great relevance for hydropower generation. Therefore, the seasonal variability and uncertainty in prediction can be high, and they should be considered as operation scenarios for a more reliable planning solution in a real-life use of the planning tool.

by generating operating scenarios based on the historical data provided by the local DSO. In order to mitigate the computational burden, we assume that the seasonal variation of the prosumption over the year can be represented with 8 typical days. All the days are independent and thus not linked to each other. For each day type, the uncertainty of the forecast is modeled by generating 1000 prosumption scenarios, which are reduced to 10 scenarios based on K-medoids clustering algorithm [71]. (See Sec. A.1 for the detailed information regarding scenario generation and reduction method used in this chapter.) The dispatch time interval for a daily operation is set to 15 min. The penalty cost for the dispatch error is set to \$700/MWh. It is worth observing that this price is intentionally set to be substantially higher than the typical imbalance cost observed in power energy markets [72] to put a high priority on achieving dispatchability of the distribution network.

Table 2.1: ESS main parameters and candidate nodes for simulation

Maximum power rating per site	7MW	Maximum energy reservoir per site	7MWh
Installation cost for energy reservoir	\$300/kWh	Installation cost for power rating	\$200/kVA
Capital investment cost per site		\$0.1Million	
Candidate nodes for ESS		4, 16, 27, 41, 45	

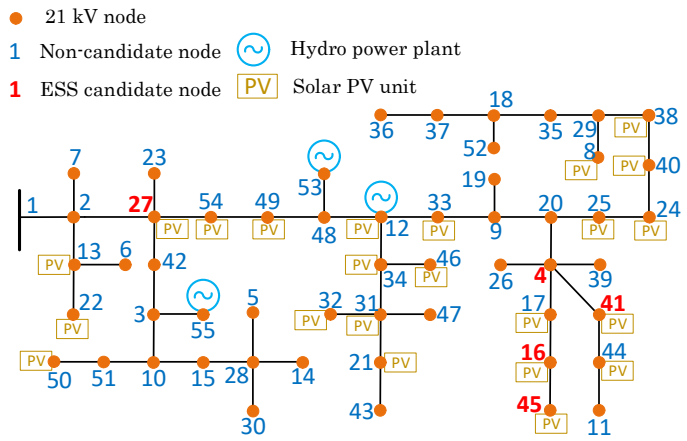

Figure 2.4: Considered real 55 node distribution network.

2.10.2 Simulation Result

To verify the effectiveness of the ESS control scheme, we analyse the simulation results considering two cases that differ in control approaches: case 1 with the offset profile embedded into a dispatch plan and case 2 without it. The optimal siting and sizing of ESSs are shown in Table 2.2 and Table 2.3, where the operational advantages of the ESS allocation are indicated in terms of penalty cost for the dispatch error and grid losses. At Node 4, both of the ESS energy reservoirs and power ratings are bigger in case 1 than in case 2. At Node 27, the ESS energy

reservoir is bigger in case 1, while the power ratings are similar in the two cases (see Table 2.2). The overall investment cost is $0.15 Million larger in case 1, and the annual uncovered dispatch error is 51.77 MWh lower in case 1 (see Table 2.3), leading to reduction of $0.2 Million in the total cost. This difference in allocation and the dispatch result can be associated with the efficiency of the ESS control scheme. Indeed, thanks to the offset profile, the utilization of the energy reservoir capacity of each dispatch interval can be optimized considering not only the dispatch error observed for the corresponding time interval but also the error anticipated in upcoming intervals by controlling the power injection into the ESSs and adjusting the SoE for each time interval.

The operational advantage of the ESS allocation and the superiority of case 1 over case 2 is well visualized in Fig. 2.5. It illustrates the operation simulation for day-type 1, showing the prosumption prediction based on 10 prosumption scenarios, the dispatch plan, and the active power flow through GCP for each scenario in the case of no ESS (see Fig. 2.5.(a)), and in the two cases associated with the optimal ESS allocation with and without the offset profile (see Fig. 2.5.(b) and Fig. 2.5.(c), respectively). Due to the prediction error of the prosumption forecast, the significant magnitude of power deviation from the scheduled power is observed, especially in the time intervals when the PV power production is high. Therefore, without the support of ESSs compensating for the dispatch error, the DSO is expected to pay a substantial amount of penalty cost. On the contrary, optimally allocated ESSs, effectively reduce the possible dispatch error, enforcing the active power flow through the GCP for each scenario to follow the dispatch plan. The difference between case 1 and case 2 is shown in the dispatch plan. In case 2, the dispatch plan is equivalent to the total prosumption profile considering the grid losses. On the other hand, the dispatch plan in case 1 deviates from the total prosumption prediction profile, especially during the daytime because of the implementation of the offset profile. The offset profile takes value, particularly at the time intervals when the notable amount of dispatch error at the GCP is anticipated for the following time intervals. The power charge/discharge of the ESSs corresponding to the offset profile can adjust their SoE levels to have enough flexibility to cope with the imminent uncertainties. In this way, the uncovered dispatch error can be additionally reduced compared to the case 2.

Table 2.2: ESS allocation results of PWL-OPF based ESS planning strategies with offset profile (Case 1) and without (Case 2).

Case	Location	Power rating	Energy reservoir
1	4	1.03MVA	1.99MWh
	27	521kVA	853kWh
2	4	915kVA	1.57MWh
	27	523kVA	773kWh

The effectiveness of the optimal ESS allocation accompanying the control scheme is assessed quantitatively by comparing the annual uncovered dispatch error in different cases. The difference in energy is then translated into a considerable gap in the total cost for 10 years of operation: $9.48 Million with the default system configuration, and $1.54 Million with

Table 2.3: Cost and Operational advantage comparison of PWL-OPF based ESS planning strategies with offset profile (Case 1) and without (Case 2).

Horizon		Case 0	Case 1	Case 2
10 yrs	Total cost ($Million)	9.48	1.54	1.74
	Investment cost ($Million)	-	1.36	1.19
	Penalty cost ($Million)	9.48	0.18	0.55
1 yr	Uncovered error (MWh)	1354.27	26.91	78.68
	Grid losses (MWh)	55.24	45.09	46.03
	Consumed energy (GWh)	7.357	7.488	7.419

the optimal ESS allocation integrating the offset profile. Consequently, the result shows the economic and technical excellence of investing in ESSs for the interest of the DSO in attaining the controllability of the active power flow through the GCP. Moreover, we successfully demonstrate that the implementation of the offset profile improves the potential of ESSs to handle the RERs uncertainties by maximizing ADN flexibility.

2.10.3 Approximation Accuracy of PWL-OPF model with Different Discretization Steps

The approximation accuracy of the PWL-OPF model depends on the number of discretization steps (Υ) and the maximum value of active power (P_l^{max}) and the reactive power (Q_l^{max}). As explained in Sec. 2.7.1, the maximum complex power value is determined based on preliminary load flow with the prosumption scenarios. Through running a daily operation with 24 time intervals, we compare the approximation accuracy of the PWL-OPF model and the computation time using different discretization steps varying from 10 to 40. As shown in (2.25), the accuracy is measured based on the error (in Ampere) between longitudinal current value expressed by the state variable of squared longitudinal current (f_l) and the value calculated by the values of complex power flow and nodal voltage. The CDF curve of approximation error is illustrated in Fig. 2.6. We can observe that the approximation accuracy substantially improved starting from the 20 discretization steps. Representative values of approximation error are given in Table 2.4 along with the computation time for each model. The error of approximation decreases with the number of discretization steps. Indeed, the higher number of discretization steps leads to an increased computational cost. Therefore, the trade-off between the approximation accuracy and the number of discretization steps should be appropriately considered when employing the PWL-OPF model.

$$err = \left(\sqrt{f_{l\phi t}} - \sqrt{\left(|P^t_{l\phi t}|^2 + |Q^t_{l\phi t} + j\, v_{up(l)\phi t} b_l|^2 \right) / v_{up(l)\phi t}} \right) * I_{base} \quad (A) \tag{2.25}$$

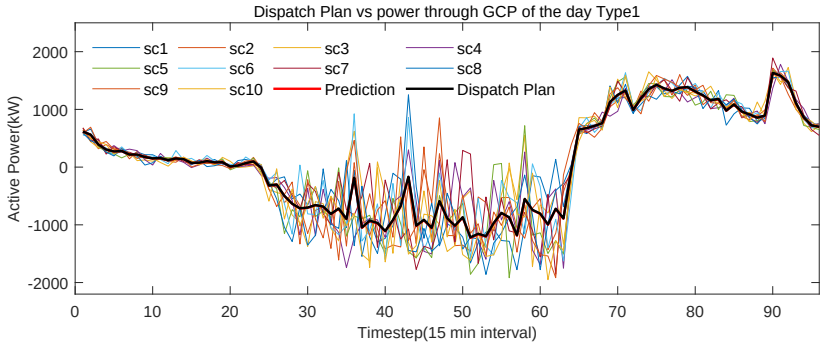

(a)

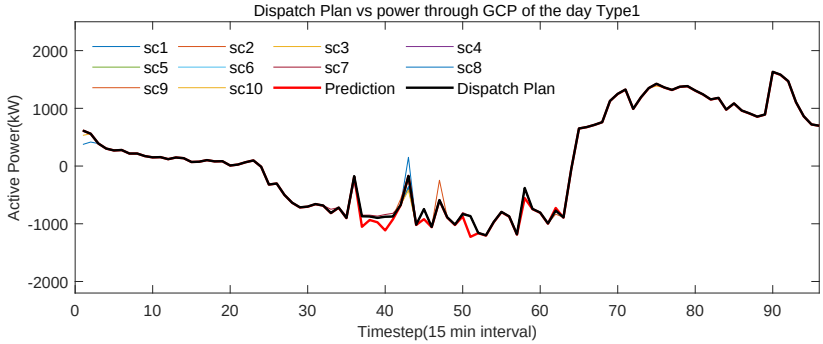

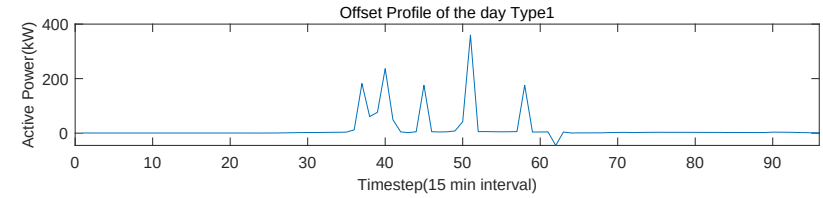

(b)

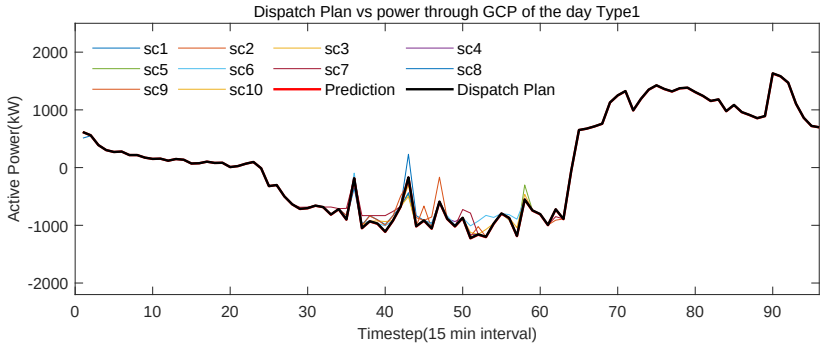

(c)

Figure 2.5: Prosumption prediction, dispatch plan and active power through the GCP in each scenario (sc): (a) Case 0 (No ESS), (b) Case 1 (With ESS integrated with offset profile), (c) Case 2 (With ESS and without offset profile).

Table 2.4: Comparison on accuracy of longitudinal current calculation with respect to PWL-OPF models with different discretization step numbers.

Υ	Error in longitudinal current (A)				Time to solve a single subproblem (s)
	min	max	mean	median	
10	3.40E-3	19.38	1.14	0.70	260
20	2.65E-6	1.33	0.07	0.03	408
40	5.11E-7	0.47	0.03	0.01	885

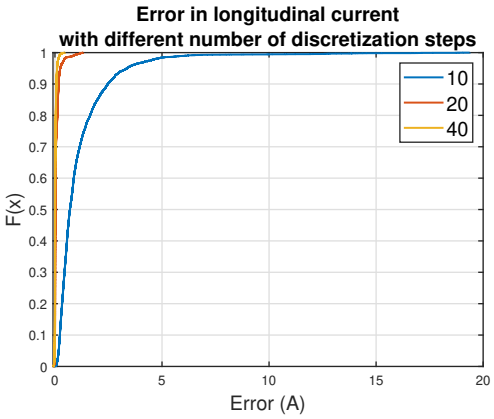

Figure 2.6: Normalized error in longitudinal current (%) with respect to PWL-OPF models with different discretization step numbers.

2.10.4 Discussion on the Integration of the Offset Profile

We showed that the integration of the offset profile improved the ADN's dispatchability by increasing the ESSs capacity, leading to a slight decrease in total planning cost compared to the ESS allocation without an offset profile. However, some concerns are worth discussing regarding the integration of the offset profile. First, the planning results differ depending on the relative weight coefficient of the offset profile and dispatch error. For example, when the weight for the offset profile is minimal, the ESS sizes get bigger such that more energy margin is procured by ESS energy reservoirs, and vice versa. Indeed, in this case, the ratio between the cost parameters of ESS investment and the dispatch error penalty will affect the economic trade-off between ESS investment cost and the dispatch error. As the offset profile's weight coefficient can largely impact the planning cost, we acknowledge that a solid strategy for determining the coefficient value is required. However, it is challenging to determine the values by quantifying the relative importance of the dispatch error and the offset profile, as it is also subjected to the stochastic characteristics of the prosumption profiles. Moreover, this ambiguity in the offset profile's weight coefficient setting complicates its value's ratio to the weight coefficient associated with grid losses. In this case, it is worth assessing the trade-off between the economic benefit the offset profile may bring vs. the discussed aspects regarding its integration into the OPF model for further application.

2.11 Conclusion

In this chapter, we have proposed an effective tool for the optimal ESS allocation within an ADN to achieve its dispatchability. The planning tool takes into account the so-called ESS offset profile into the dispatch plan. The offset profile quantifies the necessary power exchange of the ESS to optimize the exploitation of its energy reservoir capacity. The operational benefit of ESSs is evaluated through the daily operation of ADN, which is modeled by a PWL approximated convex OPF model. This model is advantageous since it guarantees the presence of a global optimal solution while accounting for the operational conditions of the network. Then, Benders decomposition is applied to handle the computational complexity of the planning problem. The effectiveness of the proposed method is validated through simulations conducted on a real Swiss ADN comprising 55 nodes hosting a large capacity of distributed renewable generation. The result underpins that the ESS allocation minimizes the ADN dispatch error.

3 Optimal Planning of Energy Storage Systems based on Exact Convexified OPF Model

3.1 Highlights

As in Ch. 2, this chapter also presents a method for the optimal siting and sizing of ESSs in ADNs to achieve their dispatchability. Compared to the linearized OPF model of Ch. 2, in this chapter, the ADN's operational constraints are accounted by an exact AC-OPF model. The proposed formulation relies on the so-called AR-OPF method: it expresses a convex full AC-OPF, which is proven to provide a global optimal and exact solution in the case of radial power networks. The AR-OPF is coupled with the proposed dispatching control resulting in a two-level optimization problem. In the first block, the site and size of the ESSs are decided along with the level of dispatchability that the ADN can achieve. Then, in the second block, the adequacy of the ESS allocation, and the feasibility of the network's operating points, are verified over operating scenarios using the Benders decomposition. Consequently, the optimal size and site of the ESSs are adjusted. To validate the proposed method, simulations are conducted on a real Swiss ADN hosting a large amount of PV generation.

This chapter presents the work published in:

Yi, Ji Hyun, Rachid Cherkaoui, and Mario Paolone. "Optimal allocation of ESSs in active distribution networks to achieve their dispatchability." ***IEEE Transactions on Power Systems*** **36.3 (2020): 2068-2081.**

3.2 Organization of the Chapter

The first part of the chapter includes the state-of-the-art of the OPF model embedded in planning strategies, with highlights on the accuracy of convexified OPF models. After defining the problem statement of this chapter, the formulation of AR-OPF model is re-called. The third part includes the structure of the ESS allocation problem employing the AR-OPF model and its decomposition to tackle the complexity of the problem. Finally, the proposed methodology is tested on a real Swiss distribution system.

3.3 State-of-the-art of the OPF Model Embedded in Planning Strategies

It is worth observing that the characteristics of the chosen control strategy and the subsequent operational conditions of the system largely influences the optimal level of ADN's dispatchability under given ESS assets. Therefore, it is needless to mention that the OPF that accurately models operation and control of the ADN is indispensable for the optimal planning of ESSs. However, the OPF-based ESSs planning is intrinsically burdensome to solve due to the non-convexity of the full AC-OPF model. A considerable amount of literature has been devoted to tackle this aspect of OPF model in order to integrate it into planning frameworks. In light of this, in this chapter, this section presents a literature review of OPF models used in ADN planning problems.

There exist meta-heuristic methods such as the particle swarm optimization (PSO) algorithm used in [63], and the fuzzy PSO algorithm used in [54] and [64]. The Author of [54] proposed a method of optimal allocation of ESSs for risk mitigation of distribution utilities with high renewable penetration, applying fuzzy particle swarm optimization algorithm to solve a non-convex OPF problem. In [73], the Authors compared three meta-heuristic methods employed in the optimization process for batteries integration in distribution systems: genetic algorithm, differential evolution, and evolutionary PSO (EPSO). The EPSO showed the best performance in terms of solution quality and computation time among the three meta-heuristic techniques. However, these meta-heuristic solution approaches cannot always guarantee the global optimum or even a feasible solution.

In Ch. 2, the non-convexity of the AC-OPF model was tackled by a linear power flow model for achieving better tractability. This type of model can achieve an optimal solution with acceptable approximation errors compared to the original OPF solution and can be applied for both radial and meshed networks. For example, the work in [74], [75] employed linear OPF models using First order Taylor's approximation of non-linear power flow equations. In [74], the Author formulated a model predictive control of ESSs by linearly approximating the OPF equations to express nodal voltages, branch currents and losses as linear products at given operating points. In [75], the Authors employed Talyor series expansion around the no-load operating point to linearly approximate the power flow. In the multi-stage joint planning model proposed in [76], the Kirchhoff's laws are used to linearize the voltage drop in the power flow formulation. The linear power flow equations in the planning strategies of [77] and [78] omitted the mathematical equation modeling the line current, thus the impact of load stochasticity (represented by scenarios) on the physical compliance with the line ampacity limit cannot be accurately evaluated. In [79], the power losses is linearized through the Venikov method, assuming that the system components are designed to operate near to the nominal current. However, the main drawback of linear OPF models lies in the approximation accuracy of physical quantities in the power flow as it depends on the operating point, possibly resulting in solutions characterized by a quality that can vary with the operating condition. In Ch. 2, we used PWL-OPF model where the nonlinear terms such as losses are approximated by employing piecewise linearized function as discussed in Sec. 2.7.1. However, as shown in

Sec. 2.10.3, the accuracy of the model highly depends on the number of discretization steps, which determines the computational burden. Besides, the preliminary awareness on the possible range of state variables is required to guarantee the solution quality, which is not always available.

Alternatively, the relaxation methods include the semi-definite programming (SDP) [21,80] and the second-order cone programming (SOCP) relaxation [49,52,53,81]. In both of [21], [80], ESSs are allocated to reduce the voltage violations. The planning problem is formulated as two-stage optimization problem that consists of investment stage and scenario-based operation evaluation stage. The SDP relaxation is adopted into the OPF model to solve operation problem for each scenario. The SOCP relaxation proposed in [82] has been implemented for the optimal ESS allocation in radial networks due to its superior computational efficiency than the SDP relaxation. The Authors of [52] further utilized the SOCP relaxed model for the ESS allocation and operation to minimize the grid losses and imported power in the ADN. In [53], an ESS planning strategy was developed relying on the SOCP-OPF model with the objective of providing ancillary services to the TSO, and to cope with the wind variability. In [62], even though the optimization problem for day-ahead operation is modeled as a non-convex OPF problem and solved by implementing a meta-heuristic method, the optimization on the real-time operation is solved thanks to the relaxed SOCP-based OPF model. The work in [49] tackled the ESS planning and operation problem by decomposing it into two stages: the first stage determines the total ESSs' size to prevent grid constraints violations due to PV power imbalance, and the second stage allocates ESSs with optimal sizes by employing the SOCP-OPF to minimize the energy cost. In the first stage, the PV power imbalance that causes grid constraint violations is calculated before determining the total required ESSs size. In the second stage, by employing the SOCP relaxed OPF, the ESSs are allocated to the optimal sites to minimize the energy cost. Meanwhile, the Authors stated that the objective function and constraints should satisfy some necessary conditions to guarantee the exactness of the SOCP-OPF solution and suggested a formula to verify the exactness a-posteriori. The main drawbacks of the SOCP-OPF model were explicitly underlined in [83] by the fact that the exactness of the solution cannot be guaranteed especially in the presence of reverse line power flows and for cases where the upper bound of nodal voltage and the line ampacity constraints are binding. This significantly limits the method's applicability to ADNs hosting DERs with large capacities. Moreover, the model neglects the transverse elements of the lines, which can produce an infeasibility of the solution, especially when ADNs are composed of underground coaxial cables.

The work in [1] solves this problem by proposing the AR-OPF model to convexify the AC-OPF for radial networks. The contribution demonstrates that, in the AR-OPF problem comprising an objective function strictly increasing with the grid losses, the conditions for the exactness of the solution are mild and hold for realistic distribution networks. The AR-OPF was implemented in subsequent works on the optimal ESS planning problem while embedding network reconfiguration with the objective of minimizing grid losses, voltage deviation and line congestion [14].

3.4 Problem Statement and Contributions

We propose an operation-driven planning strategy of ESSs to achieve the dispatchability of the ADN based on the AR-OPF model. The objective of achieving dispatchability requires a substantial and non-trivial modification of the AR-OPF as well as of the solution approach proposed in [14] in order to reach the exactness of the relaxed OPF. Moreover, we formulated the ESS allocation problem into two blocks by modifying the objective term, constraints and variables related to the dispatch error. vMeanwhile, we apply the Bender's decomposition to handle the multi-layered decisions with numerous scenarios [66]. The contributions of the chapter are two as follows.

1. The optimal allocation of ESSs is determined based on an exact convex model of the OPF to address the dispatchability of the ADN in the presence of prosumption uncertainty, while accurately reflecting the operational condition of the ADN.

2. The structure of the planning problem, and the mathematical formulation of the ADN operation, are defined accounting for the necessary conditions to ensure the tightness of the OPF relaxation.

3.5 Augmented Relaxed Optimal Power Flow

As discussed in [1], for a radial power network, the power flow equations are given as (2.10). For the sake of readability, a part of (2.10) is repeated here as (3.1a)-(3.1g). By applying the SOCP relaxation on the equation defining the longitudinal current, the equality in (3.1e) is replaced with an inequality, as in (3.1h) [82]. Hereafter, the SOCP relaxed OPF model is called as the relaxed OPF (R-OPF) model.

$$S_l^t = s_l + \sum_{m\in\mathscr{L}} \mathbf{H}_{l,m} S_l^t + z_l f_l - j(v_{up(l)} + v_l) b_l, \qquad \forall l \in \mathscr{L}, \tag{3.1a}$$

$$S_l^b = s_l + \sum_{m\in\mathscr{L}} \mathbf{H}_{l,m} S_l^t, \qquad \forall l \in \mathscr{L}, \tag{3.1b}$$

$$v_l = v_{up(l)} - 2\Re\left(z_l^*\left(S_l^t + j v_{up(l)} b_l\right)\right) + |z_l|^2 f_l, \qquad \forall l \in \mathscr{L}, \tag{3.1c}$$

$$v^{min} \le v_l \le v^{max}, \qquad \forall l \in \mathscr{L}, \tag{3.1d}$$

$$f_l = \frac{|S_l^t + j v_{up(l)} b_l|^2}{v_{up(l)}} = \frac{|S_l^b - j v_l b_l|^2}{v_l}, \qquad \forall l \in \mathscr{L}, \tag{3.1e}$$

$$I_l^t = \frac{|P_l^t|^2 + |Q_l^t|^2}{v_{up(l)}} \le I_l^{max}, \qquad \forall l \in \mathscr{L}, \tag{3.1f}$$

$$I_l^b = \frac{|P_l^b|^2 + |Q_l^b|^2}{v_l} \le I_l^{max}, \qquad \forall l \in \mathscr{L}, \tag{3.1g}$$

$$f_l \ge \frac{|S_l^t + j v_{up(l)} b_l|^2}{v_{up(l)}}, \qquad \forall l \in \mathscr{L}. \tag{3.1h}$$

In order to avoid any inexact solution of the R-OPF model (*i.e.*, any solution that makes the

left-hand side of (3.1h) strictly greater than the right-hand side), the Authors of [1] introduced auxiliary variables $\bar{f}_l$, $\bar{S}_l = \bar{P}_l + j\bar{Q}_l$, $\bar{v}_l$ and $\hat{S}_l = \hat{P}_l + j\hat{Q}_l$ to formulate the AR-OPF model. The branch power flow, nodal voltage, and current equations are defined as well with the set of the auxiliary variables, as in (3.2a)-(3.2g). Eq. (3.2a) and (3.2b) indicate the lower bound of branch power flow at the sending end and the receiving end of line l. The upper bound nodal voltage is determined correspondingly with (3.2c). Likewise, the branch power flow equations for upper bound power flow variables are shown by (3.2d) and (3.2e). Eq. (3.2f) and (3.2g) express that the upper bound of the squared longitudinal current f_l should be decided by the maximum of absolute complex power flow from both sides of line l. The magnitude of squared current at the sending and receiving end are also defined by employing maximum of absolute complex power flow variables as shown in (3.2i) and (3.2j). In this way, the ampacity limit constraints (3.1f) and (3.1g) are replaced by (3.2i)-(3.2l). The voltage constraint is modeled as in (3.2h). Eqs (3.2m) and (3.2n) indicate that the upper-bound auxiliary variable value of active and reactive power flow through each line should be bounded by maximum possible value of active and reactive power flow approximately calculated in advance by considering line ampacity limit and nodal voltage limit. The constraint is added to complete the set of equations required to guarantee the exactness.

$$\hat{S}_l^t = s_l + \sum_{m\in\mathscr{L}} \mathbf{H}_{l,m}\hat{S}_l^t - j(\bar{v}_{up(l)} + \bar{v}_l)b_l, \qquad \forall l \in \mathscr{L}, \quad (3.2a)$$

$$\hat{S}_l^b = s_l + \sum_{m\in\mathscr{L}} \mathbf{H}_{l,m}\hat{S}_l^t, \qquad \forall l \in \mathscr{L}, \quad (3.2b)$$

$$\bar{v}_l = \bar{v}_{up(l)} - 2\Re\Big(z_l^*(\hat{S}_l^t + j\,\bar{v}_{up(l)}b_l)\Big), \qquad \forall l \in \mathscr{L}, \quad (3.2c)$$

$$\bar{S}_l^t = s_l + \sum_{m\in\mathscr{L}} \mathbf{H}_{l,m}\bar{S}_l^t + z_l f_l - j(v_{up(l)} + v_l)b_l, \qquad \forall l \in \mathscr{L}, \quad (3.2d)$$

$$\bar{S}_l^b = s_l + \sum_{m\in\mathscr{L}} \mathbf{H}_{l,m}\bar{S}_l^t, \qquad \forall l \in \mathscr{L}, \quad (3.2e)$$

$$\bar{f}_l v_l \geq |\max\{|\hat{P}_l^b|, |\bar{P}_l^b|\}|^2 + |\max\{|\hat{Q}_l^b - j\,\bar{v}_l b_l|, |\bar{Q}_l^b - j\,v_l b_l|\}|^2, \qquad \forall l \in \mathscr{L}, \quad (3.2f)$$

$$\bar{f}_l v_{up(l)} \geq |\max\{|\hat{P}_l^t|, |\bar{P}_l^t|\}|^2 + |\max\{|\hat{Q}_l^t + j\,\bar{v}_{up(l)}b_l|, |\bar{Q}_l^t + j\,v_{up(l)}b_l|\}|^2, \qquad \forall l \in \mathscr{L}, \quad (3.2g)$$

$$v^{min} \leq v_l, \;\; \bar{v}_l \leq v^{max}, \qquad \forall l \in \mathscr{L}, \quad (3.2h)$$

$$I_l^t v_{up(l)} \geq |\max\{|\hat{P}_l^t|, |\bar{P}_l^t|\}|^2 + |\max\{|\hat{Q}_l^t|, |\bar{Q}_l^t|\}|^2, \qquad \forall l \in \mathscr{L}, \quad (3.2i)$$

$$I_l^b v_l \geq |\max\{|\hat{P}_l^b|, |\bar{P}_l^b|\}|^2 + |\max\{|\hat{Q}_l^b|, |\bar{Q}_l^b|\}|^2, \qquad \forall l \in \mathscr{L}, \quad (3.2j)$$

$$I_l^t \leq (I_l^{max})^2, \qquad \forall l \in \mathscr{L}, \quad (3.2k)$$

$$I_l^b \leq (I_l^{max})^2, \qquad \forall l \in \mathscr{L}, \quad (3.2l)$$

$$\bar{P}_l^t \leq P_l^{max} = \frac{v^{max} I_l^{max}}{\sqrt{2}}, \qquad \forall l \in \mathscr{L}, \quad (3.2m)$$

$$\bar{Q}_l^t \leq Q_l^{max} = \frac{v^{max} I_l^{max}}{\sqrt{2}}, \qquad \forall l \in \mathscr{L}. \quad (3.2n)$$

The nodal voltages and branches' ampacity constraints are defined with the auxiliary variables (*i.e.*, (3.2h)-(3.2j)) to construct a conservative and convex set of constraints. The

network model defined by (3.1b)-(3.1e) and (3.2a)-(3.2n) is called as the augmented-OPF (A-OPF), and its feasible solution space is proved to be a subset of the one of original OPF. As already shown in [1], the set of grid constraints employing the auxiliary variables slightly shrinks the original feasible solution space in correspondence of undesirable operation points of the network (*e.g.*, near the upper bound of nodal voltages or branches' ampacity limits).[8]

The AR-OPF model is obtained by applying SOCP relaxation on the A-OPF model (*i.e.*, by replacing (3.1e) with (3.1h)). Under the pre-requisite conditions defined in [1], it is proven that for every feasible solution of the AR-OPF, there exists a feasible solution of the A-OPF and also for the original OPF with the same power injection. Moreover, every optimal solution of the AR-OPF that satisfies (3.1e) is an optimal solution of the A-OPF. It is noteworthy that (3.1e) is satisfied in the AR-OPF model when the objective function is strictly increasing with respect to the squared longitudinal line current f_l, or the grid losses. The pre-requisite conditions to guarantee the exactness are defined by the grid parameters and they are mild enough to hold for general and realistic radial distribution networks. Since the Authors of [1] have rigorously proved all the statement above regarding the exactness of the AR-OPF solution [1], the readers are encouraged to refer to [1] for further details.

For the sake of readability, (3.1a)-(3.1c), (3.1h), and (3.2) are grouped and represented by $\Theta(\varphi) \geq 0$ where $\varphi = \{S^t, v, f, \hat{S}^t, \bar{v}, \bar{f}, \bar{S}^t, s\}$ is the set of variables. The AR-OPF problem is defined as (3.3a), where $C(r_l f_l)$ is a cost function of the grid losses. The notation without subscript corresponds to the vector of variables and parameters for buses/lines $\forall l \in \mathscr{L}$.

$$\min_{\varphi} \sum_{\forall l \in \mathscr{L}} C(r_l f_l) \tag{3.3a}$$

$$\text{subject to: } \Theta(\varphi) \geq 0. \tag{3.3b}$$

3.5.1 Discussion on the Exactness and the Applicability of the Model for Various Operational Objectives

It is noteworthy to observe a limitation of the proposed model related to the condition on the objective function for guaranteeing the exactness of the solution. The condition applies the same for general SOCP relaxation. Theoretically, the Author of [1] proved that the exactness of the AR-OPF solution is guaranteed if all the objective terms are strictly increasing with the grid losses. However, such condition may limit the applicability of the AR-OPF model to various control objectives. For example, the minimization of the nodal voltage deviations or control on ESS's energy level may not satisfy this condition, and having these objective terms within the objective function may affect the quality of the solution. Therefore, the appropriate modification of the AR-OPF model would be necessary for such control objectives. In [84],

[8] We verified that the compression of the solution space caused by the augmented constraints is small by following the some analysis reported in [1]. Under the case study shown in Sec. 5.10, we make one of two operating constraints (voltage upper bound constraint and ampacity constraint) binding at one node or line and relax the other one to find the difference between the physical state variables (nodal voltage-magnitudes and original current flow) and corresponding auxiliary variables. The difference between the nodal voltage-magnitude and the auxiliary one is 0.001%. The difference between the original current flow and the auxiliary one is equal to 0.2%.

the Authors investigated the solution inexactness of the general SOCP relaxation depending on different operational objectives, from which they observed the possible incompatibility between the identification of an exact solution and the efficient operation of the ADN with high penetration of distributed resources. In this case, instead of complying with the pre-requisite condition, the Authors proposed to tighten the relaxation by introducing an iterative algorithm that increasingly adds cutting planes to a SOCP-relaxed OPF model. The issue of the inexactness associated to the objective function given by the minimization of nodal voltages deviations is reported as well in [49]. In this regard, the Authors numerically evaluated the exactness to check the tightness of the SOCP relaxation in case the objective terms do not strictly increase with the grid losses. The Author of [85] proposed to improve the tightness of the SOCP relaxation by introducing an iterative algorithm that increases the total reactive power and adjusts its weight coefficient till the relaxation gap reduces below a tolerance value. The idea behind the approach suggests that the tightness of the SOCP relaxation highly depends on the relative dominance of the objective terms that strictly increases with the grid losses. This observation builds the basis of the modification of AR-OPF to include the modeling of ADN's dispatchability in the operation model.

3.6 Problem Formulation

The objective of the problem is to determine the optimal sizes and sites of ESSs so that the active power through the GCP follows the dispatch plan with minimal deviation. However, the dispatch error described by (2.4) does not increase while the total grid losses increase (see the necessary condition to guarantee the exactness of the AR-OPF model in Sec. 3.5). In order to verify this statement, we discuss the relationship between the dispatch error and the active power through the GCP instead of the grid losses, based on the fact that the active power through the GCP is strictly increasing with the grid losses [1]. The prediction error of the prosumption and the grid losses are random variables following normal distributions with zero mean value. Thus, it is intuitive to assume that the dispatch error, which is equivalent to the sum of prediction error of the prosumption and the grid losses over all buses/lines, is also a random variable with null mean value (a formal proof of this statement is still under investigation), and has neither positive nor negative correlation with the active power through GCP. Finally, the dispatch error does not have any correlation with the grid losses as well. Therefore, the exactness of the solution cannot be guaranteed if the objective value that corresponds to the objective term (2.4) is significant in magnitude compared to objective term regarding the total grid losses in the objective function of the AR-OPF model. This aspect leads to the undesirable coupling between the prosumption uncertainty and the exactness of the solution.

Therefore, we propose to decompose the problem into two blocks each consisting of an OPF problem. In this way, we can exclude (2.4) from the AR-OPF problem and convey it to another, approximated, OPF problem (the so-called 1st block problem), which aims to find the optimal level of dispatchability based on the ESSs investment cost and the imbalance penalty. The calculated dispatchability level, described as the leftover dispatch error rate

(LDER), is then used as a constraint in an AR-OPF model-based problem (the so-called 2nd block problem) to which the ADN must adhere.

The whole algorithm of the proposed approach is illustrated in Fig. 3.1. In the 1st block problem, the optimal ESS allocation, the daily dispatch plans, and the corresponding LDER are calculated employing linear approximated OPF ignoring the grid losses. Only the nodal voltage constraints are considered regarding the operational constraints, ignoring the ampacity limits to reduce the computational burden. Afterward, the outputs of the 1st block, which are the ESS allocation and the LDER, are used as inputs for the 2nd block problem.

In the 2nd block problem, the objective is to refine the optimal allocation of the ESSs, considering several operating scenarios and achieving the same level of LDER calculated in the 1st block problem. In this respect, the LDER is used as an additional constraint to an AR-OPF model, which considers the full AC-OPF as well as voltage constraints and branches' ampacity limits. Then, the size and site of the ESSs are iteratively adjusted thanks to the Benders decomposition. The 2nd block is decomposed into a master problem and several parallel subproblems. The master problem seeks for the optimal allocation taking into account the subproblem costs, which evaluate the sufficiency of the ESSs' capacity to comply with the LDER constraints over all prosumption scenarios. This iterative process starts initially by solving subproblems for a feasibility check of the ESS allocation resulting from the 1st block problem. The feasibility of the operation is evaluated by the unserved prosumption. Then, the ESSs' sizes and sites are re-allocated in the master problem such that the LDER constraints can be satisfied without any load curtailment. The system operation condition under the updated ESS allocation is evaluated in the parallel subproblems. Through the Benders iterations, the optimal solution of the ESS allocation is obtained as the upper-bound and the lower-bound of the total planning cost converge close to each other.

Decomposing the planning problem into two blocks avoids the exactness to rely on the relative magnitude of the dispatch error with respect to the grid losses. However, note that the unserved energy is not strictly increasing with grid losses. For instance, if RERs are curtailed in the case of normal direction of power flow, this leads to an increase of total grid losses. On the other hand, if load consumption is curtailed (increase of unserved energy), the grid losses will decrease, concluding that the condition does not hold. In this context, the solution inexactness may be observed when the ESSs sizes are not enough to satisfy the LDER constraints. However, as the planning algorithm reaches the optimal investment solution where the unserved energy will be near zero, the objective term associated with grid losses can become dominant in magnitude, and thereby, the tightness of the SOCP relaxation can be ensured. Moreover, the tightness can be numerically evaluated a-posteriori by the criterion suggested in [49].

3.6.1 Key Differences with the Planning Approach in Ch. 2

In spite of the shared objective and the similar decision making stages, the methodology introduced in the previous chapter and this chapter have significant differences in the solution approach for the OPF problem and the overall structure of the problem formulation. In Ch. 2, the attention is mainly on maximizing the controllability of the allocated ESSs by integrating

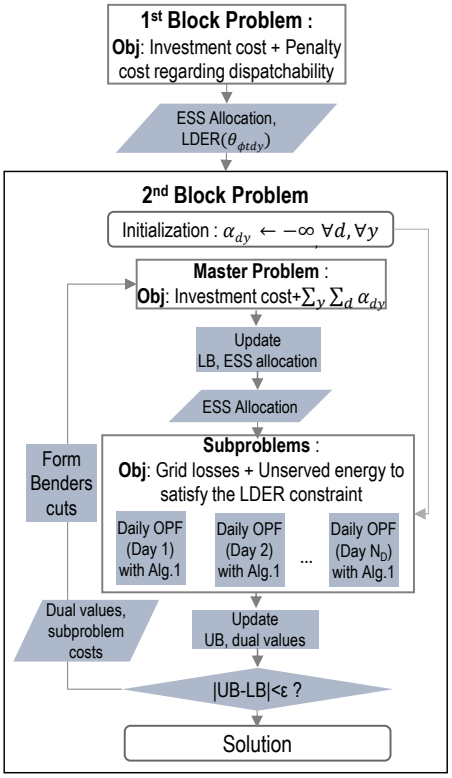

Figure 3.1: Full algorithm of the proposed method.

their control strategy in the OPF problem. In this respect, the PWL-OPF model is used to approximate the full AC-OPF. It frees up the choice of objective by relaxing the exactness of the solution, so that the ESSs' control strategy can be added to the objective function of the PWL-OPF problem along with the objective term regarding the minimization of dispatch error. The decision process of the ESS allocation can start directly with the initial stage of the Benders decomposition (see the left-hand side of Fig. 3.2). As the Benders iteration progresses, the optimal dispatchability level is determined within the subproblems in terms of the operational benefit brought by the ESS allocation.

In this chapter, in contrast, the primary interest lies in obtaining an accurate optimal solution regarding the operating points for the considered operation horizon. Therefore, the solution approach is designed to preserve the solution tightness of the SOCP relaxation of the AR-OPF model. In this regard, we separately treated the objective of minimizing the dispatch error apart from the AR-OPF problem by introducing it into another problem formulated based on a simplified linear OPF model. When the dispatchability level is calculated from this optimization problem, the AR-OPF problem is solved to check the compliance with the determined dispatchability level.

Another difference is that the offset profile is not included in the formulation in this chapter. In other words, the control strategy of ESSs is not integrated into their allocation strategy. In the previous chapter, the simulation result associated to the offset profile (Fig. 2.7) showed

that the magnitude of the offset profile is highly related to the magnitude of the prediction uncertainty. Therefore, it can be concluded that there is no specific correlation between the offset profile and the grid losses. Therefore, the objective term and constraints related to the offset profile should be removed from the 2nd block problem along with the term related to the dispatch error and conveyed to the 1st block problem. However, the offset profile that would be defined in the 1st block problem cannot guarantee the feasible operation once utilized in the 2nd block problem, because of the simplified and inaccurate network model in the 1st block. Moreover, as discussed in Sec. 2.10.4, a solid strategy of setting the relative weight coefficient of offset profile is not yet well-defined to promote the merits of the offset profile with respect to the ADN planning strategy. In this respect, the offset profile is dropped from the planning problem formulation in this chapter.

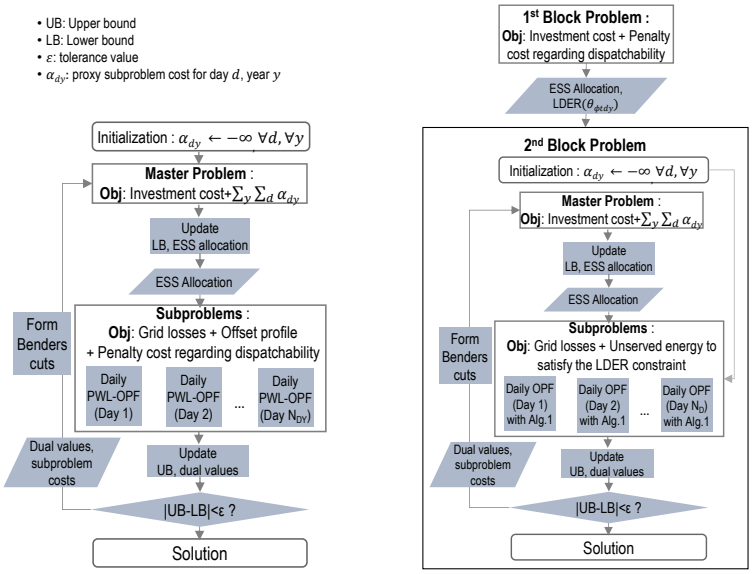

(a) (b)

Figure 3.2: The full algorithm: (a) Ch. 2, (b) this chapter.

3.6.2 1st Block Problem

We minimize the investment and total penalty costs over the planning horizon to find out the optimal allocation of the ESSs and the optimal dispatchability level. We embed an approximated OPF constraints for all operating scenarios into a two-stage mixed-integer linear programming (MILP) problem (see Sec. 5.5). The OPF is formulated by the linear Distflow model [86] in which shunt elements are considered, whereas the grid losses are neglected. In this way, the reactive power generated by the shunt impedance of the lines is considered in the nodal voltage constraints. Meanwhile, neglecting the formulation of the squared longitudinal current (f_l) (*i.e.*, losses) is less likely to affect the feasible solutions in this stage since the ampacity constraint is ignored. The dispatch plan follows the prosumption prediction, as in (3.4a), while the prosumption deviation at node l is expressed as in (3.4b). We substitute (2.1a)

into the active power balance equation, resulting in (3.4c). The lossless Distflow power flow at both sides of line l including the ESS power are expressed via (3.4c)-(3.4e). Eq. (3.4f) calculates the nodal voltage, which is governed by voltage constraint as in (3.4g). All the variables within (3.4b)-(3.4g) are defined for $l \in \mathscr{L}, \phi \in \Phi_{dy}, t \in \mathscr{T}$, $d \in \mathscr{D}$, and $y \in \mathscr{Y}$. To simplify the notations, we do not show the indices for time, day, and year.

$$DP_{tdy} = \sum_{l \in \mathscr{L}} \tilde{p}_{ltdy}, \qquad \forall t, \forall d, \forall y, \tag{3.4a}$$

$$\sum_{l \in \mathscr{L}} \Delta p_{l\phi t} = \sum_{l \in \mathscr{L}} (\epsilon_{l\phi t} + p^E_{l\phi t}), \qquad \forall \phi, \forall t, \forall d, \forall y, \tag{3.4b}$$

$$P^t_{l\phi t} = P^b_{l\phi t} = \tilde{p}_{l\phi t} - \Delta p_{l\phi t} + p^E_{l\phi t} + \sum_{m \in \mathscr{L}} \mathbf{H}_{l,m} P^t_{l\phi t}, \qquad \forall l, \forall \phi, \forall t, \forall d, \forall y, \tag{3.4c}$$

$$Q^t_{l\phi t} = q_{l\phi t} + q^E_{l\phi t} + \sum_{m \in \mathscr{L}} \mathbf{H}_{l,m} Q^t_{l\phi t} - (v_{up(l)\phi t} + v_{l\phi t}) b_l, \qquad \forall l, \forall \phi, \forall t, \forall d, \forall y, \tag{3.4d}$$

$$Q^b_{l\phi t} = q_{l\phi t} + q^E_{l\phi t} + \sum_{m \in \mathscr{L}} \mathbf{H}_{l,m} Q^t_{l\phi t}, \qquad \forall l, \forall \phi, \forall t, \forall d, \forall y, \tag{3.4e}$$

$$v_{l\phi t} = v_{up(l)\phi t} - 2\Re\Big(z^*_l (S^t_{l\phi t} + j\, v_{up(l)\phi t} b_l)\Big), \qquad \forall l, \forall \phi, \forall t, \forall d, \forall y, \tag{3.4f}$$

$$v^{min} \leq v_{l\phi t} \leq v^{max}, \qquad \forall l, \forall \phi, \forall t, \forall d, \forall y. \tag{3.4g}$$

The objective function is defined as to minimize the investment cost (the first line of (3.5)) of ESSs and the penalty cost regarding the uncovered dispatch error over the planning horizon Y. The penalty cost of day d and year y corresponds to the uncovered dispatch error over the operating scenarios for day d multiplied by ω_d, which is the cost coefficient for the imbalance. Ω_1 and Ω_2 represents the set of control variables in the first and second stage decision process, respectively. The constraints regarding the ESS allocation and operation explained in Sec. 2.9.1 are included (*i.e.*, (2.16), (3.7)), along with the linear approximated lossless OPF constraints ((3.4)).

$$\min_{\substack{\forall U,C,R \in \Omega_1; \\ \forall S^t, v, s^E \in \Omega_2}} IC_E + \sum_{y \in \mathscr{Y}} \frac{N_{dy}}{(1+r_{dis})^y} \sum_{d \in \mathscr{D}} w_d \sum_{t \in \mathscr{T}} \sum_{\phi \in \Phi_{dy}} \lambda_\phi \Big| \sum_{l \in \mathscr{L}} \epsilon_{l\phi t} \Big| \tag{3.5}$$

subject to:

$$(2.16), (3.4), \tag{3.6}$$

$$\Lambda(\pi_{l\phi dy}) \geq 0, \qquad \forall l \in \mathscr{L}, \forall \phi \in \Phi_{dy}, \forall d \in \mathscr{D}, \forall y \in \mathscr{Y}. \tag{3.7}$$

Once the OPF problem including the constraints related to the dispatchability is solved, we can calculate the capability of the ADN with the allocated ESSs. In this context, we introduce a dispatchability index called leftover dispatch error rate (LDER), and defined as $\theta_{\phi t}$. It is expressed in (3.8). It represents the ratio between the resulting dispatch error and the anticipated dispatch error in case of no ESS at scenario ϕ and time t for the daily operation on day d and year y. In the denominator, the dispatch error without ESS is indicated while the

error regarding the grid losses is ignored because its magnitude is negligible compared to that of the prosumption error.

$$\theta_{\phi t} = \frac{|\sum_{l\in\mathscr{L}} \epsilon^*_{l\phi t}|}{|\sum_{l\in\mathscr{L}} \Delta p_{l\phi t}|}, \qquad \forall \phi \in \Phi_{dy}, \forall t \in \mathscr{T}, \forall d \in \mathscr{D}, \forall y \in \mathscr{Y}. \tag{3.8}$$

The two-stage MILP problem explained above can be easily tackled with numerous commercial solvers. However, in the case where the sizes of the set $\Phi_{dy}, \mathscr{D}, \mathscr{Y}$ are significant, the size of the given MILP problem becomes too large-scaled to be handled by a commercial solver with limited computation power. In this regard, the Benders decomposition technique can be employed as an effective solution approach to break down the first and the second stage of the optimization problem into two problems. Furthermore, the second-stage problem can be decomposed into several parallel problems such that the OPF problem for each day and each year can be tackled separately.

3.6.3 2nd Block Problem

The dispatchability level is incorporated into the 2nd block problem as a constraint governed by the dispatchability index LDER. The objective of the 2nd block problem is to adjust the ESS allocation from the 1st block problem to the optimal site and size that can minimize the grid losses and unserved load. The system condition during the operation horizon is evaluated through solving the AR-OPF problem. Therefore, the 2nd block problem is formulated as a mixed-integer second-order cone programming (MISOCP) problem. We apply the Benders decomposition technique to decompose the 2nd block problem into a master problem and several parallel subproblems that each represents a daily OPF problem. The master problem determines the ESS allocation, followed by the fitness evaluation of the determined allocations in the subproblems in terms of grid losses and unserved load. The unserved load takes values to ensure the feasibility of the subproblem regardless of the ESS allocation. The optimal solution is obtained through the same Benders iterative process as explained in Sec. 2.9.

Master problem

The master problem determines the optimal ESS allocation and the lower bound of the planning problem by summing the investment cost and the lower approximation of the subsequent expected subproblem costs. Note that the formulation of the master problem is given as same as in Sec. 2.9.2. To avoid repetition of contents, the readers are suggested to refer to Sec. 2.9.2 for the mathematical formulation.

Subproblem

In the subproblem associated with day d, and year y, a daily AR-OPF model with the time-step discretization of Δt evaluates the operational advantages of ESSs while considering real operational conditions. The sufficiency of the ESS allocation is assessed by checking if the uncovered dispatch error (see (2.2)) satisfies the LDER constraints for day d and year y as in (3.9a). As indicated in (3.9b) and (3.9c), we introduce positive and negative unserved active load terms ($up^+_{l\phi t}, up^-_{l\phi t} \in \mathbb{R}^+$) and positive and negative unserved reactive load terms

($uq^{+}_{l\phi t}, uq^{-}_{l\phi t} \in \mathbb{R}^{+}$) to the active prosumption and reactive prosumption for bus l, scenario ϕ and time t, respectively. They correspond to the amount that should be curtailed from the prosumption to primarily comply with the LDER constraints along with other operational constraints, even in the case of insufficient capacity of ESSs.

$$|\sum_{l\in\mathscr{L}} \epsilon_{l\phi t}| \leq \theta_{\phi t} |\sum_{l\in\mathscr{L}} \Delta p_{l\phi t}|, \qquad \forall \phi \in \Phi_{dy}, \forall t \in \mathscr{T}, \tag{3.9a}$$

$$p'_{l\phi t} = p_{l\phi t} + up^{+}_{l\phi t} - up^{-}_{l\phi t}, \qquad \forall l \in \mathscr{L}, \forall \phi \in \Phi_{dy}, \forall t \in \mathscr{T}, \tag{3.9b}$$

$$q'_{l\phi t} = q_{l\phi t} + uq^{+}_{l\phi t} - uq^{-}_{l\phi t}, \qquad \forall l \in \mathscr{L}, \forall \phi \in \Phi_{dy}, \forall t \in \mathscr{T}, \tag{3.9c}$$

$$p'_{l\phi t} = \tilde{p'}_{ltdy} - \Delta p'_{l\phi t}, \qquad \forall l \in \mathscr{L}, \forall \phi \in \Phi_{dy}, \forall t \in \mathscr{T}, \tag{3.9d}$$

$$DP_{tdy} = \sum_{l\in\mathscr{L}} (\tilde{p'}_{ltdy} + r_l \tilde{f}_{ltdy}), \qquad \forall t \in \mathscr{T}, \tag{3.9e}$$

$$\sum_{l\in\mathscr{L}} (\Delta p'_{l\phi t} + r_l \Delta f_{l\phi t}) = \sum_{l\in\mathscr{L}} \epsilon_{l\phi t} + \sum_{l\in\mathscr{L}} p^{E}_{l\phi t}, \qquad \forall \phi \in \Phi_{dy}, \forall t \in \mathscr{T}. \tag{3.9f}$$

The AR-OPF problem embedding the dispatchability for the subproblem is formulated by replacing (2.1a) with (3.9d). In other words, we replace the prosumption $p_{l\phi t}$ by $p'_{l\phi t}$ in the relevant equations. $\tilde{p'}_{ltdy}$ is employed in place of $\tilde{p}_{ltdy}$ to determine the daily dispatch plan, as in (3.9e). $\Delta p_{l\phi t}$ of (2.2) is substituted with $\Delta p'_{l\phi t}$ to build (3.9f). Similarly, $p'_{l\phi t}$ and $q'_{l\phi t}$ replace $p_{l\phi t}$ and $q_{l\phi t}$ in the active power balance equations formulated with the state variables (*i.e.*, (3.1a), (3.1b)) and the auxiliary variables (*i.e.*, (3.2a), (3.2b), (3.2d), (3.2e)). Moreover, the power injection from the allocated ESS is introduced to the set of equations regarding AR-OPF model as shown in (3.10). Eq. (3.10) replaces the power balance equations ((3.1a), (3.1b),(3.2a),(3.2b), (3.2d),(3.2e),) of AR-OPF model given in Sec. 3.5.

$$S^{t}_{l} = s'_{l} + s^{E}_{l} + \sum_{m\in\mathscr{L}} \mathbf{H}_{l,m} S^{t}_{l} + z_l f_l - j(v_{up(l)\phi t} + v_l) b_l, \qquad \forall l \in \mathscr{L}, \tag{3.10a}$$

$$S^{b}_{l} = s'_{l} + s^{E}_{l} + \sum_{m\in\mathscr{L}} \mathbf{H}_{l,m} S^{t}_{l}, \qquad \forall l \in \mathscr{L}, \tag{3.10b}$$

$$\hat{S}^{t}_{l} = s'_{l} + s^{E}_{l} + \sum_{m\in\mathscr{L}} \mathbf{H}_{l,m} \hat{S}^{t}_{l} - j(\bar{v}_{up(l)} + \bar{v}_l) b_l, \qquad \forall l \in \mathscr{L}, \tag{3.10c}$$

$$\hat{S}^{b}_{l} = s'_{l} + s^{E}_{l} + \sum_{m\in\mathscr{L}} \mathbf{H}_{l,m} \hat{S}^{t}_{l} \qquad \forall l \in \mathscr{L}, \tag{3.10d}$$

$$\bar{S}^{t}_{l} = s'_{l} + s^{E}_{l} + \sum_{m\in\mathscr{L}} \mathbf{H}_{l,m} \bar{S}^{t}_{l} + z_l f_l - j(v_{up(l)} + v_l) b_l \qquad \forall l \in \mathscr{L}, \tag{3.10e}$$

$$\bar{S}^{b}_{l} = s'_{l} + s^{E}_{l} + \sum_{m\in\mathscr{L}} \mathbf{H}_{l,m} \bar{S}^{t}_{l}, \qquad \forall l \in \mathscr{L}. \tag{3.10f}$$

On the other hand, we can intuitively expect that having (3.9f) cannot be compliant with the mathematical formulation of the power flow equations (*i.e.*, (3.1a)-(3.1c),(3.1e)) in the case of insufficient capacity of ESSs to satisfy the LDER constraints (3.9a). The insufficient power rating of ESSs implies that possible $p^{E}_{l}, \forall l \in \mathscr{L}$ is small. It makes ϵ_l too large to comply with the LDER constraints (see (3.9f)). However, instead of making the problem infeasible, the LDER constraints and (3.9f) are both satisfied by reducing the prosumption deviation considering losses (left-hand side of (3.9f)). This leads to the violation of the physical law of power flow

because the grid losses deviation should take an unrealistic value that has the same order of magnitude as the prosumption deviation. In this way, the prosumption deviation and grid losses deviation cancel out each other to make the overall value of the left-hand side as small as the right-hand side of (3.9f). This induces the increase of the squared longitudinal current f_l such that the left-hand side of (3.1h) becomes strictly greater than the right-hand side, which leads to the inexactness of the solution. Therefore, we introduce an iterative algorithm, Alg. 3.1, comprising two additional slack variables, $\gamma^m_{\phi t}$ and $\zeta^m_{\phi t}$, to replace (3.9f) by (3.11a) and (3.11b) such that the value of the internal current would not deviate away from the real value (*i.e.*, the inexactness remains trivial). $\gamma^m_{\phi t}$ represents the realized grid losses deviation at mth iteration for scenario ϕ and time t, where $m \in \mathscr{M}$ is the index of iterations of the algorithm. $\zeta^m_{\phi t}$ indicates the unrealized part of the grid losses that should be added up to $\gamma^m_{\phi t}$ after each iteration for scenario ϕ and time t. $\gamma^m_{\phi t}$ achieves the accurate value of grid losses deviation, as the absolute value of $\zeta^m_{\phi t}$ reaches value below the defined tolerance.

$$\sum_{l\in\mathscr{L}} (\Delta p'_{l\phi t} + r_l \Delta f_{l\phi t}) = \sum_{l\in\mathscr{L}} \epsilon_{l\phi t} + \sum_{l\in\mathscr{L}} p^E_{l\phi t} + \zeta^m_{\phi t}, \qquad \forall \phi \in \Phi_{dy}, \forall t \in \mathscr{T}, \tag{3.11a}$$

$$\sum_{l\in\mathscr{L}} \Delta p'_{l\phi t} + \gamma^m_{\phi t} = \sum_{l\in\mathscr{L}} \epsilon_{l\phi t} + \sum_{l\in\mathscr{L}} p^E_{l\phi t}, \qquad \forall \phi \in \Phi_{dy}, \forall t \in \mathscr{T}. \tag{3.11b}$$

Algorithm 3.1 Iterative realization of grid losses deviation in the subproblem.

Require: θ $(LDER)$, $s = p + jq$, R^*, C^* (see (3.12d), (3.12e))

1: **Initialization :** $m \leftarrow 0, \gamma^1_{\phi t} \leftarrow 0, \zeta^1_{\phi t} \leftarrow 1, \forall \phi \in \Phi_{dy}, \forall t \in \mathscr{T}$;
2: **while** $|\zeta^{m*}_{\phi t}| \geq$ tol, $\forall \phi \in \Phi_{dy}, \forall t \in \mathscr{T}$ **do**
3: $m \leftarrow m+1$
4: Solve a subproblem including (3.11)
5: **return** $\zeta^{m*}_{\phi t}$,
6: $\gamma^{m+1}_{\phi t} \leftarrow \gamma^m_{\phi t} + \zeta^{m*}_{\phi t}, \forall \phi \in \Phi_{dy}, \forall t \in \mathscr{T}$
7: **end while**
8: **return** $\gamma^m, S, v, f, I, s^E, SC_{dy}, \mu_{dy}, \vartheta_{dy}$

In short, the modified AR-OPF model including ESSs' dispatch (*i.e.*, (3.1c), (3.1h), (3.2c), (3.2f)-(3.2n), (3.9a)-(3.9e), (3.10), (3.11)) is defined as $\Theta'(\varphi'^E) \geq 0$, where $\varphi'^E = \{S^t, v, f, \hat{S}^t, \bar{v}, \bar{f}, \bar{S}^t, s' = p' + jq', s^E = p^E + q^E, up^+, up^-, uq^+, uq^-, \zeta\}$ is the set of variables. The notation without subscript corresponds to the vector of variables and parameters for buses/lines $\forall l \in \mathscr{L}$. Hereafter, the modified AR-OPF was referred to MAR-OPF model. Finally, the subproblem is described with an objective of minimization of the total grid losses and unserved load to satisfy the LDER constraints.

$$\begin{aligned} \min_{\forall \varphi'^E, \pi} : SC_{dy} = \frac{N_{dy}}{(1+r_{dis})^y} \sum_{t\in\mathscr{T}} \sum_{\phi\in\Phi_{dy}} \lambda_\phi (w_l \sum_{l\in\mathscr{L}} r_l f_{l\phi t} \\ + w_u \sum_{l\in\mathscr{L}} (up^+_{l\phi t} + up^-_{l\phi t} + uq^+_{l\phi t} + uq^-_{l\phi t})) \end{aligned} \tag{3.12a}$$

subject to:

$$\Lambda(\pi_{l\phi}) \geq 0, \qquad \forall l \in \mathscr{L}, \forall \phi \in \Phi_{dy}, \tag{3.12b}$$

$$\Theta'(\varphi'^{E}_{\phi t}) \geq 0, \qquad \forall \phi \in \Phi_{dy}, \forall t \in \mathscr{T}, \tag{3.12c}$$

$$R_l = R_l^{(\beta)*} : \mu_{ldy}, \qquad \forall l \in \mathscr{L}, \tag{3.12d}$$

$$C_l = C_l^{(\beta)*} : \vartheta_{ldy}, \qquad \forall l \in \mathscr{L}. \tag{3.12e}$$

where w_l and w_u are the weight coefficients associated with the grid losses minimization and unserved load, respectively. The ideal ESSs' operational constraints are given as (3.12b), and the MAR-OPF model including ESSs dispatch is shown by (3.12c). (3.12d), (3.12e) describes that the ESSs' power ratings and energy reservoirs are fixed to the optimal solution values of the master problem. μ_{ldy} and ϑ_{ldy} are the duals of constraints related to the fixed ESS capacities.

$$\Gamma_{dy}^{(\beta)} = \big[SC_{dy}^{*} - \sum_{l \in \mathscr{L}} (\mu_{ldy}(R_l - R_l^{(\beta)*}) - \vartheta_{ldy}(C_l - C_l^{(\beta)*}))\big], \qquad \forall d, \forall y, \forall \beta \in \mathscr{B}. \tag{3.13}$$

The dual values obtained from the subproblem are used to form the Benders cuts for the master problems as in (3.13). The variables with subscript d, y, β are defined for $\forall d \in \mathscr{D}, \forall y \in \mathscr{Y}, \forall \beta \in \mathscr{B}$, respectively. UB is calculated summing the optimal investment cost and the subproblem costs (*i.e.*, $UB = IC^{E*} + \sum_{y \in \mathscr{Y}} \sum_{d \in \mathscr{D}} SC_{dy}^{*}$).

3.7 Simulations

3.7.1 Simulation Configuration

We validate the performance of the proposed methods with the same distribution network introduced in the previous chapter (see Fig. 3.3). The parameters related to the prosumption, the parameters required for ESS investment are given as same with the previous chapter (Table 2.1). In this section, several simulations are conducted to show the performance of the proposed method. First, a toy example of a planning exercise is carried out using operating scenarios of 1 day-type and hourly dispatch to clearly show the role of the 1st and 2nd blocks of the problem. Then, we solve the planning problem using the operating scenarios of 8 day-types and 30 minutes dispatch intervals. Unlike the previous chapter, the number of scenarios is determined as 32 and 39 for each exercise, respectively, to improve the reliability of the planning solution[9] The numbers of reduced scenarios are obtained by an algorithm that determines the minimum number of scenarios to reach a pre-defined level of statistical similarity of prosumption forecasts. The detailed algorithm is explained in Appendix. A. Notably, in this chapter, 3 representative values of imbalance costs were used in the full planning exercise for evaluating the impact of imbalance cost on the dispatchability. The

[9] However, the number of scenarios should be deliberately chosen (in other words, increasing the number of scenarios might not necessarily result in enhancement of solution quality), given the fact that if the number of scenarios becomes significant, the magnitude of probability assigned to each scenario will decrease. In this case, the relative objective value associated with the grid losses resulting from the extreme scenarios with small probability would be small as well, possibly lessening the tightness of the SOCP relaxation.

values were analyzed from the imbalance price data from 2018 to 2019 in the Swiss energy market [87] (see Table 3.1). The weight coefficients for grid losses and unserved energy are equal to 6k/MWh and 100k/MWh, respectively.

Table 3.1: Imbalance prices for ESS allocation.

	Imbalance price ($/MWh)
Mean	77
99th percentile	174
99.9th percentile	897

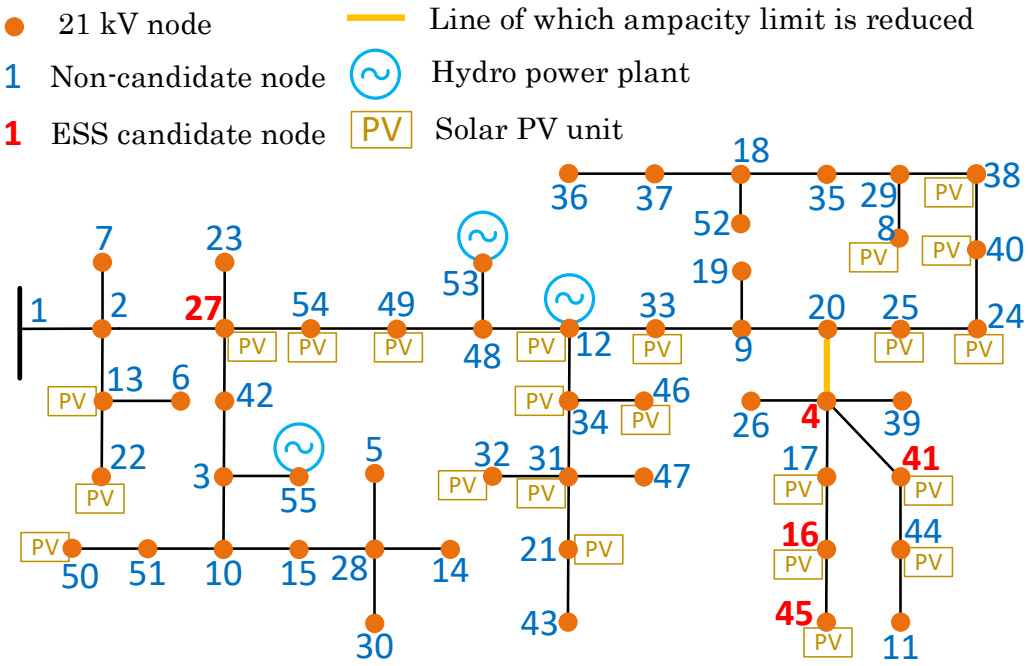

Figure 3.3: Considered real 55 bus distribution network.

3.7.2 Planning with 1 Day under Hourly Dispatch

To illustrate the role of the 1st and 2nd block of the problem, we demonstrate the result of the simplified simulation considering an hourly dispatch for 1 representative day in two cases: case 1 with the original ampacity of the lines specified for the given network and case 2 with the ampacity of line between node 4 and 20 reduced from the original value (see Fig. 3.3). Table 3.2 indicates the optimal allocation result of ESSs, followed by the cost and operation result for 10 years as shown in Table 3.3. The optimal result from the 1st block specifies the power ratings and energy reservoirs of ESSs. However, the determined allocation of ESSs cannot be guaranteed to be feasible and optimal to satisfy the LDER constraints for the real operation of the network since the grid losses and the ampacity constraint were neglected in the 1st block problem. After the 2nd block of the problem, as shown in the result for case

1 in Table 3.2, the optimal sites of the ESSs considering the minimization of the grid losses is determined as node 4, resulting in the reduction of the grid losses and unserved energy compared to the result of the 1st block problem.

In case 2, we can observe that a part of the load consumption was unserved to satisfy the LDER constraints in the condition of restrained ampacity limit with the determined ESSs' allocation from the 1st block. In this regard, the result of the 2nd block shows the change in the allocation of the ESSs due to the bottleneck of this line. The power rating and energy reservoir of the ESS on Node 4 is reduced and another ESS is allocated on Node 27. Table 3.3 shows that the unserved energy in case 2 decreased to near zero after re-allocation of the ESSs.

Table 3.2: ESS allocation result for Case 1 (original ampacity) and Case 2 (reduced ampacity).

Case	Problem	Location	Power rating	Energy reservoir
	1st Block	41	564.3 kVA	1.615 MWh
1	2nd Block	4	548.4 kVA	1.616 MWh
2	2nd Block	4	307.7 kVA	911.9 kWh
		27	238.7 kVA	705.4 kWh

Table 3.3: Comparison between the result of 1st block and 2nd block for Case 1 (original ampacity) and Case 2 (reduced ampacity).

Case	Type of cost	Allocation of 1st block	Allocation of 2nd block
case1	Investment cost ($ Million)	0.694	0.694
	Dispatch error (GWh)	2.037	2.037
	Unserved energy to satisfy the LDER constraints (MWh)	0.086	2.7E-3
	Grid losses (MWh)	292.59	292.59
	Total energy consumed (GWh)	102.90	102.90
case2	Investment cost ($ Million)	0.694	0.794
	Dispatch error (GWh)	2.037	2.037
	Unserved energy to satisfy the LDER constraints (MWh)	27.9	7.1E-4
	Grid losses (MWh)	306.30	281.85
	Total energy consumed (GWh)	102.92	102.89

3.7.3 Planning with Full Scenarios with 30 min Dispatch Intervals

The proposed planning procedure is applied to the full set of scenarios with 8 typical days with 30 min interval dispatch. Table 3.4 shows the optimal ESSs' locations and sizes. We show the results for three cases corresponding to different imbalance prices (see Table 3.1). The cost and operation result for 10 years are indicated in Table 3.5. The results show that it may not be beneficial to install ESSs under current imbalance prices (represented by the mean value of recorded imbalance prices). However, as the imbalance price grows higher with the

increase of prosumption uncertainty within the system, it will be more necessary to allocate ESSs for dispatch error compensation. Fig. 3.4 illustrates the operation result for day-type 1 in 1st year, showing the prosumption prediction considering 39 scenarios of the prosumption profiles (thick pink line), the dispatch plan (thick black line), and the active power in-feed through GCP corresponding to each scenario (thin lines) in the case of no ESS (see Fig. 3.4.(a)) and the optimal ESS allocation with imbalance price of \$897/MWh. (see Fig. 3.4.(b)). The dispatch result without ESS shows that the dispatch error is significant, especially in the time period where the production from PV is high. On the other hand, in the case with the optimal ESS allocation, the active power in-feed of every prosumption scenario follows the dispatch plan with small error. The cost analysis between the cases with ESS and without ESS in Table 3.5 demonstrates quantitatively the capability of these assets to handle uncertainties within the network. When \$897/MWh is considered for the imbalance price, the total dispatch error of the case without ESS is about 9 times of that in the case with ESSs. The difference in the dispatch error is translated into the significant gap in the total cost for 10 years of operation: \$12.45 Million with the default system configuration, and \$2.54 Million with the optimal ESS allocation. Consequently, this result demonstrates the advantages for the DSO to invest in ESSs in view of their technical and economical profit.

Table 3.4: ESS allocation results with different imbalance prices.

Imbalance price	Location	Power rating	Energy reservoir
Mean	-	-	-
99th percentile	4	497.78 kVA	1.85 MWh
99.9th percentile	4	536.08 kVA	1.46 MWh
	27	356.75 kVA	1.11 MWh

Table 3.5: Planning cost and Operational benefits with differnt imbalance prices.

	Mean	99th percentile	99.9th percentile
Investment cost (\$ Million)	-	0.75	1.15
Dispatch error (GWh)	13.875	2.881	1.552
Grid losses (MWh)	609.99	564.62	539.56
Unserved energy to satisfy the LDER constraints (MWh)	0*	1.26	1.03
Total energy consumed (GWh)	104.84	104.77	104.77

* As the LDER constraints are not calculated due to the lack of ESSs, the unserved energy is determined with only operating constraints regarding nodal voltage and ampacity limit.

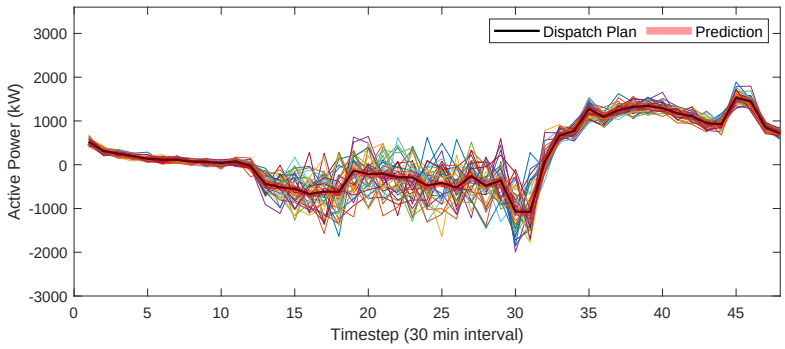

(a)

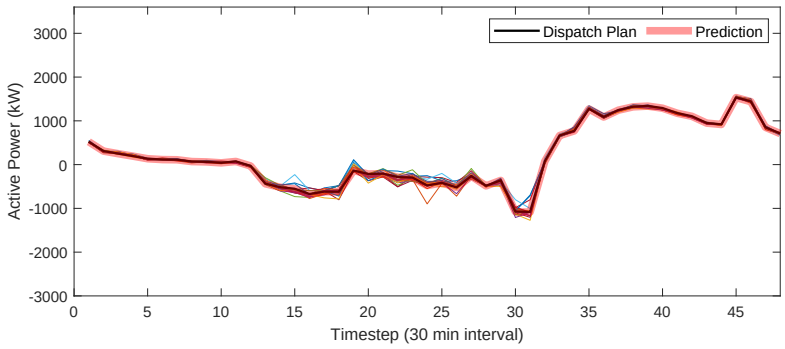

(b)

Figure 3.4: Prosumption prediction, dispatch plan and active power through GCP in each scenario (not labeled for the sake of readability): (a) Day 1(No ESS), (b) Day 1(With ESS (Imbalance price : $897/MWh)).

3.7.4 Sensitivity Analysis Regarding the Initial ESS SoE

The results of dispatching operations are sensitive to the ESSs' operational condition. In the proposed planning method, only a few days are selected as typical day-types, and they are treated discontinuously for the operation. In Sec. 2.9.1, the assumption on the initial and final SoE levels for each daily operation is discussed. In this sensitivity analysis, the initial SoE is chosen with various values to observe whether it plays a significant role in quantifying the optimal dispatchability level of ADNs, and ultimately influencing the size of ESSs. Table 3.6, Table 3.7 indicate the ESS allocation and cost result with different initial SoE values. The dispatch error in case of an initial SoE= 50% appears to be the largest. However, when the sum of investment cost and the cost related to the dispatch error are compared for all cases, the results show that setting the initial SoE= 50% gives the most economic ESS allocation.

Table 3.6: ESS allocation result with different initial SoE levels.

Initial SoE	Location	Power rating	Energy reservoir
30%	4	507.7 kWh	2.218 MWh
50%	4	548.4 kVA	1.616 MWh
70%	4	631.1 kVA	2.052 MWh

Table 3.7: Cost and Operational benefits with different initial SoE levels.

	30 %	50 %	70 %
Investment cost ($ Million)	0.867	0.694	0.842
Dispatch error (GWh)	1.995	2.037	1.964
Grid losses (MWh)	292.63	292.59	293.26
Unserved energy to satisfy the LDER constraints (MWh)	4.9E-3	0.086	2.3E-3
Total energy consumed (GWh)	103.01	101.53	102.81

3.7.5 Numerical Comparison with Operation Model Using PWL-OPF, R-OPF, and AR-OPF Model

We compare the operation results obtained from the proposed method with the AR-OPF model and with the R-OPF and PWL-OPF model (Sec. 2.7.1). For the PWL-OPF model, the number of discretization steps for approximation is set to 40 considering its superiority in approximation accuracy than the PWL-OPF model with smaller number of discretization steps as shown in the previous chapter. The comparison between three cases is analysed in terms of exactness of the OPF approximation and the SOCP relaxation at the optimal investment solution of the case with 32 scenarios and 1 day-type. According to [49], the exactness is numerically evaluated based on the error between longitudinal current value expressed by the state variable of squared longitudinal current (f_l) and the value calculated by the values of complex power flow and nodal voltage. (*i.e.*, the right-hand side and the left-hand side of (3.1h), the reference current value, (I_{base}), is 165 A.)

$$err = \left(\sqrt{f_{l\phi t}} - \sqrt{\left(|P^t_{l\phi t}|^2 + |Q^t_{l\phi t} + j\, v_{up(l)\phi t} b_l|^2 \right) / v_{up(l)\phi t}} \right) * I_{base} \quad (A) \tag{3.14}$$

Fig. 3.5 shows the CDF plot of the total approximation errors. Table 3.8 shows some of the statistical values (*i.e.*, minimum/maximum/mean/median error in A) of the distribution of the errors related to the computation of the longitudinal current. Note that the largest errors appear on the lines where the flow is near to zero. The result verifies that the SOCP-relaxed OPF models (AR-OPF and R-OPF model) are superior to the PWL-OPF model concerning the exactness of the OPF approximation. Moreover, the piecewise linearization is computationally more burdensome than the SOCP relaxation. Meanwhile, we can observe that the relaxation gap (error) of the AR-OPF model is tighter than the R-OPF model thanks to the augmented set of grid constraints. However, AR-OPF model takes more computation time than the R-OPF model. More detailed comparison between the two SOCP relaxation-based models are given in the following subsection.

Table 3.8: Comparison on accuracy of longitudinal current calculation with respect to different OPF models.

OPF model	Error in longitudinal current (A)				Time to solve a single subproblem (s)
	min	max	mean	median	
AR-OPF	7.23E-10	6.32E-4	2.87E-5	1.01E-5	27.89
R-OPF	2.25E-9	0.01	3.18E-4	8.90E-5	8.35
PWL-OPF	5.11E-7	0.47	0.03	0.01	885

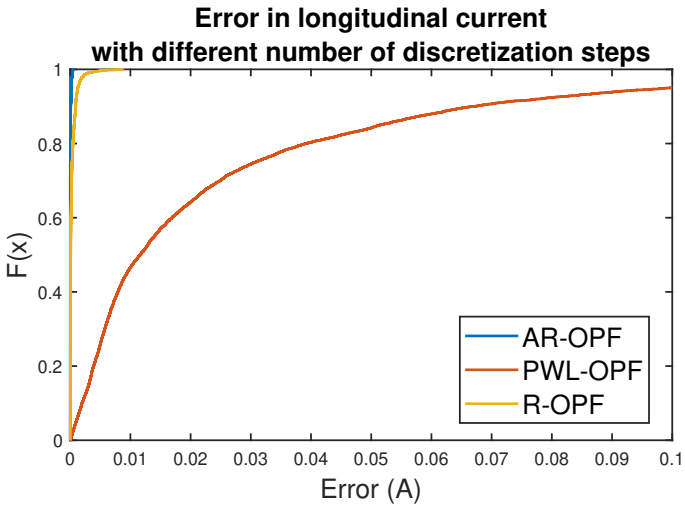

Figure 3.5: Error in longitudinal current (A).

3.7.6 Comparison with Planning Approach Using AR-OPF and R-OPF Model

It is worthwhile to compare more in detail the planning and operation results obtained from the proposed planning method employing the AR-OPF model and the planning strategy incorporating the R-OPF model which was proposed in [82]. The ESS allocation along with the cost and operational benefits are shown in Table 3.9 and Table 3.10. The ESS allocation is similar with only a small difference in ESSs' energy reservoirs, while the dispatch error is the same. The unserved energy to satisfy the LDER constraints is smaller in the AR-OPF approach than that using the R-OPF. Another comparison between the two cases is analyzed in terms of the exactness of the SOCP relaxation under the optimal allocation of ESS. The exactness is numerically evaluated based on the error between the right-hand side and the left-hand side of (3.1h). Table 3.11 shows some of the statistical values that describe the distribution of the errors over all time intervals, operating scenarios and day-types for 39 scenarios with 8 day-types. As expected, the results verify that the AR-OPF model is superior to the the R-OPF model to guarantee the exactness of the SOCP relaxation.

Table 3.9: ESS allocation result using AR-OPF and R-OPF model.

Case	Location	Power rating	Energy reservoir
using AR-OPF	4	548.4 kVA	1.616 MWh
using R-OPF	4	548.2 kVA	1.659 MWh

Table 3.10: Cost and Operational benefits using AR-OPF and R-OPF models.

	AR-OPF	R-OPF
Investment cost ($ Million)	0.694	0.707
Dispatch error (GWh)	2.037	2.036
Grid losses (MWh)	292.59	284.95
Unserved energy to satisfy the LDER constraints (MWh)	0.086	1.759
Total energy consumed (GWh)	101.53	102.89

Table 3.11: Error in longitudinal line current (A) of AR-OPF and R-OPF models.

Case	median	95th percentile	99th percentile	99.9th percentile
using R-OPF	4.7E-3	3.1E-1	9.6E-1	4.1
using AR-OPF	6E-4	1.1E-2	2.5E-1	3.7E-1

3.8 Conclusion

In this chapter, we have presented a tool for the optimal planning of ESSs within a distribution network to achieve its dispatchability. We have shown that the uncertainty of the prosumption can be compensated sufficiently with the allocation and exploitation of ESSs. The non-approximated and convex AR-OPF model is implemented to account for the distribution network's operational conditions accurately. The planning problem is decomposed into two blocks to ensure the tightness of the operational solution obtained from the AR-OPF model. In the 1st block, the allocation of ESSs is determined along with the corresponding LDER by implementing the linearly approximated OPF model. The AR-OPF model is used in the 2nd block of the problem to check the compatibility of the allocated capacity for the real operation of the network to satisfy the LDER constraints and to determine the optimal location of the ESSs to minimize the grid losses. The AR-OPF model is appropriately modified, resulting in the MAR-OPF model, to account for the operational objective of the ADN's dispatchability while ensuring the quality of the OPF solution assessed by the SOCP relaxation's tightness. We validated the effectiveness of the proposed method for a real Swiss ADN of 55 nodes by demonstrating that the allocation of ESSs successfully reduced the dispatch error.

4 Optimal Co-planning of ESS Allocation and Line Reinforcement Considering the ADN's Dispatchability

4.1 Highlights

The chapter presents a method for the co-optimization of ESS allocation and line reinforcement in ADNs. The objective is to guarantee the capability of an active distribution network to follow a dispatch plan by appropriately coping with the high uncertainties of loads and stochastic renewable generation while ensuring the secure operation of the network and minimizing the power grid losses. The proposed formulation relies on a modified formulation of the AR-OPF model. As done in the previous chapters, to tackle the complexity and computational burden of the proposed planning problem, the Benders decomposition algorithm is used and, in order to enhance the convergence speed of the numerical solution of the proposed problem, the Benders decomposition has been suitably modified to determine the assets' site and size sequentially. To assess the performance of the proposed method, simulations are conducted on the same real Swiss distribution network composed by 55 nodes and hosting a large amount of stochastic installed PV generation. The sensitivity analysis with respect to the PV capacity is carried out to assess the effectiveness of the proposed method.

This chapter presents the work published in:

Yi, Ji Hyun, Rachid Cherkaoui, Mario Paolone, Dmitry Shchetinin, and Katarina Knezovic. "Optimal Co-Planning of ESSs and Line Reinforcement Considering the Dispatchability of Active Distribution Networks." IEEE Transactions on Power Systems (2022).

4.2 Organization of the Chapter

The chapter starts with the discussion at the state-of-the-art about the joint planning problem of both line reinforcement and ESS allocation. Then, it is followed by stating the research question that cannot be addressed by the exist literature. The second part describes the line investment modeling and the OPF model's modification to incorporate the change of line characteristics (*i.e.*, ampacity limit and electrical parameters) caused by the reinforcement. Then, the reformulation of the co-optimization problem is introduced such that the siting and sizing of assets are determined separately. In the simulation part, the proposed methodology

is tested on the same real distribution network introduced in the previous chapters.

4.3 State-of-the-art of Co-optimization of Line Reinforcement and ESS Allocation

In the previous chapters, a planning methodology is proposed to optimally site and size ESSs in ADNs to achieve their dispatchability while accounting for the grid constraints and scenarios modeling the stochastic nature of local power generation and loads. As observed in the result of Sec. 3.7.2, the allocation of ESSs may be largely influenced by binding grid constraints with particular reference to line ampacity. In view of the above, the planning considering ESSs as the sole resource for DSOs may result in sub-optimal decisions. Instead, the ADNs asset investments may also take into account the line reinforcement and achieve a lower overall investment. Conventionally, DSOs have tackled the operational issues associated with ADNs hosting capacity [10] by standard line reinforcement schemes e.g., [88], [89], [90].

Numerous works discussed distribution network planning frameworks considering only network components and they are mostly used in industrial practice [91]. While the Authors of [89] considered investment decision only on the conductor type for the new and existing lines for reinforcement, the reinforcement of the substation assets (*i.e.*, high-to-medium voltage transformers) was taken into account in [88] and [90], respectively.

The installation of shunt capacitor banks [65, 92] along with voltage regulators [93] were added as planning options to improve the supply power quality issues. In [94, 95], the benefit of reconfiguration of lines is also considered to actively manage the network. Notably, several works have investigated the operational benefit of controllable DG placement [96–100], or ESS assets [8, 76, 101]. The joint planning of line and DGs to mitigate carbon emissions was proposed in [100]. The method was based on the SOCP model of the OPF, accounting for prediction errors of wind generation and loads by scenarios. However, the prosumption profile was modeled by load duration curves instead of time-series. Likewise, in [65], a two-stage stochastic MISOCP model of the joint planning problem considered the prosumption uncertainty in the same manner as in [100], making it difficult to accurately include the operational aspect of the ADN along with the prosumption changing with time. Moreover, the SOCP model employed in [65, 100] neglected the presence of shunt elements.

There is a large volume of published studies proposing joint planning strategies considering ESSs and network reinforcement. Previous studies have primarily concentrated on developing planning strategies for minimizing standard operating cost considering the cost associated to the operation of ESSs and other active assets [77, 78] and even maintenance costs [77, 78]. Another category of works put emphasis on tackling technical issues namely: (i) minimization of grid losses [79], (ii) maximization of grid reliability [76–79], In addition to the above-listed operational objectives, controllable ESSs may also be used to procure flexibility services to the local distribution system, such as peak shaving [76, 101, 102], minimization of DG

[10] The hosting capacity of a power network corresponds to the amount of loads and generation that can be hosted without violating any operational constraint.

curtailment [79] as well as ancillary services to the upper-level network [101]. Furthermore, ESSs and DG may also be controlled with the objective of reducing carbon emissions of power generation [100].

The multi-stage joint planning model proposed in [76] considered replacing/adding lines while integrating ESSs for peak shaving and enhancing the power supply reliability. The investment options for line reinforcement are treated as a number of conductor candidates, represented by integer variables. The non-linearity of the AC-OPF model was tackled by the linearization of the voltage drop in the power flow equations based on the Kirchhoff's laws, converting the planning problem into a MILP one. In [101], a probabilistic method is used to assess the ESSs size to defer network reinforcement as well as to quantify the economical benefits to provide additional peak capacity (this feature being assessed a-posteriori).

Yet, to the best of our knowledge, no study has been found so far with the obejctive of developing planning strategies to achieve ADNs dispatchability.

4.4 Problem Statement and Contributions

A co-optimization method is proposed for the allocation of ESSs and line reinforcement based on a scenario-based stochastic MISOCP model. Grid operational constraints are described by the AR-OPF model, initially proposed in [1], and modified in Ch.3 to obtain the MAR-OPF model for solving the ESS allocation problem. In this chapter, the MAR-OPF model has been suitably modified to include the reinforcement of existing lines to cope with binding operational constraints due to hosting increasing capacity of distributed stochastic resource. Along with binary and continuous decision variables representing ESSs investment decisions [103], the line reinforcement is modeled by incorporating binary and continuous decision variables associated with the line candidates for reinforcement and their conductors' size. Compared to the works in [65, 76–78, 89, 100] where line reinforcement option is treated by a set of integer variables (refering to a fixed set of available cable types with specified ampacities), in this chapter we relax it to continuous variable representing line ampacity. On the one hand, it allows better tractability. On the other hand, it provides a modeler with a better understanding of the optimal sizing decisions of the ESS and line reinforcement, while taking into account the relationship between them. The operational changes caused by line reinforcement are appropriately incorporated into the MAR-OPF model by modifying line characteristics such as line ampacity, resistance, reactance, and susceptibility.

In Ch. 2 and Ch. 3, the Benders decomposition is employed to tackle the ESS allocation problem, while binary and continuous decision variables are assigned to the ESSs' locations, and their power rating and energy reservoir capacities, respectively, and their optimal values are obtained together in the master problem. In this chapter, to better tackle the increased complexity caused by the additional numerous binary variables associated with the line reinforcement, the planning problem is reformulated to employ the Benders decomposition separately for determining the site and size of the assets investment in sequential stages. This non-trivial structural change reduces the computation time for solving the planning

problem while maintaining the optimality of the obtained solution. Consequently, it enables the scalable application of the proposed planning methodology to radial distribution networks of generic sizes. To summarize, the contributions of this work are given below.

1. A joint planning problem considering ESS allocation and line reinforcement is proposed to achieve ADN's dispatchability while ensuring sufficient hosting capacity for increasing stochastic prosumption.

2. The line reinforcement investment is suitably modeled along with corresponding adjustments on the network admittance matrix and grid constraints in order to be incorporated in the MAR-OPF model.

3. The reformulation of the planning problem is proposed to determine the siting and sizing of the assets' investment sequentially, thereby accelerating the convergence of the Benders decomposition algorithm.

4.5 System Description

The joint optimal allocation of ESSs and line reinforcement are determined based on the operation of the ADN with the same objective and condition as explained in Sec. 2.8. Multiple operational objectives are taken into account: achieving the dispatchability of the targeted ADN while minimizing the grid losses and ensuring the feasibility of the ADN operation. ESSs and line reinforcement are the assets to be planned to cope with this problem. The large amount of stochastic DG increases the risk of line congestion and may reduce the power supply reliability. In this respect, in addition to the investment decision on the ESS assets, we determine the lines to be upgraded among the existing ones (*i.e.*, $X_l \in \{0,1\}$ indicates whether to upgrade the line l). The required change in line ampacity (A_l) is decided to minimize the load curtailment, which serves as the reliability indicator for the power supply of the ADN loads.

A specific complexity of the targeted planning problem is associated with the fact that the change of line conductors produces a change of the line parameters. As the line ampacity increases, the line resistance and the reactance decrease, while the line susceptance increases. The dependence of the line parameters on its ampacity is modeled through a linear fitting for line reactance and susceptance and a hyperbolic fitting for the line resistance using realistic line data. The sensitivity coefficients of the line parameters computed from the fitted curves are introduced within the OPF to accurately model the effect of line reinforcement on the line parameters (see Sec. 4.7.1). In view of the above, the proposed ESS allocation and line reinforcement problem can be seen as a two-stage decision process: the first stage deals with the binary decision variables on the location of the ESS (U_l), the lines to be upgraded (X_l) and the continuous decision variables on the capacity of the ESSs energy reservoirs (C_l), their power rating (R_l), and the line ampacity (A_l), whereas the second stage deals with daily dispatch problems, determining the decision variables on the ESSs active and reactive power for all operating scenarios.

4.6 Problem Formulation

The operational objective associated to the co-optimization of ESSs and line reinforcement is to maintain a sufficient level of the ADN's dispatchability while complying with the network constraints in a (potentially) highly congested network due to significant penetration of uncontrollable DG units and load consumption. The planning problem is decomposed into two blocks in the same way explained in Sec. 3.6. In the 1st block, the economical benefits/penalties associated with the network dispatchability are obtained by quantifying the trade-off between the ESS allocation costs vs. the avoidance on the power dispatch imbalance penalties. In the 2nd block, the ESS allocation and the line reinforcement investment are determined by employing the AR-OPF model to satisfy a dispatch error level obtained from the 1st block, while complying with the network operating constraints.

The simultaneous decision on siting and sizing of lines and ESSs implies dealing with decision variables of different nature (continuous and binary) constituting the investment options. When following the Benders algorithm utilized in Sec. 3.6 to solve the 2nd block problem, the Benders cuts are generated based on the dual values associated with the continuous investment variables. However, they are often not efficient enough to narrow down the mixed-integer solution space. In other words, the inclusion of numerous binary investment variables makes it even more burdensome to converge to an optimal investment solution since each solution value of binary variables has to be checked with various combinations of values for the continuous investment variables. The excessive number of Benders iterations caused by inefficient Benders cuts increases the master problem's size and slows down the convergence.

Therefore, in this chapter, the planning problem employing the Benders decomposition is reformulated into two sub-stages (each employing Benders decomposition) such that siting (nodes where ESSs are allocated and branches where lines are reinforced) and sizing (ESSs' energy reservoirs, power ratings, and lines' ampacities) decisions are made consecutively in a decoupled way. We call the 1st sub-stage as *siting sub-stage*, as the sites for the ESS allocation and line reinforcement are determined. The Benders cut for the siting problem is strengthened by calculating the optimal sizes achieved at each possible siting solution while solving parallel operation problems. When the optimal siting solution is obtained, siting solution is fixed such that the master problem of the 2nd sub-stages (sizing problem) is reduced to a continuous problem. It results in faster convergence of the 2nd sub-stages to obtain optimal solutions for size variables. We call the 2nd sub-stage as *sizing sub-stage*. Note that even though both sub-stages employ the Benders decomposition, the formulation of inner master problems and subporoblems are different. The algorithm of the proposed approach is illustrated in Fig. 4.1.

4.6.1 1st Block Problem

In the 1st block problem, the optimal dispatchability level index is determined along with the preliminary ESSs' sizes and sites. Note that the 1st block problem is formulated in the same way as introduced in Sec. 3.6.2. In other words, investment associated with line reinforcement is not considered in this block. All the mathematical equations of the 1st block problem and

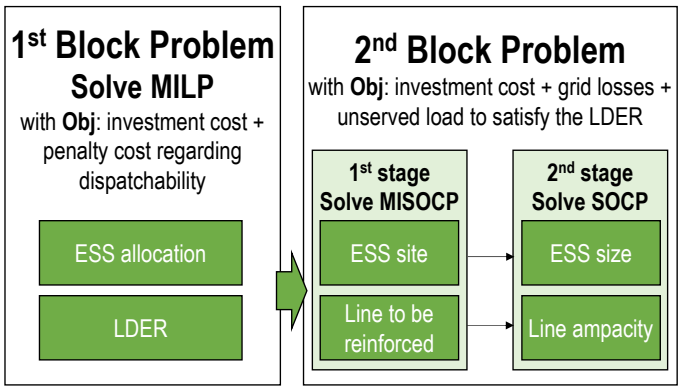

Figure 4.1: Solution algorithm overview of the proposed method.

their description can be found in Sec. 3.6.2.

4.6.2 2nd Block Problem

The objective of the 2nd block problem is to determine the ESS allocation as well as the line reinforcement scheme in order to minimize the load curtailment and the grid losses. The dispatchability level is incorporated into the 2nd block problem as a constraint governed by the dispatchability index LDER. The investment decision is optimized based on the investment cost for the ESS allocation and the line reinforcement given by (4.1). ic_l^r is the fixed cost parameter associated with reinforcement of line l. ρ_l is the length of line l. The line reinforcement cost, modeled by (4.2), consists of two parts: fixed cost, which is invariant with the conductor size and accounts for the construction, labor, etc., and the conductor cost, which varies with line ampacity and length. Based on the line cost data from [104], the cost per kilometer is modeled as a quadratic function of the ampacity, where $\delta_2, \delta_1, \delta_0$ are the coefficients for the squared, linear and constant terms in the quadratic function.

$$IC = IC_E + IC_L, \tag{4.1}$$

$$IC_L = \sum_{l \in \mathscr{L}} (ic_l^r X_l + \rho_l(\delta_2 A_l^2 + \delta_1 A_l + \delta_0 X_l)). \tag{4.2}$$

The system operating condition with each set of investment decisions is evaluated through solving the daily MAR-OPF problem. Therefore, the 2nd block problem is formulated as a MISOCP problem. Regarding the investment decisions, we tackle binary (U, X) and continuous investment decisions (R, C, A) separately in the siting sub-stage and the sizing sub-stage problems, by formulating them as a MISOCP problem and a SOCP problem, respectively. The approach is in the block diagram shown in Fig. 4.2. When the binary investment decisions are determined optimally in the siting sub-stage, the nodes to install ESS assets and the lines for reinforcement are designated in the sizing sub-stage. The energy reservoir and power rating of ESS assets, and the ampacity of reinforced lines, are optimized through the sizing sub-stage. We apply the Benders decomposition to both stages obtaining a master problem and several parallel subproblems. The detailed procedure of siting and sizing sub-stages are given in the

following paragraphs.

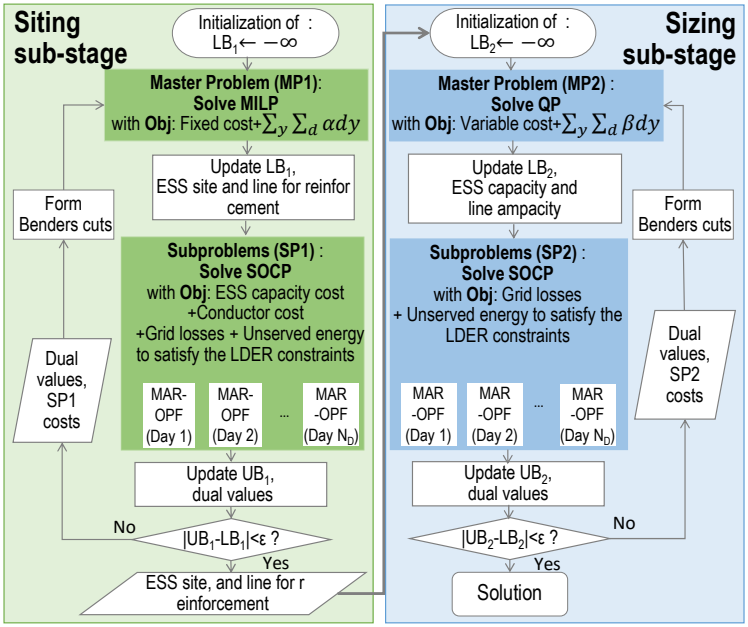

Figure 4.2: Detailed structure of the 2nd block problem.

Siting sub-stage - determination of the ESS site and line for reinforcement

Algorithm 4.1 The siting sub-stage of the 2nd block problem

Require: Network ($\mathscr{L}$), prosumption ($s_l = p_l + jq_l, \forall l \in \mathscr{L}$), ESS candidate nodes ($\mathcal{N}_E$)

1: **Initialization :** $\beta \leftarrow 1$
2: Solve master problem (MP1)
3: $LB_1 \leftarrow MC^{1st*}$
4: Update $U^{(\beta)*}, X^{(\beta)*}$ to feed the solution to subproblems
5: Solve parallel subproblems (SP1) employing Alg. 3.1
6: $UB_1 \leftarrow \sum_l ic_E^f U_l^{(\beta)*} + \sum_l (ic_l^r + \rho_l \delta_0) X_l^{(\beta)*} + \sum_y \sum_d SC_{dy}^{1st*}$
7: Update the dual values (τ, ξ)
8: **if** $|UB_1 - LB_1| \leq \epsilon$ **then**
9: **return** U^*, X^*
10: **else**
11: $\beta \leftarrow \beta + 1$
12: Update Benders cut with dual values
13: Go to step 2
14: **end if**

The problem structure of the siting sub-stage problem is illustrated on the left side of Fig. 4.2, and the detailed procedure is explained step by step in Alg. 4.1. The first iteration starts with solving the master problem, and the zero investment on ESSs and lines is given to the subproblems. The operation of each day-type is evaluated and the unserved load takes values

to ensure the feasibility of the subproblem regardless of the investment decision. Then the dual values are obtained with respect to the constraints fixing the value of the investment binary variables to zero (as given from the previous master problem). The master problem of the next iteration is updated with a set of Benders cuts constructed by the dual values and subproblems' objective values obtained from the previous subproblems.

The sites for the ESS allocation and the lines for reinforcement are accordingly updated by solving the master problem. Then, if any of the binary variable values associated with ESS sites and lines is determined as 1, each subproblem determines the capacity (ESS power rating and energy reservoir, or line ampacity) of the corresponding asset. Moreover, the operational objective is to minimize the unserved load and grid losses while complying with the LDER constraints. As the goal of this stage is to determine the best solution for the set of binary variables, the different ESSs and line conductors' sizes determined for each day-type are not the final solutions. Once the convergence of the Benders decomposition is reached, the binary solutions of the siting sub-stage are passed to the sizing sub-stage problem.

Eq.(4.3) shows the total investment cost. The part associated with binary variables is determined in the master problem as shown in (4.4), and the part linked to continuous variables, (4.5), is optimized in the subproblem specifically for each day-type and year.

$$IC = \sum_{l\in\mathscr{L}} \left(ic_E^f U_l + ic_E^e C_l + ic_E^p R_l \right) + \sum_{l\in\mathscr{L}} \left(ic_l^r + \rho_l \left(\delta_2 (A_l)^2 + \delta_1 A_l + \delta_0 \right) \right) \cdot X_l, \tag{4.3}$$

$$IC_b = \sum_{l\in\mathscr{L}} ic_E^f U_l + \sum_{l\in\mathscr{L}} \left(ic_l^r + \rho_l \delta_0 \right) \cdot X_l, \tag{4.4}$$

$$IC_c = \sum_{l\in\mathscr{L}} \left(ic_E^e C_l + ic_E^p R_l \right) + \sum_{l\in\mathscr{L}} \left(\rho_l \left(\delta_2 (A_l)^2 + \delta_1 A_l \right) \right). \tag{4.5}$$

Master problem : the formulation of the master problem is given in (4.6). The master problem only deals with the cost determined by binary variables regarding the nodes for ESS installation and line reinforcement. The objective function value of the master problem is computed by summing the fixed investment cost plus a portion of the conductor cost associated with the binary variables, and the lower approximation of the expected subproblem costs. α_{dy}^{1st} represents the subproblem cost for day-type d for year y. It is initially bounded by $\underline{\alpha}^{1st}$, which is the parameter given as the lower bound for the subproblem cost. $\beta \in \mathscr{B}_1$ is the index of the Benders iterations of the siting sub-stage problem. In every βth iteration, the Benders multi cuts represented by $\Gamma_{dy}^{(\beta)}$, $\forall d \in \mathscr{D}, y \in \mathscr{Y}$, are added, as shown in (4.6c). The lower bound of the total cost, so-called LB_1, is the optimal objective value of the master problem (*i.e.*, $LB_1 = MC^{1*}$).

$$\min_{U,X,\alpha^{1st}} : MC^1 = \sum_l ic_E^f U_l + \sum_l (ic_l^r + \rho_l \delta_0) X_l + \sum_y \sum_d \alpha_{dy}^{1st} \tag{4.6a}$$

subject to:

$$\alpha_{dy}^{1st} \geq \underline{\alpha}^{1st}, \qquad \forall d \in \mathscr{D}, \forall y \in \mathscr{Y}, \tag{4.6b}$$

$$\alpha_{dy}^{1st} \geq \Gamma 1_{dy}^{(\beta)}, \qquad \forall d \in \mathscr{D}, \forall y \in \mathscr{Y}, \forall \beta \in \mathscr{B}_1. \tag{4.6c}$$

Subproblem : the subproblem associated with day-type d and year y is formulated as a daily MAR-OPF model with varying ESSs' capacities and lines' ampacities with day-types and years. Solving each subproblem optimally sizes the ESSs capacity and lines ampacity while evaluating the investment plan based on its operational advantages on the system conditions. The optimization problem is modeled by the MAR-OPF as discussed in Sec. 3.5. In addition, the constraints modeling the line ampacity and the ESS capacity are included in the subproblem. Note that the variables for ESS energy reservoir, power rating and the line ampacity are assigned respectively for all day-types and years. The constraints linked to ESS capacities are given as (4.7).

$$R^{min} U_l \leq R_{ldy} \leq R^{max} U_l, \qquad \forall l \in \mathscr{L}, \tag{4.7a}$$

$$C^{min} U_l \leq C_{ldy} \leq C^{max} U_l, \qquad \forall l \in \mathscr{L}, \tag{4.7b}$$

$$R_{ldy} \leq \frac{C_{ldy}}{CR^{max}}, \qquad \forall l \in \mathscr{L}. \tag{4.7c}$$

The possible range of ampacity is modeled by (4.8a), while A^{min}/A^{max} represent minimum/-maximum possible line ampacity, respectively. However, as the line ampacity constraint is given with the the squared current variable (see (3.2k) and (3.2l) in Sec. 3.5), we need to model the squared ampacity to impose the ampacity constraints on the current variable. In order to avoid quadratic inequality constraints for the ampacity limit[11], the approximated value of the squared ampacity ($L(A_{ldy}^2)$) is used. The piecewise linearization technique is employed to approximate the squared ampacity as shown in (4.8c), while v is the step index and Υ_1 is the number of discretization steps. The possible range of squared ampacity is modeled as (4.8b). The ampacity constraints are modified accordingly from (3.2k) and (3.2l) to (4.8d), and (4.8e). The variables regarding the line for reinforcement and the squared ampacity are introduced in the right-hand side of (4.8d) and (4.8e). In the same way, Eqs. (4.8f) and (4.8g) replace (3.2m) and (3.2n) to consider the change of ampacity for deriving maximum possible value of active and reactive power flow of each line.

$$A^{min} X_l \leq A_{ldy} \leq A^{max} X_l, \qquad \forall l \in \mathscr{L}, \tag{4.8a}$$

$$(A^{min})^2 X_l \leq L(A_{ldy}^2) \leq (A^{max})^2 X_l, \qquad \forall l \in \mathscr{L}, \tag{4.8b}$$

$$L(A_{ldy}^2) \geq a_v A_{ldy} + b_v, \qquad \forall k \in \{1, ..., \Upsilon_1\}, \forall l \in \mathscr{L}. \tag{4.8c}$$

[11] The constraint is convex. However, quadratic inequality constraint is not preferred in the YALMIP environment and takes more computation burden for the solver as well.

$$I_l^t \le (1-X_l)\cdot(I_l^{max})^2 + L(A_{ldy}^2), \qquad \forall l \in \mathscr{L}, \forall \phi \in \Phi_{dy}, \forall t \in \mathscr{T}, \tag{4.8d}$$

$$I_l^b \le (1-X_l)\cdot(I_l^{max})^2 + L(A_{ldy}^2), \qquad \forall l \in \mathscr{L}, \forall \phi \in \Phi_{dy}, \forall t \in \mathscr{T}, \tag{4.8e}$$

$$\bar{P}_l^t \le \frac{v^{max}\big((1-X_l)\cdot I_l^{max} + A_{ldy}\big)}{\sqrt{2}}, \qquad \forall l \in \mathscr{L}, \tag{4.8f}$$

$$\bar{Q}_l^t \le \frac{v^{max}\big((1-X_l)\cdot I_l^{max} + A_{ldy}\big)}{\sqrt{2}}, \qquad \forall l \in \mathscr{L}. \tag{4.8g}$$

The constraints related to the line reinforcement described above and the ESSs investment constraints (see (4.7)) are incorporated into the OPF constraints described in Sec. 3.5.

In short, from the MAR-OPF model including ESS power dispatch, or $\Theta'(\varphi'^E) \ge 0$, where $\varphi'^E = \{S^t, v, f, \hat{S}^t, \bar{v}, \bar{f}, \bar{S}^t, s', s^E, up^+, up^-, uq^+, uq^-, \zeta\}$ (see Sec. 3.6.3), (3.2i)-(3.2n) are replaced by (4.8d)-(4.8g) to take into account the change of ampacity due to the line reinforcement into the MAR-OPF model. The changed OPF model is collectively notated as $\Theta^{A'}(\varphi'^E) \ge 0$.

In this way, we can define the subproblems of the siting sub-stage as follows. The objective function of the subproblem is defined by (4.9a). It consists of the capacity cost of the ESSs' energy reservoirs and power ratings, as well as the conductors' cost with respect to the upgraded ampacity caused by the line reinforcement. Also, it includes the operational cost, which consists of grid losses cost and the unserved energy cost. The considered constraints include capacity investment cost for ESSs and lines' conductors (4.9b), constraints modeling ideal ESSs operational characteristics (4.9c) and, finally, the changed MAR-OPF model including the line reinforcement (4.9d). Eqs. (4.9e) and (4.9f) describe how the ESSs' locations and lines to be reinforced are fixed to the optimal solution of the master problem, respectively. τ_{ldy} and χ_{ldy} are the duals of constraints related to the fixed ESSs locations and the lines for reinforcement, respectively.

$$\begin{aligned}\min_{\substack{\forall R,C,A;\\ \forall \varphi'^E,\pi}} : SC_{dy}^1 = {} & \frac{N_{dy}}{(1+r_{dis})^y}\sum_{t\in\mathscr{T}}\sum_{\phi\in\Phi_{dy}}\lambda_\phi\Big(w_l\sum_{l\in\mathscr{L}} r_l f_{l\phi t} \\ & + w_u\sum_{l\in\mathscr{L}}(up_{l\phi t}^+ + up_{l\phi t}^- + uq_{l\phi t}^+ + uq_{l\phi t}^-)\Big) \\ & + \frac{N_{dy}}{365*Y}\sum_{l\in\mathscr{L}}(ic_E^e C_{ldy} + ic_E^p R_{ldy}) \\ & + \frac{N_{dy}}{365*Y}\sum_{l\in\mathscr{L}}\rho_l(\delta_2 L(A_{ldy}^2) + \delta_1 A_{ldy})\end{aligned} \tag{4.9a}$$

subject to:

$$(4.7), (4.8a) - (4.8c), \tag{4.9b}$$

$$\Lambda(\pi_{l\phi}) \ge 0, \qquad \forall \in \mathscr{L}, \forall \phi \in \Phi_{dy}, \tag{4.9c}$$

$$\Theta^{A'}(\varphi'^E_{\phi t}) \ge 0, \qquad \phi \in \Phi_{dy}, t \in \mathscr{T}, \tag{4.9d}$$

$$U_l = U_l^{(\beta)*} : \tau_{ldy}, \qquad \forall l \in \mathscr{L}, \tag{4.9e}$$

$$X_l = X_l^{(}\beta)* : \chi_{ldy}, \qquad \forall l \in \mathscr{L}. \tag{4.9f}$$

where $\varphi'^E = \{S^t, v, f, \hat{S}^t, \bar{v}, \bar{f}, \bar{S}^t, s'{=}p'{+}jq', s^E{=}p^E{+}q^E, up^+, up^-, uq^+, uq^-, \zeta\}$ is the set of variables of MAR-OPF model. Note that we follow Alg. 3.1 to solve the formulated subproblems iteratively until the convergence criterion is satisfied (see Sec. 3.6.3).

$$\Gamma 1_{dy}^{(\beta)} = \left[SC_{dy}^{1*} - \sum_{l\in\mathscr{L}} (\tau_{ldy}(U_l - U_l^{(\beta)*}) + \chi_{ldy}(X_l - X_l^{(\beta)*}))\right], \qquad \forall d \in \mathscr{D}, \forall y \in \mathscr{Y}, \forall \beta \in \mathscr{B}_1. \tag{4.10}$$

The Benders cuts for the master problem for the next iteration are built with the dual variables and the objective value of the subproblem as shown in (4.10). The upper bound of the total planning cost, or UB_1, is calculated summing the optimal investment cost and the subproblem costs (*i.e.*, $UB_1 = \sum_l ic_E^f U_l^{(\beta)*} + \sum_l (ic_l^r + \rho_l \delta_0) X_l^{(\beta)*} + \sum_{y\in\mathscr{Y}} \sum_{d\in\mathscr{D}} SC_{dy}^{1*}$).

Sizing sub-stage - determination of the ESSs size and reinforced lines' ampacity

The problem structure of the sizing sub-stage problem is shown on the right side of Fig. 4.2. The detailed procedure of solving sizing sub-stage is described in Alg. 4.2. The nodes for ESS allocation and the lines for reinforcement determined in the siting stage are fed into the sizing sub-stage. We solve another optimization problem using the Benders decomposition to determine the optimal size of the ESS capacity and the line ampacity. Eq.(4.11) shows the total investment cost for the 2nd sub-stage, while expressing the updated ampacity (A_l) as the sum of original ampacity (I_l^{max}) and the change of ampacity (ΔA_l).

$$\begin{aligned} IC = & \sum_{l\in\mathscr{L}} \left(ic_E^f U_l^* + ic_E^e C_l + ic_E^p R_l \right) \\ & + \sum_{l\in\mathscr{L}} \left(ic_l^r + \rho_l \left(\delta_2 (I_l^{max} + \Delta A_l)^2 + \delta_1 (I_l^{max} + \Delta A_l) + \delta_0 \right) \right) \cdot X_l^* \end{aligned} \tag{4.11}$$

By keeping the installation status fixed to the siting sub-stage solution (U_l^*, X_l^*), the total investment cost now depends on the continuous investment variables. The part of investment cost associated to the continuous investment variables can be extracted as the following.

$$IC_C = \sum_{l\in\mathscr{L}} \left(ic_E^e C_l + ic_E^p R_l \right) + \sum_{l\in\mathscr{L}} \rho_l \left(\delta_2 (\Delta A_l)^2 + (2\delta_2 I_l^{max} + \delta_1) \Delta A_l \right) \tag{4.12}$$

The master problem considers the ESS capacity for the buses chosen to have ESSs investment and the line ampacity for the lines identified to be reinforced. The subproblem deals with the fitness evaluation of the determined allocations in terms of the same operational requirement and objectives as in the siting sub-stage subproblem.

Algorithm 4.2 The sizing sub-stage of the 2nd block problem.

Require: Network ($\mathscr{L}$), prosumption (s_l=p_l+$jq_l, \forall l \in \mathscr{L}$), ESS location ($U^*$), Line for reinforcement (X^*)

1: **Initialization :** $LB_2 \leftarrow 0, \beta \leftarrow 1$
2: Solve master problem (MP2)
3: $LB_2 \leftarrow MC^{2nd*}$
4: Update R^*, C^*, A^* to feed the solution to subproblems
5: Solve parallel subproblems (SP2)
6: $UB_2 \leftarrow \sum_l (ic_E^f C_l^{(\beta)*} + ic^r R_l^{(\beta)*}) + \sum_l \rho_l (\delta_2 (\Delta A_l^{(\beta)*})^2 + (2\delta_2 I_l^{max} + \delta_1)\Delta A_l^{(\beta)*}) + \sum_y \sum_d SC_{dy}^{2nd*}$
7: Update the dual values (μ, ϑ, ι)
8: **if** $|UB_2 - LB_2| \leq \epsilon$ **then**
9: **return** R^*, C^*, A^*
10: **else**
11: $\beta \leftarrow \beta + 1$
12: Update Benders cut with dual values
13: Go to step 2
14: **end if**

Master problem : the sizing sub-stage master problem is modeled only with continuous variables. The variable parts of the ESS investment cost (the part associated with energy reservoir and power rating) and the conductor cost (the part associated with the ampacity change) are only included in the objective of the master problem. The constraints associated with ESS energy reservoir and power rating are included as well (see (2.16a)-(2.16c)). The possible range for the change of line ampacity is given by (4.13c). The anticipated subproblem cost is approximated by α_{dy}^{2nd}. Starting from lower bound subproblem cost value $\underline{\alpha}^{2nd}$ (see (4.13d)), α_{dy}^{2nd} is updated by the Benders cuts $\Gamma 2_{dy}^{(\beta)}$ defined for $\forall d \in \mathscr{D}$, $\forall y \in \mathscr{Y}$, $\forall \beta \in \mathscr{B}_2$, where $\mathscr{B}_2$ is the Benders iterations of the sizing sub-stage problem as given by (4.13e). The lower bound of the sizing sub-stage cost, LB_2, is the optimal objective value of the master problem (*i.e.*, $LB_2 = MC^{2*}$).

$$\min_{\forall R,C,\Delta A,\alpha^{2nd}} : MC^2 = \sum_{l\in\mathscr{L}} (ic_E^e C_l + ic_E^p R_l) + \sum_{l\in\mathscr{L}} \rho_l (\delta_2 (\Delta A_l)^2 + (2\delta_2 I_l^{max} + \delta_1)\Delta A_l) + \sum_y \sum_d \alpha_{dy}^{2nd} \tag{4.13a}$$

subject to:

$$(2.16a) - (2.16c), \tag{4.13b}$$

$$0 \leq \Delta A_l \leq \Delta A^{max}, \qquad \forall l \in \mathscr{L}, \tag{4.13c}$$

$$\alpha_{dy}^{2nd} \geq \underline{\alpha}^{2nd}, \qquad \forall d \in \mathscr{D}, \forall y \in \mathscr{Y}, \forall \beta \in \mathscr{B}_2, \tag{4.13d}$$

$$\alpha_{dy}^{2nd} \geq \Gamma 2_{dy}^{(\beta)}, \qquad \forall d \in \mathscr{D}, \forall y \in \mathscr{Y}, \forall \beta \in \mathscr{B}_2. \tag{4.13e}$$

Subproblem : the subproblem of the sizing sub-stage evaluates the system operational condition under the investment decision given by the master problem. The optimization problem is defined with the similar set of operating constraints as in the subproblem of the siting sub-stage. However, unlike in the siting sub-stage where we consider an ESS as an ideal system, in this stage, we consider more accurate modeling for a realistic ESSs accounting for their energy losses while charging/discharging. It is done by including the model of ESS losses proposed in [2], that is by adding an additional resistive line (*i.e.*, an equivalent resistance[12] for the ESS losses) adjacent to the ESSs-allocated nodes and treating them similarly as other lines in the AC-OPF. The resistance model is shown in Fig. 4.3. In the figure, the positive sign of the ESS power denotes ESS charging power. Note that the model is originally conceived for batteries but can be used to represent the losses of other ESS technologies. The set of the virtual nodes corresponding to the additional lines is denoted as $\mathscr{L}^E$. For the virtual nodes, we introduce the ideal ESS injection (in place of load injection) to the MAR-OPF model.

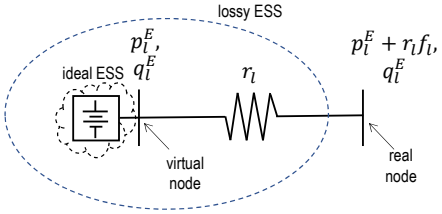

Figure 4.3: The resistance model of lossy ESS adopted from [2].

In this regard, the constraint modeling the ESSs' compensation of dispatch error need to be modified to take into account the resistance of the virtual lines connected to the ideal ESSs. By changing from (3.9f) to (4.14a), the sum of the ESS active power is replaced by the sum of the active power injected at the sending end of virtual lines. Indeed, we adopt the iterative algorithm proposed as Alg. 3.1 in Sec. 3.6.3 for solving the subproblem, and therefore, (4.14b) and (4.14c) are utilized in place of (4.14a).

$$\sum_{l\in\mathscr{L}}(\Delta p'_{l\phi t}+r_l\Delta f_{l\phi t}) = \sum_{l\in\mathscr{L}}\epsilon_{l\phi t}+\sum_{l\in\mathscr{L}^E}P^t_{l\phi t}, \qquad \forall\phi\in\Phi_{dy},\forall t\in\mathscr{T}, \tag{4.14a}$$

$$\sum_{l\in\mathscr{L}}(\Delta p'_{l\phi t}+r_l\Delta f_{l\phi t}) = \sum_{l\in\mathscr{L}}\epsilon_{l\phi t}+\sum_{l\in\mathscr{L}^E}P^t_{l\phi t},+\zeta^m_{\phi t}, \qquad \forall\phi\in\Phi_{dy},\forall t\in\mathscr{T}, \tag{4.14b}$$

$$\sum_{l\in\mathscr{L}}\Delta p'_{l\phi t}+\gamma^m_{\phi t} = \sum_{l\in\mathscr{L}}\epsilon_{l\phi t}+\sum_{l\in\mathscr{L}^E}P^t_{l\phi t}, \qquad \forall\phi\in\Phi_{dy},\forall t\in\mathscr{T}. \tag{4.14c}$$

Moreover, power balance equations including ESSs' power are changed accordingly. The lines linking the real nodes do not include the ESS injections as shown in (4.15). The ESS powers

[12]The resistances are updated in proportion to the ESS capacity using the reference value in [2]

are injected only at the lines connected to the virtual nodes as shown in (4.16).

$$S_l^t = s_l' + \sum_{m\in\mathscr{L}} \mathbf{H}_{l,m} S_l^t + z_l f_l - j(v_{up(l)\phi t} + v_l) b_l, \qquad \forall l \in \mathscr{L}, \tag{4.15a}$$

$$S_l^b = s_l' + \sum_{m\in\mathscr{L}} \mathbf{H}_{l,m} S_l^t, \qquad \forall l \in \mathscr{L}, \tag{4.15b}$$

$$\hat{S}_l^t = s_l' + \sum_{m\in\mathscr{L}} \mathbf{H}_{l,m} \hat{S}_l^t - j(\bar{v}_{up(l)} + \bar{v}_l) b_l, \qquad \forall l \in \mathscr{L}, \tag{4.15c}$$

$$\hat{S}_l^b = s_l' + \sum_{m\in\mathscr{L}} \mathbf{H}_{l,m} \hat{S}_l^t \qquad \forall l \in \mathscr{L}, \tag{4.15d}$$

$$\bar{S}_l^t = s_l' + \sum_{m\in\mathscr{L}} \mathbf{H}_{l,m} \bar{S}_l^t + z_l f_l - j(v_{up(l)} + v_l) b_l \qquad \forall l \in \mathscr{L}, \tag{4.15e}$$

$$\bar{S}_l^b = s_l' + \sum_{m\in\mathscr{L}} \mathbf{H}_{l,m} \bar{S}_l^t, \qquad \forall l \in \mathscr{L}. \tag{4.15f}$$

$$S_l^t = s_l' + s_l^E + \sum_{m\in\mathscr{L}} \mathbf{H}_{l,m} S_l^t + z_l f_l - j(v_{up(l)\phi t} + v_l) b_l, \qquad \forall l \in \mathscr{L}^E, \tag{4.16a}$$

$$S_l^b = s_l' + s_l^E + \sum_{m\in\mathscr{L}} \mathbf{H}_{l,m} S_l^t, \qquad \forall l \in \mathscr{L}^E, \tag{4.16b}$$

$$\hat{S}_l^t = s_l' + s_l^E + \sum_{m\in\mathscr{L}} \mathbf{H}_{l,m} \hat{S}_l^t - j(\bar{v}_{up(l)} + \bar{v}_l) b_l, \qquad \forall l \in \mathscr{L}^E, \tag{4.16c}$$

$$\hat{S}_l^b = s_l' + s_l^E + \sum_{m\in\mathscr{L}} \mathbf{H}_{l,m} \hat{S}_l^t \qquad \forall l \in \mathscr{L}^E, \tag{4.16d}$$

$$\bar{S}_l^t = s_l' + s_l^E + \sum_{m\in\mathscr{L}} \mathbf{H}_{l,m} \bar{S}_l^t + z_l f_l - j(v_{up(l)} + v_l) b_l \qquad \forall l \in \mathscr{L}^E, \tag{4.16e}$$

$$\bar{S}_l^b = s_l' + s_l^E + \sum_{m\in\mathscr{L}} \mathbf{H}_{l,m} \bar{S}_l^t, \qquad \forall l \in \mathscr{L}^E. \tag{4.16f}$$

The change in line ampacity are incorporated to the line ampacity limit constraints as shown in (4.17a) and (4.17b). In order to avoid quadratic inequality constraints for the ampacity limit, the squared term of ΔA_l is simply expressed by multiplication of the optimal value of ΔA_l^* determined in the previous iteration of master problem and variable ΔA_l. Likewise, the constraints on the upper-bound active and reactive power are changed to (4.17c) and (4.17d).

To summarize, from the MAR-OPF model including ESS power dispatch, or $\Theta'(\varphi'^E) \geq 0$, where $\varphi'^E = \{S^t, v, f, \hat{S}^t, \bar{v}, \bar{f}, \bar{S}^t, s', s^E, up^+, up^-, uq^+, uq^-, \zeta\}$ (see Sec. 3.6.3), (3.2i)-(3.2n) are replaced by (4.17) to take account the change of ampacity due to the line reinforcement into the MAR-OPF model of the sizing sub-stage subproblem. Moreover, by applying the lossy ESS model to the MAR-OPF model, the power balance equations (3.10) are substituted by (4.15) and (4.16) to separately consider the power flows at the real line and virtual lines. In addition, the ESS's contribution to the dispatch error compensation are represented by (4.14b) and (4.14c), replacing (3.11). The set of OPF equations obtained from $\Theta'(\varphi'^E) \geq 0$ by the

above-mentioned replacements are collectively defined as $\Theta^{\Delta A'}(\varphi'^{E}) \geq 0$.

$$I^{t}_{l\phi t} \leq (I^{max}_{l})^2 + 2I^{max}_{l}\Delta A_l + \Delta A^{*}_{l} \cdot \Delta A_l, \qquad \forall l \in \mathscr{L}, \tag{4.17a}$$

$$I^{b}_{l\phi t} \leq (I^{max}_{l})^2 + 2I^{max}_{l}\Delta A_l + \Delta A^{*}_{l} \cdot \Delta A_l, \qquad \forall l \in \mathscr{L}, \tag{4.17b}$$

$$\tilde{P}^{t}_{l} \leq \frac{v^{max}(I^{max}_{l} + \Delta A_l)}{\sqrt{2}}, \qquad \forall l \in \mathscr{L}, \tag{4.17c}$$

$$\tilde{Q}^{t}_{l} \leq \frac{v^{max}(I^{max}_{l} + \Delta A_l)}{\sqrt{2}}, \qquad \forall l \in \mathscr{L}. \tag{4.17d}$$

Finally, the subproblem of the sizing sub-stage is formulated below. As shown in (4.18a), the objective is to minimize the total grid losses and unserved prosumption to satisfy the LDER constraint. The ideal ESS operation constraints are given as (4.18b), and the constraints associated with MAR-OPF model including the change of line ampacity are indicated by (4.18c). The ESSs' power ratings, their energy reservoirs, and the change of lines' ampacity are fixed to the optimal solution values of the master problem as shown in (4.18d)-(4.18f), and μ_{ldy}, ϑ_{ldy}, and ι_{ldy} are the corresponding dual values.

$$\begin{aligned}\min_{\forall \varphi'^{E}, \pi} : SC^{2}_{dy} = \frac{N_{dy}}{(1+r_{dis})^{y}} \sum_{t \in \mathscr{T}} \sum_{\phi \in \Phi_{dy}} \lambda_{\phi} \Big(w_l \sum_{l \in \mathscr{L}} r_l f_{l\phi t} \\ + w_u \sum_{l \in \mathscr{L}} (up^{+}_{l\phi t} + up^{-}_{l\phi t} + uq^{+}_{l\phi t} + uq^{-}_{l\phi t}) \Big)\end{aligned} \tag{4.18a}$$

subject to:

$$\Lambda(\pi_{l\phi}) \geq 0, \qquad \forall l \in \mathscr{L}^{E}, \forall \phi \in \Phi_{dy}, \tag{4.18b}$$

$$\Theta^{\Delta A'}(\varphi'^{E}_{\phi t}) \geq 0, \qquad \forall \phi \in \Phi_{dy}, \forall t \in \mathscr{T}, \tag{4.18c}$$

$$R_l = R^{(\beta)*}_{l} : \mu_{ldy}, \qquad \forall l \in \mathscr{L}^{E}, \tag{4.18d}$$

$$C_l = C^{\beta)*}_{l} : \vartheta_{ldy}, \qquad \forall l \in \mathscr{L}^{E}, \tag{4.18e}$$

$$\Delta A_l = \Delta A^{\beta)*}_{l} : \iota_{ldy}, \qquad \forall l \in \mathscr{L}. \tag{4.18f}$$

The dual values are used to construct the Benders cut for βth Benders iteration at day-type d and year y, as shown in (4.19).

$$\Gamma 2^{(\beta)}_{dy} = \Big[SC*^{2*}_{dy} - \sum_{l \in \mathscr{L}} (\mu_{ldy}(R_l - R^{(\beta)*}_{l}) + \vartheta_{ldy}(C_l - C^{((\beta)*}_{l}) + \iota_{ldy}(\Delta A_l - \Delta A^{(\beta)*}_{l})) \Big]. \tag{4.19}$$

The upper bound of the sizing sub-stage problem, or UB_2, is calculated by summing the variable investment cost and the subproblem costs (*i.e.*, $UB_2 = \sum_{l \in \mathscr{L}^{E}} (ic^{e}_{E} C^{(\beta)*}_{l} + ic^{p}_{E} R^{(\beta)*}_{l})$ $+ \sum_{l \in \mathscr{L}} \rho_l (\delta_2 (\Delta A^{(\beta)*}_{l})^2 + (2\delta_2 I^{max}_{l} + \delta_1) \Delta A^{(\beta)*}_{l}) + \sum_{y \in \mathscr{Y}} \sum_{d \in \mathscr{D}} SC^{2*}_{dy}$).

4.7 Simulations

4.7.1 Simulation Configuration

The performance of the proposed method is assessed on the distribution network introduced in the previous chapters (see Fig. 3.3). Other parameters such as annual growth rate of load consumption and discount rate are the same as well. The operating scenarios are the same as in Sec. 2.10.1. The parameters associated with ESSs' investment are given as Table 2.1. The penalty cost for the dispatch error is assumed to be \$897/MWh (see Table 3.1 in Sec. 3.7 for the justifying the value assumed for the penalty cost). The weight coefficients for grid losses and unserved energy are equal to 6k/MWh and 100k/MWh, respectively(*i.e.*, the same as in Sec. 3.7).

In Table 4.1, the fixed costs associated to the lines' investment are given differently depending on the type of connection, considering that the estimated cost for constructing underground cables is roughly 4 times higher than overhead lines [105]. Fig. 4.4 shows the fittings of conductor cost and line parameters according to the line ampacity. As shown in Fig. 4.4(a), a quadratic function exhibits a better fit quality for the data. Thus, the conductor cost is modeled as the quadratic function of line ampacity and the associated equation and coefficients (δ_2, δ_1, and δ_0) are indicated in the graph. In Fig. 4.4(b), the equation of hyperbolic curve best fits the line resistance data and associated coefficients (α_2^r, α_1^r, and α_0^r) are shown as well. Likewise, the linear sensitivity coefficients for the change in the line's reactance and susceptance (Δx and Δb) are indicated in Fig. 4.4(c) and (d), respectively.

Table 4.1: Parameters related to line reinforcement.

Fixed cost for overhead lines	\$0.12M/km [96]
Fixed cost for underground cables	\$0.48M/km [106]

We solve a co-optimized planning problem using the determined operating scenario set to achieve the optimal level of dispatchability of ADNs by allocating ESS assets, while ensuring a sufficient hosting capacity by including the line reinforcement as investment options. First, we compare the two cases where different planning strategies are considered : 1) planning of only ESS assets, 2) co-optimized planning considering ESS allocation and line reinforcement. We compare the performance of the two planning approaches by analyzing the trend of investment decisions with respect to varying PV penetration levels. Then, another set of planning exercises using the co-optimized planning tool is conducted under different operating condition, namely, PV injection shifted to different set of nodes and lines with reduced ampacity, to observe how the change of operating condition affects the optimal investment solution. The performance of the solution approach based on the reformulation of planning problem to two sub-stages is analysed by comparing it in terms of computation time and the planning result with the original solution approach described in Sec. 3. Finally, the planning tool is applied on networks of different sizes ranging from 25 nodes to 123 nodes

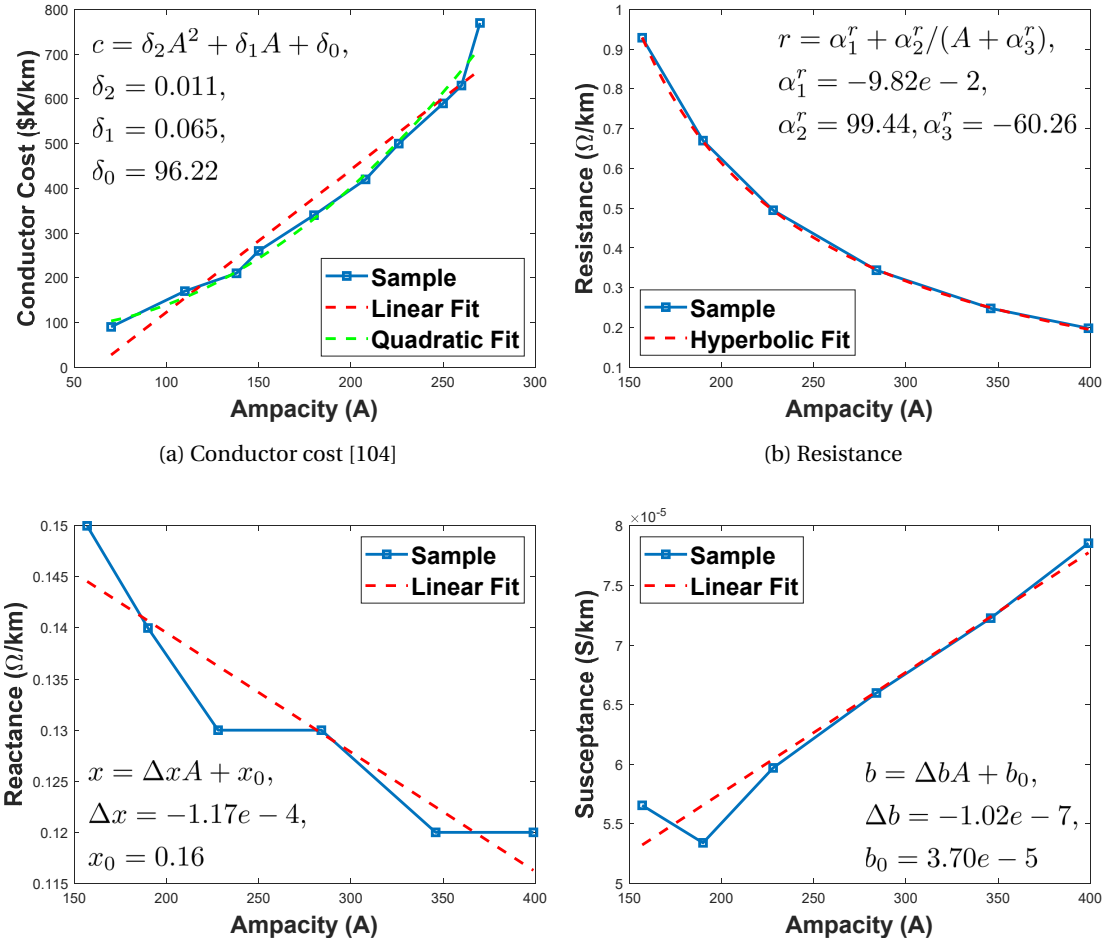

(a) Conductor cost [104]

(b) Resistance

(c) Reactance

(d) Susceptance

Figure 4.4: Fitting of line parameters as function of ampacity. Line data adapted from MV cable and overhead line manufactures.

to show its scalable applicability.

4.7.2 Effect of Co-optimized Planning : Comparison between the Case with ESSs only, and the Case with both ESSs and Line Reinforcement

We solve the planning problem by implementing two different planning strategies: 1) considering only ESSs as an investment option, and 2) considering both ESSs and line reinforcement as investment options. We considered the prosumption profile of one day-type with 24 dispatch timesteps for the simulation. We compare the investment results under different levels of PV capacities, ranging from 0 % to 500 % of existing PV capacity.

Fig. 4.5 shows the ADN topology with candidate nodes for ESS allocation, nodes where the ESSs are allocated, and the reinforced lines. Fig. 4.6(a) and Fig. 4.6(b) show the allocated energy reservoir sizes and power rating sizes with different level of PV capacity, respectively.

Each stacked bar graph in Fig. 4.6 represents the total ESSs' capacity at the specific PV level. Note that each colored section of the stacked bar graph corresponds to the allocated ESS size at the node indicated with the same color in Fig. 4.5. There is no difference in the investment solutions between the two strategies in the cases from 0 to 400% of PV capacity. In the cases of 0 PV and 100 % PV levels, an ESS asset is allocated at Node 4. Then, as the PV level increases to values higher than 100 %, the sites where ESSs are located change to Node 16 and Node 27. The high level of PV injection at Node 16 (where nearly 60 % of the total PV capacity is located) accounts for the ESS allocation at Node 16, as the allocated ESS can directly absorb the high uncertainty of the local generation. Another ESS is located closer to the GCP to tackle the prosumption uncertainty more effectively. Finally, at the level of 500 %, Strategy 1 and 2 yield different investment solutions. The investment solution of the two strategies in the case of 500 % of PV capacity are shown in Table 4.2. By Strategy 1, it is observed that the ESS size at Node 16 does not increase due to the binding ampacity constraint for the line connecting Node 9 and Node 20 (Line 9-20). Instead, the ESS is allocated at Node 45 with the maximum energy reservoir capacity (in the opposite direction from Line 9-20) such that the excess of power flow can be absorbed by the ESS and the line congestion problem is solved. In contrast, by Strategy 2, the ESS size at Node 16 is increased substantially compared to the case of 400% PV level. Accordingly, Line 9-20, which is located upstream to the ESS, is also upgraded to host the power flow considering the power dispatch from/to installed ESSs (see Fig. 4.6 for the location of updated lines and Table 4.2 for the ampacity change value.)

Thanks to the line reinforcement, the network is operated such that the grid constraints are successfully satisfied with a negligible amount of the unserved load as shown in Table 4.3. The cost results of the two strategies are shown in Table 4.3. The difference in investment costs of Strategy 1 and 2 comes from the additional allocation of ESSs by Strategy 1 at Node 45 with significant capacity due to the binding ampacity limit. The monetized cost related to grid losses and expected energy not served (EENS) are higher in Strategy 1 than 2. Therefore, the planning solution of Strategy 1 is sub-optimal compared to that of Strategy 2. The result verifies that the co-optimization of ESS allocation and line reinforcement is indispensable to achieve a sufficient level of dispatchability while guaranteeing the feasibility and reliability of the ADN operation, especially when a constant growth of load consumption and the renewable energy generation is projected within the planning horizon.

Table 4.2: The investment solutions of Strategy 1 and 2 in the case of 500 % PV capacity.

	Strategy 1			Strategy 2	
ESS nodes	16	27	45	16	27
Energy reservoir (kWh)	2767	7000	7000	6289	7000
Power rating (kVA)	1558	848	1750	3040	779
Reinforced lines	-			9-20	
Line ampacity change (ΔA)	-			30	

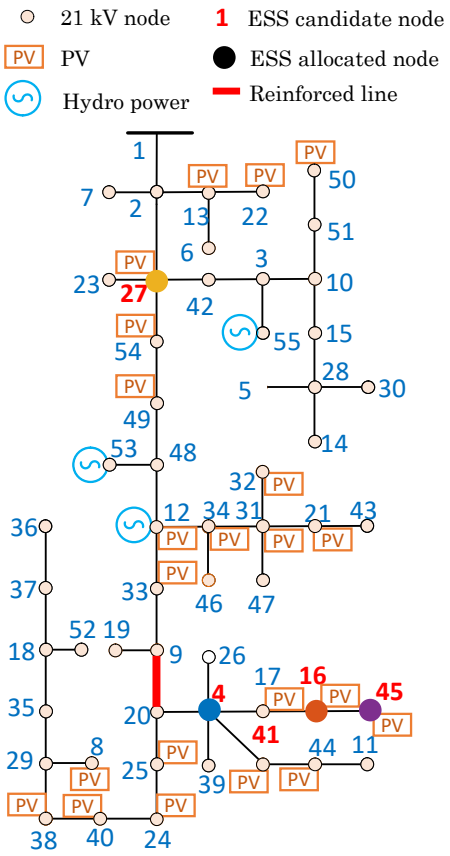

Figure 4.5: ADN topology used for the joint ESS allocation and line reinforcement.

Table 4.3: The planning cost of Strategy 1 and 2 in the case of 500 % PV capacity.

	strategy 1	Strategy 2
Investment cost ($M)	4.900	4.192
Monetized grid losses cost ($M)	1.168	1.152
Monetized EENS cost ($M)	1.93E-3	7.60E-4
Total cost ($M)	6.019	5.345

4.7.3 Planning Results with Different Levels of PV Capacities

In this subsection, we solve the planning problem with the same network topology with PV sites shifted, considering various levels of PV capacities. The lines ampacities are shrunk to make binding ampacity constraints such that we can observe more clearly the trend of investments along with changing operation condition. In this configuration, note that the PV generation with biggest capacity (60% of the total PV capacity) is located at Node 15 instead of Node 16. Fig. 4.7 shows the dispatch operation result of day-type 1 considering 100% of PV capacity. Fig. 3.4(a) shows the aggregated prosumption scenarios along with the aggregated prosumption prediction, whereas Fig. 3.4(b) represents the dispatch result after investing both on ESSs and lines. Thanks to the proposed planning strategy, the dispatch result shows

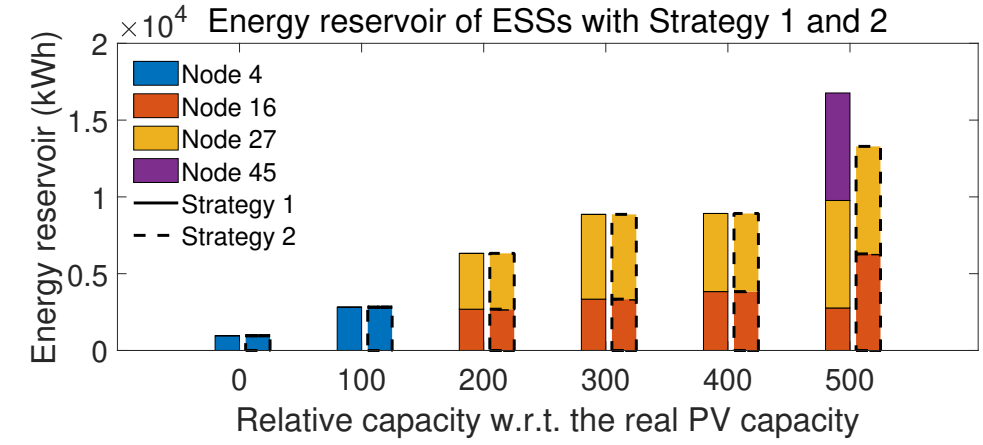

(a)

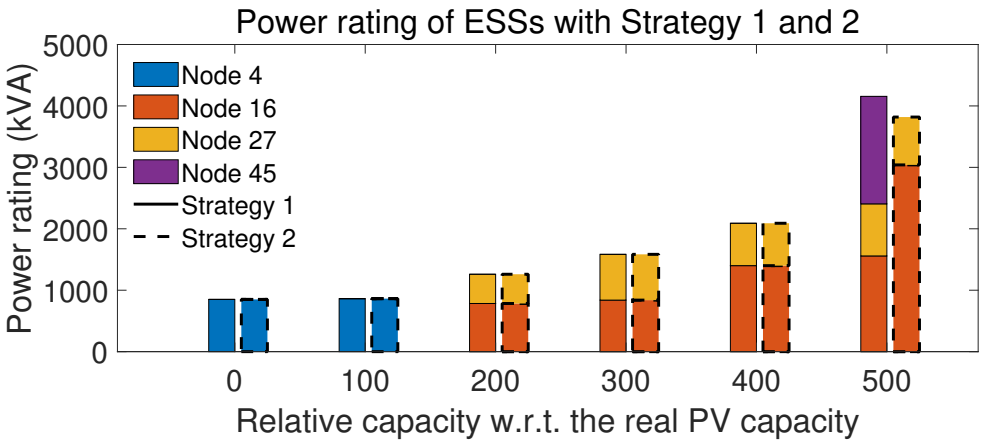

(b)

Figure 4.6: (a) Energy reservoir (kWh), (b) Power rating (kVA).

that the power flow at the GCP of all scenarios follows the dispatch plan with the dispatch error determined by the optimal dispathability level of ADN. To address the impact of the PV generation uncertainty, different levels of PV capacity (*i.e.*, 0-500% of the existing PV capacity within the ADN) are fed into the proposed planning tool. The locations of ESSs and lines to be reinforced are determined as in Fig. 4.8(a). As shown in Fig. 4.8(b), the ESSs allocated at Node 4 and Node 27 increase their power ratings and energy reservoirs with the increase of PV capacity. The capacity of ESS at Node 27 increases more with respect to the increasing PV levels than the one of the ESS at Node 4. This is to compensate for the uncertainty of PV generation mostly attributed to Node 15 where the PV panels with the biggest capacity are located (1.6MWp at 100% of the existing PV capacity). In Fig. 4.8(c), the ampacity changes of the lines indicated with bold-colored lines in Fig. 4.8(a) are shown. A decrease in ampacity change is observed in Line 48-12 and Line 49-48 as the PV penetration level increases. This is because the load consumption is mainly satisfied locally by the generation from nearby PV generation units, rather than by the power infeed from the GCP. On the other hand, four

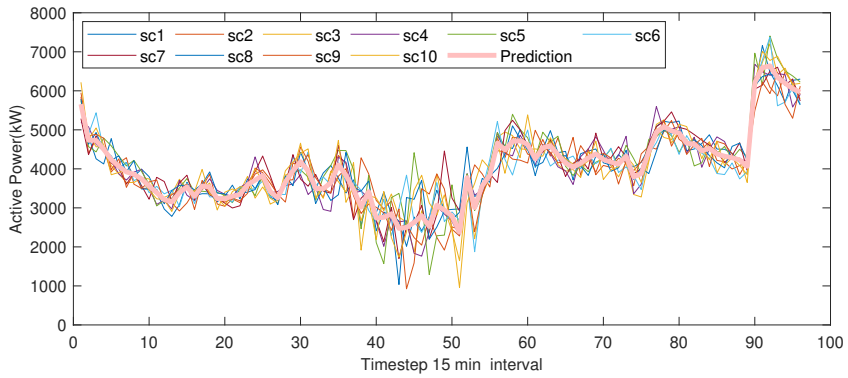

(a)

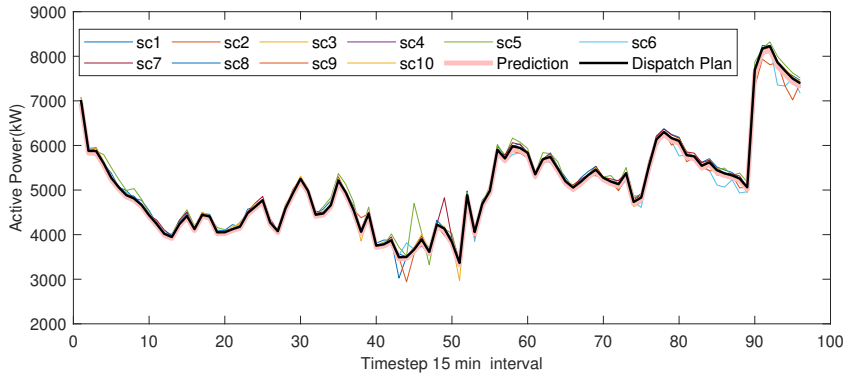

(b)

Figure 4.7: Dispatch result of Day 1: (a) Aggregated prosumption scenarios and prosumption prediction, (b) Power flow through GCP of scenarios, prosumption prediction and dispatch plan (Imbalance price : $897/MWh).

lines connecting the branches leading to GCP) and Node 15: Line 27-42, Line 42-3, Line 3-10, and Line 10-15, get updated starting from 300% and 200% of PV capacities, respectively, to support the increasing reverse power flow fed by the PV generation from Node 15. Lastly, the ampacity change of Line 2-27 decreases until the PV penetration level reaches 300% thanks to the local generation satisfying the load consumption. As the total PV generation level grows to more than 300%, the excessive PV generation, as well as the increased dispatch of bigger ESS at Node 27, increase the power flow through the branches leading to the GCP, increasing the required ampacity change of Line 2-27. Finally, Fig. 4.9(a) and Fig. 4.9(b) show the comparison of the total cost related to the operation (imbalance, grid losses and unserved energy) and investment under different PV capacities. Fig. 4.9(a) illustrates the cost of imbalance penalty and investment with and without the ESS allocation (noted as 'EX' and 'EO' which represent the planning case without ESS and with ESS, respectively) determined in the 1st block problem. The imbalance penalty cost for the case without ESS installation increases drastically along with the level of PV capacity within the ADN. As a result, the imbalance cost is expected to be less than one-tenth of the default case in all PV capacities cases. Indeed, the investment cost

associated with ESS allocation increases with larger PV capacity to achieve the optimal level of ADN's dispatchability. As shown in Fig. 4.9(b), the investment cost related to the ESS allocation and the line reinforcement increases with the increasing PV capacity. The cost related to EENS remains negligible until the PV capacity of 300% whereas when the PV capacity is beyond 300% (*i.e.*, 400% and 500%), the resulting EENS increases due to potential curtailment.

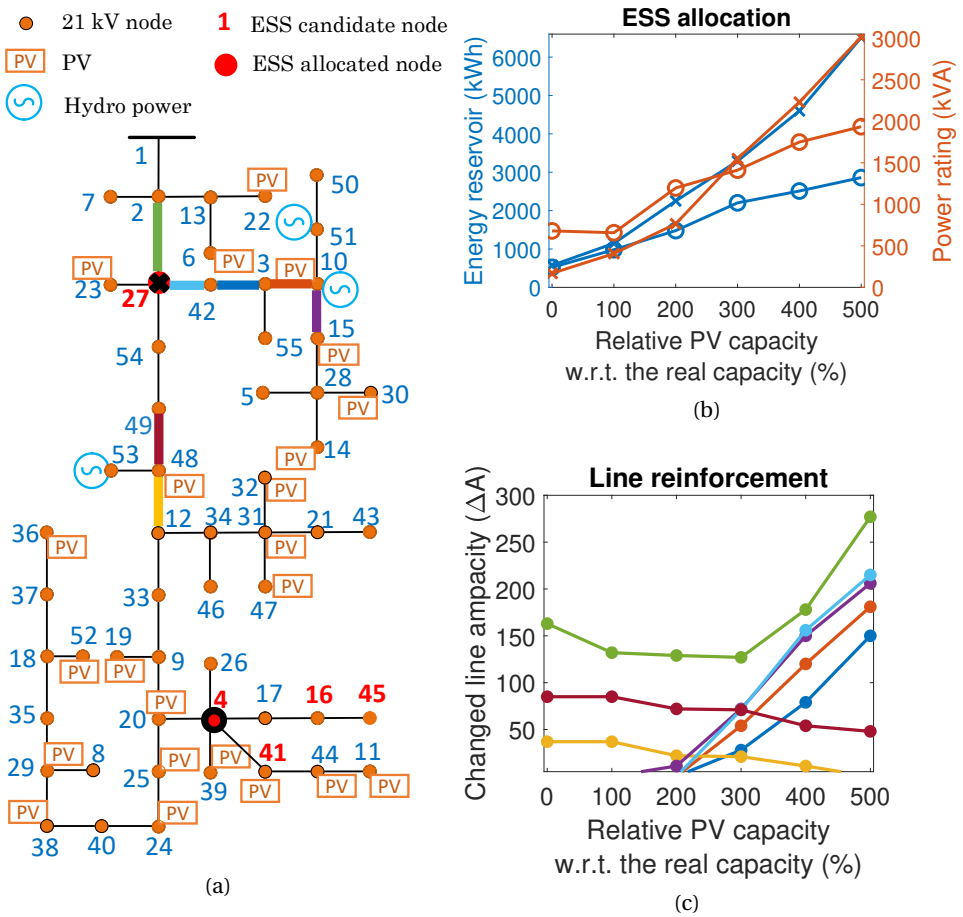

Figure 4.8: (a) Topology with ESS allocation and line reinforcement, (b) ESS allocation (2nd block problem), (c) Line reinforcement (2nd block problem).

4.7.4 Numerical Assessment on the Effect of Separation of Siting and Sizing Problems

In this section, we compare the planning result as well as the computational performance of the two solution approaches: Approach 1, where the siting and sizing decisions are made together (*i.e.*, the Benders decomposition approach used in [14] and [103]), and Approach 2, where the siting and sizing decisions are made sequentially (*i.e.*, the proposed approach in this chapter.) As shown in Fig. 4.10(a), by employing Approach 1, the evolution of the total cost over Benders iterations shows sharp changes with the change of binary investment variables, which leads to slow convergence. On the other hand, in Approach 2, the Benders cuts built

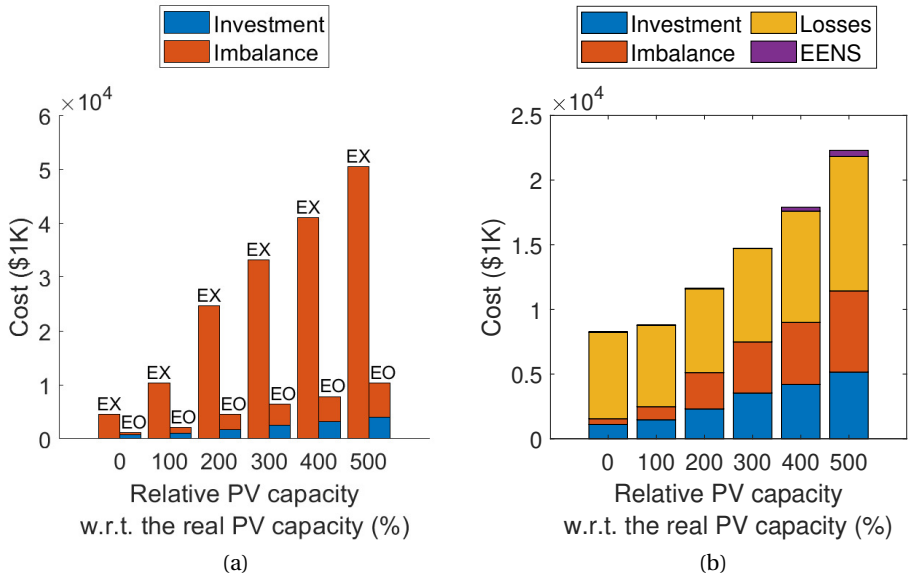

Figure 4.9: Obtained optimal cost value of (a) First block problem, (b) Second block problem.

in the siting sub-stage of 2nd block narrows down the binary solution space more effectively based on the evaluation of the best possible investment and operation decision with the given site decisions. Then, with the fixed sites, the sizing sub-stage problem converges faster to the best size solution. In this way, the fluctuating behavior in the evolution of the total planning cost is notably reduced as shown in Fig. 4.10(b) and Fig. 4.10(c). The text on the graphs show the comparison of the computation time between Approach 1 and Approach 2. The average computation times for solving a subproblem of Approach 1 are similar to those of the siting and sizing sub-stages in Approach 2. On the other hand, the average computation time to solve the master problems for Approach 1 is significantly larger than the corresponding one for Approach 2. It is due to accumulated Benders cuts as a result of large number of benders iterations for Approach 1. The sum of the Benders iteration number of the siting and sizing sub-stage of Approach 2 is smaller than the iteration number of Approach 1, verifying the superior performance of Approach 2 in the convergence speed of the algorithm. Indeed, as shown in Table 4.4, the planning results obtained from both approaches show a negligible difference in terms of ESS allocation, line reinforcements, and costs. Based on the result, it can be concluded that the Approach 2 is computationally more efficient than Approach 1 when numerous binary investment decisions have to be tackled.

4.7.5 Scalability Analysis Regarding the Network Size

The proposed method has been applied to distribution networks of various sizes to analyze its scalability. The number of dispatch intervals was 24, and 4 day-types were considered. Other parameter settings for the analysis are the same as the ones adopted in Sec. 5.10. All the network data can be found in [107] and [108]. Table 4.5 and Fig. 4.11 report the average

Table 4.4: The planning results comparison (Approach 1 vs. Approach 2).

	Approach 1			Approach 2		
ESS allocation (Node #)	4		27	4		27
Power rating (kVA)	700		341	673		387
Energy reservoir (kWh)	967		1202	1028		1151
Reinforced lines	48-12	2-27	48-49	48-12	2-27	48-49
Δampacity (ΔA)	36	133	85	37	133	85
Total cost ($M)	8.794			8.799		

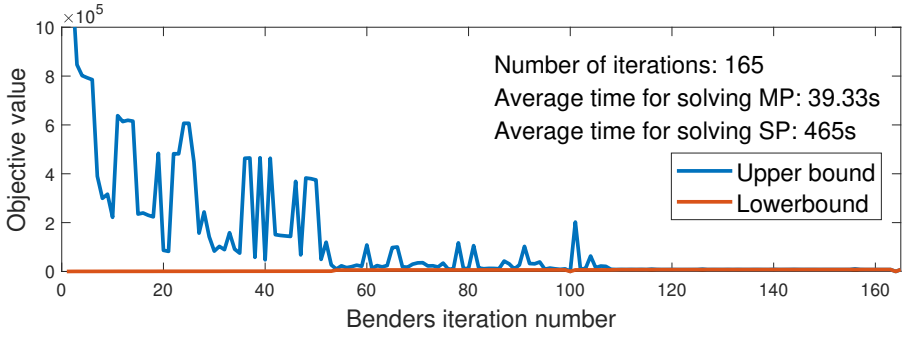

(a)

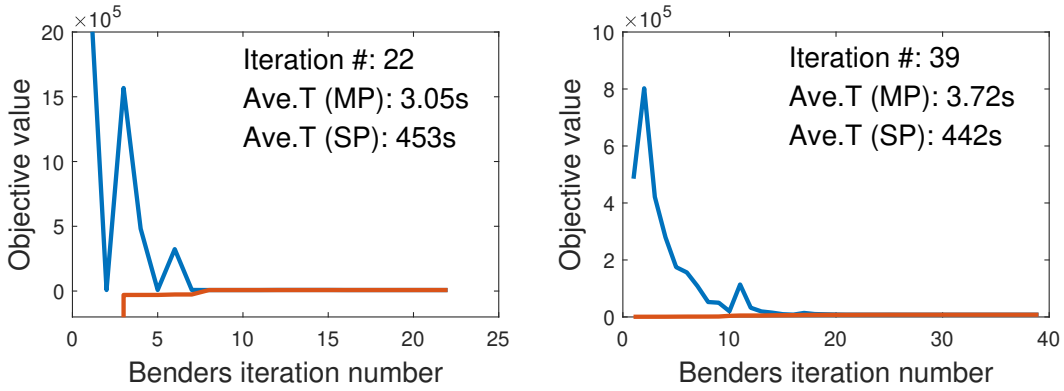

(b) (c)

Figure 4.10: Convergence of Benders decompostion: (a) Approach 1, (b) siting sub-stage (Approach 2), (c) sizing sub-stage (Approach 2).

computation time per Benders iteration (denoted by 'BI' in the table and figure) and the number of Benders iterations (including both siting and sizing sub-stage of the 2nd block problem) to solve the planning problems for available IEEE benchmark feeders with the number of nodes ranging from 25 to 123. Fig. 4.11.(a) and Fig. 4.11.(b) show respectively the trend of the average computation time per Benders iteration and total computation time concerning the system sizes. The results verify the tractability of the planning model for

distribution network feeders of a realistic size.

In each Benders iteration, solving the subproblem (*i.e.*, operation problem) takes the most computation time due to numerous operational variables and constraints determined by the system size. However, as shown in Table 4.5 and Fig. 4.11.(a), the average computation time per Benders iteration does not increase linearly with the system size. It implies that the computation time depends not only on the system (*i.e.*, problem) size but also on the solution space, which is largely affected by the network's operating condition. Furthermore, Fig. 4.11.(b) shows that the total computation time depends on the number of Benders iterations. For example, the difference in the total computation time for the 25-node system vs. the 55-node system is very small (*i.e.*, around 5% of the total computation time for 25-node system) compared to that in average computation time per Benders iteration (*i.e.*, around 115% of the average computation time per Benders iteration for 25-node system). This is attributed to the smaller number of total Benders iterations for the 55-node system in comparison to the 25-node system. Meanwhile, the total computation time for the 69-node system increased to more than 4 times compared to the 55-node system. In contrast, the total computation time for the 123-node system was 2.22 hours shorter than that with 69 nodes. The results indicate that the convergence speed of the proposed method is influenced by how the set of Benders cuts narrow down the solution space to identify the optimal solution. Given that the Benders cut is determined by the dual values obtained from solving the subproblems, the system operating condition significantly influences the optimal investment solution and the convergence speed.

Table 4.5: Total computation times and number of Benders iteration for distribution networks with different sizes.

Nodes #	Time/BI (h)	1st+2nd BI #	Total time (h)
25	0.29	43+22	18.61
55	0.61	12+20	19.67
69	1.14	59+16	85.28
123	1.22	28+40	83.06

4.8 Conclusion

The Chapter presented a tool for the co-optimized planning of ESSs and line reinforcements for ADNs to achieve their dispatchability. As in the previous chapters, ESSs are employed to compensate for the uncertainty of the prosumption such that the realized power flow at the GCP can track a day-ahead computed dispatch plan. The line reinforcement is considered to help satisfying the grid operational constraints. The lines' characteristics and the grid constraints associated with the line ampacity in the MAR-OPF model are adjusted with the change of each line ampacity to reflect the impact of its reinforcement on the grid operation. The planning problem is reformulated such that the siting and sizing problems of ESSs and line reinforcement are tackled sequentially by Benders decomposition. We assessed the per-

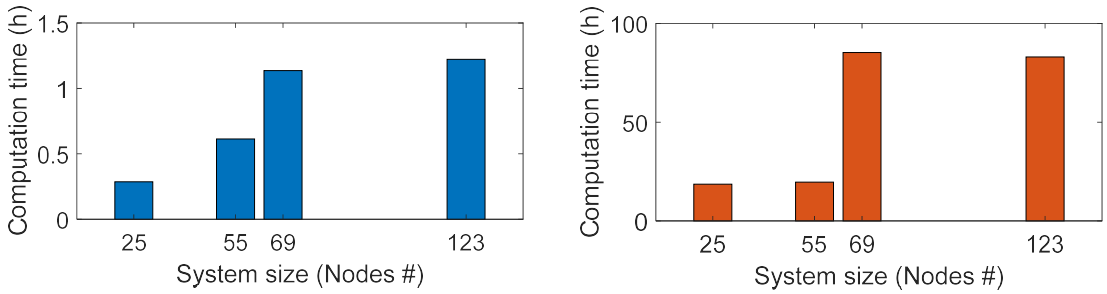

Figure 4.11: (a) Average computation time per Benders iteration (BI) for distribution networks with different sizes, (b) Total computation time for distribution networks with different sizes.

formance of the proposed method on a real Swiss ADN with substantial levels of installed PV capacity. The benefit of the co-optimization of line reinforcement and ESS allocation is shown compared to the case where only ESSs are considered. The planning results under increasing load consumption and a large amount of distributed stochastic renewable generation demonstrate that the proposed co-optimization framework can successfully guarantee the optimal level of dispatchability while securing the proper hosting capacity of the ADN. Then, the benefits associated to the separation of the siting and sizing in the planning problem are numerically assessed by comparing the computation time and investment solution to the original planning problem. The computation time for solving the reformulated problem was one-third of that of the original problem, while the difference between the investment solution and the total planning and expected operating costs of the two problems were negligible. Finally, the simulations conducted on IEEE test networks and real networks of various sizes demonstrate that the proposed planning method is sufficiently scalable to be applied to networks of generic sizes.

5 Expansion Planning of Active Distribution Networks Achieving their Dispatchability

5.1 Highlight

This chapter presents a combined framework for DNEP and ESS allocation in ADNs hosting large amount of uncontrollable RERs and loads. The proposed DNEP ensures the reliable operation of the targeted ADN with the objective of achieving its dispatchability while minimizing grid losses by determining both the network's expanded topology to connect new nodes along with the reinforcement of existing lines. As in the previous chapters, the allocated ESSs compensate for the dispatch error at GCP to achieve ADN's dispatchability. The grid constraints are modeled by using the previously introduced MAR-OPF model that convexifies the classical AC-OPF providing the global optimal and the tight solution of the OPF problem for radial networks. The DNEP problem's complexity is handled by employing two solution approaches: a sequential approach where new nodes are added one by one, following the priorities determined by the user, and a different algorithm that simultaneously optimizes the investment on new lines. In both approaches, the siting and sizing problems associated with ESSs and line investment are solved separately to enhance the convergence speed of the Benders decomposition. Simulations are conducted on the same real 55-node Swiss ADN hosting sizeable stochastic PV generation.

This chapter presents the work published in:

Yi, Ji Hyun, et al. "Expansion planning of active distribution networks achieving their dispatchability via energy storage systems." Applied Energy 326 (2022): 119942.

5.2 Organization of the Chapter

In the beginning of the chapter, the state-of-the-art of the expansion planning problem for distribution networks is presented. Then, the peculiarity of the research problem distinguished from the existing literature. The contributions of this chapter are then summarized. The second part starts with the system description. Then, in the section giving the problem formulation, we discuss the challenges associated with the solution of the defined planning problem and the solution approaches to tackle each of computational hurdles. Especially,

two solution approaches - the so-called sequential approach, and the simultaneous one - are introduced to handle the new lines investment in a more efficient way. For each of the solution approaches, the global structure of the planning problem is elaborated. Each process of the expansion planning algorithm is explained in detail with mathematical formulation. It includes the modeling of investment on new lines and the modification of the OPF model employing the big-M method to selectively activate the OPF constraints depending on the installation status of each specific line candidate. The reformulation of the planning problem to separate siting and sizing problems are also explained. Finally, the performance of the two solution approaches are compared in terms of computational efficiency and optimality. A comparative study comparing the two solution approaches is carried out on the same network example introduced in the previous chapters, followed by several numerical analysis with different system settings.

5.3 State-of-the-art of ADN Expansion Planning

As already discussed in the previous chapters, RERs' stochasticity in power systems causes difficulties to secure the reliable operation of distribution network, such as degradation in quality of supply mainly associated with voltage control, as well as lines and transformers congestions. A conventional solution to tackle these problems is to increase the network's hosting capacity by line reinforcement and expansion, referred to as the DNEP problem. The DNEP decides optimal investment strategies tackling the challenges associated with operating condition varying over time, such as load growth. The considered options include construction of additional infrastructures, substations, or power plants [6, 109]. On the other hand, DSOs need to develop a DNEP strategy that increases the distribution network's flexibility to handle technical issues related to system volatility, as well as achieve enough controllability of flexible resources to balance out the uncertainty or even provide ancillary services to TSOs in an effort to mitigate system imbalances [110].

As already discussed in the previous chapters, ESS assets are employed for multiple purposes and thereby to support the integration of RERs. However, according to [6], conventional DNEP is inefficient to handle the above-mentioned challenges as active elements, such as ESSs, are not considered. For example, in [109], the planning strategy was developed based on a heuristic approach where the reconfiguration scheme is first applied to check operational feasibility in contingency cases, and the construction plan candidates were sought once the violation of the system operating conditions is observed. However, such conventional framework is not appropriate to proactively handle issues caused by various sources of uncertainties, nor to reflect potential support provided by active assets in the network. In this context, DSOs require a robust DNEP strategy to incorporate DERs to be installed in locations not covered by the ADN topology, while minimizing their impact on ADNs and maximizing their benefits for DSO's interest.

In the existing literature, DNEP problems are often proposed to size and site ESSs (e.g., [8, 76, 77, 79, 98, 102]), DG units (e.g., [97, 98]), voltage regulators [94], static var compensators and on-load-tap-changers [111]. These problems are solved with various objectives, such

as minimizing power losses [8, 76, 77, 79, 97, 98, 102], assuring the reliability of power supply [8, 76, 77, 79, 98, 102], improving quality of power supply (*e.g.*, voltage) [97], reducing operation costs [76, 94, 111], and peak shaving [112]. The planning strategy proposed in [112] integrated the ESSs considering their benefit on peak-shaving and operation cost along with other active management schemes such as DG curtailments, demand side management, and on-load tap changer tap adjustments. The given planning problem was formulated as a MISOCP problem embedding the distflow OPF model. Some studies used the DNEP strategy while procuring local flexibility by exploiting flexible resources. The Authors of [77, 113] considered ESSs and price-induced flexibility provided by consumers within the proposed planning framework while suitably modeling the uncertainties caused by high PV penetration. The planning problem was formulated as a scenario-based stochastic programming framework with the operational objective consisting operation cost, reliability and investment costs. In [114], a bi-level approach-based expansion planning is proposed considering concurrently the uncertainty of plug-in electric vehicles and its potential capability to serve as an alternative supply source to enhance network flexibility. The network expansion considering the EV charging station is carried out by evaluating the DSO's benefit coupled with calculation of EV parking lots owners' revenue. In [115], the DNEP problem was used while considering DGs as candidate flexibility resources in the presence of V2G features of EV parking lots and curtailable RERs. The DNEP problem was formulated as a MILP problem to minimize the investment cost and operating costs including flexibility-oriented penalties for RERs' curtailment. In [116], uncontrollable and controllable DGs, and ESSs are considered as investment options. The assets allocation were determined based on their ramping value to compensate for the load variability, reducing the operation costs and, furthermore, total planning costs.

Although the above-mentioned studies proposed DNEP frameworks with particular reference to allocating system flexibility, far too little attention has been paid to enhancing the local flexibility to achieve ADN's dispatchability. In view of this, the objective of this chapter is to develop a DNEP strategy that ensures ADN's sufficient dispatchability and reliable system operation. However, due to the nature of the objective itself, the specific DNEP problem should be coupled with accurate network operation model, fully accounting for the system uncertainties.

In this regard, one notable difficulty reported commonly by the studies mentioned-above concerning the modern DNEP problem is solution tractability and computation burden. The operation-aware planning embeds operation stage where the non-linear and non-convex power flow based optimization problem needs to be tackled. Moreover, the operational conditions and decision variables are inter-linked with complicating integer variables associated with assets investment, rendering the DNEP problem a large-scale multi-layered mixed integer non-linear programming problem. Due to its inherent complexity, this type of problems are often solved by meta-heuristic algorithms [93, 97, 102, 114]. However, these solution techniques do not guarantee optimality, or even feasibility with respect to the ADN operation. Other studies used convexification schemes of OPF models such as linear approximation [8, 76, 99] or SOCP relaxation [65, 111]. For example, the multi-stage expansion planning

tool developed in [8] evaluates the operation through a probabilistic linear OPF model while embedding the ESSs' daily schedule identified by dynamic programming. Alternatively, the SOCP model [65, 111] can improve the modeling accuracy of the load flow but at the cost of higher computation time compared to the linear OPF. In [14], to guarantee the exactness of the solution obtained from the SOCP model, augmented bounds are built upon the grid constraints when solving an operation-stage optimization problem within the planning problem. In order to handle the computational burden associated with multi-layered decision process, several studies utilized decomposition method such as the bi-level approach [114], the and Benders decomposition technique [14, 116].

5.4 Problem Statement and Contributions

In Ch.4, the planning tool proposed in Ch.3 was extended to consider line reinforcement in addition to the ESS allocation to identify a better optimal investment solution even in binding operational conditions caused by growing PV generation capacity within the ADN. The co-optimization of line reinforcement and ESS allocation assured the feasible operation of the network by updating the line ampacity. At the same time, the allocated ESSs compensated for the increased stochasticity stemming from the PV injection. Finally, this chapter extends the method proposed in Ch.3 and Ch.4 to a DNEP strategy to host newly integrated RERs and customers. It takes into account the updates of the grid topology to connect new nodes as decision variables. The proposed tool co-optimizes the investment in new line installations and line reinforcement, as well as ESS allocation to achieve ADNs dispatchability.

The inclusion of network investment option in the DNEP requires fundamental modification of power flow equations and operating constraints associated with changes in topology and network adjacency matrix. By employing the big-M method, the power flow equations and grid constraints are selectively activated only when the optimal connection among candidate lines are chosen, such that the system operation under the optimal connection to the new node is evaluated. The admittance matrix is adjusted along with the change of ampacities of new lines and the lines to be reinforced, following the relation between the line parameters and the line ampacity presented in Sec. 4.5.

Moreover, the increased problem complexity caused by the simultaneous management of ESSs and lines investment necessitates a change in the solution approach to improve the tractability of the planning problem. To cope with the computational complexity of the proposed planning framework, in Ch.4, the reformulation of the planning problem has been proposed to determine the investment decisions regarding the sites and sizes of assets in separate sub-stages. The planning problem reformulated into siting and sizing sub-stages showed faster convergence of the Benders decomposition in the performance comparison with the original problem. In view of its advantage, essential when solving a planning problem consisting of numerous binary variables, the reformulation technique is fittingly applied to the DNEP problem.

Nevertheless, the DNEP problem requires a substantial changes in the solution approach

to tackle the computational complexity associated with the determination of the optimal topology changes. In view of this, two approaches are proposed to tackle the binary decisions related to the new line installation: the so-called the *Sequential approach*, and the *Simultaneous approach*. The sequential approach is introduced to add new nodes to the existing network in a sequential way, making the proposed DNEP strategy capable of handling the scalability issue associated with large number of new nodes. On the other hand, the simultaneous approach optimizes the connections to new nodes all at once along with other investment decisions. To do that, the siting sub-stage problem is reformulated such that the new lines can be determined without going through inefficient and excessive iterations of the Benders algorithm. In summary, the contributions of the chapter are threefold:

- The DNEP strategy relying on a scenario-based stochastic programming approach is proposed to ensure sufficient hosting capacity and achieve ADNs dispatchability when increasing stochastic renewable generation and demand.
- The ESSs and lines investment decisions are optimized based on the accurate evaluation of ADN operation via the MAR-OPF model, appropriately converted to consider the change of network topology and adjacency matrix associated with assets investment.
- The computational burden of the DNEP problem is mitigated by employing two approaches: the sequential approach and the simultaneous approach. Both of the algorithms consist of siting and sizing sub-stages. In the sequential approach, the siting sub-stage sequentially integrates new nodes while determining lines for reinforcement and nodes for ESS allocation, and the sizing sub-stage determines the capacity of lines and ESSs. On the other hand, in the simultaneous approach, the problem structure of the siting sub-stage is transformed to determine all of the new lines installation simultaneously.

5.5 System Description

The goal of the DNEP problem is to determine: (i) the optimal routing from the existing ADN topology to new nodes hosting additional stochastic resources (consumption/renewable generation), (ii) the reinforcement of existing lines, and (iii) the allocation of ESSs[13] to maintain a feasible and dispatchable operation of the network, while minimizing the total investment and operating costs. The inputs to the DNEP problem include the characteristics of the existing network and the new assets (ESSs and lines), locations and capacities of newly integrated load and RERs, the existing candidate nodes that can be connected to new nodes, and the ESS candidate nodes.

The DNEP is applied to a MV distribution network with a radial topology, where $l \in \mathscr{L}(|\mathscr{L}| = L)$ is the generic line, $i \in \mathscr{N}(|\mathscr{N}| = L{+}1)$ is the generic node, and $n' \in \mathscr{N}'(|\mathscr{N}'| = N')$ is the new node. The set of candidate nodes that can be connected to a new node are defined

[13]The considered planning problem does not take into account hybrid PV-ESS systems since their behavior is user-defined and hard to predict. Future research has to focus on integrating these systems in the proposed planning tool.

for each new node n' and indicated as $\mathscr{K}(n')$. The number of candidates for new node n' is given as $\mathscr{K}(n') = K$. Its element is indexed as $k \in \mathscr{K}(n')$. The binary variable for line reinforcement is denoted by $X_l \in \{0,1\}, \forall l \in \mathscr{L}$. The decision variable associated with the ampacity of the generic reinforced line is denoted by $A_l, \forall l \in \mathscr{L}$. For the sequential approach, new nodes are integrated into the existing network one by one, implying that only a single new node, and the corresponding line candidates, are considered into each round of the planning problem. The number of new nodes N' corresponds to the number of solution rounds of the proposed planning problem to complete the network expansion framework. In this approach, the installation of the line connecting node candidate $k \in \mathscr{K}(n')$ and new node $n' \in \mathscr{N}'$ is denoted by the variable $X'_k \in \{0,1\}, \forall k \in \mathscr{K}(n'), \forall n' \in \mathscr{N}'$, whereas line ampacities of the candidates for the new line are denoted by $A'_k, \forall k \in \mathscr{K}(n'), \forall n' \in \mathscr{N}'$. Line ampacities A_l and A'_k are determined for the lines where the line investment takes place (*i.e.*, $X_l = 1, \forall l \in \mathscr{L}$, and $X'_k = 1, \forall k \in \mathscr{K}(n'), \forall n' \in \mathscr{N}'$).

On the other hand, for the simultaneous approach, new nodes are connected all at once to the existing network. In this approach, for the sake of clarity regarding the mathematical notation, we denote the new line candidates with a pair of indices representing sending and receiving end of the line. In other words, the installation of the line connecting node candidate $k \in \mathscr{K}(n')$ and new node $n' \in \mathscr{N}'$ is denoted by the variable $X'_{k(n')} \in \{0,1\}, \forall k \in \mathscr{K}(n'), \forall n' \in \mathscr{N}'$. The same indexing is applied to the line ampacities of the line candidates, that is, $A'_{k(n')}, \forall k \in \mathscr{K}(n'), \forall n' \in \mathscr{N}'$.

Another set of binary variables is defined for each node $i \in \mathscr{N}$ to determine the ESS allocation (while ESS candidate nodes can be given by the user) and its array is denoted as $U_i \in \{0,1\}$, $\forall i \in \mathscr{N}$. The energy reservoir ($C_i$) and power rating ($R_i$) are determined at the node where the ESS is allocated ($U_i = 1, \forall i \in \mathscr{N}$).

The DNEP strategy is determined based on the operation of the ADN with the same objective and condition explained in Sec. 2.8. Multiple operational objectives are taken into account: namely, achieving the dispatchability of the targeted ADN while minimizing the grid losses and ensuring the feasibility of the ADN operation. The detailed introduction on the dispatching operation of the ADN can be found in Sec. 2.8.

To summarize, the DNEP problem is structured as a two-stage decision process: (1) the first stage determines the binary decision variables of the ESS location (U_i), the line to be newly constructed (X'_k for the sequential approach, and $X'_{kn'}$ as its counterpart for the simultaneous approach), the existing lines to be reinforced (X_l), and the continuous decision variables on the ESS energy capacity (C_i), their power rating (R_i), the line ampacity of the new line (A'_k for the sequential approach, and $A'_{kn'}$ as its counterpart for the simultaneous approach) and the reinforced lines (A_l); and (2) the second stage dealing with the daily operation problem, where the decision variables on the ESSs active and reactive power are determined for all operating scenarios and the power state variables accordingly.

5.6 Problem Formulation

The complexity of the considered DNEP problem stems mainly from three points: (i) the two-layered decision-making process on planning and operation; (ii) the simultaneous decision on siting and sizing of lines and ESSs; and (iii) the numerous possible connections between the existing and new nodes that introduce numerous binary decision variables.

Point (i) can be tackled by employing the Benders decomposition [66], which has already been used as a powerful algorithm for solving the planning problem formulated in the previous chapters with suitable modifications to enhance the convergence of the DNEP.

Point (ii) is related to the decision variables of different nature (continuous and binary) constituting the investment options. As proposed in Sec. 4.6, the planning problem (to be specific,the 2nd block problem) using the Benders decomposition is restructured into two sub-stages (each using the Benders decomposition) such that ESSs' and lines' siting and sizing decisions are separated. When the optimal siting solution is found, it is fixed such that the sizing problem's master problem is reduced to a continuous programming problem.

To tackle the computational issue regarding point (iii), we introduce two solution approaches: 1) considering connecting all the new nodes; and 2) considering sequentially connecting the new nodes.

First approach is considering all the possible connections of new nodes at once. When the binary variables related to the new lines' candidates are introduced into the planning options, the Benders algorithm becomes more difficult to converge in the siting sub-stage. In this regard, the problem structure is modified such that the new lines can be decided in a distributed manner (*i.e.*, by including the associated binary variables into the subproblems) rather than in a central way (*i.e.*, by including the variables into the master problem). In this way, the computation burden is mitigated. Nevertheless, the problem still may become intractable as the number of new nodes becomes significant. Such scalability issue is difficult to avoid when considering all the possible connections of new nodes at once for the sake of achieving the global optimal investment solution.

An alternative formulation is to consider a sequential approach for connecting the new nodes, while sacrificing the solution's global optimality. Yet, given that the integration of loads and DG units is spread over a long-term horizon following the pre-established targets set by DSO and customers, the sequential approach is in accordance with such standard planning process adopted by DSOs as it follows the priority order of new nodes.

The sequential approach is introduced first in Sec. 5.7, followed by the simultaneous approach discussed in Sec. 5.8. In Sec. 5.9, the two approaches are tested on the real distribution network introduced in Sec. 5.10.1 to compare their computational efficiency and solution optimality, and thereby to demonstrate the practical superiority of the sequential approach.

5.7 Sequential Approach

In this section, the DNEP problem is solved by a sequential approach comprising several rounds of the planning problem, each tackling the addition of a single new node to the existing network in a sequential priority order defined by the user. Each planning problem is decomposed into two blocks. In the 1st block, the economic benefits/penalties associated with the network dispatchability are obtained considering the prosumption of the new node by quantifying the optimal trade-off between the ESS allocation costs and the avoidance of the power dispatch imbalance penalties. In the 2nd block, the new lines, the reinforcement of the existing lines, and the ESS allocation are determined to comply with the dispatch error level (obtained from the 1st block) and with the network operating constraints. The reader is referred to Ch.3 for more details regarding the two-block structure. In Ch.4, we propose to decompose the 2nd block problem into two sub-stages: the siting sub-stage where the binary investment decisions are determined, and the sizing sub-stage where values of the continuous investment variables are obtained. The Benders decomposition technique is applied to both sub-stages to tackle the computational complexity. The MAR-OPF based operation model considered in the subproblems are substantially modified to consider the change in network's topology and/or line parameters properly adjusted according to the investment solution obtained from the master problems.

The whole algorithm of the proposed approach is illustrated in Fig. 5.1 and described step by step in Alg. 5.1. We start the planning algorithm by selecting a new node $n' = 1$ from the pool of new N' nodes accordingly to the priority defined by the user. First, the 1st block problem is solved to determine the optimal level of dispatchability when node n' is added to the existing network. Then, a set of candidate nodes $\mathscr{K}(n')$ are chosen based on the modeler's choice. In this study, we selected the candidate nodes based on their distance from the new node. After solving the siting sub-stage of the 2nd block problem, the optimal allocation of a new line connecting the new node is determined along with the possible reinforcement of existing lines and the ESS allocation. The network is thus expanded by having one more line (*i.e.*, $L \leftarrow L+1, \mathscr{L} \leftarrow \mathscr{L} \cup k^*$, where k^* indicates the optimally determined candidate for the connection to the new node) and node (*i.e.*, $N \leftarrow N+1, \mathscr{N} \leftarrow \mathscr{N} \cup n'$), and the determined line candidate's fixed cost parameter ($ic^c_{k^*}$) becomes the cost parameter of line L (ic^r_L). The node next in the queue (*i.e.*, $n' = 2$) is tackled in the next iteration of the planning problem. Once all new nodes are connected to the existing network through this procedure, the sizing sub-stage of the 2nd block problem is solved to determine the ESSs' sizes and the optimal line ampacities.

5.7.1 1st Block Problem

The 1st block problem determines the optimal ESS allocation and the ADN's dispatchability level by evaluating the dispatch operation for all operating scenarios with the PV generation and load consumption of a new node integrated into the existing network. The formulation of the 1st block problem is the same as the one already proposed in Sec. 3.6.2. The new node is assumed connected to any possible node in the existing network when solving the 1st block

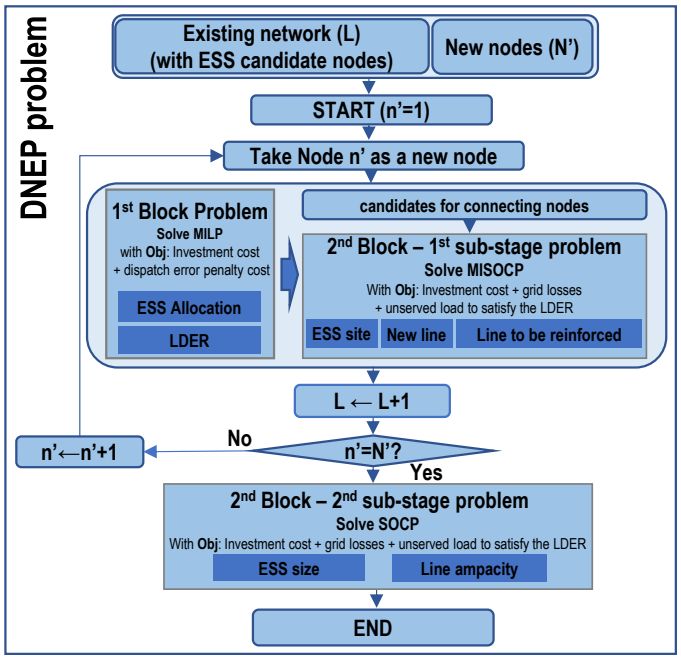

Figure 5.1: Full algorithm of the proposed method.

problem. This assumption can be made as the main interest of solving the 1st block problem is to find the economically optimal point considering the trade-off between the ESS size and the dispatchability level. Note that the 1st block problem gets re-visited each time a new node is added sequentially.

5.7.2 2nd Block Problem

The objective of the 2nd block problem is to determine the optimal connection between the existing network and node n', line reinforcement, and ESS allocation to minimize the grid losses and load curtailment while satisfying LDER constraints. The investment cost consists of the construction cost of the new line, the reinforced lines, and the ESS allocation (5.1). The new line investment and the line reinforcement cost consist of two parts: fixed cost, which is invariant with the ampacity of the line and accounts for the construction, labor, etc., and the line conductor cost, which varies with line ampacity. ic_k^c denotes the fixed cost parameter of the new line investment for line candidate $k \in \mathcal{K}(n')$.

$$\begin{aligned} IC = IC_E + & \sum_{k \in \mathcal{K}(n')} ic_k^c X'_k + \sum_{l \in \mathcal{L}} ic_l^r X_l \\ & + \sum_{k \in \mathcal{K}(n')} \rho_k (\delta_2 A'^2_k + \delta_1 A'_k + \delta_0 X'_k)) \\ & + \sum_{l \in \mathcal{L}} \rho_l (\delta_2 (A_l)^2 + \delta_1 A_l + \delta_0 X_l)) \end{aligned} \tag{5.1}$$

Regarding the investment decisions, we have binary (U, X, X') and continuous investment decisions (R, C, A, A') separately in the 1st and the sizing sub-stage problems, making them

Algorithm 5.1 Full algorithm of the proposed expansion planning method.

Require: Existing network ($\mathscr{L}$), prosumption ($s = p + jq$), ESS candidate nodes ($\mathscr{N}_E$), new nodes ($\mathscr{N}'$)

Initialization : $n' \leftarrow 1$;
while $n' \leq N'$ **do**
  Consider Node n' as a new node
  Solve 1st block problem to determine the optimal level of dispatchability when node n' is added to the existing network
  Select candidate nodes $\mathscr{K}(n')$ for connecting the existing nodes to the new node according to the modeler's criteria
  Solve siting sub-stage of 2nd block problem to determine $U_i^*, \forall i \in \mathscr{N}_E$ (ESS site), $X_k^{'*}, \forall k \in \mathscr{K}(n')$ (connection to the new node), $X_l^*, \forall l \in \mathscr{L}$ (line to be reinforced)
  $L \leftarrow L+1, \mathscr{L} \leftarrow \mathscr{L} \cup k^*$, $N \leftarrow N+1, \mathscr{N} \leftarrow \mathscr{N} \cup n'$ {Integrate new node n' to the network}
  $n' \leftarrow n'+1$
end while
return $\mathscr{L}, U^*, X^*$
Solve the sizing sub-stage of 2nd block problem to determine ESS size ($R_i^*, C_i^*, \forall i \in \mathscr{N}_E$), line ampacities of new lines and lines to be reinforced ($A_l^*, \forall l \in \mathscr{L}$)
return R^*, C^*, A^*

MISOCP problem and SOCP problem, respectively. The structure of the 2nd block problem is illustrated by the diagram shown in Fig. 5.2. We apply the Benders decomposition technique

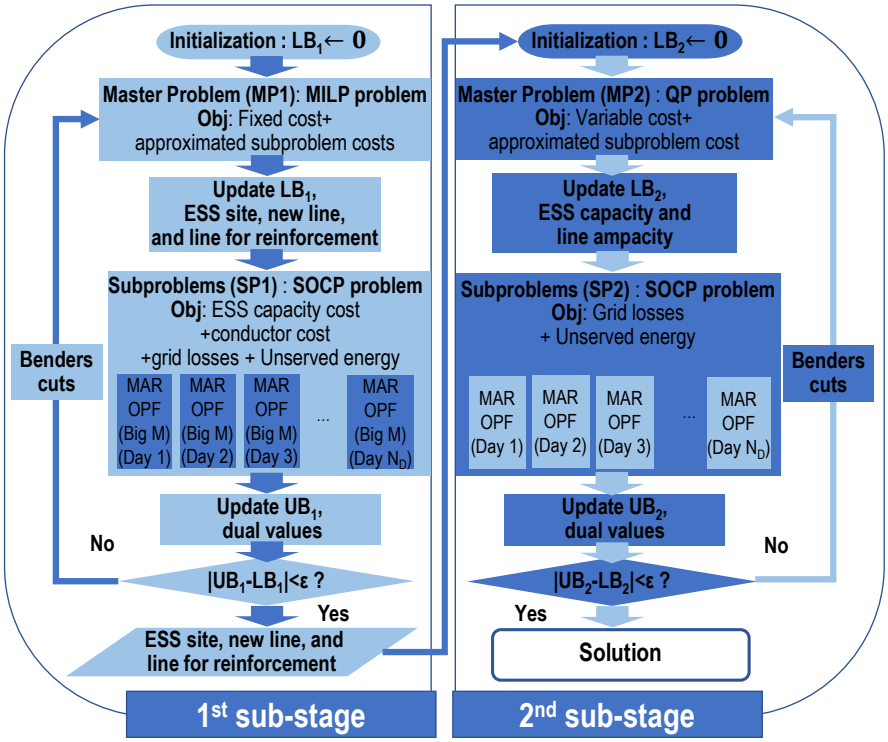

Figure 5.2: Full structure of the 2nd block problem.

to solve both sub-stage problems. In the siting sub-stage, the Benders master problem determines the route connecting the existing network and the new node, the line for reinforcement, and the site of the ESSs. Then, each subproblem, which solves a daily OPF modeled by the AR-OPF model, determines the ESSs capacity and the line ampacity of the new and the reinforced lines for each day-type and year to minimize the unserved load and comply with the dispatchability constraint. The change of network topology associated with the choice of the new line is modeled by employing the big M method [117], as it enables the selective activation of power flow equations and the network constraints depending on the choice of the new line. The unserved load takes values to ensure the feasibility of the subproblem regardless of the investment. When the convergence of the Benders decomposition is reached, the binary solutions regarding the site of ESSs and lines investment are determined. The siting sub-stage problem of the 2nd block (along with the 1st block) is solved repetitively till all the connections to the new nodes are decided. Then, the siting solutions are passed to the sizing sub-stage problem. In the sizing sub-stage problem, the master problem considers the ESSs' capacities and the lines' ampacities for the buses and lines to be invested. The subproblem evaluates the fitness of the determined allocations with the same problem formulation introduced in Sec. 4.6.2.

Use of the Big M method into the MAR-OPF model

The big M method is employed to selectively activate the OPF constraints for the new line and node only when a new line is chosen among the candidates. In this regard, let arrays Π and A'' be the investment status of existing lines and the candidate routes represented by binary variables, and line ampacities, respectively. Ψ represents the connection status of existing lines and the candidate routes. Note that the size of the introduced column vectors are given as $(L+K)$.

$$\Pi = [X^\top \; X'^\top]^\top, \; A'' = [A^\top \; A'^\top]^\top, \; \Psi = [\mathbb{1}_{|\mathscr{L}|}^\top \; X'^\top]^\top. \tag{5.2}$$

All the power flow variables of nodes and lines take values only when the corresponding nodes and lines are connected within the system. In other words, when a line from $k \in \mathscr{K}(n')$ is not connected to the new node n', the state variables of the new node and the line are fixed to zero. Otherwise, the state variables are imposed by the given operating constraints. In the following equations, all the variables with index j and i are defined for $j \in (\mathscr{L} \cup \{\mathscr{K}(n')\})$ and $i \in (\mathscr{N} \cup \{n'\})$, respectively. By employing the big M method, (5.3b) and (5.3c) replace (3.2m) and (3.2n) to redefine the ranges for the upper-bound power flow variables at line j to updated value when line j is determined to be invested (both for line reinforcement and for new line installation.) Likewise, (5.3a) imposes the possible ranges on the values of longitudinal current, its upper-bound variable, and currents at sending/receiving end of line j considering the investment status of line j.

$$0 \leq \left\{ f_j, \bar{f}_j, I_j^t, I_j^b \right\} \leq (I_j^{max})^2 \cdot (1-\Pi_j) + (A''_j)^2, \qquad \forall j \in (\mathscr{L} \cup \mathscr{K}(n')), \tag{5.3a}$$

$$0 \leq \bar{P}_j^t \leq P_j^{max} \cdot (1-\Pi_j) + A''_j \sqrt{v^{max}/2}, \qquad \forall j \in (\mathscr{L} \cup \mathscr{K}(n')), \tag{5.3b}$$

$$0 \leq \bar{Q}_j^t \leq Q_j^{max} \cdot (1-\Pi_j) + A''_j \sqrt{v^{max}/2}, \qquad \forall j \in (\mathscr{L} \cup \mathscr{K}(n')). \tag{5.3c}$$

The formulation of the branch power flow equations for both power flow variables and auxiliary bound variables does not change mathematically from (3.1a)-(3.2e) due to the equations above that selectively activate the variables according to the investment status of the lines. For the sake of implementation, Ψ, (*i.e.*, the connection status of the candidate nodes and the new node), is multiplied by the terms quantifying the impact of shunt capacitance on the line power flow as shown in (5.4a), (5.4b), and (5.4c). Note that the value X_k in Ψ is parameterized to the optimal value obtained from the previous master problem.

$$S_j^t = s_j + \sum_{m \in \mathscr{L}} \mathbf{H}_{j,m} S_j^t + z_j f_j - j\Psi_j^* (v_{up(j)} + v_j) b_j, \qquad \forall j \in (\mathscr{L} \cup \mathscr{K}(n')), \tag{5.4a}$$

$$\hat{S}_j^t = s_j + \sum_{m \in \mathscr{L}} \mathbf{H}_{j,m} \hat{S}_j^t - j\Psi_j^* (\bar{v}_{up(j)} + \bar{v}_j) b_j, \qquad \forall j \in (\mathscr{L} \cup \mathscr{K}(n')), \tag{5.4b}$$

$$\bar{S}_j^t = s_j + \sum_{m \in \mathscr{L}} \mathbf{H}_{j,m} \bar{S}_j^t + z_j f_j - j\Psi_j^* (v_{up(j)} + v_j) b_j, \qquad \forall j \in (\mathscr{L} \cup \mathscr{K}(n')). \tag{5.4c}$$

The power balance equation including the power injection from ESSs, defined at the sending end of line l, and its counterparts associated with upper-bound and lower-bound auxiliary variables are given as below by employing the big M method.

$$S_j^t = s_j + s_j^E + \sum_{m \in \mathscr{L}} \mathbf{H}_{j,m} S_j^t + z_j f_j - j\Psi_j^* (v_{up(j)} + v_j) b_j, \qquad \forall j \in (\mathscr{L} \cup \mathscr{K}(n')), \tag{5.5a}$$

$$\hat{S}_j^t = s_j + s_j^E + \sum_{m \in \mathscr{L}} \mathbf{H}_{j,m} \hat{S}_j^t - j\Psi_j^* (\bar{v}_{up(j)} + \bar{v}_j) b_j, \qquad \forall j \in (\mathscr{L} \cup \mathscr{K}(n')), \tag{5.5b}$$

$$\bar{S}_j^t = s_j + s_j^E + \sum_{m \in \mathscr{L}} \mathbf{H}_{j,m} \bar{S}_j^t + z_j f_j - j\Psi_j^* (v_{up(j)} + v_j) b_j, \qquad \forall j \in (\mathscr{L} \cup \mathscr{K}(n')). \tag{5.5c}$$

The voltage equations (3.1c) and (3.2c) are replaced by (5.6a) and (5.6b) by employing the big-M method. The voltages of the nodes connected to line j take values only when line j is connected.

$$\left| -\Psi_j^* v_j + \Psi_j^* v_{up(j)} - 2\Re(\bar{z}_j (S_j^t + j\Psi_j^* v_{up(j)} b_j)) + |z_j|^2 f_j \right| \leq M(1-\Psi_j), \quad \forall j \in (\mathscr{L} \cup \mathscr{K}(n')), \tag{5.6a}$$

$$\left| -\Psi_j^* \bar{v}_j + \Psi_j^* \bar{v}_{up(j)} - 2\Re(\bar{z}_j (\hat{S}_j^t + j\bar{v}_{up(j)} b_j)) \right| \leq M(1-\Psi_j), \qquad \forall j \in (\mathscr{L} \cup \mathscr{K}(n')). \tag{5.6b}$$

The parameterized line connection status is incorporated into the inequality constraints defining the longitudinal current ((5.7a)) and its auxiliary variable ((5.7b) and (5.7c)). As shown in (5.7d) and (5.7e), the line current at the sending end and the receiving end are expressed

while considering the connection status of lines.

$$f_j(\Psi_j^* v_{up(j)}+(1-\Psi_j^*)) \geq |S_j^t + j\Psi_j^* v_{up(j)} b_j|^2, \qquad \forall j \in (\mathscr{L} \cup \mathscr{K}(n')), \quad (5.7a)$$

$$\begin{aligned}\bar{f}_j(\Psi_j^* v_{up(j)}+(1-\Psi_j^*)) \geq & |\max\{|\hat{P}_l^t|, |\bar{P}_l^t|\}|^2 \\ & +|\max\{\{|\hat{Q}_l^t + j\Psi_j^* \bar{v}_{up(l)} b_l|, |\bar{Q}_l^t + j\Psi_j^* v_{up(l)} b_l|\}\}|^2, \end{aligned} \qquad \forall j \in (\mathscr{L} \cup \mathscr{K}(n')), \quad (5.7b)$$

$$\begin{aligned}\bar{f}_j(\Psi_j^* v_j+(1-\Psi_j^*)) \geq & |\max\{|\hat{P}_l^b|, |\bar{P}_l^b|\}|^2 \\ & +|\max\{|\hat{Q}_l^b - j\Psi_j^* \bar{v}_l b_l|, |\bar{Q}_l^b - j\Psi_j^* v_l b_l|\}|^2, \end{aligned} \qquad \forall j \in (\mathscr{L} \cup \mathscr{K}(n')), \quad (5.7c)$$

$$I_j^t(\Psi_j^* v_{up(j)}+(1-\Psi_j^*)) \geq |\max\{|\hat{P}_j^t|, |\bar{P}_j^t|\}|^2 + |\max\{|\hat{Q}_j^t|, |\bar{Q}_j^t|\}|^2, \qquad \forall j \in (\mathscr{L} \cup \mathscr{K}(n')), \quad (5.7d)$$

$$I_j^b(\Psi_j^* v_j+(1-\Psi_j^*)) \geq |\max\{|\hat{P}_j^b|, |\bar{P}_j^b|\}|^2 + |\max\{|\hat{Q}_j^b|, |\bar{Q}_j^b|\}|^2, \qquad \forall j \in (\mathscr{L} \cup \mathscr{K}(n')). \quad (5.7e)$$

For the sake of readability, the equations regarding the MAR-OPF employing the big M method includes (3.1b), (3.2b), (3.2e), (3.2h), (5.3)-(5.7), and grouped as $\Theta^B(\varphi^B) \geq 0$, where $\varphi^B := \{S^t, v, f, \hat{S}^t, \bar{v}, \bar{f}, \bar{S}^t, s, \Pi, A'', \Psi\}$ is the set of variables.

Likewise, the big M method employed MAR-OPF model that includes ESS injections is formulated by (3.1b), (3.2b), (3.2e), (3.2h), (3.9a)-(3.9e),(3.10b), (3.10d), (3.10f), (3.11), (5.3),(5.5)-(5.7), and the equations are grouped as $\Theta'^B(\varphi'^{(B,E)}) \geq 0$, where $\varphi'^{(B,E)} := \{S^t, v, f, \hat{S}^t, \bar{v}, \bar{f}, \bar{S}^t, s', s^E, up^+, up^-, uq^+, uq^-, \zeta, \Pi, A'', \Psi\}$ is the set of variables. The notation without subscript corresponds to the vector of variables for all buses/lines.

Siting sub-stage - determination of the site

The problem structure of the siting sub-stage problem is illustrated by the left-hand side of Fig. 5.2 and Alg. 5.2. The new line that connects the new node to the existing node, the nodes for ESS, and the lines for reinforcement are determined in the master problem. The optimal ESSs' sizes and lines' ampacities for the invested lines specific to each day-type, and resulting operational benefit are evaluated within each subproblem. As this stage aims to determine the best solution for the binary variables, the different ESSs and line conductors' sizes determined for each day type are not the final optimal solutions. The Benders iteration terminates when the upper-bound and the lower-bound of the total cost become sufficiently close to each other. As the new line connecting to the new node is determined at the end of the Benders iteration, the adjacency matrix and the array of line parameters get modified considering the new line.

Master problem : the formulation of the master problem is given in (5.8). Its objective function is the sum of the fixed investment cost for ESS installation, new line installation, and the line reinforcement, and the constant part of the conductor cost for both of the new and the reinforced lines. In addition, the lower approximation of the total expected subproblem cost is added. As the targeted networks are supposed to operate with a radial configuration, only

Algorithm 5.2 Siting sub-stage of the 2nd block problem.

Require: Existing network ($\mathscr{L}$), prosumption ($s_i = p_i + jq_i, \forall i \in (\mathscr{N} \cup n')$), ESS candidate nodes, new node (n'), candidate nodes $\mathscr{K}(n')$

1: **Initialization :** $LB_1 \leftarrow 0, \beta \leftarrow 1$
2: Solve master problem (MP1)
3: $LB_1 \leftarrow MC^{1*}$
4: Update $U^{(\beta)*}, X^{'(\beta)*}, X^{(\beta)*}$ to feed the solution to subproblems
5: Solve parallel subproblems (SP1)
6: $UB_1 \leftarrow \sum_i ic_E^f U_i^{(\beta)*} + \sum_l (ic_l^r + \rho_l \delta_0) X_l^{(\beta)*} + \sum_k (ic_k^c + \rho_k \delta_0) X_k^{'(\beta)*} + \sum_y \sum_d SC_{dy}^{1*}$
7: Update the dual values (τ, ξ)
8: **if** $|UB_1 - LB_1| \leq \epsilon$ **then**
9: **return** $U^*, X^{'*}, X^*$
10: **else**
11: $\beta \leftarrow \beta + 1$
12: Update Benders cut with dual values
13: Go to step 2
14: **end if**

a single line must be connected to the new node (see (5.8b).) Eq. (5.8c) indicates that if any new node is already added to the existing network (*i.e.*, $n' \geq 2$), the investment statuses for the added lines are 1 to update their required line ampacity while determining a new connection. (5.8d) and (5.8e), and their roles in the master problem are given as same in Sec. 4.6.2. The lower-bound of the total cost LB_1 is the optimal objective value of the master problem (*i.e.*, $LB_1 = MC^{1*}$).

$$\min_{U,\Pi,\alpha^{1st}} : MC^1 = \sum_{i \in \mathscr{N}} ic_E^f U_i + \sum_{k \in \mathscr{K}(n')} (ic_k^c + \rho_k \delta_0) X_k' + \sum_{l \in \mathscr{L}} (ic_l^r + \rho_l \delta_0) X_l + \sum_{\in \mathscr{Y}} \sum_{d \in \mathscr{D}} \alpha_{dy}^{1st} \quad (5.8a)$$

subject to:

$$\sum_{k \in \mathscr{K}(n')} X_k' = 1, \quad (5.8b)$$

$$X_{(L-n'+1):L} = 1, \qquad \forall n' \geq 2, \quad (5.8c)$$

$$\alpha_{dy}^{1st} \geq \underline{\alpha}^{1st}, \qquad \forall d \in \mathscr{D}, \forall y \in \mathscr{Y}, \quad (5.8d)$$

$$\alpha_{dy}^{1st} \geq \Gamma 1_{dy}^{(\beta)}, \qquad \forall d \in \mathscr{D}, \forall y \in \mathscr{Y}, \forall \beta \in \mathscr{B}_1. \quad (5.8e)$$

Subproblem : in the subproblem associated with day-type d and year y, a daily MAR-OPF model employing the big M method sizes the ESSs' capacities and lines' ampacities based on the investment constraints, and evaluates its operational advantages on the system conditions. The lines' ampacities are optimally sized not only for the new line candidates (connecting the network to the new node n') but also for the lines added by the previous rounds of siting sub-stage optimization problem and for the existing to-be-reinforced lines.

Conductor's possible ampacity range is modeled by (5.9a), where A^{min}/A^{max} represent

minimum/maximum possible line ampacity, respectively. As the line ampacity limit is given by the squared current variable, it is important to include the piece-wise linearized approximation constraints for the squared line ampacity value as given in (5.9c), along with constraints defining the range of piece-wise linearized value of the squared line ampacity as shown in (5.9b).

$$A^{min}\Pi_j \leq A''_{jdy} \leq A^{max}\Pi_j, \qquad \forall j \in (\mathscr{L} \cup \mathscr{K}(n')), \tag{5.9a}$$

$$(A^{min})^2\Pi_j \leq L((A''_{jdy})^2) \leq (A^{max})^2\Pi_j, \qquad \forall j \in (\mathscr{L} \cup \mathscr{K}(n')), \tag{5.9b}$$

$$L((A''_{jdy})^2) \geq a_v A_{jdy} + b_v, \qquad \forall v \in \{1,...,\Upsilon_1\}, \forall j \in (\mathscr{L} \cup \mathscr{K}(n')). \tag{5.9c}$$

The subproblem is modeled based on the MAR-OPF with big-M method as discussed in Sec. 5.7.2. The equations modeling the investment constraints on the conductor size and the ESSs capacity ranges are included as in (5.9). The operational constraints of ideal ESSs are given as (5.10d), while the MAR-OPF model employing big M method is indicated as (5.10c). Note that the ESS power injection and its contribution in achieving dispatchability are embedded within (5.10c). The objective function of the subproblem is the combination of the capacity cost of the ESSs' energy reservoirs, power ratings, the conductor cost for new lines and the reinforced lines, as well as the operational cost, given by (5.10a). The operational cost consists of grid losses and the unserved energy costs. Eq. (5.10e) and (5.10f) shows that the ESSs' locations and the lines to be invested are fixed to the optimal solution values of the master problem. τ_{idy} and χ_{jdy} are the duals of constraints related to the fixed ESSs' locations and the lines for investment.

$$\begin{aligned}\min_{\substack{\forall R,C,A'';\\ \forall \varphi'^{(B,E)},\pi}} : SC^1_{dy} = \frac{N_{dy}}{(1+r_{dis})^y} \sum_{t\in\mathscr{T}} \sum_{\phi\in\Phi_{dy}} \lambda_\phi (w_l \sum_j r_j f_{j\phi t} \\ + w_u \sum_j (up^+_{j\phi t} + up^-_{j\phi t} + uq^+_{j\phi t} + uq^-_{j\phi t})) \\ + \frac{N_{dy}}{365 * Y} \sum_i (ic^e_E C_{idy} + ic^p_E R_{idy}) \\ + \frac{N_{dy}}{365 * Y} \sum_j \rho_j (\delta_2 (A''_{jdy})^2 + \delta_1 A''_{jdy})\end{aligned} \tag{5.10a}$$

subject to:

$$(4.7), (5.9), \tag{5.10b}$$

$$\Theta'^B(\varphi'^{(B,E)}_{\phi t}) \geq 0, \qquad \forall t \in \mathscr{T}, \forall \phi \in \Phi_{dy}, \tag{5.10c}$$

$$\Lambda(\pi_{l\phi}) \geq 0, \qquad \forall l \in \mathscr{L}, \phi \in \Phi_{dy}, \tag{5.10d}$$

$$U_{idy} = U^{(\beta)*}_i : \tau_{idy}, \qquad \forall i \in (\mathscr{N} \cup \{n'\}), \tag{5.10e}$$

$$\Pi_{jdy} = \Pi^{(\beta)*}_j : \chi_{jdy}, \qquad \forall j \in (\mathscr{L} \cup \mathscr{K}(n')). \tag{5.10f}$$

As shown in (5.11), as a result of solving the subproblem, the Benders cut is obtained for day d and year y by employing the dual values linked to the location of ESS and line investment.

$$\Gamma 1_{dy}^{(\beta)} = \left[SC_{dy}^{1*} - \sum_{i}(\tau_{idy}(U_i - U_i^{(\beta)*})) - \sum_{j}(\chi_{jdy}(\Pi_j - \Pi_j^{(\beta)*}))\right]. \tag{5.11}$$

The upper-bound (UB_1) of the planning cost is the sum of the fixed cost from the master problem and the total subproblem cost.

Sizing sub-stage-determination of ESSs and lines sizes
At each run of siting sub-stage, a new node and corresponding optimal line candidate is added to the existing network using the Alg. 5.1. In this way, after N' runs of 1st block and siting sub-stage problems, $\mathscr{N}$ and $\mathscr{L}$ contain both the initial nodes and lines as well as all the new ones. Since the network is still radial, lines and nodes (both the existing and new lines ones) can be indicated by a single index $l \in \mathscr{L}$, *i.e.*sending end index of line l. Moreover, the reinforcement for existing lines and the optimal sites for ESSs are fixed by the optimal binary solutions from the final run of the siting sub-stage.

The binary solutions are passed to the sizing sub-stage, then decisions on ESSs power/energy capacities, and line ampacities are determined. We refer to the formulation of the master and the subproblem associated with the 2nd sub-stage detailed in Sec. 4.6.2.

5.8 Simultaneous Approach

In this section, a solution approach that simultaneously connects all the new nodes to the existing network is introduced. It is expected that the simultaneous approach provides a better solution compared to the sequential approach as the latter's solution space is restricted by the pre-defined sequence concerning integration of new nodes. In Sec. 5.7, the binary variables associated with line and ESS investment are determined in the master problem of the siting sub-stage, while the optimal sizing decisions with the given site solution from the master problem and the operation condition, are evaluated through solving the parallel subproblems. The optimal solution is achieved when the convergence of the Benders decomposition is reached. In this specific problem formulation, considering more than one node for a new connection requires including numerous binary variables associated with the new line candidates, which significantly increases the computational burden. Therefore, it is observed that introducing these binary variables into the master problem may hinder the convergence of the Benders algorithm. The significant number of Benders iterations due to slow convergence make the master problem inefficient due to the accumulation of Benders cuts. In this regard, the substantial reformulation on the problem structure is essential to consider the new lines investment in the planning problem.

Fig. 5.3 illustrates the optimization process by reformulating the planning problem. For clearer description of the whole process, Alg. 5.3 is also included. In the 1st block problem, the ESS investment is optimized to minimize the penalty of the dispatch error. Note that the new nodes are assumed to be connected to any node in the network when optimally allocated

Algorithm 5.3 Full algorithm of the simultaneous approach.

Require: Existing network ($\mathscr{L}$), prosumption ($s = p + jq$), ESS candidate nodes, new nodes ($\mathscr{N}'$)

Solve **1st block problem** to determine the optimal level of dispatchability when nodes $\mathscr{N}'$ are added to the existing network
Select candidate nodes $\mathscr{K}(n'), \forall n' \in \mathscr{N}'$ according to the modeler's criteria
while $Convergence = 0$ **do**
  Initialization : $\beta \leftarrow 1$ {**Siting sub-stage of 2nd block problem**}
  Solve the master problem to determine $U_i^{(\beta)*}, \forall i \in \mathscr{N}$, $X_l^{(\beta)*}, \forall l \in \mathscr{L}$
  Update LB
  Solve MISOCP modeled subproblems for $\forall d \in \mathscr{D}$ to determine $X'^*(d)$ (see (5.12a) and (5.19a)) specific to each day-type for β^{th} Benders iteration
  Solve SOCP modeled subproblems (with Alg. 3.1), with each problem fixed by $X'^*(d)$ to determine the subproblems objective values for $\forall d \in \mathscr{D}$, $\forall y \in \mathscr{Y}$
  Update UB
  if $|UB - LB| \leq \varepsilon$ **then**
    $Convergence \leftarrow 1$
  else
    Build Benders cut with dual values and subproblem objective values
    $\beta \leftarrow \beta + 1$
  end if
end while
Identify the unique solutions among $X'^*(d), \forall d \in \mathscr{D}$ and index them with $D \in \mathscr{D}^*$
for $D \leftarrow 1$ to $|\mathscr{D}^*|$ **do**
  Calculate the total planning cost $TP(D)$ by solving master problem and parallel SOCP modeled subproblems, with all subbroblems fixed by $X'(d) \leftarrow X'^*(D), \forall d \in \mathscr{D}, \forall y \in \mathscr{Y}$
end for
$D^* = \arg\min_{d \in \mathscr{D}}(TP(D))$
return $\Pi^* \leftarrow \Pi^*(D), N \leftarrow N + N', L \leftarrow L + N'$
Solve **Sizing sub-stage of 2nd block problem** to determine ESS size ($R_i^*, C_i^*, \forall i \in \mathscr{N}_E$), line ampacities of new lines and lines to be reinforced ($A_l''^*, \forall l \in \mathscr{L}$)
return R^*, C^*, A''^*

ESSs are identified. The substantial modification of the planning problem takes place in the siting sub-stage of the 2nd block problem, where the new lines installation is determined. In the master problem, as formulated in Sec. 4.6.2, the binary variables related to the line reinforcement and the ESS allocation are included. On the other hand, the binary variables for new lines investment are included in the subproblem, along with the size associated investment variables and the operation related variables. This changes the subproblem from a SOCP to a MISOCP problem when compared to the subproblem formulated in Sec. 4.6.2. After obtaining the solution of the new line investment by solving the subproblem, we solve another round of subproblem modeled as a SOCP problem by fixing the binary value of the new line investment. The step is indispensable to obtaining dual values associated with the values of line reinforcement and ESS allocation investment. After reaching convergence of the

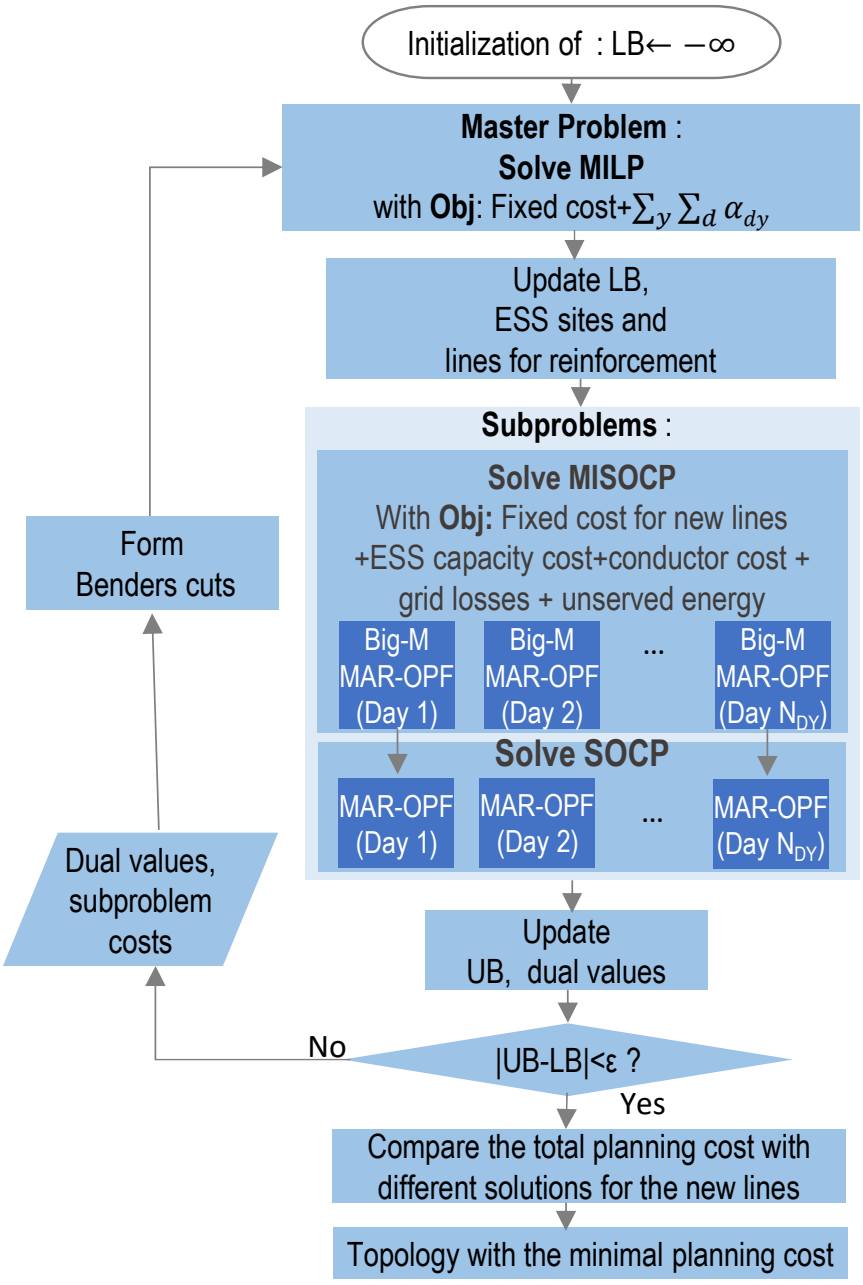

Figure 5.3: Flow chart of the simultaneous approach.

Benders algorithm, we obtain the optimal binary solution for all day-types regarding the line to be reinforced and the ESSs' sites. The binary solutions for the new lines may be determined differently for each day-type. The distinct solutions of new lines with different day-types form the solution set of new lines. The final step is to check which solution brings the minimal total planning cost among the solution set of new lines. By comparing the total planning cost with different solutions associated with new lines, the optimal solution among the solution set is

chosen as the optimal new lines placement. Then, it is followed by the sizing sub-stage of the 2nd block problem to obtain the optimal size of the assets.

5.8.1 Master Problem

The master problem is formulated in the same way as in the master problem of the siting sub-stage for co-optimization of line reinforcement and ESS allocation. The mathematical formulation and its description are detailed in Sec. 4.6.2.

5.8.2 Subproblem

The formulation of the subproblem is modified from that described in Sec. 4.6.2 to include the modeling of the new lines investment. In this subsection, only the parts that are modified are explicitly explained.

The investment in new lines : the candidate connections to the new nodes are represented as binary variables, while 1 indicates that the specific candidate is chosen to be installed. Array X' is re-defined to include all the candidate lines to connect new nodes $\mathcal{N}'$, as shown in (5.12a). The conditions for the new lines investment are modeled as shown below. Since the studied distribution network is radial, it signifies that there should be only single line connected upstream to each new node. This is enforced by (5.12b). Only one candidate must be chosen among the candidate connections to each new node and this condition is enforced by (5.12c). Finally, in case a line connecting any two new nodes is sorted as one of the possible connection candidates for both new nodes, only one of the two is chosen as described by (5.12d).

$$X' = \Big[[X'_{1(1)} \cdots X'_{(K-1)(1)}\ X'_{K(1)}],\ [X'_{1(2)} \cdots X'_{K(2)}], \cdots [X'_{1(N'-1)} \cdots X'_{K(N'-1)}], [X'_{1(N')} \cdots X'_{K(N')}] \Big]^{\top}, \tag{5.12a}$$

$$\sum_{n' \in \mathcal{N}'} \sum_{k \in \mathcal{K}(n')} X'_{k(n')} = N', \tag{5.12b}$$

$$\sum_{k \in \mathcal{K}(n')} X'_{k(n')} = 1, \tag{5.12c}$$

$$X'_{k(n')} + X'_{j(n'')} = 1, \text{where } \ k(n') : n'' \rightarrow n', \ \ j(n'') : n' \rightarrow n'', \quad \forall n', n'' \in \mathcal{N}'. \tag{5.12d}$$

Modification of the OPF equations

The power flow equations and the operational constraints are modeled based on MAR-OPF employing big-M method introduced in Sec. 5.7.2. The additional modification from the OPF model described in Sec. 5.7.2 is the inclusion of binary variables associated with new lines. Note that the equations are defined for all lines encompassing existing network and the candidate lines for connecting all of the new nodes, (the index of line is j, $\forall j \in \mathcal{L} \cup \{\mathcal{K}(n') | \forall n' \in \mathcal{N}'\}$. For the sake of simplicity, we define, $\mathcal{S} = \{\mathcal{K}(n') | \forall n' \in \mathcal{N}'\}$). The modified parts of the branch power flow equations (including ESS power dispatch) for both power flow variables and auxiliary bound variables are expressed by (5.13a)-(5.13c), which replace (5.5).

Unlike in (5.5) where the values of Ψ are parameterized, the part of the new line candidates in Ψ is modeled by the array of binary variable $X'_{k(n')}$. In other words, the nodal voltages related terms in the power balance equation are indicated by the multiplication of binary variable and continuous variable, making the corresponding power balance equations a set of non-convex constraints. Due to the same reason, the voltage equations are expressed as (5.13d) and (5.13e) by including Ψ as well, replacing (5.6).

$$S_j^t = s_j + s_j^E + \sum_{m\in\mathscr{S}} \mathbf{H}_{j,m} S_j^t + z_j f_j - j\Psi_j(v_{up(j)} + v_j)b_j, \qquad \forall j \in \mathscr{S}, \tag{5.13a}$$

$$\hat{S}_j^t = s_j + s_j^E + \sum_{m\in\mathscr{S}} \mathbf{H}_{j,m} \hat{S}_j^t - j\Psi_j(\bar{v}_{up(j)} + \bar{v}_j)b_j, \qquad \forall j \in \mathscr{S}, \tag{5.13b}$$

$$\bar{S}_j^t = s_j + s_j^E + \sum_{m\in\mathscr{S}} \mathbf{H}_{j,m} \bar{S}_j^t + z_j f_j - j\Psi_j(v_{up(j)} + v_j)b_j, \qquad \forall j \in \mathscr{S}, \tag{5.13c}$$

$$\left|-\Psi_j v_j + \Psi_j v_{up(j)} - 2\Re(\bar{z}_j(\hat{S}_j^t + j\Psi_j v_{up(j)} b_j)) + |z_j|^2 f_j\right| \leq M(1-\Psi_j), \qquad \forall j \in \mathscr{S}, \tag{5.13d}$$

$$\left|-\Psi_j \bar{v}_j + \Psi_j \bar{v}_{up(j)} - 2\Re(\bar{z}_j(\hat{S}_j^t + j\Psi_j \bar{v}_{up(j)} b_j))\right| \leq M(1-\Psi_j), \qquad \forall j \in \mathscr{S}. \tag{5.13e}$$

The array of line connection status with binary variables is also incorporated into the inequality constraints defining the longitudinal current ((5.14a) and (5.14b)) and its auxiliary variable ((5.14c) and (5.14d)). As shown in (5.14e) and (5.14f), the line current at the sending and the receiving ends are expressed while considering the connection status of lines. In this way, (5.14) replaces (5.7).

$$f_j(\Psi_j v_{up(j)} + (1-\Psi_j)) \geq |\max\{|\hat{P}_j^t|, |\bar{P}_j^t|\}|^2 + |\max\{|\hat{Q}_j^t - j\Psi_j \bar{v}_j b_j|, |\bar{Q}_j^t - j\Psi_j v_j b_j|\}|^2, \qquad \forall j \in \mathscr{S}, \tag{5.14a}$$

$$f_j(\Psi_j v_j + (1-\Psi_j)) \geq |\max\{|\hat{P}_j^b|, |\bar{P}_j^b|\}|^2 + |\max\{|\hat{Q}_j^b - j\Psi_j \bar{v}_j b_j|, |\bar{Q}_j^b - j\Psi_j v_j b_j|\}|^2, \qquad \forall j \in \mathscr{S}, \tag{5.14b}$$

$$\bar{f}_j(\Psi_j v_{up(j)} + (1-\Psi_j)) \geq |\max\{|\hat{P}_j^t|, |\bar{P}_j^t|\}|^2 + |\max\{|\hat{Q}_j^t + j\Psi_j \bar{v}_{up(j)} b_j|, |\bar{Q}_j^t + j\Psi_j v_{up(j)} b_j|\}|^2, \qquad \forall j \in \mathscr{S}, \tag{5.14c}$$

$$\bar{f}_j(\Psi_j v_j + (1-\Psi_j)) \geq |\max\{|\hat{P}_j^b|, |\bar{P}_j^b|\}|^2 + |\max\{|\hat{Q}_j^b - j\Psi_j \bar{v}_j b_j|, |\bar{Q}_j^b - j\Psi_j v_j b_j|\}|^2, \qquad \forall j \in \mathscr{S}, \tag{5.14d}$$

$$I_j^t(\Psi_j v_{up(j)} + (1-\Psi_j)) \geq |\max\{|\hat{P}_j^t|, |\bar{P}_j^t|\}|^2 + |\max\{|\hat{Q}_j^t|, |\bar{Q}_j^t|\}|^2, \qquad \forall j \in \mathscr{S}, \tag{5.14e}$$

$$I_j^b(\Psi_j v_j + (1-\Psi_j)) \geq |\max\{|\hat{P}_j^b|, |\bar{P}_j^b|\}|^2 + |\max\{|\hat{Q}_j^b|, |\bar{Q}_j^b|\}|^2, \qquad \forall j \in \mathscr{S}. \tag{5.14f}$$

The compound nodal voltage terms $\Psi_j v_{up(j)}, \Psi_j v_j, \Psi_j \bar{v}_{up(j)}, \Psi_j \bar{v}_j$ are reformulated such that the power balance and nodal voltage equations are expressed as linear equations. In this regard, a new set of auxiliary variables associated with voltage labeled as $vv_{up(j)}$, vv_j, $\bar{v}v_{up(j)}$, and $\bar{v}v_j$, are introduced along with the related constraints (see (5.15)) to define their values.

$$vv_{up(j)} \le v_{up(j)}, \quad vv_{up(j)} \le 2\Psi_j, \quad vv_{up(j)} \ge 0, \qquad \forall j \in \mathscr{S}, \tag{5.15a}$$
$$vv_j \le v_j, \quad vv_j \le 2\Psi_j, \quad vv_j \ge 0, \qquad \forall j \in \mathscr{S}, \tag{5.15b}$$
$$\bar{v}v_{up(j)} \le \bar{v}_{up(j)}, \quad \bar{v}v_{up(j)} \le 2\Psi_j, \quad \bar{v}v_{up(j)} \ge 0, \qquad \forall j \in \mathscr{S}, \tag{5.15c}$$
$$\bar{v}v_j \le v_j, \quad \bar{v}v_j \le 2\Psi_j, \quad \bar{v}v_j \ge 0, \qquad \forall j \in \mathscr{S}. \tag{5.15d}$$

The set of constraints makes the auxiliary variable bind to the physical nodal voltage value only when the line which connects the node j and its upstream node $up(j)$ is selected, otherwise, it is fixed to zero. To do that, it is necessary to add the total negative sum of the voltage auxiliary variable values to the objective function (see (5.18a)). In this way, we can replace the compound nodal voltage terms with the defined auxiliary variables in the power balance, and nodal voltage equations. Mathematically, (5.16) replaces (5.13).

$$S_j^t = s_j + s_j^E + \sum_{m \in \mathscr{S}} \mathbf{H}_{j,m} S_j^t + z_j f_j - j(vv_{up(j)} + vv_j) b_j, \qquad \forall j \in \mathscr{S}, \tag{5.16a}$$
$$\hat{S}_j^t = s_j + s_j^E + \sum_{m \in \mathscr{S}} \mathbf{H}_{j,m} \hat{S}_j^t - j(\bar{v}v_{up(j)} + \bar{v}v_j) b_j, \qquad \forall j \in \mathscr{S}, \tag{5.16b}$$
$$\bar{S}_j^t = s_j + s_j^E + \sum_{m \in \mathscr{S}} \mathbf{H}_{j,m} \bar{S}_j^t + z_j f_j - j(vv_{up(j)} + vv_j) b_j, \qquad \forall j \in \mathscr{S}, \tag{5.16c}$$
$$\left| -vv_j + vv_{up(j)} - 2\Re(\bar{z}_j(S_j^t + jvv_{up(j)} b_j)) + |z_j|^2 f_j \right| \le M(1-\Psi_j), \qquad \forall j \in \mathscr{S}, \tag{5.16d}$$
$$\left| -\bar{v}v_j + \bar{v}v_{up(j)} - 2\Re(\bar{z}_j(\hat{S}_j^t + j\bar{v}v_{up(j)} b_j)) \right| \le M(1-\Psi_j), \qquad \forall j \in \mathscr{S}. \tag{5.16e}$$

The compound nodal voltage terms in the current associated equations are also replaced with the defined auxiliary variables. Mathematically, (5.17) replaces (5.14).

$$\begin{aligned} f_j(vv_{up(j)} + (1-\Psi_j)) \ge & |\max\{|\hat{P}_j^t|, |\bar{P}_j^t|\}|^2 \\ & + |\max\{|\hat{Q}_j^t + i\bar{v}v_{up(j)} b_j|, |\bar{Q}_j^t + ivv_{up(j)} b_j|\}|^2, \end{aligned} \qquad \forall j \in \mathscr{S}, \tag{5.17a}$$
$$\begin{aligned} f_j(vv_j + (1-\Psi_j)) \ge & |\max\{|\hat{P}_j^b|, |\bar{P}_j^b|\}|^2 \\ & + |\max\{|\hat{Q}_j^b - i\bar{v}v_j b_j|, |\bar{Q}_j^b - j\Psi_j vv_j b_j|\}|^2, \end{aligned} \qquad \forall j \in \mathscr{S}, \tag{5.17b}$$
$$\begin{aligned} \bar{f}_j(vv_{up(j)} + (1-\Psi_j)) \ge & |\max\left\{|\hat{P}_j^t|, |\bar{P}_j^t|\right\}|^2 \\ & + |\max\left\{|\hat{Q}_j^t + j\bar{v}v_{up(j)} b_j|, |\bar{Q}_j^t + jvv_{up(j)} b_j|\right\}|^2, \end{aligned} \qquad \forall j \in \mathscr{S}, \tag{5.17c}$$
$$\begin{aligned} \bar{f}_j(vv_j + (1-\Psi_j)) \ge & |\max\left\{|\hat{P}_j^b|, |\bar{P}_j^b|\right\}|^2 \\ & + |\max\left\{|\hat{Q}_j^b - j\bar{v}v_j b_j|, |\bar{Q}_j^b - jvv_j b_j|\right\}|^2 \end{aligned} \qquad \forall j \in \mathscr{S}, \tag{5.17d}$$
$$I_j^t(vv_{up(j)} + (1-\Psi_j)) \ge |\max\{|\hat{P}_j^t|, |\bar{P}_j^t|\}|^2 + |\max\{|\hat{Q}_j^t|, |\bar{Q}_j^t|\}|^2, \qquad \forall j \in \mathscr{S}, \tag{5.17e}$$
$$I_j^b(vv_j + (1-\Psi_j)) \ge |\max\{|\hat{P}_j^b|, |\bar{P}_j^b|\}|^2 + |\max\{|\hat{Q}_j^b|, |\bar{Q}_j^b|\}|^2, \qquad \forall j \in \mathscr{S}. \tag{5.17f}$$

Finally, the MAR-OPF model that includes ESS injections for the siting sub-stage of the simultaneous approach is formulated by (3.1b), (3.2b), (3.2e), (3.2h), (3.9a)-(3.9e),(3.10b),

(3.10d), (3.10f), (3.11), (5.3),(5.15), (5.16), (5.17), and the equations are grouped as $\Theta'^{S}(\varphi'^{(S,E)}) \geq 0$, where $\varphi'^{(S,E)} := \{S^t, v, f, \hat{S}^t, \bar{v}, \bar{f}, \bar{S}^t, s', s^E, up^+, up^-, uq^+, uq^-, \zeta, \Pi, A'', \Psi\}$ is the set of variables. The notation without subscript corresponds to the vector of variables for $\forall j \in \mathscr{S}$.

The MISOCP subproblem is shown as (5.18). The constraints related to the new line investment are incorporated (see (5.12)) into the modified OPF constraints. The constraints for ESSs' energy reservoirs, and their power ratings are given by (5.18c)-(5.18e) and the constraints for lines' ampacities are (5.18f)-(5.18h). The ESSs' operational constraints are indicated by (5.18i). The MAR-OPF model considering new line candidates is included (see (5.18j).) The investment status related to ESS allocation and the line reinforcement on the existing lines are fixed to the solution of the master problem of the previous Benders iteration ((5.18k) and (5.18l)). As given by (5.18a), the objective function of the subproblem consists of three parts: investment cost, operational cost, and finally additional term associated with the auxiliary nodal voltage variables. The investment cost included in the subproblem is the new line investment cost (both fixed and conductor cost), the conductor cost for the reinforced lines, the capacity cost of ESSs. The operational cost relates to the grid losses and the unserved energy. Finally, the negative sum of the voltage auxiliary variables is added for accurate calculation of nodal voltage values.

$$\begin{aligned}
\min_{\substack{\forall X',R,C,A'';\\ \forall \varphi'^{(S,E)},\pi}} : SC_{dy}^{MISOCP} = & \frac{N_{dy}}{365*Y}\sum_{n'}\sum_{k}(ic^{f}_{k(n')}X'_{k(n')}+\rho_{k(n')}\delta_0 X'_{k(n')}) \\
& + \frac{N_{dy}}{365*Y}\sum_{i}(ic^{e}_{E}C_i+ic^{p}_{E}R_i) \\
& + \frac{N_{dy}}{365*Y}\sum_{j}\rho_j(\delta_2(A''_j)^2+\delta_1 A''_j) \\
& + \frac{N_{dy}}{(1+r_{dis})^y}\sum_{t\in\mathscr{T}}\sum_{\phi\in\Phi_{dy}}\lambda_\phi(w_l\sum_{j}r_j f_{j\phi t} \\
& + w_u\sum_{j}(up^{+}_{j\phi t}+up^{-}_{j\phi t}+uq^{+}_{j\phi t}+uq^{-}_{j\phi t}) \\
& - \sum_{j}(v v_{up(j)\phi t}+v v_{j\phi t}+\bar{v}\bar{v}_{up(j)\phi t}+\bar{v}\bar{v}_{j\phi t})
\end{aligned} \tag{5.18a}$$

subject to:

$$(5.12), \tag{5.18b}$$

$$R^{min}U_i \leq R_{idy} \leq R^{max}U_i, \qquad \forall i \in \mathscr{N}, \tag{5.18c}$$

$$C^{min}U_i \leq C_{idy} \leq C^{max}U_i, \qquad \forall i \in \mathscr{N}, \tag{5.18d}$$

$$R_{idy} \leq \frac{C_{idy}}{CR^{max}}, \qquad \forall i \in \mathscr{N}, \tag{5.18e}$$

$$A^{min}\Pi_j \leq A''_{jdy} \leq A^{max}\Pi_j, \qquad \forall j \in \mathscr{S}, \tag{5.18f}$$

$$(A^{min})^2\Pi_j \leq L((A''_{jdy})^2) \leq (A^{max})^2\Pi_j, \qquad \forall j \in \mathscr{S}, \tag{5.18g}$$

$$L((A''_{jdy})^2) \geq a_v A_{jdy} + b_v, \qquad \forall v \in \{1,...,\Upsilon_1\}, \forall j \in \mathscr{S}, \tag{5.18h}$$

$$\Lambda(\pi_{i\phi}) \geq 0, \qquad \forall i \in \mathscr{N}, \forall \phi \in \Phi_{dy}, \tag{5.18i}$$

$$\Theta'^{S}(\varphi'^{(S,E)}_{\phi t}) \geq 0, \qquad \forall t \in \mathscr{T}, \forall \phi \in \Phi_{dy}, \tag{5.18j}$$

$$U_{idy} = U_i^{(\beta)*} : \tau_{idy}, \qquad \forall i \in \mathscr{N}, \tag{5.18k}$$

$$\Pi_{jdy} = \Pi_j^{(\beta)*} : \chi_{jdy}, \qquad \forall j \in \mathscr{S}. \tag{5.18l}$$

By solving the MISOCP-modeled subproblems for different day-types, we obtain the new lines investment specifically determined for each day-type. Note that solving the above mentioned subproblems cannot yield dual values related to the line reinforcement and the ESS allocation. Therefore, we solve another set of subproblems modeled in Sec. 4.6.2, under the topology determined by the day-type specific binary solution obtained from the MISOCP-modeled subproblems. In this way, the dual values related to the line reinforcement and the ESS allocation can be obtained to build the Benders cuts required for the next iteration of master problem.

5.8.3 Selection of the Best Network Topology

After reaching the convergence of the Benders algorithm, we obtain a unique and optimal line reinforcement and ESS allocation with the related binary solution. However, the optimal topology with new nodes may be different for each day-type, as shown in (5.19). In this regard, we first identify the unique solutions and index them with $D \in \mathscr{D}^*$ as shown in (5.19a). In this way, the compound array of line investment solution $\Pi^*(D)$, indicated in (5.19b), consists of investment decisions on line reinforcement (uniquely determined for all day-types) and D^{th} solution of new lines among the solution set $\mathscr{D}^*$. The corresponding connection status is indicated by $\Psi^*(D)$. The final step of the siting sub-stage is to compute the total planning cost while fixing the line investment status and the connection status to the corresponding solution array obtained from the solution set $\mathscr{D}^*$ (*i.e.*, $\Pi \leftarrow \Pi^*(D), \Psi \leftarrow \Psi^*(D)$). The total planning cost with the network topology $\Psi^*(D)$ (*i.e.*, $TP(D)$) is computed considering different topology solutions of $D, \forall D \in \mathscr{D}^*$. The total planning cost is mathematically indicated as shown in (5.19d), while the subproblem cost of day d and y under the network configuration $\Psi^*(D)$ is calculated as shown in (5.19c).

$$X'^*(D) = \Big[[X'^*_{1(1)}(D) \cdots X'^*_{K(1)}(D)], [X'^*_{1(2)}(D) \cdots X'^*_{K(2)}(D)] \cdots, [X'^*_{1(N')}(D) \cdots X'^*_{K(N')}(D)] \Big]^\top, \quad \forall D \in \mathscr{D}^*, \tag{5.19a}$$

$$\Pi^*(D) = [X^{*\top}\ X'^*(D)^\top]^\top, \quad \Psi^*(D) = [\mathbf{1}^\top\ X'^*(D)^\top]^\top, \qquad \forall D \in \mathscr{D}^*, \tag{5.19b}$$

$$SC^{1*}_{dy}(D) = \frac{N_{dy}}{365 * Y}\Big(\sum_i ic^e_i C^*_{idy} + ic^p_i R^*_{idy} + \sum_j \Pi^*_j(D)\cdot(\delta_2 A''_{jdy}\cdot A''_{jdy} + \delta_1 A''_{jdy})\Big) + \frac{N_{dy}}{(1+r_{dis})^y}\sum_{t\in\mathscr{T}}\sum_{\phi\in\Phi_{dy}}\lambda_\phi(w_l\sum_j r_j f_{j\phi t} + w_u\sum_j(up^+_{j\phi t} + up^-_{j\phi t} + uq^+_{j\phi t} + uq^-_{j\phi t})), \tag{5.19c}$$

$$TP(D) = \sum_i ic^c_i U^*_i + \sum_l (ic^r_l + \rho_l\delta_0)X^*_l + \sum_{n'}\sum_k (ic^{n'}_k + \rho_{k(n')}\delta_0)X^{'*}_{k(n')}(D) + \sum_y\sum_d SC^{1*}_{dy}(D). \tag{5.19d}$$

The topology which gives the minimal planning cost is determined to be the optimal topology connecting the new nodes as shown in (5.20a). Finally, the network is expanded by including the optimal candidate lines identified by index D^* as expressed by (5.20b).

$$D^* = \underset{d\in\mathscr{D}}{\arg\min}\big(TP(D)\big), \tag{5.20a}$$

$$\mathscr{L} \leftarrow \mathscr{L} \cup \{k^*(1)(D^*), \cdots, k^*(N')(D^*)\}. \tag{5.20b}$$

The binary solutions are then fed into the sizing sub-stage to determine the optimal size of ESSs and line ampacities. The sizing sub-stage can be referred to Sec. 4.6.2.

5.9 Comparison between the Sequential and the Simultaneous Approach

The two developed approaches can be compared based on two main factors: the optimality that can be reached by determining the network topology; and the computation time. With the simultaneous approach, the computational burden is mainly loaded with the MISOCP subproblem due to numerous binary variables and the associated operational constraints. The conservative bounds constraints modeled in the AR-OPF problem make the problem even more demanding to solve. One measure to reduce the number of variables and related operational constraints is to solve the MISOCP subproblems by employing the R-OPF model instead of the AR-OPF model. The R-OPF model is the standard SOCP relaxed OPF model [82] without conservative bound on current and voltage, which makes the MISOCP subproblem computationally lighter than the one with AR-OPF model. In view of this, the two OPF models are employed for modeling the MISOCP subproblems to evaluate the trade-off between the computation burden and the modeling accuracy of OPF constraints, as well as its effect on the investment solutions. However, note that, in both of the simultaneous approaches, the SOCP subproblems (subproblems that come after solving the MISOCP subproblems) are formulated by utilizing the MAR-OPF model. In short, we compare the three approaches: sequential approach, simultaneous approach employing the AR-OPF model, and simultaneous approach employing the R-OPF model.

5.9.1 Simulation Configuration

The comparative study is carried on the same system with the same settings as set in Sec. 4.7.1. Additionally, in the first test case, three new nodes are considered to be included in the existing network. For each new node, 4 candidate lines are considered. The candidate lines are determined based on the distance between the new node and the existing nodes. It is also possible to consider a connection between any two new nodes if the distance between the two are close enough to be sorted as one of the candidates. The number of considered operating scenarios is 10 with 24 timesteps, and 1 day-type. The same kind of test case is carried on while adding 10 new nodes to compare the scalability of the proposed approaches.

5.9.2 Planning Results Comparison between the Sequential and the Simultaneous Approach

The investment solutions with the sequential approach and the simultaneous approach (based on the MAR-OPF model) are shown in Table 5.1.

The test case with 3 new nodes

The investment solutions with the sequential approach and the simultaneous approach (based on the MAR-OPF model) are shown in Table 5.1. The indices of the new nodes are 56, 57, and 58. The result indicates that the simultaneous approach employing AR-OPF model and the sequential approach yield the same investment solutions in terms of ESS sites, and lines to be invested (both reinforcement, and new installation), while difference in the unserved energy is negligible. Note that the simultaneous approach that employs the R-OPF model gave different ESS site from the two previous approaches. The difference in the investment results is converted into the final objective values. As shown in Table 5.1, the objective values obtained by the simultaneous approach with AR-OPF model and the sequential approach are the same. Meanwhile, the planning cost obtained by the simultaneous approach with R-OPF model is \$19K higher than the other approaches. On the other hand, the simultaneous approach with R-OPF model took the shortest computation time, followed by the sequential approach. The computation time by the simultaneous approach with the AR-OPF model was the longest. The difference in Benders iterations number between the simultaneous approaches and the sequential approach shows that the simultaneous approaches are more efficient to the grid convergence than the sequential approach. However, including the binary variables makes the subproblems of the simultaneous approach take more time to solve. Therefore, ultimately, the simultaneous approach with AR-OPF model takes the longest time to solve among the suggested approaches even with the smallest number of Benders iterations.

The test case with 10 new nodes

In order to assess the scalability of the proposed approaches, the number of new nodes is increased to 10 new nodes, and the number of possible connections to those new nodes is 40 in total. In other words, the sequential approach requires 10 runs of solving the planning problem to connect all the new nodes, while taking into account 4 candidate lines per new node. On the other hand, in the simultaneous approach, 40 candidate lines are introduced

Table 5.1: Investment solutions with the sequential approach and the simultaneous approaches (AR-OPF and R-OPF)

Approach		Simultaneous (with R-OPF)	Simultaneous (with AR-OPF)	Sequential
Assets	Node with ESS	16, 27	4, 27	4, 27
	Reinforced lines	Line (48-12) Line (2-27)	Line (48-12) Line (2-27)	Line (48-12) Line (2-27)
	New lines	Line (15-56) Line (56-57) Line (56-58)	Line (15-56) Line (56-57) Line (56-58)	Line (15-56) Line (56-57) Line (56-58)
Unserved energy (siting sub-stage)		0.13 kWh	0.13 kWh	0.21 kWh

Table 5.2: Objective values and the computation times with the sequential approach and the simultaneous approaches (AR-OPF and R-OPF models).

		Iteration #	MP/SP	Computation time	Objective
Simultaneous approach (with R-OPF)		21	1.06s/2.5598E+3	5.38E+4	$ 29.489 M
Simultaneous approach (with AR-OPF)		20	1.18s/5.3660E+3	1.07E+5	$ 29.470 M
Sequential	Node 56	99	2.26s/316.9s	6.95E+4	$ 29.470 M
	Node 57	88	1.95s/220.1s		
	Node 58	73	3,16s/273.6s		

in the MISOCP-subproblem to connect 10 new nodes. The investment solutions, the total planning cost, and the total computation time are presented in Table 5.3 and Table 5.4. Note that the simultaneous approach with AR-OPF model was not able to tackle the given planning problem (*i.e.*, took too much time to converge to an optimal solution in subproblems.)

The investment solutions obtained in the simultaneous approach with R-OPF model and the sequential approach are shown in Table 5.3, with their differences highlighted in bold font. As shown in Table 5.4, the simultaneous approach with R-OPF model took 3.3 times of computation time than the sequential approach. The number of Benders iterations is only 14, which is relatively small compared to the Benders iterations of sequential approach, but the average computation time for solving the subproblems was significantly higher than sequential approach. The optimality gained by using simultaneous approach (with R-OPF model) compared to sequential approach is $10K, which corresponds to only 0.025% of the total planning cost.

In summary, when adding small number of nodes, the sequential approach exhibited the performance that is as good as the simultaneous approach with the AR-OPF model in terms of optimality, while its computation time was around 30% smaller. The simultaneous approach with R-OPF model showed the shortest computation time, while sacrificing optimality of

0.06%. On the other hand, as the number of nodes increased to 10, the sequential approach turned out to be significantly more efficient in computation over the simultaneous approaches while the quantified sub-optimality gap is almost negligible. In conclusion, the comparative analysis demonstrated the superior scalability of the sequential approach to apply to the generic exercise of expansion planning of distribution networks. In this regard, in the rest of the simulation section, only the sequential approach is tested for the performance validation of the planning tool.

Future work can be associated with developing the simultaneous approach further such that the limitation on the scalability of the planning tool can be improved. One possible approach is to hybridize the simultaneous approach and the sequential approach. By clustering the set of new nodes into several subgroups according to reasonable, data-driven criteria, the expansion planning process can be conducted by connecting each subgroup sequentially. For each round of planning process, the network is expanded by utilizing the simultaneous approach.

Table 5.3: Investment solutions with sequential approach and simultaneous approaches (10 new nodes).

Approach	Simultaneous (with R-OPF)	Simultaneous (with AR-OPF)	Sequential
Node with ESS	4, 27	-	4,27
Reinforced lines	48-12 2-27 **54-49** **27-54**	-	48-12 2-27
New lines	15-56 56-57 56-58 6-59 **61-60** 3-61 **59-62** **60-63** **63-64** **56-65**	-	15-56 56-57 56-58 6-59 **3-60** 3-61 **61-62** **59-63** **60-64** **60-65**

5.10 Performance Validation of the Expansion Planning Tool with the Sequential Approach

5.10.1 The simulation Configuration

The proposed DNEP is applied to a real Swiss 21kV distribution network with 55 nodes (see Fig. 5.4(a)). Initially, 2.7MWp of PV generation and 805kVA of hydropower generation are installed. The initial network topology and parameters can be found in [107]. The planning horizon is set to 10 years and other parameters such as annual growth rate of load consumption and discount

Table 5.4: Objective values and the computation times with sequential approach and simultaneous approaches (10 new nodes).

		Iteration #	MP/SP time	Total time	Objective
Simultaneous approach (with R-OPF)		14	1.12s/6.0798E+4	8.54E+5	$ 41.418 M
Simultaneous approach (with AR-OPF)		-	-	-	-
Sequential	Node 56	99	2.26s/316.9s	2.61E+5	$ 41.428 M
	Node 57	80	1.95s/220.1s		
	Node 58	73	3,16s/273.6s		
	Node 59	65	1.33s/241s		
	Node 60	66	1.86s/246.7s		
	Node 61	76	2.11s/251.2s		
	Node 62	95	1.88s/261.2s		
	Node 63	103	2.80s/352.9s		
	Node 64	92	1.75s/243.3s		
	Node 65	64	2.75s/267.2s		

rate are the same as in the previous chapters (see Fig. 3.3). The ESS cost parameters and possible ranges of energy reservoirs and power ratings are shown in Table 2.1. The candidate nodes for ESS installation are set according to the indications of the operator of this specific network. The new nodes are given on the network topology with their indices indicating their priorities for integration. Both load consumption and PV system with capacity of 1MWp are located on each new node. Each new node can be connected to the ones of the existing network among 4 candidates given by the user. In Table 5.5, the fixed costs associated with the line investment are given depending on the type of investment and connection. The estimated cost for constructing underground cables (UC) is set to four times higher than the one for overhead lines (OL) considering the cost range reported in [105]. The coefficient values for quadratic, linear and constant term of conductor cost function are given in Table 5.5 (see Sec. 5.7.2.) The penalty cost for the dispatch error is assumed as $897/MWh as set in Sec. 4.7.1. The same set of operating scenarios (10 operating scenarios and 8 day-types) are considered for the planning problem as set in Sec. 4.7.1.

Table 5.5: Parameters related to line investment.

New line installation		Line reinforcement	
Fixed cost (OL)	$0.2M/km	Fixed cost (OL)	$0.12M/km
Fixed cost (UC)	$0.8M/km	Fixed cost (UC)	$0.48M/km
Coefficients for conductor cost function		$\delta_2 : 0.011$, $\delta_1 : 0.065$, $\delta_0 : 95.22$	

5.10.2 Distribution Network Expansion Assessment on a Real Swiss Power Distribution Network

This subsection shows the solution of the planning problem using the determined set of operating scenarios to achieve the optimal level of dispatchability of the targeted ADNs by allocating ESSs. Moreover, the line investment regarding new line installation and existing line reinforcement are co-optimized to minimize the grid losses and the expected energy not served (EENS) while complying with the grid constraints regarding nodal voltage and line ampacity.

Fig. 5.4(a) illustrates the network topology with 8 new nodes (green circle), and the candidate nodes for ESS allocation (purple circle). The new nodes are integrated to the network by ascending order of the node index number. In Fig. 5.4(b), the line candidates to the new nodes are indicated (green dotted line). Fig. 5.4(c) shows the result in terms of the location of the new lines (green line), line to be reinforced (thick red line), and the nodes to host ESSs (orange circle) determined by the proposed planning tool. Table 5.6 shows the capacities of ESSs and the invested lines ampacities.

Table 5.6: Investment result

ESS	Node #	Energy reservoir (kWh)	Power rating (kVA)
	16	4657	1196
	27	5733	1431
Line	Investment type	Line #	Ampacity (A)
	Reinforcement	3-10	134
	New lines	10-56	51
		35-57	38
		56-58	34
		43-59	35
		16-60	34
		14-61	51
		61-62	43
		28-63	39

The connection to each new node is optimally determined based on the conductor cost (which relies on the line length, and the type of line installation) and the evaluation on the system operation. For example, the connecting node for Node 56 is decided to be Node 10 considering the relatively low fixed cost for overhead lines and the shorter distance to Node 56 than other candidate nodes. In this way, Node 58 is connected to Node 56, making the two new nodes connected in series to Node 10. The line ampacity of line between Node 56 and 58 is optimally decided to host the prosumption injection from Node 58. The ampacity of Line 10-56 is larger than Line 56-58, to host the total prosumption of Node 56 and 58. 5 new nodes are determined to be connected downstream to Node 10. These connections result in investment on upgrading the line between Node 10 and Node 3, because its initial

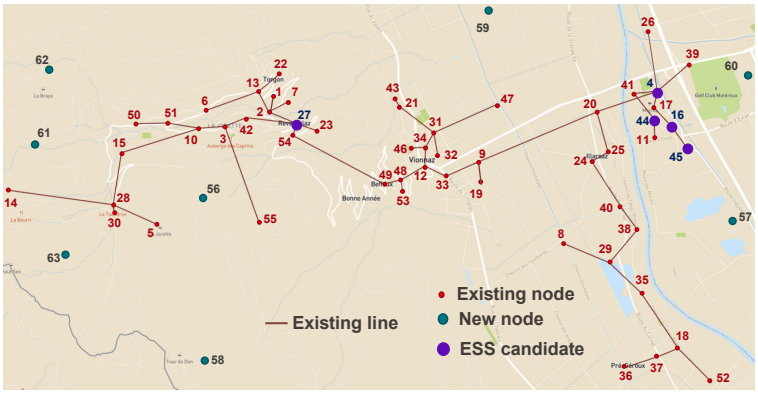

(a)

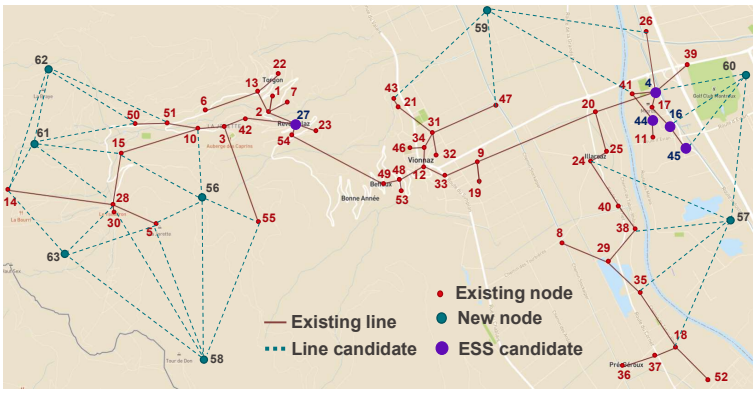

(b)

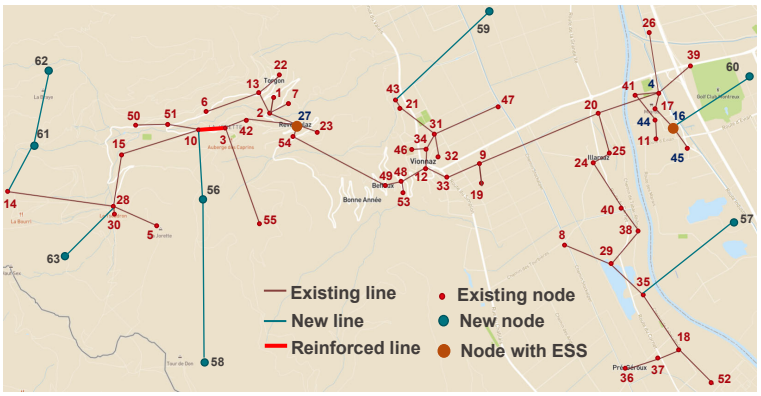

(c)

Figure 5.4: Network topology with: (a) candidate nodes for ESS allocation and new nodes, (b) with line candidates, (c) with ESSs, new lines and line reinforcement.

line ampacity (which was 90 A) was insufficient to host the additional PV injection from the 5 new nodes. The line is replaced to have ampacity of 134 A. The ESS installed at Node 27 with 4.66 MWh energy reservoir and 1.20 MVA power rating to compensate for the increased prosumption uncertainty from the 5 new nodes. Another ESS is installed at Node 16 to mainly

compensate for the uncertainty of the additional PV injection of Node 60 and the existing PV generation at Node 16 (as it hosts the biggest PV plant of 1.6 MWp).

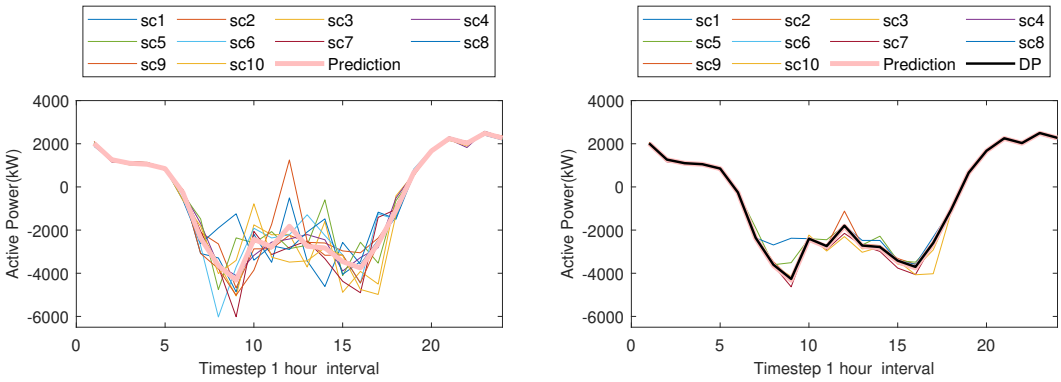

Figure 5.5: Example of dispatch result for Day-type 4, year 10: (a) aggregated prosumption scenarios and prosumption prediction, (b) power flow through GCP of scenarios, prosumption prediction and dispatch plan (DP).

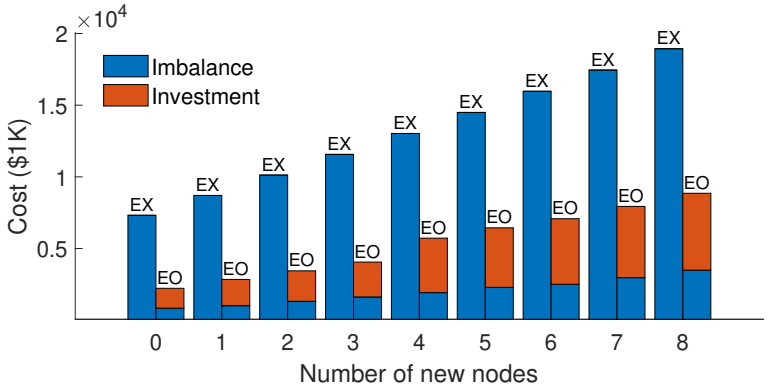

Figure 5.6: The 1st block cost result.

Table 5.7: Planning cost and Operational benefits.

Investment cost ($ Million)	6.86
Dispatch error penalty cost ($ Million)	3.49
Grid losses (GWh)	2.16
EENS (kWh)	14.99
Total energy served (GWh)	241.2

Fig. 5.5(a) shows the aggregated prosumption scenarios along with the aggregated prosumption prediction, whereas Fig. 5.5(b) represents the dispatch result after investment on ESS and lines. Thanks to the proposed planning strategy, the dispatch result shows that the power flow at the GCP of all scenarios follows the dispatch plan with the dispatch error

Table 5.8: Computation time (sec) for the expansion planning with the sequential approach.

Sub-stage	New Node ID	MP	SP	BI#
1st	56	8.47	2484	48
	57	8.86	2478	54
	58	6.54	2836	44
	59	9.44	2563	53
	60	8.46	2704	49
	61	7.11	2816	42
	62	9.26	2945	51
	63	6.40	2964	37
2nd		2.66	2300	25
Total		1.08E+6 (≈ 300hrs)		

determined by the optimal dispathability level of ADN. Furthermore, Fig. 5.6 illustrates the optimal ESSs investment and the resulting dispatch error penalty cost determined from the 1st block problem. 'EO' and 'EX' represent the case with and without the ESS allocation. The graphs of 'EO' show the increase of ESSs investment cost with the integration of new nodes hosting PV generation and load. The resulting benefit concerning the imbalance penalty cost corresponds to 82% reduction of dispatch error compared to the case without ESS.

The total planning cost, consisting investment and operational objectives costs, is shown in Table 5.7, along with total grid losses and active power served in the network for 10 years horizon. The final penalty cost for 10 years horizon regarding the dispatch error is $3.49 Million (which corresponds to 3.89 GWh). The total investment cost is $6.86 Million, where the ESS investment cost is $3.85 Million and the line investment cost is $3.01 Million. The EENS is only 15 kWh, which is negligible enough to conclude that the reliability of the power supply is successfully assured by the planning result. Table 5.8 shows the computation time of the 1st block problem, the siting, sizing sub-stages, and the total time for solving the given planning problem. Note that there are 8 rounds of the 1st block problem and the siting sub-stage of 2nd block problem. 2nd block problem takes more computation time than the 1st block problem due to its exact system operation evaluation based on the MAR-OPF model (subproblem of the 2nd block, which is indicated as 'SP' in the table). Based on the reported total computation time for solving master problems (indicated as 'MP') and subproblems along with the number of Benders iterations (indicated as 'BI'), the average computation time of MP and SP (4 (day-types) x 10 (years) parallel subproblems) per each iteration are calculated as 7.78s and 2541s, respectively. It is observed that the computation times for determining the connection to each new node are within the same order of magnitude, implying that the running time of the proposed framework increases linearly with the size of the new nodes. Lastly, the master problem and subproblem computation time of the sizing sub-stage are shown. Thanks to the fixed binary investment decision obtained in the siting sub-stage, the sizing sub-stage problem converges swiftly to the final investment solution in 25 Benders iterations.

5.10.3 Scalability Analysis Regarding Varying Investment Candidates

In this section, we analyze the computation time for solving a planning problem considering various candidates for ESS nodes and connections to a new node from the existing network. We tested the proposed planning framework on a 28-node benchmark distribution network [118]. We solved the planning problem for 16 cases accounting for the numbers of candidate nodes for ESS allocation and candidate connections to a new node ranging from 2 to 8 as shown in Table 5.9. The number of considered operating scenarios for each day type was 10, while the number of day types was 4. The local consumption and generation are considered fixed over the planning horizon. Fig. 5.7 illustrates the trend of computation times associated with the number of candidate nodes for ESS (indicated as 'ESSs #' in Table 5.9) and the number of candidates of new lines (indicated as 'New lines #' in Table 5.9), and it ranges from 1.18 hours to 29.50 hours. Regarding the given system, the computation time increases more rapidly with the increase of the number of new line candidates than the number of ESS candidates.

Table 5.9: Computation time (hours) with various number of candidates (28-node system).

New lines # \ ESSs #	2	4	6	8
2	1.18	1.84	2.25	2.92
4	2.13	2.96	3.75	6.86
6	7.05	10.83	14.02	14.69
8	8.09	11.15	19.13	29.50

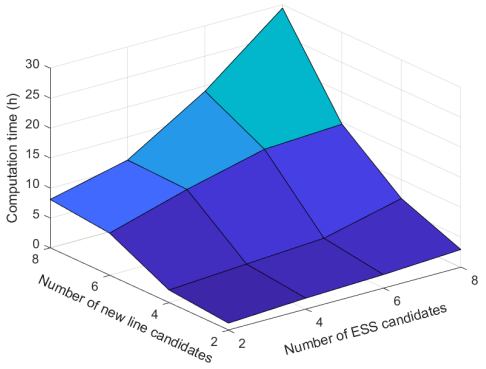

Figure 5.7: Computation time with different number of candidates.

5.10.4 Scalability Analysis Regarding Varying System Size

The planning methodology is also tested on distribution systems of different sizes ranging from 13 nodes to 123 nodes (13-node and 28-node systems are from [118], 55-node system is from [107], and 123-node IEEE benchmark system can be found in [108]). 5 candidate nodes for ESS allocation and the 4 candidate connections for a new node are considered, while the number of scenarios, day-types and the growth of prosumption is set to be the same as in the previous analysis. Table 5.10 reports the average computation time for the master problem and the subproblem for siting and sizing sub-stage problems. Note that only

the computation times for the 2nd block problems are reported in this table. It is observed that the subproblems (*i.e.*, operation problem) take most of the total computation time. Its computation time increases with the system size, suggesting that the subproblem size is determined by the number of constraints and variables varying with the system size. Solving the planning problem for the system with 28 nodes takes 1.8 times longer than the 13-node system. However, for 55-node system, it took a shorter computation time than for 28-node system despite the longer computation time for the subproblems thanks to the smaller number of Benders iterations. The lower average computation time to solve the master problem for the 55-node system implies a smaller number of accumulated Benders cuts in the master problem. On the other hand, the total computation time for solving the case of 123-node system was more than 20 times higher than the case of 55-node system, significantly exceeding the proportion of the subproblem computation time for 123-node system compared to the case of 55-node system. It suggests that the convergence speed of the proposed method depends not only on the size of the network, but also on how the Benders cuts pin down the solution space to identify the optimal solution. In fact, this optimal solution is affected mainly by the structure of the solution space which is subjected to the network's operation condition.

Table 5.10: Computation time (sec) of the 2nd block with respect to system size.

System size (Number of nodes)	Average siting MP	Average siting SP	Average sizing MP	Average sizing SP	Total
13	1.7	72.5	0.5	31.6	7579
28	1.3	74.8	1.3	158.9	13488
55	0.9	98.4	0.7	172.5	13299
123	7.2	816.7	2.1	425.0	297000

5.10.5 Statistical Analysis on Varying Number of Operating Scenarios

We analyzed the relationship between the number of operating scenarios and the trade-off between the computation time and the solution quality. Note that the operating scenario set considered for the planning problem is the outcome of K-medoids clustering technique (see Alg. A.1 in Sec. 5.10.1) applied to the initial scenario set. Therefore, the number of clusters (*i.e.*, operating scenarios to be used in the planning problem) determines how the reduced scenario subset can represent the stochastic characteristic of the initial scenario set. Fig. 5.8.(a) shows the cumulative distribution function (CDF) of the initial scenario set and different reduced scenario sets regarding the value of a single random variable (PV irradiation value at timestep 15, day-type 1, and year 1). It is obvious that the stochastic similarity between the reduced scenario set and the initial scenario set improves with the number of operating scenarios, as shown in Fig. 5.8.(a).

In this regard, it is worthwhile investigating a-posteriori the impact of the number of operating scenarios on the computation time and the optimal solution quality of the planning problem by observing the distribution of the objective values throughout the repetitive runs of planning exercises with the different number of operating scenarios. 100 runs of simulation are conducted for each case considering 10, 40, 70, and 100 reduced scenarios, respectively,

to observe the average computation time, the average expected objective value, and the normalized standard deviation as shown in Table 5.11. Fig. 5.8.(b) indicates the median of the objective values, and the 25% and 75% percentile of the objective value along with outliers (shown as red 'x's). The number of reduced scenarios 40 is obtained from the algorithm introduced in [103], which determines the number of reduced scenarios by evaluating the statistical similarities between the initial and reduced scenarios set. The reader can find the details about the algorithm in [103]. The 70 scenarios with and 100 scenarios are chosen as the reference cases to compare the solution quality with 10 and 40 scenarios cases.

All the metrics (*i.e.*, the average expected objective value, the normalized standard deviation values, and the range between 25-75% percentile) show a relatively small difference between the case with 40 scenarios and those with a larger number of scenarios in contrast to the significant gap in the average computation time between 40 scenarios case and other cases. The result demonstrates that 40 scenarios can yield an acceptable level of solution reliability while maintaining a reasonable computation time. Then, the solution's reliability in the case of 10 operating scenarios (which is used for the previous simulation exercises) is evaluated with reference to 40 scenarios. While the average computation time for 10 scenarios case is nearly a quarter of the time for solving 40 scenarios case, the average expected objective value difference is merely 0.3%. The difference in the average objective value of 10 scenarios case with other cases (40, 70, and 100 scenarios) is at a maximum of 2.6%, which is an acceptable magnitude of error considering the merit of 10 scenarios case in terms of significantly short computation time. However, the normalized standard deviation, and the 25-75% percentile interval remain larger compared to the other number of scenarios cases. In view of this, the modeler can choose to consider 40 scenarios to improve solution reliability in realistic planning practices, but at the cost of significantly higher computation time.

Table 5.11: Post analysis with respect to different number of scenarios (tested on 13-node system, 4 day-types, 24 timesteps, 2 ESS node candidates, 1 new line candidate).

Number of scenarios	Average Computation time (hr)	Average objective value	Normalized standard deviation
10	0.29	2124.7	0.0810
40	1.08	2130.6	0.0454
70	4.02	2180.6	0.0413
100	6.15	2158.7	0.0375

5.11 Conclusion

This chapter presents a DNEP tool for ADNs to achieve their dispatchability. The connections to the new nodes and line reinforcement are determined based on a proper evaluation of the network operation modeled by means of the AR-OPF model. ESSs are employed to compensate for the prosumption uncertainty such that the realized power flow at the GCP can track a day-ahead computed dispatch plan. The big M method is employed into the MAR-OPF model to selectively activate the operational constraints related to the change of

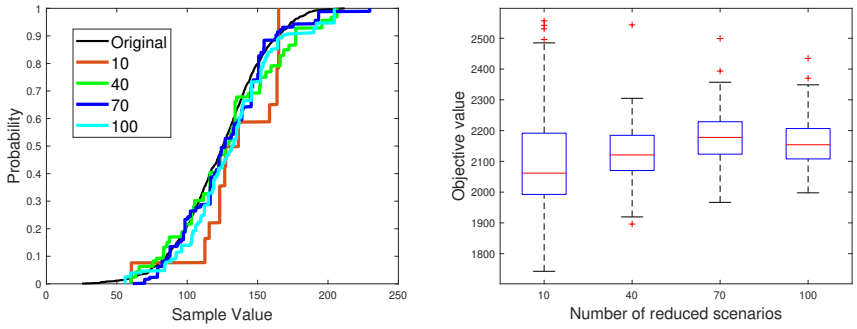

(a) (b)

Figure 5.8: (a) CDF of initial scenario set and reduced scenario sets with different number of reduced scenarios regarding the value of a single random variable (PV irradiation value at timestep 75, day-type 1, and year 1), (b) Boxplot of objective values of planning problem with different number of prosumption scenarios.

topology. Two solution approaches are proposed to solve the DNEP problem: the sequential approach (new nodes are added one by one according to the pre-defined priorities); and the simultaneous approach, (new nodes are added simultaneously by decision-making on the topology changes in distributed manner). The performance of the two approaches are compared through two test cases on a real Swiss ADN, in which 3 new nodes and 10 new nodes are added, respectively. The comparative analysis showed that the sequential approach is superior to the simultaneous one in terms of scalability, which stands as the main factor determining the practicability and serviceability of the proposed planning tool. In this regard, we tested the proposed sequential approach on a real Swiss ADN with 8 new nodes hosting in total 8MWp of new PV capacity. The results show that the DNEP strategy with the sequential approach can successfully determine the optimal level of dispatchability while securing the required hosting capacity of the ADN under increasing stochastic prosumption. Moreover, the extended computation time analysis for solving the planning problem indicates that the running time of the proposed method increases linearly with the number of the new nodes, avoiding a scalability issue associated with the size of network expansion. The scalability analysis on various candidates and different system sizes is also carried out to demonstrate that the proposed planning strategy can be applicable to distribution networks with generic sizes considering multiple investment options. The post-analysis of the planning problem's objective values with a different number of operating scenarios shows the trade-off between the computation time and the reliability of the planning solutions, providing helpful insight for choosing an operating scenario set to the modeler.

6 Conclusion

In this thesis, we proposed methodologies for optimal infrastructure planning of ADNs with particular reference to achieving their dispatchability by means of ESSs. In this respect, we focused on the following three main problems:

- Optimal allocation of ESSs aiming at achieving the ADN's dispatchability;
- Optimal co-planning of ESS allocation and line reinforcement;
- Optimal expansion planning incorporating ESS allocation and line reinforcement.

Optimal allocation of ESSs aiming at achieving ADN's dispatchability
First, two approaches for the optimal ESS allocation are proposed to achieve ADN's dispatchability. ESSs are employed to compensate for the uncertainty of the prosumption such that the realized power flow at the GCP can track a day-ahead computed dispatch plan.

The first planning method proposed in Chapter 2 accounts for the ESS control that integrates so-called offset profile into the dispatch plan. The offset profile quantifies the necessary power injection into each ESS to optimize its exploitation of energy reservoir capacity. The operational benefit of ESSs with this control strategy is evaluated through a daily operation of ADNs, which is modeled by a linear approximated convex OPF, or the PWL-OPF model. Then, the Benders decomposition is applied to handle the computational complexity of the planning problem. The effectiveness of the proposed method is validated through simulations conducted on a real Swiss ADN comprising 55 nodes and a large capacity of distributed renewable generation. The result underpins that the ESS allocation eliminates the dispatch error, and the dispatchability can be further enhanced with the integration of the ESS offset profile compared to the ESS planning approach without it.

Given the close coupling between operation and planning, the second planning strategy proposed in Chapter 3 puts emphasis on the use of an accurate ADN operation model to enhance the investment solution's quality and reliability. The non-approximated and convex OPF model, *i.e.*, the AR-OPF model, is implemented to account for the operational conditions of the distribution network. The integration of ADN's dispatchability necessitated a non-trivial

modification in the AR-OPF model, resulting in the modified AR-OPF or MAR-OPF model. Moreover, the planning problem was converted into two blocks to ensure the tightness of the operational solution obtained from the MAR-OPF model. In the 1st block, the allocation of ESSs is optimally determined along with the corresponding dispatchability level by implementing the linearly approximated OPF model. The MAR-OPF model is used in the 2nd block of the problem to check the compatibility of the allocated capacity for the real operation of the grid to satisfy the calculated dispatchability level and to determine the optimal location of the ESSs to minimize the grid losses. We validated the effectiveness of the proposed method for the real Swiss ADN by demonstrating that the allocation of ESSs successfully reduced the dispatch error. Moreover, the exactness of the optimal solution from the MAR-OPF model is assessed with respect to standard SOCP relaxed OPF model and the PWL-OPF model, showing the superiority of the MAR-OPF model in providing the exact evaluation of the system state. In this way, the MAR-OPF-based planning can guarantee reliable and optimal planning solutions for achieving ADN's dispatchability while ensuring the secure network operation.

Optimal co-planning of ESS allocation and line reinforcemt

In Chapter 4, the co-optimized planning strategy of ESSs and lines reinforcement for ADNs is proposed with particular reference to procurement of the sufficient ADN hosting capacity for increasing capacity of RERs while achieving ADN's dispatchability. The line reinforcement is considered to help satisfying the grid operational constraints. The line characteristics and the grid constraints associated with the line ampacity in the MAR-OPF model are adjusted with the change of line ampacity to reflect the impact of line reinforcement on the grid operation. The planning problem is reformulated such that the siting and sizing problems of ESSs and lines reinforcement are tackled sequentially by the Benders decomposition. We assessed the performance of the proposed method on the real Swiss ADN with substantial levels of installed PV capacity. The planning results under increasing load consumption and a large amount of distributed stochastic renewable generation demonstrate that the proposed co-optimization framework can successfully guarantee optimal ADN dispatchability while securing the proper hosting capacity. Then, the benefits associated to the separation of the siting and sizing in the planning problem of ESSs and lines reinforcement are numerically assessed by comparing the computation time and investment solution to the original planning problem. Thanks to the reformulation of the planning problem, the simulation results additionally showed that the proposed planning method is sufficiently scalable to be applied to networks of generic sizes.

Optimal expansion planning incorporating ESS allocation and line reinforcement

The final chapter is devoted to the development of a DNEP tool. Such a tool is based on the planning strategies presented in the previous chapters. The connections to the new nodes and line reinforcement are determined based on a proper evaluation of the network operation modeled by the MAR-OPF model. The big-M method is employed in the MAR-OPF model to selectively activate the power flow constraints depending on the choice of new lines. Two solution approaches are proposed to solve the DNEP problem: the sequential approach, where the new nodes are added one by one according to the pre-defined priorities; the simultaneous

approach, where the new nodes are added simultaneously, and the best topology including the new nodes are determined in a distributed manner. The two solution approaches have considerable differences in modifying the planning problem structure due to the ways they tackle the numerous binary variables. The comparative analysis of the two approaches showed that the sequential method is superior to the simultaneous method in terms of scalability, which is the main factor determining the practicability and serviceability of the proposed planning tool. Meanwhile, the cost result of the sequential approach showed a negligible sub-optimality compared to the simultaneous method. Moreover, the computation time analysis for solving the planning problem indicates that the running time of the proposed sequential method increases linearly with the number of new nodes, avoiding a scalability issue associated with the size of network expansion. The scalability analysis on various candidates and different system sizes are also carried out for the sequential method to demonstrate that the proposed planning strategy can be applied to distribution networks with generic sizes considering multiple investment options.

Future Works

In the continuation of this work, the following tasks are suggested for further investigation.

- We have developed the planning strategy for radial distribution networks. The planning strategy can be further developed to take into account meshed networks.
- In this thesis, the initial topology of ADNs is considered to be fixed. The line reconfiguration can be considered in the proposed planning tool to consider an effect of adaptive ADN topology on the investment solutions. [14]
- In this thesis, we considered the ESSs and lines investment as the investment options. The proposed procedure could be further extended to other resources such as DG units, and DR resources. Moreover, allocation of auxiliary assets such as on-load tap changers, capacitor banks can be considered for the support of system flexibility and reliability.
- In this thesis, the planning strategy is developed to achieve dispatchability of ADNs. The operational objective could be extended further to consider providing multiple flexibility services to TSOs, while taking into account the interactive TSO-DSO's coordination, such as providing ancillary services (ex., frequency control, voltage support, etc) to TSOs. The objective function should be modified to consider the DSO's revenues defined according to market rules. The operating constraints should include the contribution of ESSs to each service governed by ESSs control schemes designed to be compatible with each service's physical characteristics.
- In this thesis, the planning strategy is developed in the economic perspective of DSOs assuming static power market conditions. Dynamic interactions with power market and the market uncertainties can be incorporated into the planning strategy for ADNs.

[14] The additional feature can be straightforwardly included in the structure of proposed formulation, but it will increase the number of binary variables associated with line switching in the planning problem.

A Appendix

A.1 Scenario Generation

The operating scenarios for the planning problem are generated following the scenario generation algorithm described in Alg. A.1. First, we classified the historical load data at each node based on the season and weekdays/weekends, grouping them into different day-types representing seasonal variability of the prosumption. The mean and standard deviation values of the magnitude of prosumptions at each timestep are extracted from the consumption profiles classified in each day-type. A similar process is conducted for PV generation. The historic PV irradiation data is grouped by seasons and separated into sunny/cloudy days. With the extracted mean and standard deviation value of the load and PV irradiation, 1000 prosumption scenarios are generated with equal probabilities to model the prediction uncertainty based on the assumption that both the load and PV irradiation follow the normal distribution [30]. Then, the number of operating scenarios for each day-type is reduced by K-medoids clustering technique [71], selecting a subset of the initial scenario set.

It should be noted that the adopted scenario generation process has some limitations in modeling accurate prosumption profiles. Firstly, using representative day-types instead of complete 8760-hour operation profiles may not be enough to picture the total variation of the prosumption profiles over a year. Therefore, the number of day-types should be chosen carefully considering the trade-off between the computation burden and the accuracy of seasonal variability modeling. The criteria for categorizing day-types can largely affect the number of day-types as well as the reliability of the planning solution. Moreover, operating scenarios are modeled as discontinuous representative days. Therefore, continuous ESS operation over consecutive days is not modeled[15] Secondly, the prosumption scenarios are generated while the prosumption day-ahead prediction uncertainty is modeled as a uni-dimensional normal distribution. The user can, however, generate these scenarios according to other parametric or non-parametric prosumption models that may be available. Moreover, one can improve the quality of prosumption modeling by considering of temporal auto-correlation of prosumption uncertainty. Given that the ESS investment decisions are influenced by how accurately the

[15] Instead, the final SoE of each representative day is constrained to be 10% higher or lower than the initial SOE of each representative day to ensure the feasibility of consecutive day operation.

scenarios model the prosumption uncertainty, in practice, the modeler should have a reliable forecasting and scenario generation tool. It is finally worth pointing out that the modeling of prosumption uncertainty is beyond the scope of this paper.

Algorithm A.1 Scenario generation

1: Group the historical load data at each node based on seasons and weekdays/weekends
2: Calculate the mean and standard deviation value of the historical load profiles in each group
3: Group the historical solar irradiation data based on the seasons and sunny/cloudy days
4: Calculate the mean and standard deviation values of the historical solar irradiation profiles in each group
5: Generate 1000 prosumption scenarios (Φ_{dy}) assuming that the prosumption follows the normal distribution
6: Set the number of desired clusters (i.e., the number of reduced scenarios) for scenario reduction
7: Run the K-medoids clustering function
8: The members within each cluster are counted to calculate the probability set (λ_{Φ}) of the reduced scenario set
9: Save the medoids as the reduced scenario set Φ'_{dy}
10: **return** $\Phi'_{dy}, \lambda_{\Phi_{dy}}, d \in \mathscr{D}, y \in \mathscr{Y}$

A.1.1 Defining the Operating Scenario set: Discussion on the Decision on the Minimum Number of Scenarios to Represent the Uncertainty

The quality of a stochastic optimization solution highly depends on how much the scenarios in the subset can properly preserve the probabilistic properties of the original scenario set. There have been specific studies on the scenario reduction where the minimum number of reduced scenarios is usually identified a-posteriori by observing the converging trend of the objective value with different number of reduced scenarios (*e.g.* [119]). However, for the sake of simplicity, we adopted the algorithm shown in Alg. A.2 to a-priori obtain the minimum number of reduced scenarios that can approximate the distribution function of the uncertainty.

Each of the generated scenarios is expressed as vector defined as,

$$\boldsymbol{\nu}_{\phi} = \{\nu_{\phi}^{1}, ..., \nu_{\phi}^{H}\}, \forall \phi \in \Phi_{dy}, \qquad \text{where } H = \sum_{l \in \mathscr{L}} (T^{AL(l)} + T^{RL(l)} + T^{PV}). \tag{A.1}$$

where $T^{AL(l)}$, $T^{RL(l)}$, and T^{PV} are the time duration of the daily active, reactive load at node l, and PV irradiation profiles, respectively.

Firstly, we construct a CDF for each random variable $\boldsymbol{\nu}^{h}$ ($h \in \{1, ..., H\} = \mathscr{H}$) with scenario

set Φ_{dy}, which is given by,

$$y_{\phi}^{h} = cdf(v_{\phi}^{h}) = P(\boldsymbol{v}^{h} \leq v_{\phi}^{h}), \forall \phi \in \Phi_{dy}, h \in \{1, ..., H\} = \mathscr{H}, \tag{A.2}$$

and its inverse function is given by,

$$cdf^{-1}(y_{\phi}^{h}), y_{\phi}^{h} \in [0, 1]. \tag{A.3}$$

The objective of the algorithm is to find the minimal number of reduced scenarios such that the average distance between the CDF of the initial scenario set and that of the reduced scenario set over number of check points becomes smaller than a given tolerance. We define the check points for calculating the distance between the CDF curve of scenario set Φ_{dy} with another CDF curve as,

$$cdf^{-1}(y_{\Phi_{dy}}(q)), y_{\Phi_{dy}}(q) \in [0, 1], \forall q \in \{1, ..., N_q\}. \tag{A.4}$$

For instance, we can set $N_q = 5$, with quantile ranging $[0.05, 0.95]$. The scenario reduction process is initialized by applying K-Medoids clustering method [71] based on the Euclidean distance between each scenario pairs to reduce the original scenario set into set Φ'_{dy} with a single representative scenario. The average distance between CDFs of different scenario set Φ_{dy} and Φ'_{dy} is calculated by index defined by

$$\Delta = \sum_{q} \omega_q \sqrt{\frac{1}{H} \sum_{h} \left(\frac{cdf^{-1}(y_{\Phi_{dy}}^{h}(q)) - cdf^{-1}(y_{\Phi'_{dy}}^{h}(q))}{cdf^{-1}(y_{\Phi_{dy}}^{h}(q))} \right)^2}. \tag{A.5}$$

where ω_q is the weight coefficient assigned to qth check point. As the distance is bigger than a threshold value, the scenario reduction is re-applied to produce a scenario set with incremented number of scenarios than the previous iteration. Fig. A.1 shows a CDF of original scenario set with the CDFs of different reduced scenario sets regarding a single random variable. The proposed algorithm determines that the minimum number of scenarios required is 39. Then, the generated 39 scenarios and probability value that corresponds to each scenario become the set of operating scenarios and probabilities fed into the dispatching problem. Fig. A.1 shows the evolution of Δ w.r.t the number of reduced scenarios.

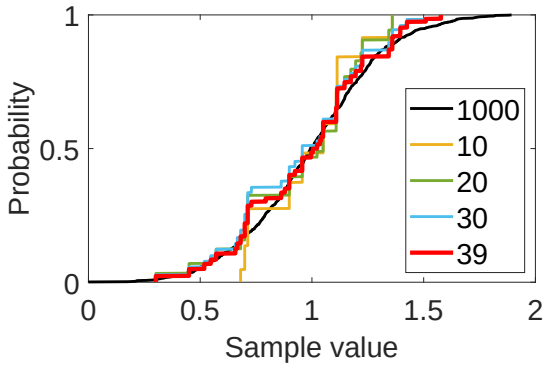

(a)

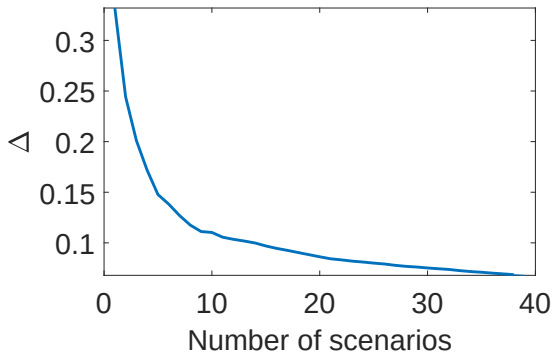

(b)

Figure A.1: (a) CDF of initial scenario set and reduced scenario sets with different number of reduced scenarios, (b) Average of normalized distance between initial and reduced scenario sets with different number of reduced scenarios

Algorithm A.2 Scenario reduction

1: Generate $N_{\Phi_{dy}}$ scenarios for $\boldsymbol{\nu}$
2: Draw CDF graphs of $\boldsymbol{\nu}^h, \forall h \in \mathscr{H}$ with scenario set Φ_{dy}
3: **Initialization:** $N_{\Phi'_{dy}} = 0, \Delta = \infty$
4: **while** $|\Delta| \geq tolerance$ **do**
5: $N_{\Phi'_{dy}} \leftarrow N_{\Phi'_{dy}} + 1$
6: Obtain $N_{\Phi'_{dy}}$ scenarios for $\boldsymbol{\nu}$ via K-medoids clustering
7: Draw CDF graphs of $\boldsymbol{\nu}^h, \forall h \in \mathscr{H}$ with scenario set Φ'_{dy}
8: Compute Δ between the two CDFs of set Φ_{dy} and Φ'_{dy}
9: **end while**
10: **return** $N_{\Phi'_{dy}}, \boldsymbol{\nu}_{\phi'}, \forall \phi' \in \Phi'_{dy}$

A.2 Benders Decomposition

The Benders decomposition is a method for breaking down certain kind of large-scale optimization problems. It decomposes the main problem into small sub-problems with less number of variables. Since solving the complete problem with large number of variables and constraint requires very high computational power, splitting the problem into multiple smaller problems helps to make it solvable. The Benders decomposition is well described in [120, 121] and briefly described here:

Lets consider the following optimization problem:

$$\arg\min_{x,y} \; c^T x + \sum_{s\in\Omega} a_s^T y_s \tag{A.6a}$$

subject to:

$$Fy_s = g - T_s x \qquad \forall s \in \Omega, \tag{A.6b}$$

$$c(x) \leq 0, \tag{A.6c}$$

$$d(y_s) \leq 0 \qquad \forall s \in \Omega. \tag{A.6d}$$

Above problem can be decomposed by using Benders decomposition into following problems:

A.2.1 Master problem

The master problem can be expressed as

$$\arg\min_{x,\mathcal{Z}} \; \zeta^{(n)} = c^T x + \sum_{s\in\Omega} \mathcal{Z}_s \tag{A.7a}$$

subject to:

$$c(x) \leq 0, \tag{A.7b}$$

$$\mathcal{Z}_s \geq A_s^{(k)*} - \alpha_s^{(k)}(x - x^{(k)*}). \tag{A.7c}$$

A.2.2 Sub-problems

The set of subproblems are defined for each scenario set $s \in \Omega$,

$$\arg\min_{y_s} A_s^{(n)} = a_s^T y_s \tag{A.8a}$$

subject to:

$$Fy_s = g - T_s x^{(n-1)*}, \tag{A.8b}$$

$$d(y_s) \leq 0, \tag{A.8c}$$

$$x = x^{(n-1)*} : \alpha_s^{(n)}. \tag{A.8d}$$

where $\alpha_s^{(n)}$ represent the dual constraints of constraint Eq. (A.8d).

The algorithm of the Benders decomposition is progressed following the steps described below.

Algorithm A.3 Benders decomposition algorithm

1: **Initialization :** $n \leftarrow 0$
2: Solve master problem to find the optimal solution $x^{(n)*}$
3: $LB \leftarrow \zeta^{(n)*}$
4: Feed the solution $x^{(n)*}$ to subproblems
5: Solve parallel subproblems to find the optimal solution $y_s^{(n)*}$
6: $UB \leftarrow c^T x^{(n)*} + \sum_{s\in\Omega} A_s^{(n)*}$
7: Update the dual values ($\alpha_s^{(n)}$)
8: **if** $|UB - LB| \leq \epsilon$ **then**
9: **return** $x^{(n)*}, y^{(n)*}$
10: **else**
11: $n \leftarrow n + 1$
12: Update Benders cut with dual values
13: Go to step 2
14: **end if**

As shown in the above algorithm, the convergence of Benders decomposition is given by |UB - LB| $\leq \epsilon$, where

$$\text{LB} = \zeta^{(n)}, \tag{A.9a}$$

$$\text{UB} = c^T x^{(n)*} + \sum_{s\in\Omega} A_s^{(n)*}. \tag{A.9b}$$

For further details we refer the interested reader to [120].

Bibliography

[1] M. Nick, R. Cherkaoui, J. L. Boudec, and M. Paolone, "An exact convex formulation of the optimal power flow in radial distribution networks including transverse components," *IEEE Trans. Autom. Control*, vol. 63, no. 3, pp. 682–697, March 2018.

[2] E. Stai, L. Reyes-Chamorro, F. Sossan, J.-Y. Le Boudec, and M. Paolone, "Dispatching stochastic heterogeneous resources accounting for grid and battery losses," *IEEE Transactions on Smart Grid*, vol. 9, no. 6, pp. 6522–6539, 2017.

[3] F. Pilo, S. Jupe, F. Silvestro, K. El Bakari, C. Abbey, G. Celli, J. Taylor, A. Baitch, and C. Carter-Brown, "Planning and optimisation of active distribution systems-an overview of cigre working group c6. 19 activities," 2012.

[4] M. Paolone, "Editorial," *Sustainable Energy, Grids and Networks*, vol. 1, pp. A1–A3, 2015. [Online]. Available: https://www.sciencedirect.com/science/article/pii/S2352467715000089

[5] N. Hatziargyriou, J. Amantegui, B. Andersen, M. Armstrong, P. Boss, B. Dalle, G. DeMontravel, A. Negri, C. A. Nucci, and P. Southwell, "Cigre wg "network of the future" electricity supply systems of the future," *ELECTRA*, vol. No 256, pp. 42–49, 06 2011.

[6] C. Abbey, A. Baitch, B. Bak-Jensen, C. Carter, G. Celli, K. El Bakari, M. Fan, P. Georgilakis, T. Hearne, L. N. Ochoa *et al.*, *Planning and optimization methods for active distribution systems*. CIGRE, 2014.

[7] H. Laaksonen, H. Khajeh, C. Parthasarathy, M. Shafie-khah, and N. Hatziargyriou, "Towards flexible distribution systems: Future adaptive management schemes," *Applied Sciences*, vol. 11, no. 8, p. 3709, 2021.

[8] G. Celli *et al.*, "A comparison of distribution network planning solutions: Traditional reinforcement versus integration of distributed energy storage," in *2013 IEEE Grenoble Conference*. IEEE, 2013, pp. 1–6.

[9] R. Li, W. Wang, Z. Chen, J. Jiang, and W. Zhang, "A review of optimal planning active distribution system: Models, methods, and future researches," *Energies*, vol. 10, no. 11, p. 1715, 2017.

[10] P. Gao, H. Chen, X. Zheng, and B. Wu, "Framework planning of active distribution network considering active management," *The Journal of Engineering*, vol. 2017, no. 13, pp. 2093–2097, 2017.

[11] M. Kabirifar, M. Fotuhi-Firuzabad, M. Moeini-Aghtaie, and N. Pourghaderia, "Joint distributed generation and active distribution network expansion planning considering active management of network," in *2019 27th Iranian Conference on Electrical Engineering (ICEE)*. IEEE, 2019, pp. 702–708.

[12] X. Xu, D. Niu, L. Peng, S. Zheng, and J. Qiu, "Hierarchical multi-objective optimal planning model of active distribution network considering distributed generation and demand-side response," *Sustainable Energy Technologies and Assessments*, vol. 53, p. 102438, 2022.

[13] Y. Xiang, J. Liu, F. Li, Y. Liu, Y. Liu, R. Xu, Y. Su, and L. Ding, "Optimal active distribution network planning: a review," *Electric Power Components and Systems*, vol. 44, no. 10, pp. 1075–1094, 2016.

[14] M. Nick, R. Cherkaoui, and M. Paolone, "Optimal planning of distributed energy storage systems in active distribution networks embedding grid reconfiguration," *IEEE Trans. Power Syst.*, vol. 33, no. 2, pp. 1577–1590, March 2018.

[15] S. Zhang, H. Cheng, D. Wang, L. Zhang, F. Li, and L. Yao, "Distributed generation planning in active distribution network considering demand side management and network reconfiguration," *Applied Energy*, vol. 228, pp. 1921–1936, 2018.

[16] A. Piccolo and P. Siano, "Evaluating the impact of network investment deferral on distributed generation expansion," *IEEE Transactions on Power Systems*, vol. 24, no. 3, pp. 1559–1567, 2009.

[17] V. Mendez, J. Rivier, J. De La Fuente, T. Gomez, J. Arceluz, J. Marin, and A. Madurga, "Impact of distributed generation on distribution investment deferral," *International Journal of Electrical Power & Energy Systems*, vol. 28, no. 4, pp. 244–252, 2006.

[18] M. Esmaili, E. C. Firozjaee, and H. A. Shayanfar, "Optimal placement of distributed generations considering voltage stability and power losses with observing voltage-related constraints," *Applied energy*, vol. 113, pp. 1252–1260, 2014.

[19] S. F. Santos, D. Z. Fitiwi, A. W. Bizuayehu, M. Shafie-Khah, M. Asensio, J. Contreras, C. M. Cabrita, and J. P. Catalao, "Impacts of operational variability and uncertainty on distributed generation investment planning: A comprehensive sensitivity analysis," *IEEE Transactions on Sustainable Energy*, vol. 8, no. 2, pp. 855–869, 2016.

[20] A. S. Awad, T. H. El-Fouly, and M. M. Salama, "Optimal ess allocation for load management application," *IEEE Transactions on Power systems*, vol. 30, no. 1, pp. 327–336, 2014.

[21] A. Giannitrapani, S. Paoletti, A. Vicino, and D. Zarrilli, "Optimal allocation of energy storage systems for voltage control in lv distribution networks," *IEEE Transactions on Smart Grid*, vol. 8, no. 6, pp. 2859–2870, 2016.

[22] C. K. Das, O. Bass, T. S. Mahmoud, G. Kothapalli, N. Mousavi, D. Habibi, and M. A. Masoum, "Optimal allocation of distributed energy storage systems to improve performance and power quality of distribution networks," *Applied Energy*, vol. 252, p. 113468, 2019.

[23] E. Dehnavi, F. Aminifar, and S. Afsharnia, "Congestion management through distributed generations and energy storage systems," *International Transactions on Electrical Energy Systems*, vol. 29, no. 6, p. e12018, 2019.

[24] B. Jeddi, V. Vahidinasab, P. Ramezanpour, J. Aghaei, M. Shafie-khah, and J. P. Catalão, "Robust optimization framework for dynamic distributed energy resources planning in distribution networks," *International Journal of Electrical Power & Energy Systems*, vol. 110, pp. 419–433, 2019.

[25] N. J. Cutler, N. D. Boerema, I. F. MacGill, and H. R. Outhred, "High penetration wind generation impacts on spot prices in the australian national electricity market," *Energy Policy*, vol. 39, no. 10, pp. 5939–5949, 2011.

[26] E. Ela, M. Milligan, A. Bloom, A. Botterud, A. Townsend, and T. Levin, "Evolution of wholesale electricity market design with increasing levels of renewable generation," National Renewable Energy Lab.(NREL), Golden, CO (United States), Tech. Rep., 2014.

[27] H. Holttinen, A. Tuohy, M. Milligan, E. Lannoye, V. Silva, S. Müller, L. Sö *et al.*, "The flexibility workout: managing variable resources and assessing the need for power system modification," *IEEE Power and Energy Magazine*, vol. 11, no. 6, pp. 53–62, 2013.

[28] G. Koeppel and M. Korpås, "Improving the network infeed accuracy of non-dispatchable generators with energy storage devices," *Electr. Pow. Syst. Res.*, vol. 78, no. 12, pp. 2024–2036, 2008.

[29] T. Boutsika and S. Santoso, "Sizing an energy storage system to minimize wind power imbalances from the hourly average," in *2012 IEEE Power and Energy Society General Meeting*. IEEE, 2012, pp. 1–8.

[30] F. Sossan, E. Namor, R. Cherkaoui, and M. Paolone, "Achieving the dispatchability of distribution feeders through prosumers data driven forecasting and model predictive control of electrochemical storage," *IEEE Trans. Sustain. Energy*, vol. 7, no. 4, pp. 1762–1777, Oct 2016.

[31] M. Bozorg, F. Sossan, J.-Y. Le Boudec, and M. Paolone, "Influencing the bulk power system reserve by dispatching power distribution networks using local energy storage," *Electr. Power Syst. Res.*, vol. 163, pp. 270–279, 2018.

[32] R. R. Appino, J. Á. G. Ordiano, R. Mikut, T. Faulwasser, and V. Hagenmeyer, "On the use of probabilistic forecasts in scheduling of renewable energy sources coupled to storages," *Applied energy*, vol. 210, pp. 1207–1218, 2018.

[33] S. Lavrijssen, A.-A. Marhold, and A. Trias, "The changing world of the dso in a smart energy system environment: Key issues and policy recommendations," *TILEC Discussion Paper*, no. 2018-015, pp. 1–98, 2016.

[34] S. Kim, M. Pollitt, Y. Jin, J. Kim, and Y. Yoon, "Contractual framework for the devolution of system balancing responsibility from the transmission system operator to distribution system operators," *EPRG Working Paper*, no. 1715, 2017.

[35] Y. V. Makarov, P. Du, M. C. Kintner-Meyer, C. Jin, and H. F. Illian, "Sizing energy storage to accommodate high penetration of variable energy resources," *IEEE Transactions on sustainable Energy*, vol. 3, no. 1, pp. 34–40, 2011.

[36] H.-I. Su and A. El Gamal, "Modeling and analysis of the role of energy storage for renewable integration: Power balancing," *IEEE Transactions on Power Systems*, vol. 28, no. 4, pp. 4109–4117, 2013.

[37] A. ENTSO-E, "Entso-e network code on electricity balancing," 2014.

[38] "Directive (eu) 2019/944 of the european parliament and of the council of 5 june 2019 on common rules for the internal market for electricity and amending directive 2012/27/eu," *Official Journal of the European Union L 158*, vol. 62, pp. 125–199, 2019.

[39] S. Ugarte, J. Larkin, B. Van der Ree, V. Swinkels, M. Voog, N. Friedichsen, J. Michaels, A. Thielmann, M. Wietschel, and R. Villafafila, "Energy storage: Which market designs and regulatory incentives are needed?" *Eur. Parliament Committee Ind., Res. Energy, Brussels, Belgium*, pp. 1–5, 2015.

[40] E. Perez, H. Beltran, N. Aparicio, and P. Rodriguez, "Predictive power control for pv plants with energy storage," *IEEE Trans. Sustain. Energy*, vol. 4, no. 2, pp. 482–490, April 2013.

[41] J. P. Chaves-Ávila, R. A. Hakvoort, and A. Ramos, "The impact of european balancing rules on wind power economics and on short-term bidding strategies," *Energy Policy*, vol. 68, pp. 383–393, 2014.

[42] R. R. Appino, J. Á. G. Ordiano, R. Mikut, T. Faulwasser, and V. Hagenmeyer, "On the use of probabilistic forecasts in scheduling of renewable energy sources coupled to storages," *Applied energy*, vol. 210, pp. 1207–1218, 2018.

[43] E. Stai, L. Reyes-Chamorro, F. Sossan, J. Le Boudec, and M. Paolone, "Dispatching stochastic heterogeneous resources accounting for grid and battery losses," *IEEE Trans. Smart Grid*, vol. 9, no. 6, pp. 6522–6539, Nov 2018.

[44] R. S. Go, F. D. Munoz, and J.-P. Watson, "Assessing the economic value of co-optimized grid-scale energy storage investments in supporting high renewable portfolio standards," *Applied energy*, vol. 183, pp. 902–913, 2016.

[45] S. Dehghan and N. Amjady, "Robust transmission and energy storage expansion planning in wind farm-integrated power systems considering transmission switching," *IEEE Trans. Sustain. Energy*, vol. 7, no. 2, pp. 765–774, April 2016.

[46] M. Kalantar-Neyestanaki, M. Bozorg, F. Sossan, and R. Cherkaoui, "Allocation of frequency control reserve from aggregated resources of active distribution systems," in *2018 Power Systems Computation Conference (PSCC)*, June 2018, pp. 1–8.

[47] H. Doagou-Mojarrad, G. Gharehpetian, H. Rastegar, and J. Olamaei, "Optimal placement and sizing of dg (distributed generation) units in distribution networks by novel hybrid evolutionary algorithm," *Energy*, vol. 54, pp. 129–138, 2013.

[48] J. Xiao, Z. Zhang, L. Bai, and H. Liang, "Determination of the optimal installation site and capacity of battery energy storage system in distribution network integrated with distributed generation," *IET Gener. Transm. Distrib.*, vol. 10, no. 3, pp. 601–607, 2016.

[49] Q. Li, R. Ayyanar, and V. Vittal, "Convex optimization for des planning and operation in radial distribution systems with high penetration of photovoltaic resources," *IEEE Trans. Sustain. Energy*, vol. 7, no. 3, pp. 985–995, 2016.

[50] M. Nick, M. Hohmann, R. Cherkaoui, and M. Paolone, "On the optimal placement of distributed storage systems for voltage control in active distribution networks," in *2012 3rd IEEE PES Innov. Smart Grid Technol. Eur.* IEEE, 2012, pp. 1–6.

[51] G. Carpinelli *et al.*, "A hybrid method for optimal siting and sizing of battery energy storage systems in unbalanced low voltage microgrids," *Applied Sciences*, vol. 8, no. 3, p. 455, 2018.

[52] E. Grover-Silva, R. Girard, and G. Kariniotakis, "Optimal sizing and placement of distribution grid connected battery systems through an socp optimal power flow algorithm," *Applied Energy*, vol. 219, pp. 385–393, 2018.

[53] M. Qin *et al.*, "Optimal planning and operation of energy storage systems in radial networks for wind power integration with reserve support," *IET Gener. Transm. Distrib.*, vol. 10, no. 8, pp. 2019–2025, 2016.

[54] Y. Zheng, Z. Y. Dong, F. J. Luo, K. Meng, J. Qiu, and K. P. Wong, "Optimal allocation of energy storage system for risk mitigation of discos with high renewable penetrations," *IEEE Trans. Power Syst.*, vol. 29, no. 1, pp. 212–220, Jan 2014.

[55] P. Fortenbacher, A. Ulbig, and G. Andersson, "Optimal placement and sizing of distributed battery storage in low voltage grids using receding horizon control strategies," *IEEE Transactions on Power Systems*, vol. 33, no. 3, pp. 2383–2394, 2018.

[56] K. Baker, G. Hug, and X. Li, "Energy storage sizing taking into account forecast uncertainties and receding horizon operation," *IEEE Trans. Sustain. Energy*, vol. 8, no. 1, pp. 331–340, Jan 2017.

[57] M. Cao, Q. Xu, J. Cai, and B. Yang, "Optimal sizing strategy for energy storage system considering correlated forecast uncertainties of dispatchable resources," *Int. J. Elec. Power*, vol. 108, pp. 336–346, 2019.

[58] P. Pinson, G. Papaefthymiou, B. Klockl, and J. Verboomen, "Dynamic sizing of energy storage for hedging wind power forecast uncertainty," in *2009 IEEE Power & Energy Society General Meeting*. IEEE, 2009, pp. 1–8.

[59] H. Bludszuweit and J. A. Domínguez-Navarro, "A probabilistic method for energy storage sizing based on wind power forecast uncertainty," *IEEE Transactions on Power Systems*, vol. 26, no. 3, pp. 1651–1658, 2010.

[60] Q. Li, S. S. Choi, Y. Yuan, and D. Yao, "On the determination of battery energy storage capacity and short-term power dispatch of a wind farm," *IEEE Trans on Sustain. Energy*, vol. 2, no. 2, pp. 148–158, April 2011.

[61] X. Ke, N. Lu, and C. Jin, "Control and size energy storage systems for managing energy imbalance of variable generation resources," *IEEE Transactions on Sustainable Energy*, vol. 6, no. 1, pp. 70–78, 2014.

[62] Y. Zheng, J. Zhao, Y. Song, F. Luo, K. Meng, J. Qiu, and D. J. Hill, "Optimal operation of battery energy storage system considering distribution system uncertainty," *IEEE Transactions on Sustainable Energy*, vol. 9, no. 3, pp. 1051–1060, 2017.

[63] J. Qiu, Z. Xu, Y. Zheng, D. Wang, and Z. Y. Dong, "Distributed generation and energy storage system planning for a distribution system operator," *IET Renewable Power Generation*, vol. 12, no. 12, pp. 1345–1353, 2018.

[64] Y. Zheng, D. J. Hill, and Z. Y. Dong, "Multi-agent optimal allocation of energy storage systems in distribution systems," *IEEE Trans on Sustain. Energy*, vol. 8, no. 4, pp. 1715–1725, 2017.

[65] H. Haghighat and B. Zeng, "Stochastic and chance-constrained conic distribution system expansion planning using bilinear benders decomposition," *IEEE Trans. Power Syst.*, vol. 33, no. 3, pp. 2696–2705, 2017.

[66] A. M. Geoffrion, "Generalized benders decomposition," *J. Optimiz. Theory App.*, vol. 10, no. 4, pp. 237–260, 1972.

[67] J. F. Franco, M. J. Rider, M. Lavorato, and R. Romero, "Optimal conductor size selection and reconductoring in radial distribution systems using a mixed-integer lp approach," *IEEE Trans. Power Syst.*, vol. 28, no. 1, pp. 10–20, Feb 2013.

[68] M. Shafie-Khah, P. Siano, D. Z. Fitiwi, N. Mahmoudi, and J. P. S. Catalão, "An innovative two-level model for electric vehicle parking lots in distribution systems with renewable energy," *IEEE Trans. Smart Grid*, vol. 9, no. 2, pp. 1506–1520, March 2018.

[69] P. L. Cavalcante, J. C. López, J. F. Franco, M. J. Rider, A. V. Garcia, M. R. R. Malveira, L. L. Martins, and L. C. M. Direito, "Centralized self-healing scheme for electrical distribution systems," *IEEE Trans. Smart Grid*, vol. 7, no. 1, pp. 145–155, Jan 2016.

[70] E. Namor, D. Torregrossa, F. Sossan, R. Cherkaoui, and M. Paolone, "Assessment of battery ageing and implementation of an ageing aware control strategy for a load leveling application of a lithium titanate battery energy storage system," in *2016 IEEE 17th Workshop on COMPEL*. Ieee, 2016, pp. 1–6.

[71] A. K. Jain, R. C. Dubes *et al.*, *Algorithms for clustering data*. Prentice hall Englewood Cliffs, NJ, 1988, vol. 6.

[72] J. Abrell, "The swiss wholesale electricity market," *tech. rep., wiss Competence Center for Energy Research*, 2016.

[73] C. A. Sepulveda Rangel, L. N. Canha, M. Sperandio, and V. Miranda, "Mixed-integer stochastic evaluation of battery energy storage system integration strategies in distribution systems," *IET Generation, Transmission & Distribution*, vol. 16, no. 4, pp. 641–655, 2022.

[74] R. Gupta, F. Sossan, and M. Paolone, "Performance assessment of linearized opf-based distributed real-time predictive control," in *2019 IEEE Milan PowerTech*, June 2019, pp. 1–6.

[75] R. A. Jabr, "High order approximate power flow solutions and circular arithmetic applications," *IEEE Trans. Power Syst.*, pp. 1–1, 2019.

[76] X. Shen, M. Shahidehpour *et al.*, "Expansion planning of active distribution networks with centralized and distributed energy storage systems," *IEEE Trans. Sustainable Enery*, vol. 8, no. 1, pp. 126–134, 2016.

[77] M. Asensio *et al.*, "Joint distribution network and renewable energy expansion planning considering demand response and energy storage—part i: Stochastic programming model," *IEEE Trans. on Smart Grid*, vol. 9, no. 2, pp. 655–666, 2016.

[78] P. M. de Quevedo, G. Munoz-Delgado, and J. Contreras, "Impact of electric vehicles on the expansion planning of distribution systems considering renewable energy, storage, and charging stations," *IEEE Trans. on Smart Grid*, vol. 10, no. 1, pp. 794–804, 2017.

[79] B. Canizes *et al.*, "Optimal expansion planning considering storage investment and seasonal effect of demand and renewable generation," *Renewable Energy*, vol. 138, pp. 937–954, 2019.

[80] M. Bucciarelli, S. Paoletti, and A. Vicino, "Optimal sizing of energy storage systems under uncertain demand and generation," *Applied Energy*, vol. 225, pp. 611–621, 2018.

[81] M. Nick, R. Cherkaoui, and M. Paolone, "Optimal allocation of dispersed energy storage systems in active distribution networks for energy balance and grid support," *IEEE Transs on Power Syst.*, vol. 29, no. 5, pp. 2300–2310, Sep. 2014.

[82] R. A. Jabr, "Radial distribution load flow using conic programming," *IEEE Trans. Power Syst.*, vol. 21, no. 3, pp. 1458–1459, 2006.

[83] K. Christakou, D.-C. Tomozei, J.-Y. L. Boudec, and M. Paolone, "Ac opf in radial distribution networks – part i: On the limits of the branch flow convexification and the alternating direction method of multipliers," *Electr. Pow. Syst. Res.*, vol. 143, pp. 438 – 450, 2017.

[84] S. Abdelouadoud, R. Girard, F.-P. Neirac, and T. Guiot, "Optimal power flow of a distribution system based on increasingly tight cutting planes added to a second order cone relaxation," *International Journal of Electrical Power & Energy Systems*, vol. 69, pp. 9–17, 2015.

[85] Z. Yuan, "On the tightness of convex optimal power flow model based on power loss relaxation," in *2021 IEEE PES Innovative Smart Grid Technologies Europe (ISGT Europe)*, 2021, pp. 1–5.

[86] M. Baran and F. F. Wu, "Optimal sizing of capacitors placed on a radial distribution system," *IEEE Transactions on power Delivery*, vol. 4, no. 1, pp. 735–743, 1989.

[87] (2020) The prices for balance energy in swissgrid. [Online]. Available: https://www.swissgrid.ch/en/home/customers/topics/bgm/balance-energy.html

[88] R. C. Lotero and J. Contreras, "Distribution system planning with reliability," *IEEE Trans. Power Del.*, vol. 26, no. 4, pp. 2552–2562, 2011.

[89] J. F. Franco, M. J. Rider, M. Lavorato, and R. Romero, "Optimal conductor size selection and reconductoring in radial distribution systems using a mixed-integer lp approach," *IEEE Trans. Power Syst.*, vol. 28, no. 1, pp. 10–20, 2012.

[90] G. Munoz-Delgado, J. Contreras, and J. M. Arroyo, "Distribution network expansion planning with an explicit formulation for reliability assessment," *IEEE Trans. Power Syst.*, vol. 33, no. 3, pp. 2583–2596, 2017.

[91] K. El Bakari, C. Carter-Brown, S. Jupe, A. Baitch, C. Abbey, A. R. Aoki, M. Fan, C. Nakazawa, and F. Pilo, "Survey on methods and tools for planning of'active'distribution networks," 2012.

[92] S. R. Gampa, S. Makkena, P. Goli, and D. Das, "Fpa pareto optimality-based multiobjective approach for capacitor placement and reconductoring of urban distribution systems with solar dg units," *International Journal of Ambient Energy*, pp. 1–17, 2020.

[93] N. C. Koutsoukis, P. S. Georgilakis, and N. D. Hatziargyriou, "Multistage coordinated planning of active distribution networks," *IEEE Trans. Power Syst.*, vol. 33, no. 1, pp. 32–44, 2017.

[94] A. Tabares, J. F. Franco, M. Lavorato, and M. J. Rider, "Multistage long-term expansion planning of electrical distribution systems considering multiple alternatives," *IEEE Trans. Power Syst.*, vol. 31, no. 3, 2015.

[95] J. M. H. Ortiz, M. Pourakbari-Kasmaei, J. López, and J. R. S. Mantovani, "A stochastic mixed-integer conic programming model for distribution system expansion planning considering wind generation," *Energy Systems*, vol. 9, no. 3, pp. 551–571, 2018.

[96] I. Ziari, G. Ledwich, A. Ghosh, and G. Platt, "Optimal distribution network reinforcement considering load growth, line loss, and reliability," *IEEE Trans. Power Syst.*, vol. 28, no. 2, pp. 587–597, 2012.

[97] M. E. Samper and A. Vargas, "Investment decisions in distribution networks under uncertainty with distributed generation—part i: Model formulation," *IEEE Trans. Power Syst.*, vol. 28, no. 3, pp. 2331–2340, 2013.

[98] G. Muñoz-Delgado *et al.*, "Multistage generation and network expansion planning in distribution systems considering uncertainty and reliability," *IEEE Trans. Power Syst.*, vol. 31, no. 5, pp. 3715–3728, 2015.

[99] X. Shen, M. Shahidehpour *et al.*, "Multi-stage planning of active distribution networks considering the co-optimization of operation strategies," *IEEE Trans. on Smart Grid*, vol. 9, no. 2, 2016.

[100] J. M. Home-Ortiz, O. D. Melgar-Dominguez, M. Pourakbari-Kasmaei, and J. R. S. Mantovani, "A stochastic mixed-integer convex programming model for long-term distribution system expansion planning considering greenhouse gas emission mitigation," *International Journal of Electrical Power & Energy Systems*, vol. 108, pp. 86–95, 2019.

[101] D. M. Greenwood, N. S. Wade, P. C. Taylor, P. Papadopoulos, and N. Heyward, "A probabilistic method combining electrical energy storage and real-time thermal ratings to defer network reinforcement," *IEEE Trans. Sustain. Energy*, vol. 8, no. 1, pp. 374–384, 2016.

[102] H. Saboori, R. Hemmati, and V. Abbasi, "Multistage distribution network expansion planning considering the emerging energy storage systems," *Energy Convers. Manag.*, vol. 105, pp. 938–945, 2015.

[103] J. H. Yi, R. Cherkaoui, and M. Paolone, "Optimal allocation of esss in active distribution networks to achieve their dispatchability," *IEEE Trans. Power Syst.*, 2020.

[104] Z. Zhao and J. Mutale, "Optimal conductor size selection in distribution networks with high penetration of distributed generation using adaptive genetic algorithm," *Energies*, vol. 12, no. 11, p. 2065, 2019.

[105] S. A. Fenrick *et al.*, "Cost and reliability comparisons of underground and overhead power lines," *Utilities Policy*, vol. 20, no. 1, 2012.

[106] Z. Zhu, S. Lu, B. Gao, T. Yi, and B. Chen, "Life cycle cost analysis of three types of power lines in 10 kv distribution network," *Inventions*, vol. 1, no. 4, p. 20, 2016.

[107] J. H. Yi. (2022) 55nodes-swiss-distribution-grid. [Online]. Available: https://github.com/DESL-EPFL/55nodes-Swiss-distribution-grid

[108] ——. (2022) Ieee-benchmark-distribution-grids. [Online]. Available: https://github.com/DESL-EPFL/IEEE_benchmark_distribution_grids

[109] T. Asakura, T. Genji, T. Yura, N. Hayashi, and Y. Fukuyama, "Long-term distribution network expansion planning by network reconfiguration and generation of construction plans," *IEEE Transactions on Power Systems*, vol. 18, no. 3, pp. 1196–1204, 2003.

[110] B. Muruganantham, R. Gnanadass, and N. Padhy, "Challenges with renewable energy sources and storage in practical distribution systems," *Renew. Sust. Energ. Rev.*, vol. 73, pp. 125–134, 2017.

[111] S. Xie *et al.*, "Multi-objective active distribution networks expansion planning by scenario-based stochastic programming considering uncertain and random weight of network," *Applied Energy*, vol. 219, pp. 207–225, 2018.

[112] H. Xing, H. Cheng, Y. Zhang, and P. Zeng, "Active distribution network expansion planning integrating dispersed energy storage systems," *IET Generation, Transmission & Distribution*, vol. 10, no. 3, pp. 638–644, 2016.

[113] H. Hamidpour, J. Aghaei, S. Pirouzi, T. Niknam, A. Nikoobakht, M. Lehtonen, M. Shafiekhah, and J. P. Catalão, "Coordinated expansion planning problem considering wind farms, energy storage systems and demand response," *Energy*, vol. 239, p. 122321, 2022.

[114] M. Moradijoz, M. P. Moghaddam, and M.-R. Haghifam, "A flexible distribution system expansion planning model: a dynamic bi-level approach," *IEEE Trans. on Smart Grid*, vol. 9, no. 6, pp. 5867–5877, 2017.

[115] S. Karimi-Arpanahi, M. Jooshaki, M. Moein-Aghtaie, M. Fotuhi-Firuzabad, and M. Lehtonen, "Considering forecasting errors in flexibility-oriented distribution network expansion planning using the spherical simplex unscented transformation," *IET Generation, Transmission & Distribution*, vol. 14, no. 24, pp. 5970–5983, 2020.

[116] S. Ghaemi and J. Salehi, "Assessment of flexibility index integration into the expansion planning of clean power resources and energy storage systems in modern distribution network using benders decomposition," *IET Renewable Power Generation*, vol. 14, no. 2, pp. 231–242, 2020.

[117] M. Cococcioni and L. Fiaschi, "The big-m method with the numerical infinite m," *Optimization Letters*, vol. 15, no. 7, pp. 2455–2468, 2021.

[118] R. K. Gupta. (2020) Estimated medium voltage distribution network models for switzerland. [Online]. Available: https://github.com/DESL-EPFL/Estimated-Medium-Voltage\-Distribution-Network-Models-for-Switzerland

[119] J. Hu and H. Li, "A new clustering approach for scenario reduction in multi-stochastic variable programming," *IEEE Transactions on Power Systems*, vol. 34, no. 5, pp. 3813–3825, 2019.

[120] A. J. Conejo, E. Castillo, R. Minguez, and R. Garcia-Bertrand, *Decomposition techniques in mathematical programming: engineering and science applications*. Springer Science & Business Media, 2006.

[121] F. You and I. E. Grossmann, "Multicut benders decomposition algorithm for process supply chain planning under uncertainty," *Annals of Operations Research*, vol. 210, no. 1, pp. 191–211, 2013.

Ji Hyun Yi

ELL 140, Station 11, EPFL, Lausanne, Switzerland 1015
ji.yi@epfl.ch, +41-782414307, GoogleScholar|ResearchGate|LinkedIn|Orcid

Education

- **Ph.D. in Electrical Engineering**, 04/2018 - 11/2022
  Distributed Electrical Systems Laboratory,
  École Polytechnique Fédérale de Lausanne, Switzerland
  Thesis title: *"Optimal infrastructure planning including Energy Storage Systems for Achieving Active Distribution Network Dispatchability"*
  Thesis directors: *Prof. Mario Paolone, Rachid Cherkaoui.*

- **M.Sc. in Electrical Engineering** 03/2016 - 02/2018
  Electric Power Network Economics Laboratory (EPNEL),
  Seoul National University (SNU), Republic of Korea
  Thesis title: *"The impact of carbon reduction target on the optimal design of photo voltaic integrated small-scale multi energy system"*
  Thesis director: *Prof.Jong Keun Park.*

- **B.Tech (double major) in Electrical Engineering and Biology** 03/2010 - 08/2015
  Yonsei University, Seoul, Republic of Korea

Experience

Doctoral Researcher, EPFL, Switzerland 04/2018 - 11/2022

- Operation-aware optimal expansion planning of Medium Voltage Distribution Networks, by employing Optimal Power Flow (OPF)-based scheduling and energy storage systems (ESSs) control frameworks.
- Experimental validation of the optimal planning strategy of ESSs on a real lower voltage and medium voltage distribution network
- Development of day-ahead and real-time OPF-based dispatching tools to control ESS units, which is applied for a real medium voltage distribution network hosting Photo Voltaic resources.

Master Student Researcher, EPNEL, SNU, Republic of Korea 03/2016 - 02/2018

- Evaluation of impact of carbon-emission limit on the optimal planning of multi-energy system.
- Optimal planning of multi-energy system considering operation of combined heat and power generation (CHP) units.
- Analysis of impact of power converters on electromagnetic transient phenomenon in the power system.

Student Intern, Biophotonics Nanoengineering Laboratory, SNU, Republic of Korea 04/2016 - 08/2016

- Development of cell-capturing micro-structures isolating circulating tumor cells

Student Intern, Smartgrid Laboratory, Yonsei University, Republic of Korea 08/2015 - 01/2015

- Power system modeling utilizing MATPOWER

Publications

Journal Articles (published)

1. **Ji Hyun Yi**, Rachid Cherkaoui, Mario Paolone, Dmitry Shchetinin, and Katarina Knezovic. Expansion planning of active distribution networks achieving their dispatchability via energy storage systems. *Applied Energy*, 326:119942, 2022

2. **Ji Hyun Yi**, Rachid Cherkaoui, Mario Paolone, Dmitry Shchetinin, and Katarina Knezovic. Optimal co-planning of esss and line reinforcement considering the dispatchability of active distribution networks. *IEEE Transactions on Power Systems*, 2022

3. **Ji Hyun Yi**, Rachid Cherkaoui, and Mario Paolone. Dispatch-aware planning of energy storage systems in active distribution network. *Electric Power Systems Research*, 190:106644, 2021

4. **Ji Hyun Yi**, Rachid Cherkaoui, and Mario Paolone. Optimal allocation of esss in active distribution networks to achieve their dispatchability. *IEEE Transactions on Power Systems*, 36(3):2068–2081, 2020

5. **Ji Hyun Yi**, Woong Ko, Jong-Keun Park, and Hyeongon Park. Impact of carbon emission constraint on design of small scale multi-energy system. *Energy*, 161:792–808, 2018

6. Rahul Gupta, Antonio Zecchino, **Ji Hyun Yi**, and Mario Paolone. Reliable dispatch of active distribution networks via a two-layer grid-aware model predictive control: Theory and experimental validation. *IEEE Open Access Journal of Power and Energy*, 2022

7. Hungyu Kwon, Jong-Keun Park, Dam Kim, **Ji Hyun Yi**, and Hyeongon Park. A flexible ramping capacity model for generation scheduling with high levels of wind energy penetration. *Energies*, 9(12):1040, 2016

Conference Papers

1. **Ji Hyun Yi**, Woong Ko, and Jong-Keun Park. Optimal planning of energy resources for integrated energy systems considering operation of combined heat and power generation. In *2017 International Conference of Electrical Engineering, Weihai, China*, 2017

2. **Ji Hyun Yi**, Woong Ko, and Jong-Keun Park. Optimal planning of energy resources for integrated energy systems using mixed integer linear programming. In *Summer Conference of Korean Institute of Electrical Engineering, Busan, Korea*, 2017

3. Hyeongon Park, Jip Kim, **Ji Hyun Yi**, , and Jong-Keun Park. Impact of dynamic thermal line rating on generation scheduling. In *2016 Energy Systems Conference, London, UK*, 2016

Presentations

Oral

1. *14^{th} PowerTech Conference, Madrid, Spain (Virtual):* Optimal allocation of ESSs in active distribution networks to achieve their dispatchability, Yi, J., Cherkaoui, R., Paolone, M., 2021.

2. *XX Power Systems Computation Conference, Porto, Portugal (Virtual):* Dispatch-aware planning of energy storage systems in active distribution network, Yi, J., Cherkaoui, R., Paolone, M., 2020.

Poster

1. *SCCER-FURIES Annual Conference, EPFL, Lausanne, Switzerland:* Optimal allocation of ESSs in active distribution networks to achieve their dispatchability, Yi, J., Cherkaoui, R., Paolone, M. 2019.

2. *Europe-Korea Conference on Science and Technology (EKC), Glasgow, Scottland:* Impact of carbon emission constraint on design of small scale multi-energy system, Yi, J., Ko, W., Park, J.-K., Park, H., 2018.

Expertise

- Expansion and grid reinforcement planning of power distribution networks,
- Stochastic-based optimization for power network,
- Optimal power flow,
- Convex optimization, Convexification methods (linearization, relaxation etc.)
- Mixed-Integer Linear Programming, Mixed-Integer Second Order Cone Programming,
- Machine Learning, data analysis
- Scenario modeling of stochastic resources such as PV generation and demand,
- **Programming:** Matlab, Python, Express-MP, GAMS, C++,
- **Power System Analysis:** EMTP-RV, PSS/E, MATPOWER

Involvement in Research Projects

Customer-oriented distribution grid design and operation to enable a sustainable and green future
sponsored by Swiss Innovation Agency, Hitachi energy, and ABB Corporate Research 2018 - 2021

- Optimal ESS allocation based on an exact convexified OPF model
- Optimal line reinforcement and grid expansion planning of distribution network

SCCER-FURIES REEL Demonstrator
sponsored by Swiss Federal Office of Energy and Swiss Innovation Agency 2019 - 2022

- Validation of OPF-based real-time control algorithm on a real-life medium voltage distribution network in Aigle, Switzerland hosting 2.5MWh/1.5MW battery storage capacity, 3.2MWP photovoltaic, 3.4 MVA hydro and 2.8MW base demand.
- Development of the software for operation of the battery energy storage system for real-time control.

CircuBAT project
sponsored by Swiss Innovation Agency 2019 - 2022

- Advancing the technical and economical potential of a circular economy for batteries
- Optimal siting and sizing of batteries within a real Low Voltage distribution network

Supervised Student Projects

- **Cluster-and-connect expansion planning algorithm for distribution network**, Master Semester Project, Mr. Valentin Michel René Jarry-Cammas, Fall, 2022

Awards & Honors

- **National Science & Technology Outstanding Talent Scholarship**,
  funded by **Korea Student Aid Foundation**, 03. 2010 – 08. 2015

Language

- English (Full professional proficiency), French (B1), German (A1), Korean (Mother tongue)

Extra Curricular Activities

Member of **"Yonsei Energy & Environmental Economics Forum"** 03/2014 - 08/2015

- Academic research/discussion on energy & environment issues and their economic/social/political impacts

Member of **Humanities Forum "Plato Academy"** 03/2013 - 08/2015

- Organizing and leading humanities activities for students such as seminars, workshops, exihibition, volunteering and etc.

Referees

Prof. Mario Paolone
DESL, EPFL
mario.paolone@epfl.ch
☎ +41 21 693 26 62

Dr. Rachid Cherkaoui
Senior Scientist, EPFL
rachid.cherkaoui@epfl.ch
☎ +41 21 693 20 58

Dr. Dmitry Shchetinin
Senior Scientist, Hitachi Energy
dmitry.shchetinin@hitachienergy.com